Characterisation of ADAM15-mediated changes to cellular behaviour in breast cancer cells

Thesis submitted in partial fulfilment of the requirements of the degree of Doctor of Philosophy (PhD)

Jens Mattern, BSc (Hons), BSc

2016

School of Medicine
Cardiff University
Cancer & Genetics Building
Cardiff, CF14 4XN
Wales, United Kingdom

Schifferstadt, January 26, 2017

Affidavit

Declaration

This work has not been submitted in substance for any other degree or award at this or any other university or place of learning, nor is being submitted concurrently in candidature for any degree or other award.

Signed ..... (candidate) Date .....

Statement 1

This thesis is being submitted in partial fulfilment of the requirements for the degree of Doctor of Philosophy (PhD)

Signed ..... (candidate) Date .....

Statement 2

This thesis is the result of my own independent work/investigation, except where otherwise stated. Other sources are acknowledged by explicit references. The views expressed are my own.

Signed ..... (candidate) Date .....

Statement 3

I hereby give consent for my thesis, if accepted, to be available online in the University's open access repository and for inter-library loan, and for the title and summary to be made available to outside organisations

Signed ..... (candidate) Date .....

Statement 4

I hereby give consent for my thesis, if accepted, to be available online in the University's open access repository and for inter-library loans after expiry of a bar on access previously approved by the Academic Standards & Quality Committee.

Signed ..... (candidate) Date .....

I dedicate my PhD thesis to my beloved parents, Stephanie and Bernd. Thank you both for your never-ending love and support throughout my life and education

Acknowledgements

I would like to thank my supervisors Dr Zaruhi Poghosyan and Dr Vera Knäuper for their support and guidance throught my PhD, and for giving me this opportunity. I would also like to thank Cancer Research Wales for funding my project and Prof Dr Chris Pepper, Dr Stephen Man and Dr Paul Brennan for all the good advices before, during and after my annual appraisals. I would also like to thank our collaborator Prof Dylan Edwards from the University of East Anglia in Norwich. Thanks to Melanie, Kayleigh and Sara for beeing amazing colleagues and friends and for sharing great memories inside and outside the lab. I'd like to thank Dr Dodd specially for sharing lab equipment throughout my PhD. A big thanks to Julia Grimstead, the mastermind technician, who patiently answered hundreds of my questions and helped me with general issues in the lab and department. Thanks to Maria Clarke for supporting our lab and thus giving me more time for my project. Thanks to Sam Hyatt which was always available for great discussions, healthy food and sporting activities. Thanks to Wenbin Wang for valuable conversations and discussions during and after work hours and long weekends in the lab. Thanks to Dr Spyros Zissimopoulos, Dr Andreas Heil, Dr Lea Bauer and Laura Escudero for sharing great moments during the last years. Thanks to Dr Rhiannon Robinson and Dr Katie Evans which were regularly available for a good chat during incubation times. Special thanks to Dr Ellie Rad for all her time and support, and for making my stay in Cardiff memorable. Last but not least, my deepest graditude go to my parents. All this would not have been possible without your love and support.

“ *A scientist is never certain. We absolutely must leave room for doubt or there is no progress and there is no learning.* ”

Richard Phillips Feynman, *theoretical physicist*, 1918-1988

Abstract

ADAM15 is a multidomain multifunction transmembrane protein. It participates in protein ectodomain shedding via the metalloproteinase domain. ADAM15 also interacts with integrins via the disintegrin domain. ADAM15 mRNA is subject to complex processing, generating different isoforms as a result of alternative splicing. The splicing affects the intracellular domain (ICD) of the protein, generating distinct SH3 domain binding regions. The expression of specific splice forms correlates with breast cancer prognosis.

We aimed to test if ADAM15 isoforms have distinct functions that may affect multiple aspects of cell behaviour in isoform-specific unique ways. We generated an isogenic panel expressing each ADAM15 isoform in MDA-MB-231 acells. Comparative characterisation of the panel demonstrated distinct differences between isoforms, such as catalytic function dependant or independent effects on proliferation rate, changes in cell size, isoform-specific reorganisation of the actin cytoskeleton.

We discovered ADAM15 isoform-dependant upregulation of tight junction protein claudin1. Immunofluorescence analysis demonstrated co-localisation of ADAM15 with claudin1 and another tight junction protein ZO1 at cell-cell junctions. Further immunoprecipitation analysis showed potential complex formation with ADAM15 and ZO1. Pharmacological analysis showed claudin1 upregulation is mediated via PI3K/mTOR-pathway. Claudin1 upregulation depended on the metalloproteinase catalytic function of ADAM15, suggesting that ADAM15 isoforms have distinct substrates. Claudin1 was also found in the nucleus of MDA/ADAM15 A expressing cells where it could potentially function as a transcription factor.

Focal adhesion (FA) turnover was influenced by ADAM15 isoform expression. In MDA/ADAM15 C expressing cells impairment of FA reassembling was observed, while ADAM15 D expression showed reduced FA disassembly. Comparison of spreading of ADAM15 isoform expressing cells on fibronectin (FN) and vitronectin (VN) revealed that most cell lines preferred FN over VN. Expression of ADAM15 E reduced this preference while ADAM15 A altered it in favour of VN over FN. Changes in subcellular localisation of $\beta 3$, but not $\beta 1$-integrin was observed.

Table of contents

List of Figures

List of Tables

Listings

Abbreviations

β-PIX	Pak-interacting exchange factor-β
βAPP	β-amyloid precursor protein
µL	Microlitre
µM	Micromolar
CO_2	Carbon dioxide
IC_{50}	Half maximal inhibitory concentration
$MgCl_2$	Magnesium chloride
Na^+/K^+ – ATPase	Sodium-potassium adenosine triphosphatase
PIP_2	Phosphatidylinositol 4,5-bisphosphate
PIP_3	Phosphatidylinositol 3,4,5-triphosphate
.jpeg	Joint Photographic Experts Group
.tsv	Tab-separated values
3'UTR	3' untranslated region
4E-BP1	4E-binding protein 1
A	Ampere
ADAM	A disintegrin and metalloproteinase
ADAMTS	A disintegrin and metalloprotease with thrombospondin motifs
AF	AlexaFluor
AHI1	Abelson helper integration site 1
AJCC	American Joint Committee on Cancer
ALDH1	Aldehyde dehydrogenase isoform 1
AN	Accession number
ANOVA	Analysis of variance
APC	Adenomatous polyposis coli
APS	Ammonium persulfate
ATP	Adenosine triphosphate
au	Arbitrary unit
B&W	Black & White
Bcl2	B-cell lymphoma 2
BD	Becton Dickinson
BH	Bcl2 homology
Bim1	Bisindolylmaleimide 1
Bit	Binary digit
BLAST	Basic Local Alignment Search Tool

BLBC	Basal-like breast cancer
BRCA1	Breast Cancer 1
BSA	Bovine serum albumin
Btk	Bruton's tyrosine kinase
C	Cysteine
CAK	CDK-activating kinase
Cat. No.	Catalogue Number
Cav1	Caveolin1
CCS	Clathrin-coated structure
CCV	Clathrin-coated vesicles
Cdc42	Cell division control protein 42 homologue
CDK	Cyclin dependent kinase
cDNA	Complementary DNA
CE	Cytoplasmic cell extract
CHX	Cycloheximide
CIP4	Cdc42 interacting protein 4
CKI	CDK inhibitor protein
CLAHE	Contrast Limited Adaptive Histogram Equalization
cm	Centimetres
CME	Clathrin-mediated endocytosis
Crk	v-crk sarcoma virus CT10 oncogene homologue
Csk	C-terminal Src kinase
CST	Cell Signalling
CTF	C-terminal fragment
Ctn	Catenin
D-loop	Disintegrin loop
D6	Six-sided dice
Da	Dalton
Dab	Disabled
Dab2	Disabled homologue 2
DCIS	Ductal carcinoma *in situ*
DEPTOR	DEP domain-containing mTOR-interacting protein
DLC1	Deleted in liver cancer 1
DMSO	Dimethyl sulfoxide
DNase	Deoxyribonuclease
dNTP	Deoxyribonucleotide triphosphates
Dock180	Dedicator of cytokinesis, 180 kDa
DTT	Dithiothreitol
E	Glutamic acid

E-cadherin	Epithelial-cadherin
EBCTCG	Early Breast Cancer Trialists' Collaborative Group
ECD	Extracellular domain
ECL	Enhanced Chemoluminescence
EDTA	Ethylenediaminetetraacetic acid
EGF	Epidermal Growth Factor
EGFR	Epidermal growth factor receptor
EIF4E	Eukaryotic initiation factor 4E
ELMO1	Engulfment and motility
EMSO	European Society for Medical Oncology
EMT	Epithelial-Mesenchymal-Transition
Eps8L	Epidermal growth factor receptor kinase substrate 8-like protein
ER	Oestrogen receptor
ES cells	Embryonic stem cells
ESACG-motif	Exon skipping-associated C- or G-rich motifs
ESE	Exonic splice enhancer
ESR	Exonic splice-regulatory sequences
ESS	Exonic splice silcener
EtOH	Ethanol
FAC	fluorouracil, doxorubicin, cyclophosphamide
FAH	Formaldehyde
FAK	Focal adhesion kinase
FBP17	Formin-binding protein 17
FBS	Fetal Bovine Serum
Fc	Fragment crystallisable
FEC	fluorouracil, epirubicin, cyclophosphamide
FGFR2IIIb	Fibroblast growth factor receptor-2IIIb
FKBP12	FK506-binding protein 12
FLIM	Fluorescence-lifetime imaging microscopy
FRET	Fluorescence resonance energy transfer
FRT	Flp recombination target
FSC	Forward Scatter
FSC-A	Forward Scatter Area
FSC-H	Forward Scatter Height
FSH	Follicle stimulating hormone
G	Glycine
GAIP	Gα interactin protein
GAP	GTPase-activating protein

GAPDH	Glyceraldehyde-3-phosphate dehydrogenase
GDP	Guanosine diphosphate
GE	General Electric
GEF	Guanine nucleotide exchange factor
GIPC1	GAIP interacting protein, member 1
GLISA	GTPase-linked immunosorbent assay
GLP-2	Glucagon-like peptide-2
GnRHa	Gonadotropin-releasing hormone analogues
GPCR	G-protein coupled receptor
Grb2	Growth factor receptor-bound protein 2
GSK3	Glycogen synthase kinase 3 β
GSK3	Glycogen synthase kinase-3
GST	Glutathione-S-transferase
GTP	Guanosine triphosphate
h	Hours
HAT	Histone acetyltransferase
HB-EGF	Heparin-binding EGF-like growth factor
HCl	Hypochloric acid
HCV	Hepatitis C Virus
HDAC	Histone deacetylase
HEAT	(Huntingtin, elongation factor 3 (EF3), protein phosphatase 2A (PP2A), and the yeast kinase TOR1)
Her	Human epidermal growth factor receptor
HIF-1	Hypoxia-inducible factor-1
HMC	Human mesangial cell
hnRNP	Heterogeneous nuclear ribonucleoprotein
HSP90	Heat Shock Protein 90
HUVEC	Human umbilical vein endothelial cells
IBC	Inflammatory breast cancer
IBS	Irritable bowel syndrome
ICD	Intracellular Domain
IDC	Invasive ductal carcinoma
IGF-1	Insulin-like growth factor 1
IgG	Immunoglobulin G
IGV	Integrative Genomics Viewer
ILK	Integrin-linked kinase
ILKAP	ILK-associated phosphatase
IP	Immunoprecipitation
IPEC	Intestinal porcine epithelial cells

ISE	Intronic splice enhancer
ITC	Isolated tumour cells
Itk	Interleukin-2-inducible T-cell kinase
JAM	Junctional Adhesion Molecule
kbp	Kilobase pair
KCl	Potassium chloride
kDa	Kilodalton
L	Litre
L-Glu	L-Glutamine
LCWGS	Low-coverage whole genome sequencing
LDL	Low density lipoprotein
lif	Leica Image File
LIMK	LIM-motif containing kinase
LoG	Laplacian of Gaussian
LPA	Lysophosphatidic acid
LPS	Lipopolysaccharide
M	Molar
MAD2	Mitotic arrest deficient 2
MAGUK	Membrane-associated guanylate kinase
MAP	Mitogen-activated protein
MBNL1	Muscleblind-like protein 1
MDCK	Madin-Darby canine kidney
mDia	Mammalian Diaphanous formin
ME	Membrane cell extract
MEF	Mouse embryonic fibroblast
MEM	Minimal Essential Medium
MeOH	Methanol
MesNa	Sodium 2-mercaptoethanesulfonate
MET	Mesenchymal-epithelial transition
MHC	Major histocompatibility complex
MICB	MHC class I polypeptide-related sequence B
min	Minutes
miRNA	Micro RNA
mL	Millilitre
MLC	Myosin II light chain
MLCP	Myosin light chain phosphatase
mLST8	Mammalian lethal with SEC13 protein 8
mM	Millimolar
mm	Millimetre

MMP	Matrix Metalloprotease
MMP9	Matrix metalloproteinase 9
MP	Metalloproteinase
mSIN1	Mammalian stress-activated protein kinase-interacting protein 1
MT-MMP	Membrane-type metalloproteinases
mtDNA	Mitochondrial DNA
mTOR	Mechanistic target of rapamycin
mTORC1	mTOR complex 1
mTORC2	mTOR complex 2
MTS	3-(4,5-dimethylthiazol-2-yl)-5-(3-carboxymethoxyphenyl)-2-(4-sulfophenyl)-2H-tetrazolium
MUPP1	Multi-PDZ Domain Protein 1
N-cadherin	Neural-cadherin
NaOH	Sodium hydroxide
NCCN	National Comprehensive Cancer Network (NCCN)
NCF1	Neutrophil cytosolic factor 1
NE	Nuclear cell extract
NEAA	Non-essential amino acids
NGS	Next generation sequencing
NISCH	Neonatal ichthyosis and sclerosing cholangitis
nM	Nanomolar
NPF	Nucleation promoting factor
Nrp1	Neuropilin 1
NSCLC	non-small cell lung cancer
nt	Non target
OB	Osteoblast
OSTF1	Osteoclast stimulating factor 1
P/S	Penicillin/Streptomycin
PAA	Polyacrylamide
PAGE	Polyacrylamide gel electrophoresis
PAK	Serine/threonine-protein kinase PAK
PAR3	Proteinase-activated receptor 3
PARP1	Poly-ADP-ribose polymerase 1
PBS	Phosphate buffered saline
PC3	Prostate cancer 3
PCR	polymerase chain reaction
PDAC	Pancreatic ductal adenocarcinoma

PDK1	Phosphoinositide-dependent kinase 1
PDZ	Post synaptic density protein (PSD95), Drosophila disc large tumor suppressor (Dlg1), and zonula occludens-1 protein (ZO1)
pH	pH-value
PH domain	pleckstrin homology domain
PHLLPP	PH domain leucine-rich repeat protein phosphatase
PI	Propidium iodide
PI3K	Phosphatidylinositol-3-kinase
PIKK	PI3K-related kinase
PINCH	Particularly interesting cysteine- and histidine-rich protein
PKC	Protein kinase C
PKCζ	Protein kinase C ζ
PKL	Paxillin-kinase linker
PMA	Phorbol myristic acid
PMSF	Phenylmethanesulfonyl fluoride
PP2A	Protein phosphatase 2A
PR	Progesterone receptor
PRAS40	Proline-rich Akt substrate 40 kDa
pRB	Retinoblastoma protein
Protor	Protein observed with Rictor
PTB domain	Phosphotyrosine-binding domain
PTEN	Phosphatase and tensin homolog
PTK6	Protein-tyrosine kinase 6
PTP-1B	Protein-tyrosine phosphatase 1B
PTP-PEST	Protein-tyrosine phosphatase-PEST
PVDF	Polyvinylidene fluoride
Pyk2	Proline-rich tyrosine kinase 2
R	Arginine
R&D	R&D Systems
Rab	Ras-related protein
Rac	Ras-related C3 botulinum toxin substrate
Raptor	Regulatory-associated protein of mTOR
RFS	Relapse Free Survival
Rheb	Ras homologue enriched in brain
Rho	Ras homologue
Rho-GDI	Rho-GDP dissociation inhibitors
Rictor	Rapamycin-insensitive companion of mTOR

RIM	Regulating synaptic membrane exocytosis protein
RIMBP	RIM-binding protein
RIP	Regulated intramembrane proteolysis
RIPA	Radioimmunoprecipitation assay buffer
RNase	Ribonuclease
ROCK	Rho-associated coiled-coil kinase
ROI	Regions of interest
RON	Recepteur d'origine nantais (RON)
ROP	Retinopathy of prematurity
ROS	Reactive oxygen species
RRM	RNA-recognition motif
RT-PCR	Reverse transcription polymerase chain reaction
RTK	Receptor tyrosine kinase
S	Serine
S6K	Ribosomal protein S6 kinase
sAPPα	soluble amyloid precursor protein α
sc	Santa Cruz
SDS	Sodium dodecyl sulfate
SEA	Serine-glutamic acid-alanin
SERM	Selective oestrogen receptor modulator
SHIP	SH2-containing phosphatases
SHP2	Src homology phosphotyrosyl phosphatase2
siRNA	short interference RNA
SNP	Single nucleotide polymorphism
SNX	Sorting nexin
SR-protein	Serine/Arginine-protein
STAT3	Signal transducer and activator of transcription 3
SVMP	Snake venom metalloproteinas
T	Threonine
T3	Triiodothyronine
TACE	TNFα converting enzyme
TAE	Tris-acetate-EDTA
TBS	Tris buffered saline
TBST	Tris buffered saline Tween
TC	Tissue culture
TE	Total cell extract
TEER	Transepithelial electrical resistance
TEMED	N,N,N',N'-Tetramethylethylendiamine
TGFα	Transforming growth factor α

TGFβ1	Transforming growth factor-β1
Tis	Tumour *in situ*
TKI	Tyrosine kinase inhibitor
TMT-MS-TAILS	Tandem Mass Tag® terminal amino isotopic labelling of substrates
TNM	Tumour node metastasis
TOCA1	Transducer of Cdc42-dependent actin assembly protein 1
Tris	Tris(hydroxymethyl)-aminomethan
TSA	Trichostatin A
TSC1	Tuberous sclerosis complex 1
TSC2	Tuberous sclerosis complex 2
TSP	Thrombospondin
UICC	International Union for Cancer Control
UK	United Kingdom
UT	Untreated
UV	Ultraviolet
V	Voltage
VCAM1	Vascular cell adhesion molecule-1
VE-cadherin	Vascular endothelial-cadherin
VEGF	Vascular endothelial growth factor
WASP	Wiskott-Aldrich syndrome proteins
WAVE	Wiskott-Aldrich syndrome protein-family verprolin homologous protein
WB	Western Blot
WT	Wildtype
Y	Tyrosine
ZO1	Zona occludens protein 1
ZONAB	ZO1-associated nucleic-acid binding

Chapter 1

General Introduction

1.1 Cancer

Cancer is a common name for more than 200 types of diseases. In total this disease accounts for approximately 20% of deaths in all industrialised countries of the Western world[1]. In the UK, over 350,000 new cases of cancer were diagnosed, and over 160,000 patients died in 2014[2]. Statistically, one in two people born after 1960 will develop some form of cancer during their lifetime[2].
Years of research in the field of cancer has provided a substantial amount of knowledge, revealing that this disease and its characteristics are triggered by genome instability. Mutations that result in the upregulation of oncogenes and also the loss of function of tumour suppressor genes have been recognised in both human and animal cancer cells[3]. There are indications that tumourigenesis is indeed a complex and multi-step procedure, with every step containing genetic alternations that drive the transformation of normal cells into tumour cells. The main question concerning cancer development is what kind and how many regulatory defects must occur before the transformation of a normal cell into a cancer cell. In year 2000, Robert Weinberg and Douglas Hanaham published an article, proposing six hallmarks for cancer, which provided a better understanding of the biology underlying this complex disease[4]. Over a decade later, two emerging hallmarks and two enabling characteristics were added. The hallmarks are reprogramming of energy consumption and evading immune destruction. The characteristics are tumour-promoting inflammation as well as genome instability and mutation[3]. A summary of hallmarks is depicted in figure 1.1.

1. Sustaining proliferative signalling

One of the essential features of cancer cells is their ability to sustain proliferation. While normal cells closely control their growth and division cycle to insure the normal function of tissues, cancer cells tend to deregulate the cell cycle and cell growth signals. Enabling cells to become highly proliferative. The sustained mitogenic signalling in cancer cells is achieved via various methods; these cells might overexpress growth factor receptors followed by the production of growth factors by themselves, this results in the stimulation of an autocrine proliferation. Moreover cancer cells have the ability to send signals to normal cells located within the stroma, causing production of growth factors by these cells[3].

2. Evading growth suppressors

While cancer cells have the ability to sustain proliferative behaviour via the production of cell cycle and cell growth regulators, it is also necessary for these cells to be able to evade negative regulators of proliferation. There are numerous

tumour suppressor genes that act as negative regulators of cell growth and division. In cancer cells inactivation of such genes results in uncontrolled proliferation. Retinoblastoma protein (pRB) and p53 are two of the main tumour suppressor proteins that play an important role in allowing cell proliferation or cell death[5].

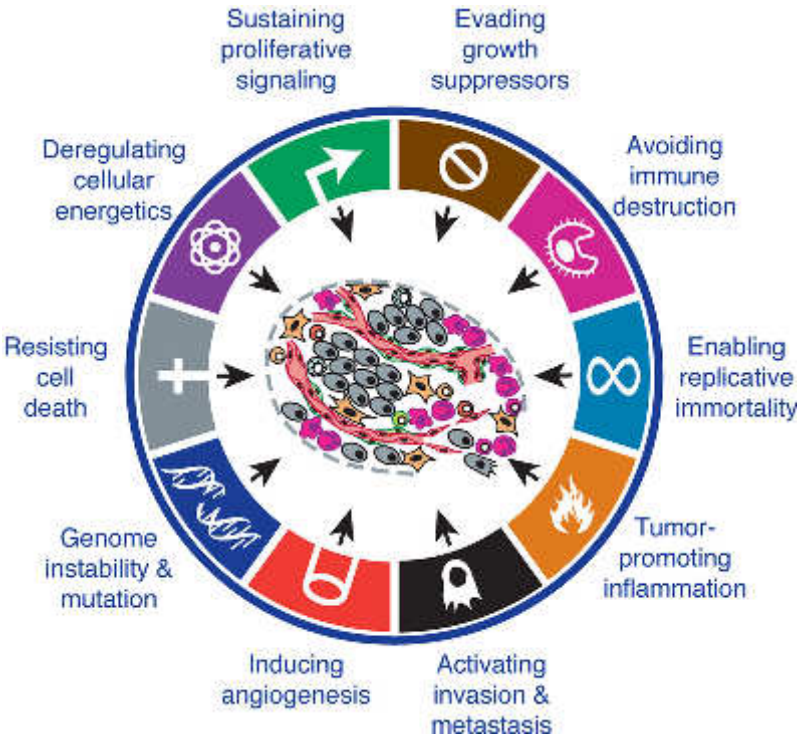

Figure 1.1: The hallmarks of cancer proposed by Hanahan and Weinberg in 2011. The figure was adapted and modified from their review[3]

.

3. Avoiding immune destruction

According to the theory of immune surveillance nascent cancer cells are cleared from the immune system by early recognition. However, solid tumours evaded this process either by avoiding detection or survived the immunological killing. The importance of the immune system is shown in different mouse models. Deficiencies in cytotoxic T-lymphocytes, T-helper or natural killer cells led to increased tumour size. Cancer cells may be able to evade by disabling immune system components. Natural killer cells and cytotoxic T-cells may be paralysed by transforming growth factor-β (TGF-β) secretion[6]. A more subtle way is to recruit immunosuppressive cells to repress cytotoxic T-cells. These compromises not only regulatory T-cells, but also myeloid-derived suppressor cells[7]. Immunoevasion is still an emerging hallmark and a deeper insight needs to be established.

4. Enabling replicative immortality

Most normal cells can only go through a limited number of cell division cycles, on

the contrary cancer cells have the ability to multiply indefinitely. This limitation in normal cells is due to the existence of two main barriers: senescence (non-proliferative state) and crisis. The state of crisis describes apoptosis, karyotypic disarray with telomeric end-to-end fusion. Occasionally, a cell can escape crisis (1:10,000,000). This is described as immortilsation[8]. These two crucial barriers against proliferation are used in cells as anticancer defences, resulting in a normal and healthy cell division. However tumour cells have the potential to become immortalised by maintaining a sufficient telomere length, which can prevent the activating of the senescence or apoptosis process. This is possible by the upregulation of telomerase expression in these cells[9].

5. Tumour promoting inflammation

Several mechanisms exist in which parts of or the whole cell is degraded. Some of those functions by inducing an inflammatory response, some do not. Usually, autophagy plays a role in clearing misfolded proteins or damaged organelles. The first step is to surround the target molecule isolating it from the rest of the cell generating an autophagosome. In the next step it fuses with a lysosome to an autolysosome in which the inside is broken down by lysosomic enzymes. Another destructive mechanism is apoptosis. A dying cell contracts and is degraded from the inside. In a final step the cell is engulfed and endocytosed by macrophages. Together, both process are executed without inflammation. In contrast, necrotic cells enlarge and burst, releasing their contents into the environment triggering an immune response. Necrosis normally occurs due to bacterial or viral infection. In context of neoplasia, inflammatory cells can be tumour promoting. These cells are capable of inducing angiogenesis, cell proliferation and invasiveness[3]. For example, necrotic cells can release interleukin 1-α, which can stimulate adjacent cells to proliferate[10]. This may facilitates neoplastic progression.

6. Activating invasion and metastasis

A main characteristic of malignant tumours is their ability to move through the extracellular matrix (ECM) and invade other tissues. In order to do so, tumour cells have the ability to alter their shape and develop changes in their attachment to adjacent cells and the ECM. This could be achieved by the loss of Epithelial-cadherin (E-cadherin; a cell-cell adhesion molecule). Furthermore the down-regulation or mutation inactivation of E-cadherin has been observed in various tumour cells, suggesting that this adhesion molecule plays an important role in the invasive and metastatic behaviour of tumour cells. In addition, abnormal expression of other cell-cell and cell-ECM adhesion molecules has been observed in more aggressive carcinomas.

7. Inducing angiogenesis

For tumour cells to survive, just like normal cells, they require nutrients and oxygen. It is also essential for these cells to discard their metabolic waste and carbon dioxide. This is achieved by neovascularisation via angiogenesis. In normal tissues the process of angiogenesis is only activated briefly when required, however during tumourgenesis, the angiogenic switch is constantly on, resulting in the formation of new blood vessels that cause expanding neoplastic growth.

8. Genome instability and mutation

The acquisition of hallmarks largely depends on the accumulation of genomic alterations and maintaining them. Selective advantage of those cells enable them to outgrow other cells which let them dominate in their environment. Inactivation of a tumour suppressor can be acquired by epigenetic mechanism like histone modification, DNA methylation, by direct mutation due to UV light or exposure to chemicals. Each cell has a DNA-maintenance machinery. Defects in genes which drive these machineries are crucial. They comprise: (1) Detection of DNA damage and activation of repair mechanisms. (2) Direct repair of damaged DNA. (3) Interception of mutagenic agents prior to DNA damage. When introduced in mouse germline, mutant copies of genes involved in these machineries resulted in elevated cancer incidences[11]. This supports their role in human cancer development.
Replicative potential induced by telomerase is another hallmark of cancer, this action also plays a role in genome stability. Loss of telomeric DNA generates karyotypic instability in tumours. This can lead to deletion or amplification of chromosomal segments. Comparative genomic hybridisation studies revealed the loss and gains of gene copy numbers during tumour progression. Amplifications and deletions at particular genomic sites indicate location of genes which mutations favour neoplastic progression.

9. Resisting cell death

Apoptosis is a crucial process used by cells to eliminate dysfunctional and damaged cells. One of the hallmarks of malignant tumours is indeed the ability to evade apoptosis, allowing these tumour cells to grow and divide uncontrollably. Studies have shown that apoptosis is a natural process which can prevent cancer development when activated. Research regarding the signalling pathway related to apoptosis has revealed that the apoptotic program can be activated in response to numerous physiological stress events seen in many developing cancer cells. As mentioned earlier DNA damage caused by hyper-proliferation can induce apoptosis in these cells. However, of interest, studies carried out on different types of tumour

cells have shown that apoptosis is reduced in tumour cells that develop in to high-grade malignancies and become resistant to therapy.

10. Deregulating cellular energetics

Another emerging hallmark is the altered cellular energetics. Uncontrolled cell proliferation does not only involve deregulated cell growth, but also a higher energy metabolism to support growth and division. Normal cells generate energy needed for they metabolism mainly by mitochondrial oxidative phosphorylation, in contrary to this cancer cells tend to depend on aerobic glycolysis. This was first observed by Otto Warburg, therefore this phenomenon in cancer cells is known as "The Warburg effect"[12]. Cancer cells tend to use aerobic glycolysis even in the presents of adequate oxygen. The underlying mechanisms are not completely understood how a cancer cells compensate for the approximately 18-fold decreased efficiency of adenosine triphosphate (ATP) production. This is partially achieved by upregulation of glucose transporters which increase the uptake of glucose into the cytoplasm[13]. Another interesting process found in some tumours is the presence of two subpopulations. Glucose-dependent cells secrete lactate which is used by the second subpopulation as energy source to partially employ the citric acid cycle. Deregulated metabolism is not part of the core hallmarks yet and needs further investigation. Hypoxic conditions are not necessarily static in tumours. Temporarily normoxic environment could possibly compensate the lack of oxygen. It is also important to note that neovascularisation supports tumour progression in many cases.

1.2 Breast Cancer

Breast cancer is the most common type of cancer in the UK. In 2014, over 55,000 cases of cancer were reported. In 2014, over 11,000 patients died from this disease[2]. It is estimated that almost 1.7 million women were diagnosed worldwide in 2012[2]. The majority of cases occur after the menopause, but also many young women are affected. Known risk factors are ionising radiation, smoking, a high-fat diet, and prolonged exposure to oestrogens. Genetics also play a role in developing this disease. In rare occasions men are diagnosed with breast cancer (<1%). Breast cancer is comprised of several different subtypes, this is based on: The location of the tumour, invasiveness, abnormal expression of hormone receptors, metastatic rate and the occurrence of inflammation.

1.2.1 Stages of breast cancer

Staging of cancer is important to understand changes in cancer incidence within the population, the extent of the disease at initial presentation as well as the impact on cancer treatment. It is an important benchmark for physicians and patients for defining prognosis and the probability to overcome this disease. Moreover, it is a crucial base of clinical trials. For breast cancer there are several systems available. The two most common system, TNM and number/roman staging system, will be discussed in more detail below. A comparison of both system is depicted in table 1.1.

1.2.1.1 TNM staging system

The "T" stands for tumour and describes the size, the "N" for involvement of the lymph node and "M" whether the cancer has established far distant metastases.

The TNM system was developed by Pierre Denoix in the 1940s. Since the 1980s the *International Union for Cancer Control* (UICC) and the *American Joint Committee on Cancer* (AJCC) coordinate and refine the guidelines. These guidelines are published in *TNM Classification of Malignant Tumours*[14] and the *AJCC Cancer Staging Manuel*[15].

TNM staging has four different types. (1) The *clinical staging* is used based on information identified prior to neoadjuvant therapies or surgery. It is based on imaging tests, biopsies and physical examination. (2) *Pathologic staging* is determined individually post surgery. This staging is combined with clinical staging. (3) *Post-therapy* or *Post-neoadjuvant theraphy staging* explains how much cancer remains after initial systemic and/or radiotherapy treatment prior to surgery (or no surgery). Either clinical or pathologic staging guidelines are assessed. (4) *Restaging* is used to assess recurring disease. It helps to determine the best treatment options. As a matter of simplicity only the clinical staging system will be explained in detail.

The T stages

The T is followed by a letter, digit or abbreviation to give further details. **TX** means that the tumour could not be found or measured. **T0** indicated that there is no proof of a primary tumour. **Tis** means "tumour *in situ*" and is used to describe DCIS. **T1-4** are based on the size of the tumour and in which extend the adjacent tissue is affected. In general **T1** means that the tumour is 2 cm in size or less. However, T1 is sub-grouped, depending on the size of the tumour, into: T1mi, T1a, T1b and T1c: **T1mi** indicates a tumour size of 0.1 cm or less. **T1a:** The tumour is larger than 0.1 cm, but not more than 0.5 cm. **T1b:** The size varies between 0.5-1 cm. **T1c:** The tumour is between 1-2 cm. **T2** means the tumour has a size

between 2-5 cm. **T3** means the tumour is larger than 5 cm. **T4** is subdivided into four groups based on the location of metastasis: T4a, T4b, T4c and T4d: **T4a** If the tumour has spread to the chest wall. **T4b** indicates that the cancer has spread into the skin and the breast might be swollen. **T4c** means chest wall and skin are infiltrated by tumour cells. **T4d** is a rare form of breast cancer (1-4%) and is described as an inflammatory cancer with symptoms such as swollen breast. Cancer cells might be found in both the skin and lymph nodes.

The N stages

The N is followed by a letter, digit or abbreviation to give further details. **NX** means that no tumour is found in the lymph nodes or they cannot be assessed. One reason could be that they were previously removed. **N0** indicates that no cancer cells were found in nearby lymph nodes. There is a threshold for lymph node scoring: A lymph node can have cancer cells however can be counted as negative if they only contain isolated tumour cells (ITCs). ITCs are defined either as single tumour cell, small cluster of cancer cells with less than 0.2 mm in size or less than 200 cells in one part of the lymph node. **N1**: Cancer has spread to the lymph nodes in the armpit, but is not detected in surrounding tissue. A subtype of N1 is **pN1mi** which is diagnosed if one or more lymph nodes contain micrometastasis which are larger than 0.2 mm or contain more than 200 cancer cells with less than 2 mm in size. **N2** is categorised in two groups - N2a and N2b. **N2a:** Metastases are found in axillary lymph nodes which are fixed to one another or to other structures. **N2b:** Cancer cells are clinically detected in the internal mammary nodes, but are absent in the axillary nodes. **N3** is divided into three groups: **N3a:** If metastases are found within lymph nodes below the collarbone. **N3b:** If tumours are detected in the internal mammary and axillary lymph nodes. **N3c:** If cancer cells are found in the lymph nodes superior to the collarbone.

The M stages

The M stages indicate if cancer has not spread **(M0)** or has spread **(M1)** to other body parts. In M1 stage tumours are larger than 0.2 mm. However, there is one exemption within the **cMo(i+)** stage where neither clinical nor radiographical evidence of distant metastases were found. However, molecularly or microscopically detected tumour cells are found in circulating blood, bone marrow or other distant nodal tissue with a size of more than 0.2 mm. Patients in this stage are without symptoms or signs of metastases.

1.2.1.2 Number/Roman numeric staging system

The number staging system divides breast cancer in four stages. As the TNM system, the number stage system also considers if the cancer is node negative or positive as well as tumour size and spreading to other body parts. Sometimes, a fifth stage is included in the system. Stage 0 is the pendant to Tis of the TNM system and refers to non-invasive breast cancer such as DCIS. Following stages, however, describe all invasive cancer.

Stage I is further divided into two subcategories IA and IB. Invasion can be observed, but invaded cells measure less than 1 mm in surrounded tissue. Stage IA is an invasive tumour with up to 2 cm in size, but has not yet spread to the lymph nodes. Stage IB describes invasive breast cancer with or without a tumour not larger than 2 cm as well as small groups of breast cancer cells which vary between 0.2 and 2 mm in size and infiltrated the lymph nodes.

Stage II is also subcategorised into two groups: IIA and IIB. Three scenarios are considered in stage IIA cancer: 1) No tumour is found in the breast, but 1 to 3 tumours are seen within the axillary lymph nodes or in the lymph nodes near the breast bone. These are larger than 2 mm. 2) If the tumour has a maximum size of 2 cm and has spread to the axillary lymph nodes. 3) If a tumour is between 2-5 cm, but has not yet spread to the axillary lymph nodes. Stage IIB distinguishes also three scenarios: 1) The tumour is between 2-5 cm in size. Additionally, small tumours with a size of 0.2-2 mm are found in the lymph nodes. 2) The tumour is between 2-5 cm in size and the cancer has spread to lymph nodes near the breastbone or to 1 to 3 axillary lymph nodes. 3) The tumour is larger than 5 cm, but has not infiltrated the axillary lymph nodes.

Stage III has thee subcategories: IIIA, IIIB and IIIC. IIIA: In this stage different size tumours might be present or in some cases no tumours are found, however 4-9 axillary or breast bone lymph nodes are affected. In some cases tumours grow larger than 5 cm and small groups of breast cancer cells (0.2 -2 mm) are seen in the lymph nodes. Alternatively, larger tumours (<5cm) have spread to 1 to 3 axillary or lymph nodes located near the breastbone. Stage IIIB: In this stage there is no restriction regarding tumour size. Cancer may or may not have spread to the chest wall. Also the skin of the breast might be infiltrated which causes ulcers and swelling. Alternatively, the cancer may have spread to 9 axillary lymph nodes. In the other case the tumour might have infiltrated the lymph nodes near the breastbone. Inflammatory cancer, as described in the previous section would be considered as stage IIIB. IIIC: In this stage it is possible that no tumour is observed or one tumour with no restricted size is present. Is is also possible that the cancer has metastasised to the breasts' chest wall and/or skin. For a type of breast cancer to be grouped in this

stage the features described above need to be accompanied by one of the following: Cancer cells have spread to 1) ten or more axillary lymph nodes or 2) lymph nodes above or below the collarbone or 3) axillary lymph nodes or to lymph nodes near the breastbone.

Stage IV breast cancer is metastasised and spread to other organs distant from the primary tumour site such as lung, bones or liver.

Table 1.1: Represenation of how the number and TNM staging system correlate. [a] Ti includes T1mi; [b] Nodal micrometastases of T0 and T1 are classified as stage IB instead of stage IIA. M0 includes M0(i+).

Number staging system	**TNM staging system**		
Stage 0	Tis	N0	M0
Stage IA	T1	N0	M0
Stage IB	T0	N1mi	M0
	T1[a]	N1mi	M0
Stage IIA	T0	N1[b]	M0
	T1	N1[b]	M0
	T2	N0	M0
Stage IIB	T2	N1	M0
	T3	N0	M0
Stage IIIA	T0	N2	M0
	T1[a]	N2	M0
	T2	N2	M0
	T3	N1	M0
	T3	N2	M0
Stage IIIB	T4	N0	M0
	T4	N1	M0
	T4	N2	M0
Stage IIIC	Any T	N3	M0
Stage IV	Any T	Any N	M1

1.2.2 Subtypes and treatments of breast cancer

In the past five years international experts proposed and refined new classification systems for breast cancer. Six subtypes are known: 1) Slow growing Luminal A type, 2) luminal A-like type, 3) fast growing Luminal B type, 4) luminal B-like, 5) basal-like/triple negative and 6) Her2-positive cancer. It was just recently proposed that luminal A-like should be added to the subtypes[16]. Luminal A-like breast cancer responses much worse to chemotherapy compared to luminal B-like disease. An

overview of classification is shown in table 1.2. The thresholds are not shown.

Table 1.2: Subtype classification system for breast cancer[16,17]. Her2: Human epidermal growth factor receptor; ER: Oestrogen receptor; PR: Progesterone receptor.

Subtype	**Trait**
Luminal A	ER +ve and/or PR +ve
	Her2 -ve
	Low Ki-67
Luminal A-like	ER +ve
	High Ki-67
	High PR
	Her2 -ve
Luminal B	ER +ve
	Her2 -ve
	Either Ki-67 high or PR low
Luminal B-like	ER +ve
	High Her2
	Any Ki-67
	Any PR
Basal-like/Triple-negative	ER -ve
	PR -ve
	Her2 -ve
Her2 positive	ER -ve
	PR -ve
	High Her2

In breast cancer different treatment strategies are available as recommended by the European Society for Medical Oncology (ESMO) and the National Comprehensive Cancer Network (NCCN). In this section I will focus on the guidelines published by ESMO[18]. Discrepancies between both guidelines were recently debated by Zagouri et al.[19].

In early breast cancer three scenarios post diagnosis are possible. Scenario 1: The patient has no wish for the breast or conservation (lumpectomy) is not possible due to e.g. presence of more tumours which formed separately from one another (multicentric breast cancer) or a part or the whole breast is removed (mastectomy). This is followed by different options of therapies including chemo-, radio- and endocrine therapy as illustrated in figure 1.2. Scenario 2: The tumour is less than 2 cm in size and/or optimal surgery can be achieved. The patient would undergo a lumpectomy followed by different therapies. Scenario 3: The tumour is larger than 2 cm

or optimal surgery is not feasible and the patient decides against mastectomy. The prerequisite is that lumpectomy is potentially feasible. The patient needs to start the systemic induction therapy, normally chemotherapy which can have two outcomes. If the response is unsatisfactory the patients needs to undergo a mastectomy followed by the mentioned postoperative therapies. If the repsonse to chemotherapy is satisfactory a lumpectomy can be performed followed by postoperative therapies. An overview of this scheme is illustrated in figure 1.2.
(Neo)adjuvant treatment should start within 2-6 weeks post surgery as efficacy is decreased if administration is delayed for more than 12 weeks[20]. In figure 1.3 treatment choices, according to expression of biomarker and intrinsic phenotype, are illustrated.
After initial screening, including the hormone receptors ER, Her2 and PR, the treatment pursues following choices: ER-negative tumours with Her2 expression receive chemotherapy in combination with anti-Her2 medication such as trastuzumab. Ductal triple-negative tumours receive chemotherapy. For special histological types of triple-negative disease the recommendations of the St. Gallen consensus are endorsed[21]. They propose endocrine therapy for endocrine responsive histologies. For high-risk endocrine non-responsive breast cancer chemotherapy is recommended while for low-risk endocrine non-responsive disease no systemic therapy is endorsed. In contrast, ER-positive, luminal B and Her2-positive breast cancer a combination of chemo- and endocrine therapy with trastuzumab is applied. In ER-positive, luminal B, but Her2-negative cancer a combination of chemo- and endocrine therapy is applied. For ER-positive, Her2-negative and luminal A-type cancer endocrine therapy only is recommended. However, for high risk cases additional chemotherapy is proposed[18].

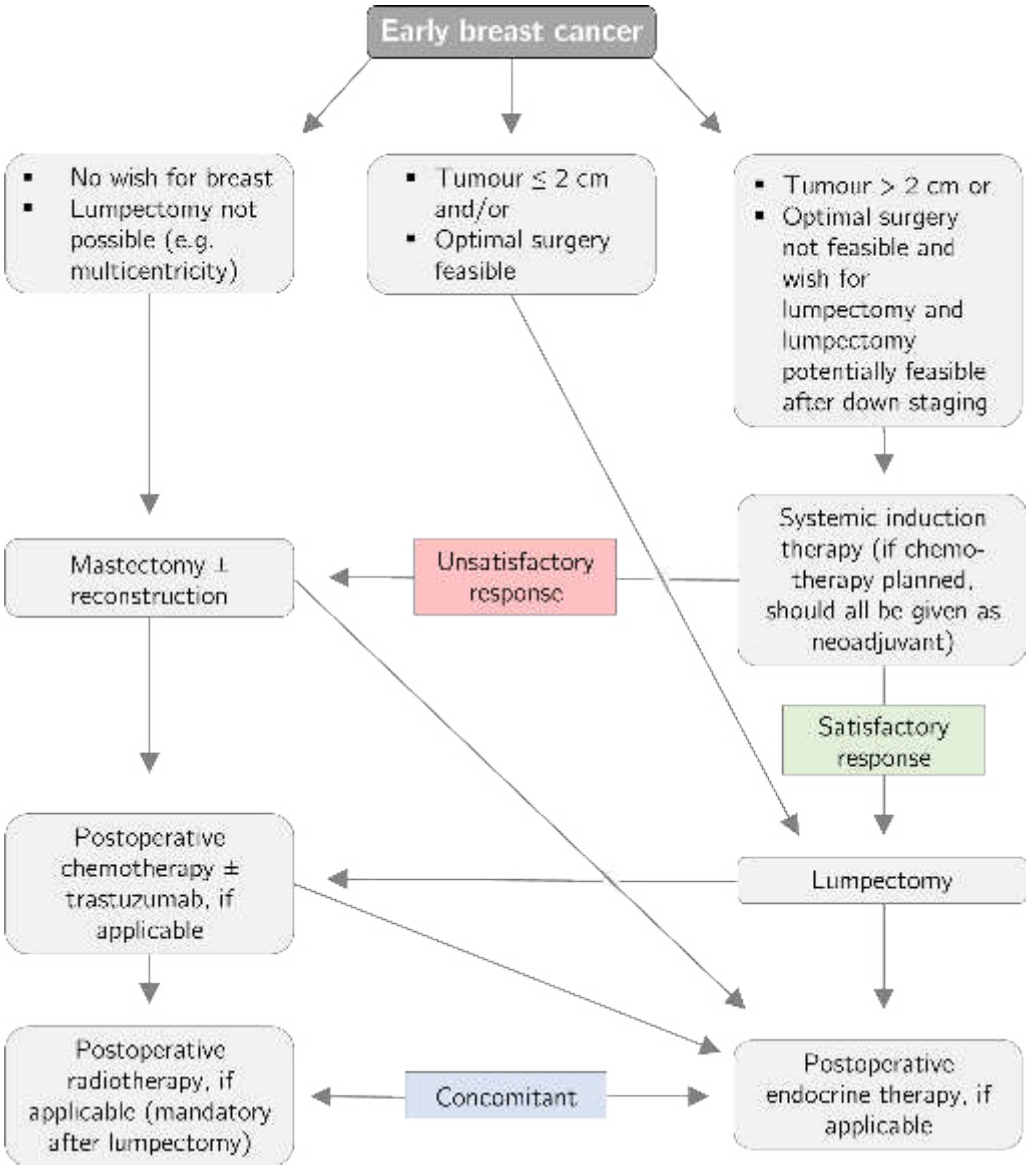

Figure 1.2: Schematic illustration of the early breast cancer treatment algorithm proposed by ESMO. Adapted and modified from Senkus et al., *Primary breast cancer: ESMO Clinical Practice Guidelines for diagnosis, treatment and follow-up*, Annals of Oncology, 2015[18].

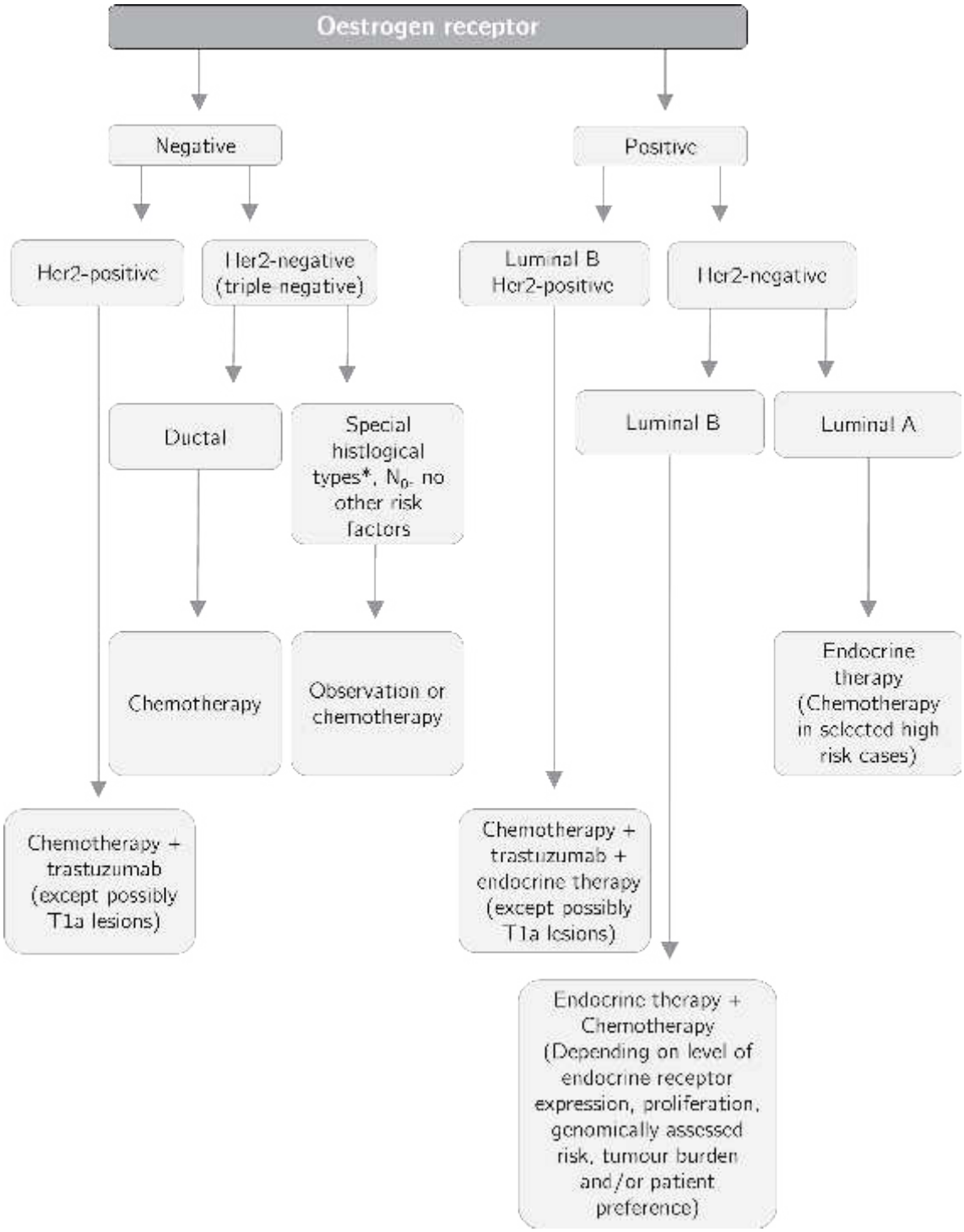

Figure 1.3: Schematic illustration of (neo)adjuvant systemic treatment options based on instrinsic phenotype and biomarker expression proposed by ESMO.
* EMSO endorses the recommendations of St. Gallen consensus for special histological types of triple-negative disease[21]. Endocrine therapy is recommended for endocrine responsive histologies while chemotherapy is proposed for high-risk endocrine non-responsive breast cancer. No systemic therapy is recommended for low-risk endocrine non-responsive disease.
Adapted and modified from Senkus et al., *Primary breast cancer: ESMO Clinical Practice Guidelines for diagnosis, treatment and follow-up*, Annals of Oncology, 2015[18].

A precursor of breast cancer is the *ductal carcinoma in situ (DCIS)*, which is a non-invasive neoplastic proliferation of epithelial cell and initiates within the lactiferous ducts. These cells show a varying degree of cytologic atypia. Around 4,800 women are diagnosed with DCIS in the UK every year[2]. Metastasis is uncommon in DCIS, however it could occur if the disease is diagnosed at a late stage or left untreated. In some cases DCIS can undergo malignant transformation leading to invasive ductal carcinoma (IDC). Genomic hybridisation studies revealed an almost identical pattern of genomic alterations in DCIS and IDC[22]. On the contrary, a lot of research has shown differences between non-invasive and invasive breast cancers. A recent study using gene profiling has identified 74 genes that are involved in the invasive behaviour of breast cancer[23]. Gene expression profiling revealed a total of 470 genes which are differently expressed between DCIS and invasive breast cancer. Especially genes involved in ECM synthesis and organisation were prominent in epithelium of invasive breast cancer. Lee et al. compared their results to eight similar studies and found overlap of 74 genes. *In silico* analysis of these genes correctly categorised about 90% of breast cancer samples in this and two other studies. An experimental approach was performed with human DCIS, in which four genes were knockdown that are elevated in clinical samples of DCIS. These cells were used in a DCIS xenograft model which resulted in reduced progression to invasive breast cancer. *In silico* and *in vivo* analysis showed that the identified set of genes may have clinical benefits. Detection, diagnosis and therapy of this disease may be improved by targeting some of the identified genes.

Oestrogens and progesterones are two important hormones that play a crucial role in the development of breast cancer. In about 70% of the cases ERα and PR are present. However, ERβ is often lost. In other breast cancer incidents ERα and PR are often epigenetically downregulated. Breast cancer which express ERα can be treated with selective ER modulator (SERM). The action of SERMs is varying depending on the tissue. In some tissue it can act as agonist in others as antiagonist. One of the most common drugs to treat breast cancer is tamoxifen. This is used in early and advanced ER-positive breast cancer in pre- and postmenopausal women. In the liver tamoxifen is metabolised to 4-hydroxytamoxifen and acts as low affinity antagonist for oestrogen. This leads to reduced oestrogen activity such as transcription of genes which respond to ER activation. Tamoxifen is mostly given in combination with gonadotropin-releasing hormone analogues (GnRHa). Tamoxifen and GnRHa are the standard treatment of pre-menopausal patients suffering from breast cancer[24] since two-third of patients express ER independent of age[25]. For ER-positive breast cancer the mortality is reduced by 31% if treated with tamoxifen for a period of five years[26]. However, patients respond differently to tamoxifen treatment. Some tumours do not respond to treatment despite maintaining ER ex-

pression[27]. Aromatase inhibitors have been developed to overcome this problem. The cytochrome P-450 enzyme aromatase catalyses the synthesis of oestrogens from androgen precursors[28]. Its expression occurs in many organs such as ovary, muscles, placenta, hypothalamus, liver, adipose tissue and breast cancer itself. During puberty the aromatase expression in ovaries is induced by the release of follicle stimulating hormone (FSH). While the ovary contributes most to aromatase expression the organ loses this ability again after menopause[28]. Aromatases inhibit the release of gonadotropin (negative feedback). Blockage of aromatase leads to decrease in oestrogens which stimulates gonadotropin synthesis which activates the release of oestrogens and aromatase. As reviewed by Hiscox et al.[29], due to the oestrogenic effects of tamoxifen in other organs such as uterus and vasculature the use of tamoxifen is associated with endometrial cancer, stroke and thromboembolic events. Additionally, after five years of treatment tamoxifen does not improve survival. In contrast, aromatase inhibitors do not exert an oestrogenic effect resulting in fewer side effects. Also for prevention of disease recurrence seem aromatase inhibitors superior to tamoxifen[30]. In clinical trials it was found that the aromatase inhibitor anastrozole was more effective alone than in combination with tamoxifen suggesting to interfere with each others metabolism[29]. In combination with signal transduction inhibitors (e.g. imatinib) a significant reduction in tumour growth was found. However, aromatase inhibitors have a response rate of 50-70% in patients suggesting limited sensitivity or some level of *de novo* resistance[29]. Combinatorial targeting of other pathways may improve the efficiency of aromatase inhibitors. Nevertheless, the observed superior effect with less side effects, compared to tamoxifen, makes these inhibitors already clinically relevant.

It has been observed that more aggressive breast cancer often lacks ERs. Predominantly, proliferation is driven through Her2 familiy receptor tyrosine kinases (RTKs) via Ras-MAPK pathway. It also inhibits apoptosis via mTOR. To function, Her2 heterodimerises with Her3 and Her4. Thus, gene amplification and overexpression of Her2 correlates with breast cancer progression. In Her2 overexpressing patients trastuzumab is given as an anti-cancer drug. Trastuzumab is a monoclonal antibody targeting the extracellular segment of the receptor. Analysis by the *Early Breast Cancer Trialists' Collaborative Group* (EBCTCG) revealed that 6 month polychemotherapy using anthracyclines such as FAC (fluorouracil, doxorubicin, cyclophosphamide) or FEC (fluorouracil, epirubicin, cyclophosphamide) reduces the mortality rate by 38% for women when aged 50 years or younger at diagnosis. The death rate is reduced by 20% when diagnosed with the age of 50-69. The outcome is largely regardless of tamoxifen treatment, ER as well as nodal status or other tumour characteristics[26]. Anthracyclines have a wide spectrum of anti-tumour activity. The most known mechanisms comprise 1) inhibition of macromolecule synthesis by inter-

calation with DNA and RNA, 2) induction of lipid peroxidation and DNA damage by generation of free radicals, 3) alkylation and binding of DNA, 4) crosslinking of DNA, 5) interfering with DNA unwinding, strand separation and helicase activity, 6) effects on cell membrane and 7) topoisomerase II inhibition resulting in DNA damage and eventually apoptosis[31–33]. In ER-positive disease, five years of tamoxifen treatment reduced the mortality rate by 31%, regardless of age, PR status, chemotherapy or other tumour characteristics[26]. The same study also showed that five years of tamoxifen treatment are more effective than just 1-2 years. ER-positive women (middle-age) have a approximately 50% reduced mortality rate when subjected to 6 month anthracycline polychemotherapy (e.g. FAC or FEC) followed by 5 years of tamoxifen treatment. The anthracycline-based therapy prior to tamoxifen further reduced the mortality rate in women aged younger than 50 years (38%) and 50-69 years (20%) to a final mortality reduction of 57% and 45%, respectively[26].
Results of a 8.4 year long study showed that adding trastuzumab to chemotherapy of Her2-positive patients the overall survival improved by 37%. After 10 years, the overall survival increased from 75.2% to 84%. The relapse-free survival (RFS) was improved by 40% and the 10-year RFS from 62.2% to 73.7%[34].
A subtype which is considered to be highly aggressive is basal or triple negative breast cancer. Patients suffering from this disease lack ER, Her2 and PR. Lacking these receptors make treatment difficult since common drugs, as trastuzumab or tamoxifen, are inactive without target. In this case conventional therapy such as chemotherapy is still the preferred treatment option. Good results are shown by platinum-containing agents like carboplatin oder cisplatin[35]. Platinum-based durgs interfere with DNA replication, thus most effective in fast proliferating cells as cancer. The chloride ions of e.g cisplatin are displaced by H_2O once inside the cell due to the low cellular ion concentration. The aquated cisplatin favours binding of DNA by crosslinking covalently purines[36]. This induces difference repair pathways and eventually, when the cell fails to repair the DNA, apoptosis is induced leading to cell degradation. The platinum-based therapy shows a higher response rate (88%) in triple-negative breast cancer compared to other subtypes (55%). However the overall survival after 5 years was worse in triple-negative disease compared to other breast tumours[37]. Immunohistochemical analysis investigated the expression of epidermal growth factor receptor/Her1 (EGFR) in benign lesions and 84 samples with invasive breast cancer[38]. The samples were classified on a molecular level and stained for EGFR. EGFR was expressed in 41.66% of basal-like cancer, 50% of luminal B carcinoma and 21.42% of cases with Her2 overexpression[38]. EGFR is a potential target for therapy, because it stimulates cell replication similarly to Her2. Blocking the EGF receptor could cease the stimulating effect resulting in cell cycle arrest and potential tumour regression[39]. Targeting of EGFR can be achieved in

two ways. One is to apply monoclonal antibodies which block ligand binding and receptor internalisation by binding to the extracellular domain of EGFR. The other way is to block internal signalling by tyrosine kinase inhibitors (TKIs) which target the intracellular domain[40].

In a clinical phase II trial with hormone resistant tumours the TKI gefitinib was found to be not very effective if applied alone.[41]. However, *in vitro* experiments with triple-negative breast cancer cell lines showed that gefitinib enhanced the response to docetaxel and carboplatin. In combination of all three drugs a syngerstic effect in these cells was observed[42]. Docetaxel interferes with microtuble dynamics. It binds to microtubles thus preventing disassembly/depolymerisation. Accumulation of these eventually induces apoptosis[43]. A phase I/II trial with stage IV Her2-positive breast cancer patients found that a combination therapy with docetaxel, trastuzumab and gefitinib is effective[44]. Lapatinib, another TKI inhibitor, showed complete response in Her2-positive disease, but only little effect in other cancer[45].
The basal-like subtype of breast cancer (BLBC) is associated with triple-negative status[46] and is known for its aggressive behaviour. However, a study showed that triple-negative and BLBC are not the same[47]. They were able to show that only 123 out of 172 triple-negative tumours were BLBC, according to gene expression profiling. From 160 samples, which were tested to be BLBC by gene profiling, only 123 were triple-negative based on histological staining. This suggests that not all BLBC are triple-negative. These findings were not only confirmed by other studies[48,49], they also showed that triple-negative breast cancer do not form a homogeneous subtype in transcriptional terms, unlike BLBC[47]. This suggests that within the heterogeneous group of triple-negative breast cancer, a homogeneous subtype of BLBC forms an entity. Thus the poor prognosis of triple-negative breast cancer may be a result of the basal-like subtype and is rather a symptom than a subtype[39].
A rare and aggressive form is inflammatory breast cancer (IBC). It is characterised by its aggressive behaviour and fast progression. Due to blocked lymph nodes following symptoms can occur in the breast: Swelling, reddening, hot sensation and firmer tissue. Other symptoms comprise thickened and/or perforated skin, lumps or inversion of the nipple. IBC commonly lacks ER/PR and is subjected to amplification of Her2 oncogene[50]. Overexpression of p53 and EGFR can be observed in some cases and correlate with poor prognosis[51,52]. In 90% of all tumours RhoC GTPase is upregulated and its involved in cytoskeletal reorganisation and regulation of angiogenic growth factors as well as inflammatory cytokines[53,54]. Evidence suggests claudin1 is a tumour suppressor involved in invasive breast cancers[55].
It has been shown that ER-negative tumours tend to be claudin1 positive compared to ER positive cancer. In fact ER-positive tumours showed a very weak positivity of claudin1 or showed complete loss[56]. In basal-like subtype of breast cancer a signifi-

cant high association with claudin1 was found, which correlated with poor prognosis in patients suffering from this type of breast cancer[56,57]. Basal-like breast cancer (BLBC) is a very aggressive subtype of cancer and is defined by the expression of a distinct set of genes that encode for proteins such as the EGFR and cytokeratins 5 and 17. These proteins are characteristic in the basal or outer layer of the mammary gland epithelium. These tumours often occur in young women and cause short relapses[58]. However, a recent study[59] identified a significant correlation between high levels of claudin1 and BLBC incidents in women aged 55 years or older. A significant association of high claudin1 expression and patient survival was not found. Knockdown of claudin1 in BLBC cells led to reduced cancer cell migration[59]. However, this type of cancer still remains poorly characterised. A recent study also identified high levels of claudin1 in a small percentage of luminal and Her2 subtypes[57] which emphasises the heterogeneity of cancer. High levels of claudin1 and 6 were found in breast cancer 1 (BRCA1) type breast cancer[60]. Due to the characteristic expression pattern of claudin1 and 6 it is thought that they can be used to help to distinguish between sporadic breast cancer incidents and BRCA1 mutation carriers[60]. BRCA1 is a tumour suppressor gene and the encoded protein plays a role in DNA repair, more precisely the BRCA1 protein repairs double-strand breaks of the DNA by homologous recombination. BRCA1 breast cancer is a hereditary cancer and mutation carriers are also prone to develop ovarian and fallopian tube cancer[61]. For women the cumulative risk of beeing diagnosed with breast cancer is about 12% in their lifetime[62,63]. The risk of breast cancer at an age of 70 is 3.84%[63] while carriers of the BRAC1 mutation have a likelihood of developing breast cancer of 65%[62]. *In vitro* and *in vivo* experiments showed that heterozygous inactivation of BRCA1 resulted in genomic instability in non-cancerous somatic breast cells[64]. Deletion of AG at position 185 led to impaired DNA repair and enhanced sensitivity to genotoxic stress. Thus it is believed that the sufficiency of BRCA1 may accelerate carcinogenesis in breast tissue by promoting additional genetic alterations[64]. Yet it is not known how this leads to differential regulation of claudins. It could be that regulatory genes for claudins lie in areas which are hotspots for double-strand breaks. If BRCA1 is defective these double-strand breaks then accumulate which may lead to distortion of claudin expression.

A novel strategy targeting BRCA1 mutation carriers are poly-ADP-ribose polymerase 1 (PARP1) inhibitors. PARP1 is involved in the base excision DNA repair pathway of DNA upon single-strand breaks[65]. PARP1 binds to exposed ends of damaged DNA and recruits other repair enzymes to the site of single-strand breaks. Upon PARP1 inhibition cell replication is arrested at site of single-strand breaks leading do double-strand breaks. Healthy cells then execute homologous recombination in which BRCA1 plays an important role. BRCA1-deficient cells cannot be

repaired this way and activate an alternative pathway called non-homologous end joining. The latter is much prone for errors compared to error-free homologous recombination due to its use of intact DNA as a template. Non-homologous end joining accumulates DNA lesions which ultimately result in genomic instability and eventually apoptosis[39]. BRCA2 has similar function working in the same pathway, thus lack of this protein make the cell susceptible to PARP inhibitors too[66]. Phase I and II trials confirmed the anti-tumour activity of PARP inhibitor in BRCA1/2 mutations carriers with little adverse side effects. In a phase I trial with 60 patients (22 BRCA1/2 carriers) showed the PARP inhibitor olaparib anti-tumour activity against mutation carriers while mutation-free tumours were unaffected[67]. In a consecutive phase II trial with only BRCA1/2 carriers a higher dose of olaparib was applied which correlated with better response and RFS while the toxicity of the drug remained low (comparable to mutation-free tumours)[68].
Another phase II trial, but solely on triple-negative breast cancer, showed improved survival when treated with the PARP inhibitor BSI-201 in combination with carboplatin and gemcitabine[69]. The positive effect lies on the fact that triple-negative breast cancer has often a significantly elevated expression of PARP1[69].
Another subtype of breast cancer is identified as claudin-low breast cancer, but remains poorly described. A summary is found in figure 1.4.

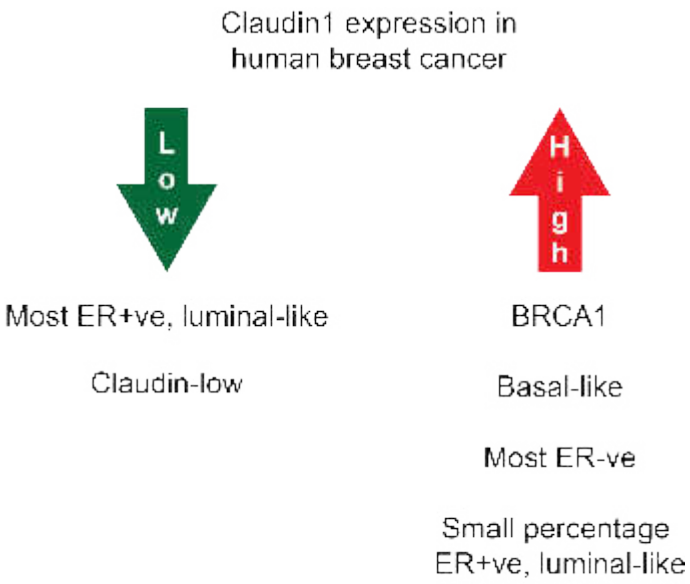

Figure 1.4: Claudin1 expression in subtypes of breast cancer. The image was adapted from Blanchard et al.[56], Zhou et al.[70] and Prat et al.[71].

Claudin-low tumours can be characterised by cancer stem cell-like features including reduced expression of luminal- and proliferative-associated genes such as aldehyde dehydrogenase isoform 1 (ALDH1), immune response genes such as CD14, CD79b and vav1, enrichment of EMT markers such as vimentin, twist and snail and

low expression or absence of luminal differentiation markers such as ER, PR, keratins 18 and 19[71]. In contrast to BLBC, claudin-low subtypes have a lower frequency of being triple negative[72]. These tumours are the most undifferentiated along the mammary epithelial type tumours with poor prognosis[72].
The expression pattern of claudins, especially claudin1, in different cancer subtypes indicate claudin1 as potential biomarker for breast cancer diagnosis, treatment and predicting disease progression.

1.3 The ADAM family: A Disintegrin and Metalloproteinase

ADAMs are a family of transmembrane glycoproteins that belong to the zinc protease superfamily - Metzincin. The name Metzincin is derived from the methinoineturn sequence within its metalloprotease domain (MP), which is able to bind zincions. A family tree of endopeptidases is shown in figure 1.5. They have a vast spectrum of biological functions such as cytokine and growth factor shedding, a process by which biologically active and soluble molecules are released from membrane-bound precursors. Other functions involve cell migration, control of membrane fusion, muscle development, fertilisation, cell fate determination in the nervous system, axon guidance and intracellular signalling. The ADAM family is comprised of 40 members of which 22 are found in human. 13 are considered or predicted as proteolytic active. The existence of ADAM36-40 is only predicted based on genomic sequences[73]. A table of all ADAMs discovered is kept up-to-date by White and Wolfsberg[73].

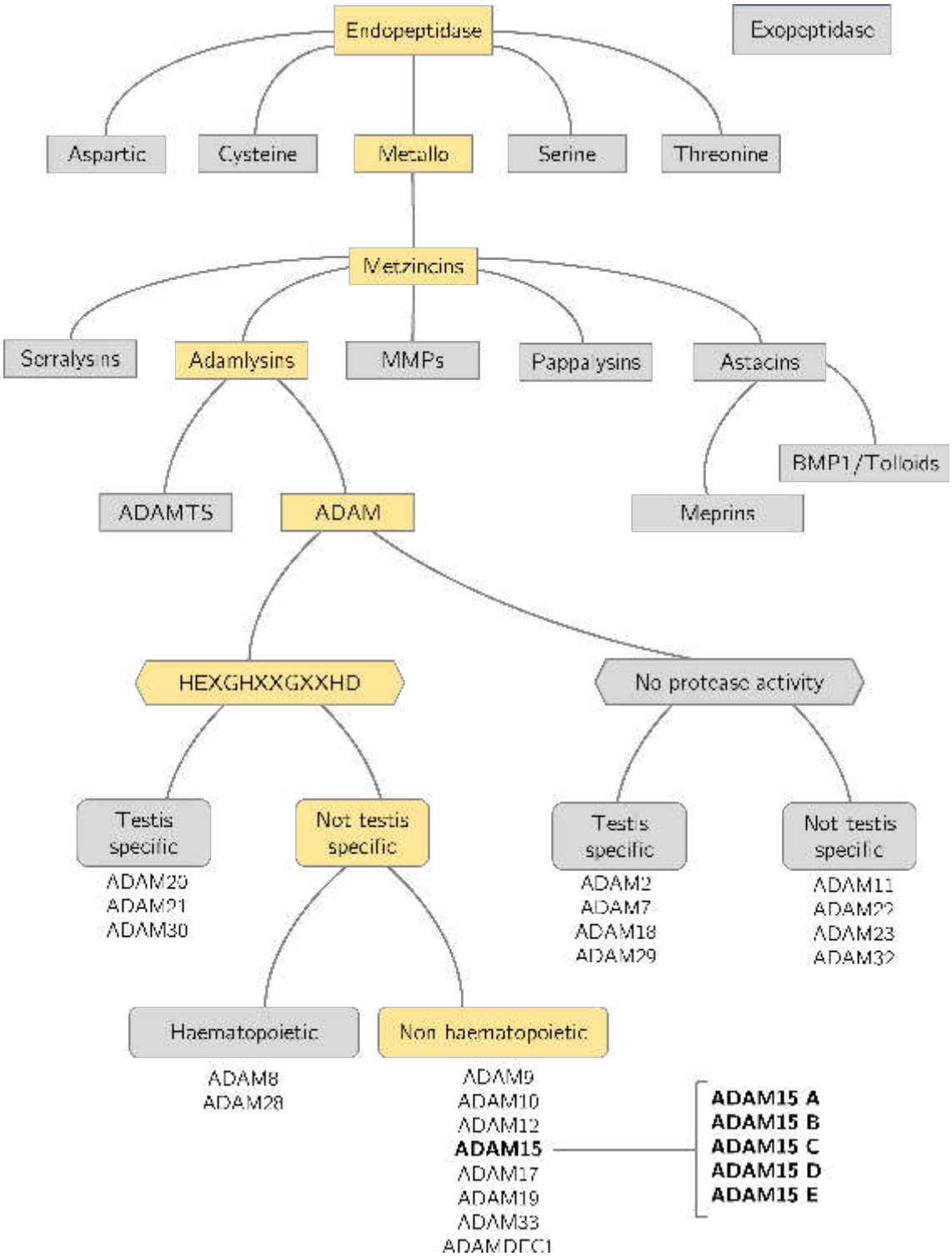

Figure 1.5: Overview of functional ADAM family members in relation to their MP activity and site of expression, in comparison with other metzincin superfamily members. Family members are outlined with rectangles, protease activity with hexagons and site of expression with rounded rectangles. The tree was adapted and modified from Vandenbroucke & Libert[74] and Edwards, Handsley & Pennington[75].

1.3.1 Structural differences of ADAMs and other metalloproteases

ADAMs are multidomain proteins consisting of a signal-sequence, a pro-, a metalloproteinase (MP), a disintegrin, cysteine-rich, epidermal growth factor (EGF)-like, transmembrane and intracellular (ICD) domain (or cytoplasmic tail, respectively). The functions of each domain will be discussed in more detail in the following subsection. An overview of the structure of ADAMs as well as close relatives, which will be described briefly in this section, are illustrated in figure 1.6. ADAMs share many characteristics with other metalloproteinases. Close relatives are the ADAMs with thrombospondin motifs (ADAMTS), matrix metalloproteases (MMPs), snake venom metalloproteinases (SVMPs) and the membrane-bound MMPs. These proteins all share a signal peptide, pro-domain and a zinc-dependent MP domain. However, they differ in the addition or absence of other motifs.

Kuno et al. named a new family of ADAMs based on the presence of a thrombospondin (TSP) homologous domain containing TSP-1 motif. ADAMTS1 for example has three TSP-1 motifs. The first is flanked by the disintegrin and cysteine-rich domain whereas the other two are located as a tandem at the C-terminus[76]. Compared to ADAMs, ADAMTS proteases lack the transmembrane region hence they are secreted. All known ADAMTS share the first TSP-1 motif. However, the C-terminal region is highly dynamic and varies within the family. Physiological processes include extracellular matrix turnover, ovulation, blood coagulation, melanoblast development and wound healing. They also play a role in pathological processes such as cancer, atherosclerosis, arthritis, cancer and angiogenesis[77].

SVMPs are the closest to ADAMs. They not only share the signal peptide, pro- and MP-domain, but also have similar disintegrin- and cysteine-rich domain (figure 1.6). Metalloproteinases are very common toxins in snakes and SVMPs are considered as the primary factors for haemorrhage. Based on the domain organisation SVMPs are classified into P-I to P-III. P-I is the simplest protease with just a MP-domain whereas P-II has an additional disintegrin domain. P-III SVMPs consist of a MP-, disintegrin- and cysteine-rich domain and are characterised by more biological functions and higher haemorrhagic activity[78]. Apart from haemorrhage, other activities include fibrino(geno)lysis[79], apoptosis[80] and activation of members of the coagulation cascade such as factor x[81,82] or prothrombin[83,84]. It is believed that the RGD motif within the disintegrin loop (D-loop) plays a role in platelet aggregation and cell-matrix interactions[85]. The D-loop will be discussed in subsection 1.3.1.3.

MMPs and membrane-type-MMPs (MT-MMPs) are other relatives of ADAMs. They differ in the presence or absence of a transmembrane region and a cytoplasmic tail. One important difference in the MMP family is that some of them contain a

haemopexin-like domain (figure 1.6). The natural function of haemopexin is to bind free haem in the body and deliver it to the liver, to prevent oxidative stress. However, there are MMPs which only contain a signal peptide, pro- and MP-domain such as MMP7 and MMP26. Their major functions are degradation of various connective-tissue proteins such as laminin[86], collagen IV[86], fibrin[87], elastin[88] or growth factors such as latent transforming growth factor-β1 (TGFβ1)[89] or latent vascular endothelial growth factor (VEGF)[90]. Due to their natural function of ECM degradation the overexpression of MMPs can lead to various pathological conditions. In various types of cancers the expression and activity of MMPs is elevated. This is associated with higher invasion[91] and migration[92] rate leading to a more advanced tumour stage[93] and reduced survival[94]. Although MMPs play a big role in disease progression in some cases they can also be beneficial. Expression of MMP12 in colorectal carcinoma cells is associated with increased survival[95]. Another model of human colorectal cancer suggests that MMP9 expression is associated with smaller metastasis[96].

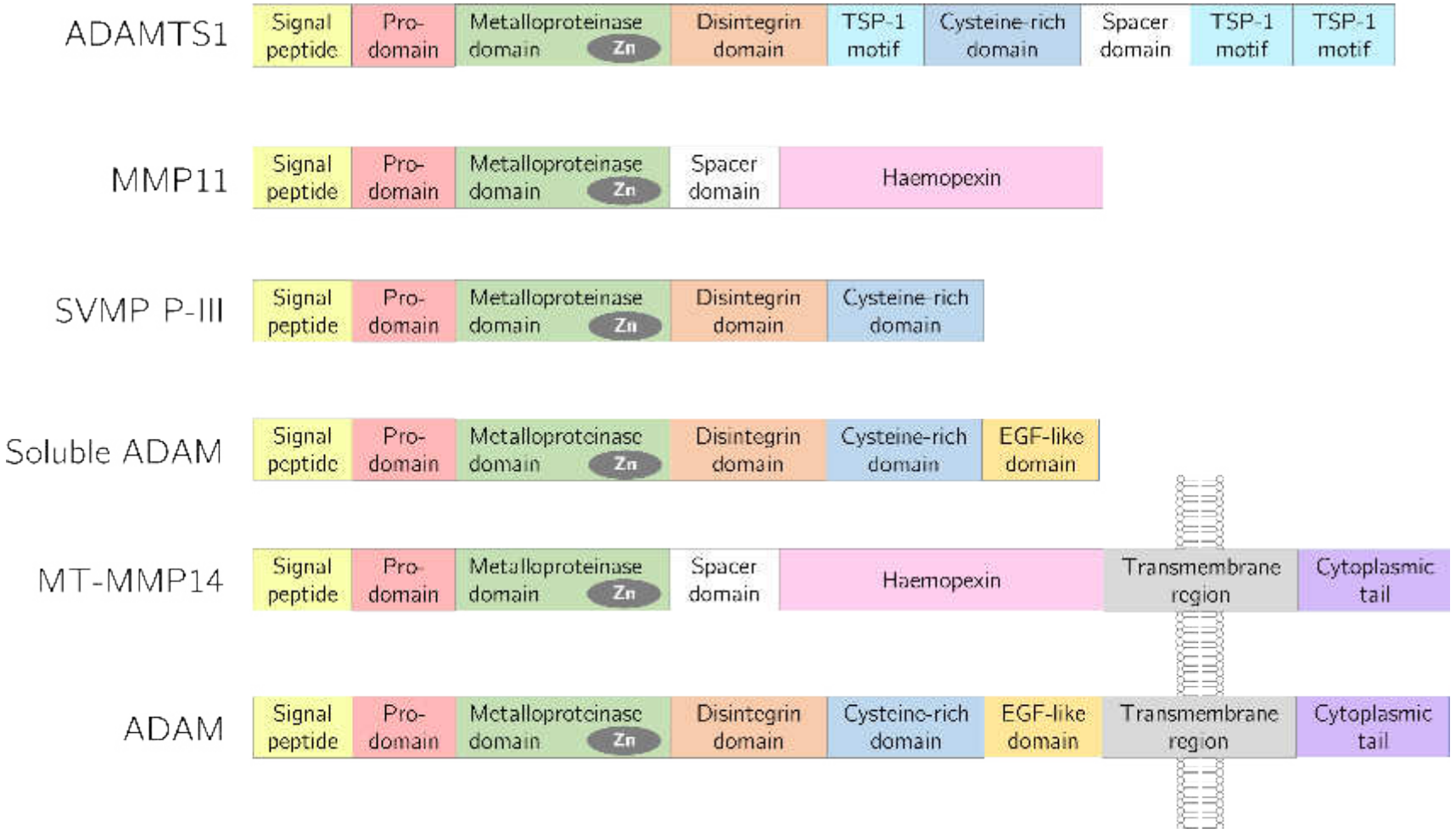

Figure 1.6: Schematic representation of the ADAM family in comparison with other metalloproteases. Common structures of SVMPs (P-III), ADAMTS (ADAMTS1), MMPs (MMP11) and MT-MMPs (MT-MMP14) are depicted. Domain addition and organisation varies among the family members. Figure adapted from Wolfsberg & White[97], Tang[98] and Parks, Wilson & López-Boado[99]

1.3.1.1 Signal sequence and pro-domain

Since ADAMs are localised to the membrane they possess an N-terminal signal sequence which guides the protein into the secretory pathway followed by fusion with the cell membrane[100]. Two forms of these proteins exist, a 110 kDa non-active (containing pro-domain) and an 85 kDa active form (without the pro-domain)[100,101]. The pro-domain has two functions: Firstly, it ensures correct folding of the protein[102]. Secondly, it keeps the MP-domain inactive through a cysteine switch[103]. The cysteine residues interact with the zinc ion of the MP domain causing inactivation[97,104,105]. ADAMs have consensus sequences RRRR[102,106] and RXKR[107,108] between the pro- and MP-domain, which are targets for furin proteases. The consensus RRRR sequence is also found in ADAM15.

1.3.1.2 MP-domain

Metzincin family proteins contain an evolutionary conversed Met-turn sequence, located within the core of the protein structure. It provides structural integrity, supports zinc-binding and is indispensable for the function. The Met-turn is inserted into the core structure and supports zinc-binding[109]. Depending on the metalloprotease the catalytic domain contains between 130 and 260 residues which folds into globular moieties. These are divided in an upper N-terminal and lower C-terminal subdomain by an active site cleft. The N-terminal subdomain contains the active-site helix which embeds the HEXGHXXGXXHD zinc binding sequence and the general base/acid glutamate which acts as catalyst and zinc binding histidines. The MP domain also contains a binding site for calcium which modulates enzymatic activity[110] (figure 1.7). Therefore, calcium chelators can inhibit the protease reversibly.

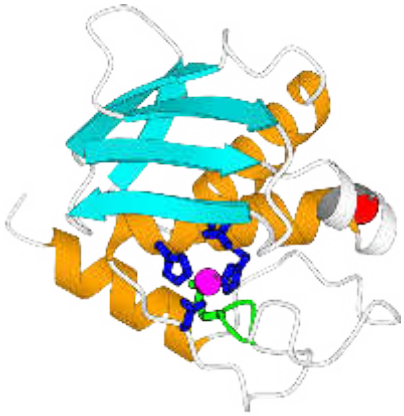

Figure 1.7: Three dimensional structure of the catalytic cleft of the MP domain. β-sheets in cyan, α-helix in orange, Met-turn in green, Zinc binding histidines in blue, zinc ion in magenta and calcium ion in red. Image taken from Tallant et al, *On the relevance of the met-turn methionine in metzincins*, Journal of Biological Chemistry, 2009[109].

1.3.1.3 Disintegrin-domain

The name of the disintegrin-like domain derives from its function. In haemorrhagic snake venom small proteins are found which block platelet aggregation by binding platelet integrin αIIbβIIIa[111]. Within the domain a so called *disintegrin loop* or D-loop is found which is necessary for binding to integrins[112]. The general motif of this 14 amino acid long sequence is RXXXXXCDXXEXC which is present in most ADAMs. This sequence is missing in ADAM10 and 17[112]. Eto at al.[113] identified a specific integrin-binding site within the disintegrin loop which is required for binding α9β1 integrin. The identified RX_6DLPEF-motif is crucial for the binding of α9β1 to ADAMs, including ADAM15. Due to the lack of the D-loop in ADAM10 and 17 α9β1 is not believed to interact with these ADAMs. ADAM15 is the only known ADAM within the family with an RGD-motif (at residues 484-486). It has been shown that ADAM15 interacts via this RGD-motif with α5β1[114] and αvβ3[113–115]. Zhang[115] and colleagues were the first who found that ADAM15 interacts with integrins in an RGD dependent manner. They showed that the recombinant ADAM15 disintegrin domain were found to interact with αvβ3, but not with α2β1, α3β1, α4β1, α5β1, α6β1, α6β4, αvβ1, αIIbβ3 and αLβ2. Mutation of RGD to SGA completely inhibited the interaction with αvβ3. Interestingly, upon mutation of the region adjacent to the RGD-motif (RPTRGD to NWKRGD) the disintegrin domains were recognised not only by αvβ3, but also αIIbβ3. This suggests that the flanking regions of the RGD-motif mediate the receptor binding specificity which is observed for snake venom disintegrins[116,117].

As mentioned before Zhang et al. were not able to visualise the interaction between ADAM15 and α5β1. However, Nath et al[114] were able to deliver evidence years later. They used a chimeric protein which contain the ECD of ADAM15 fused to the Fc-portion of IgG. The binding activity was analysed by solid-phase cell-adhesion assays on haemopoietic cells. Binding was not only observed for α5β1, but also αvβ3 integrin. Furthermore, they found evidence that these interactions depended on the RGD-motif since blockage by RGD-peptide inhibited cell adhesion.

1.3.1.4 Cysteine-rich domain

Some ADAMs possess a hydrophobic stretch within the cysteine-rich domain which are believed to play a role in membrane fusion. This hypothesis is based on the comparison of ADAM1 with viral fusion proteins which share most characteristics especially a rather hydrophobic region within the cysteine-rich domain[118]. Today it is known that ADAMs are involved in cell fusion processes in mammals. Examples are ADAM1 and 2 in fertilisation[97,118], in multinucleated giant cell and osteoclast formation[119], myoblast fusion[120] and trophoblast fusion[118]. A study dis-

covered that the cysteine-rich domain of recombinant ADAM12 interacts *in vitro* with heparan-sulfate proteoglycans in various cell types[121]. A series of transfections with syndecans in low level heparan expressing cells enabled cells to adhere to recombinant ADAM12[122] This shows that the heparan sulfate chains of syndecans interact with the cystein-rich region of ADAM12. Affinity chromatography showed interaction of ADAM12 and syndecan-4 which was confirmed with a solid phase binding assay[122]. In contrast to the mentioned ADAMs ADAM15 does not contain a hydrophobic region within the cysteine-rich domain. Therefore, it is unlikely that it contributes directly to membrane fusion[100].

1.3.1.5 EGF-like domain

The cysteine-rich domain is followed by an EGF-like domain. It contains six cysteine residues which form three disulfide bonds[123]. It forms a two-stranded β-sheet followed by a loop to another two-stranded β-sheet[124].
In P-selectin, a cell adhesion molecule in endothelial cells and platelets, it is involved in both ligand recognition and adhesion[125]. During maturation, dendritic cells seem to require EGF-like mediated interaction with selectins to mature. Blocking of the domain attenuates this process[126]. The cysteine-rich region of ADAM10 is only separated by 26 residues from the cell membrane which is believed to be disordered[127]. Unlike ADAM10 and 17[127] all other known ADAMs contain the EGF-like domain. Surprisingly, it is also reported ADAM17 multimerisation is mediated by its EGF-like domain[128]. While Janes et al.[127] report that the EGF-like domain is missing in ADAM10/17 is Lorenzen et al.[128] reporting the cysteine-rich domain is missing, but is compensated by the EGF-like domain. It seems there is confusion about the less understood structures of ADAMs. An explaination could be due to a misinterpretation of the structure. As the cysteine-rich domain, the EGF-like domain is rich in cysteins too[123].

1.3.1.6 Cytoplasmic domain

The ECD and the ICD are linked via a transmembrane domain. While the ECD is similar throughout the ADAM family, there is great variation within the ICDs. Three examples of ICDs are illustrated in figure 1.8. The example comprise very common members of the ADAM family, ADAM10, ADAM12 and ADAM17. The cytoplasmic tail among ADAMs is very versatile which explains how they are capable of fulfilling many different functions. As illustrated, the length of the ICD is varying. While the cytoplasmic tail of ADAM10 has a length of 54 amino acids, the ICD of ADAM17 is over 2-fold and ADAM12 is over 3-fold longer. This statistically leads to a higher number of interaction and phosphorylation sites. ADAM10 ICD possesses

various PXXP-motifs serving as SH3 binding site. Additionally it has a threonine (T) which can be phosphorylated. ADAM12 has two consensus class I (RXXPXXP) SH3 binding motifs plus an additional class II motif (PXXPXR). A tyrosine serves as phosphorylation site at the C-terminus. The cytoplasmic tail of ADAM17 only contains two PXXP motifs, but various phosphorylation sites. Two T and three serines (S) can be found.
The ICD of ADAM15 and its isoforms is discussed in detail in the following section.

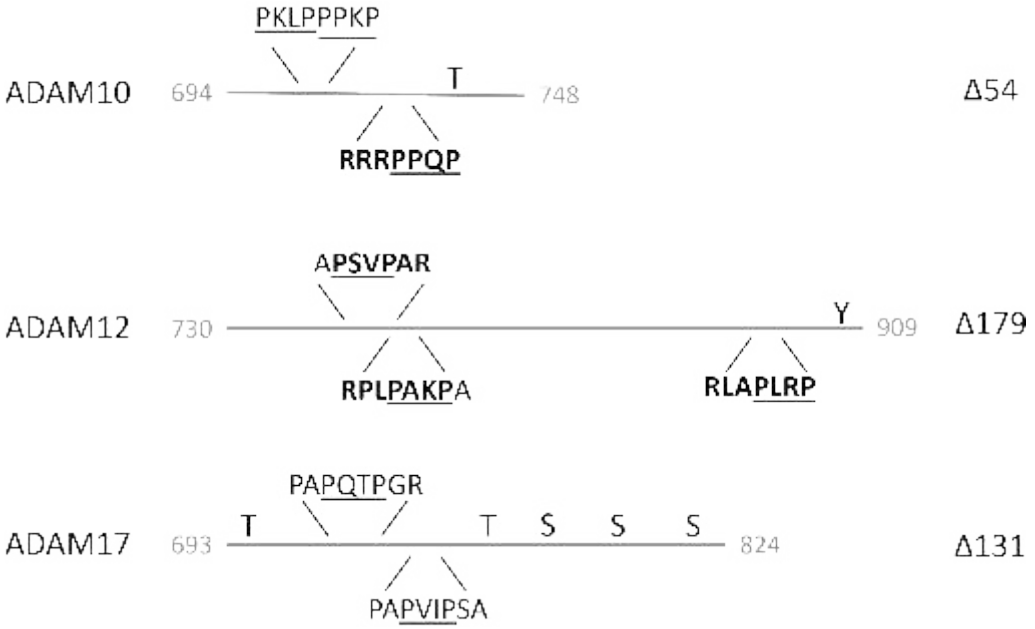

Figure 1.8: Illustration of the cytoplasmic tails of ADM10, 12 and 17. Consensus SH3 class I (RXXPXXP) and class II (PXXPXR) binding sequences are shown in boldface. The PXXP-motifs are underlined. The image is based on data from Uniprot[129].

1.3.2 ADAMs in normal and disease

1.3.2.1 ADAM functions in normal biological processes

This section will shed light on some functions of better characterised ADAMs in normal biological processes.
ADAM1 (fertilin-α) and ADAM2 (fertilin-β) were the first discovered mammalian ADAMs[130]. Their first implication was fertilisation since antibody blockage of ADAM2 inhibited sperm-egg fusion in guinea pigs[131]. During sperm differentiation ADAM1 and 2 are cleaved between their MP- and disintegrin domains resulting in an N-terminal disintegrin domain of each ADAM subunit in mature sperm[132]. Due to the high sequence homology of the disintegrin domain and disintegrin peptides of snake venom[130], and the fact these peptides bind integrins[133], it was hypothesised that the N-terminal domain of ADAM1 and 2 can interact with integrins on the egg. ADAM3 has also been associated with fertilisation[134]. Sperm-egg adhesion

and fusion is inhibited by an eight-residue peptide from the D-loop by almost 90%. In contrast, equivalent sized peptides from ADAM1,4 and 5 D-loop had either little or no effect on sperm-egg adhesion and fusion[134].

ADAM11 is considered to play a role in pain perception. ADAM11$^{-/-}$ mice showed only reduced pain response to inflammation caused by nociception tests (acetic acid and formalin injection). In non-inflammatory experiments (von Frey hair and hot plate test) the response remained unaltered[135]. This suggests that ADAM11 is involved in inflammatory mediated pain transmission.

For a limited period of time it was believed that a continuous expression of ADAM12 plays a role in muscle differentiation. It has been shown that it is required for fusion of mouse myoblasts into myotubes[120]. Further studies showed that ADAM12 is only transiently upregulated in the beginning of myoblast differentiation. In undifferentiated cells ADAM12 levels remained low[136]. The interaction of ADAM12 and α-actinin-2 seems to be important for the process of myoblast fusion[136].

ADAM22 and 23 were found to be highly expressed in the brain[137], alongside ADAM11[138]. Since it had been reported that ADAM2 interacts with α6/β1-subunits[139], which is independent of the RGD-motif[113], it was hypothesised whether these ADAMs also interact with cerebral integrins[137]. This hypothesis has been confirmed since it was shown that ADAM11, 22 and 23 are able to bind the integrin subunits α6, α9 and β3[138]. Furthermore, it appears that ADAM22 inhibits cell proliferation in αvβ3 expressing cells[138].

A large field of ADAM activity is antigen and ectodomain shedding. ADAM10 and ADAM17 are the most well characterised sheddases with more than 25 and 77 known substrates reviewed by Edwards[75] and Scheller[140]. However, substrate shedding is not only restricted to these ADAMs. There are also a number of substrates known for other ADAM family members. In 1997, ADAM17 was known as MP, but no physiological function was identified yet. However, the release of TNFα was already intensively studied due to its physiological importance. Hydroxamic acid-based inhibitors suggested the involvement of one or more MPs in TNFα shedding. By knockdown experiments of ADAM17 a significant decrease in soluble TNFα was found. The enzyme involved in releasing soluble TNFα was given the name TNFα converting enzyme (TACE). Experiments with expression of recombinant TACE resulted in the production of functional TNFα from its inactive precursor[141]. ADAM17 cleaves, like other ADAMs, within the stalk sequences which lies N-terminal of the transmembrane region and is activated by kinases such as PKC or MAPK[142]. Some ADAMs seem to work very closely together as published for ADAM9 and ADAM10. Inhibition of ADAM9 in various cell lines reduced cleavage of cellular prion protein (PrP^c) which releases a small N-terminal fragtment named N1[143]. Concomitantly, the release of soluble amyloid precursor protein α (sAPPα) from βAPP via α-secretase

pathway was reduced[143]. Since PrP^c is a known substrate for ADAM10[144], a resuce experiment was attempted in $ADAM10^{-/-}$ fibroblasts[143]. Interestingly, release of N1 and sAPPα was not recovered suggesting both ADAMs are necessary. Accordingly, a fluorimetric substrate for α-secretase activity could not be cleaved in ADAM10 null cells. However, upon co-transfection of both, ADAM9 and ADAM10, the fluorimetric substrate was hydrolysed. This confirms the interplay of both ADAMs in this process.

This is not the only example were ADAMs have a common substrate. CD23 (described in more detail in section 1.3.3.4) can be shed by several ADAMs such as ADAM8[145], ADAM10[146], ADAM15[145], ADAM28[145] and ADAM33[147].

A more complex mechanism of proteolytic processing is the regulated intramembrane proteolysis (RIP) in which ADAMs are involved. As an example, Notch signalling is a highly conserved and one of the most used intercellular communication pathways. ADAM10 (figure 1.9) or ADAM17 are considered as the major sheddase in RIPing of Notch. It is critical for various cellular processes such as homoeostasis, cell proliferation and differentiation. However, deregulated signalling is found in many types of cancer. In mammals, the pathway is activated if one of five available ligands bind to one of the four existing receptors. The membrane bound receptors are either cleaved by ADAM10 or ADAM17. Upon cleavage the presenilin dependent γ-secretase releases the Notch ICD into to the cytosol. From there it translocates into the nucleuss regulating and activating various processes and pathways as reviewed by Yuan et al[148].

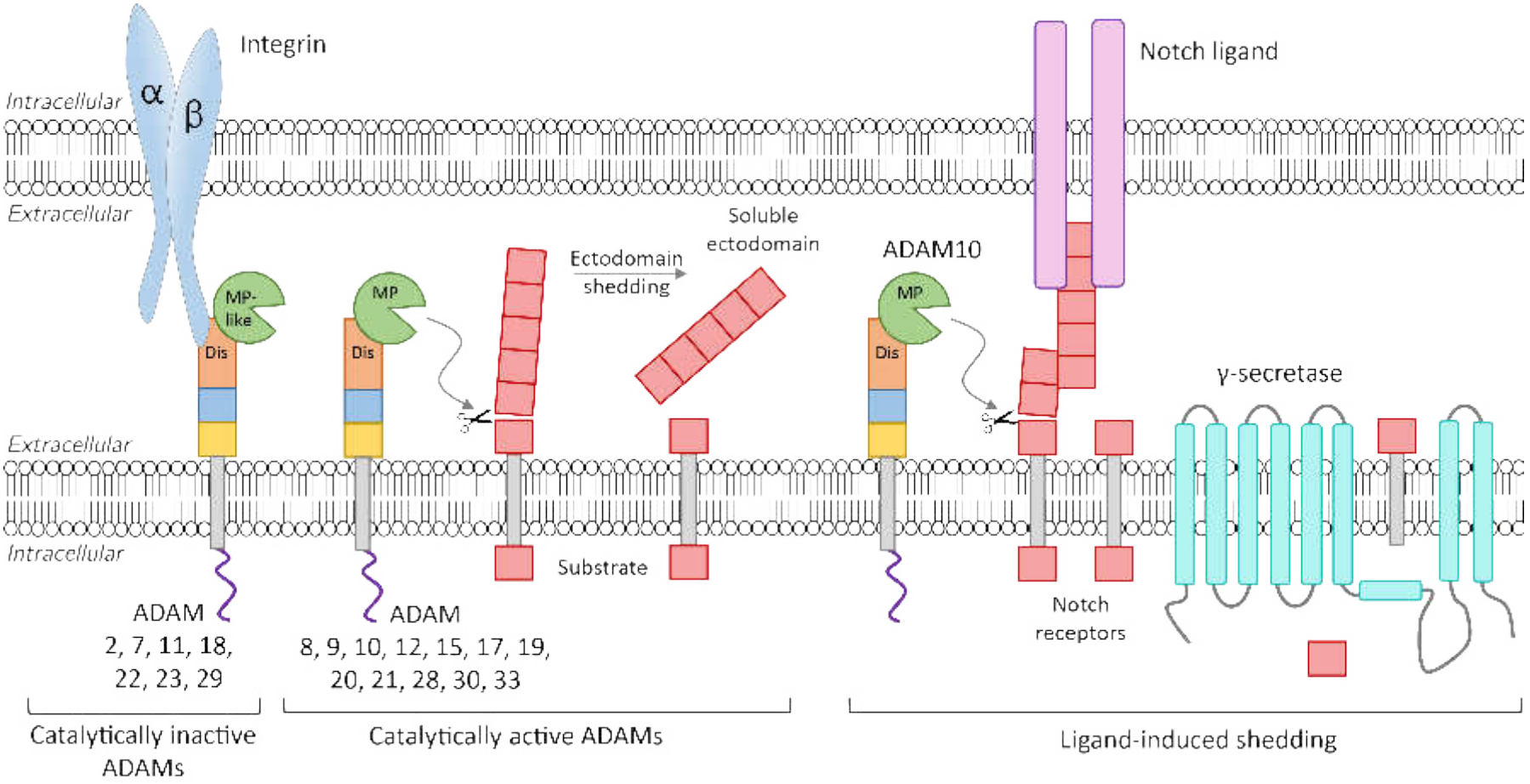

Figure 1.9: Comparison of catalytically active and inactive ADAMs in RIPing. ADAMs, especially inactive member seem to be important in integrin (blue) mediated adhesion. Proteolytically active ADAMs are involved in membrane-bound substrate (red) shedding. The ectodomain is released leaving a stub behind. ADAM10 is a well known example for ligand-induced shedding. Upon interaction of a Notch receptor (red) to a Notch ligand (pink) ectodomain shedding is induced by ADAM10 leaving a stub with ICD behind. Subsequently, a γ-secretase (cyan) cleaves the ICD from the stub releasing it to the cytosol. This event is known as regulated intramembrane proteolysis (RIP). Legend: MP = Metalloproteinase domain; Dis = Disintegrin domain; Adapted and modified from Weber & Saftig, *Ectodomain shedding and ADAMs in developments*, Development, 2012[149].

1.3.2.2 Involvement in diseases

Since ADAMs possess many functions and are present in almost all tissues and organs throughout the body, dysregulation of these contribute to pathology. ADAMs have been involved in inflammation, infection, asthma, arthritis, cardiovascular and neurological diseases and several types of cancers. Some implications will be discussed in more detail in the other chapters.

In multiple sclerosis, expression of ADAM17 was associated with parenchymal astrocytes, activated microglia/macrophages and blood vessel endothelium[150]. Elevated levels of ADAM17 were found in active lesions with recent breakdown of myelin. Since ADAM17 is the major sheddase of TNFα it is assumed that this contributes to the disease progression. TNFα is a major cytokine of proinflammation and was identified to play a pathogenic role in diseases affecting the central nervous system including multiple sclerosis[150].

TNFα and other proinflammatory cytokines play also a role in diabetes type 2. Increased concentrations are found, together with soluble adhesion molecules, in the plasma. Adhesion molecules and cytokines are involved in endothelial-leukocyte interaction. Low density lipoprotein (LDL) from type 2 diabetes patients increased the expression of ADAM8, 15, 17 and 28, compared to normal LDL[151]. The LDL from type 2 diabetes patients differs structurally and biochemically from LDL of normal people.

Upregulation of ADAM8 correlated with rheumatoid arthritis[152]. ADAM8 is naturally expressed in intracellular granules and on the cell surface of human neutrophils. Activation of the neutrophils induced translocation of ADAM8 to the plasma membrane where it was released by cleavage. Neutrophils from the synovial fluid of patients suffering from rheumatoid arthritis expressed much higher amounts of ADAM8 than peripheral blood neutrophils. The degree of joint inflammation directly correlates with the concentrations of soluble ADAM8 found in the synovial fluid[152]. ADAM17 was also found to be upregulated in rheumatoid arthritis. Low concentration of TNFα and oxygen led to hypoxia-inducible factor-1 (HIF-1) mediated increase in mRNA levels of ADAM17[153].

ADAM10 contributes to disintegration of adherens junctions during endothelial activation and apoptosis[154]. ADAM10 regulates the release of VE-cadherin in human umbilical vein endothelial cells (HUVEC) cells. VE-cadherin is important in the control of endothelial cell permeability, leukocyte transmigration, angiogenesis and vascular integrity. Increased levels of soluble VE-cadherin are associated with coronary atherosclerosis[154].

ADAMs are also associated with asthma on a genetic level[155]. Asthma is a respiratory disorder with recurrently occurring symptoms such as wheezing, breathlessness

and coughing. A survey of SNPs in a variety of genes identified ADAM33 as being significantly associated with this disease[155].

In prostate cancer nuclear localisation of ADAM10 was found while it was absent in benign prostate hypertrophy[156]. Immunocytochemistry experiments showed ADAM10 translocated from the membrane to the nucleus. Intensity of the staining directly correlated with different prostate cancer staging methods. In breast cancer ADAM12 was found to contribute to breast cancer progression[157]. In human breast cancer, apoptosis of stromal cells is observed, while it is absent in non-malignant lesions. ADAM12 was found to decrease tumour cell apoptosis, but increased stromal cell apoptosis[157]. In gliomas elevated expression of ADAM8 and ADAM19 were found. In these tumours the expression levels and protease activity of both ADAMs correlated with enhanced invasiveness[158]. In contrast, ADAM22 is expressed in normal brain tissue, but is lost in high-grade gliomas[138]. ADAM10 showed an unwanted function in treatment of lymphoma patients[159]. CD30 is a transmembrane protein which is often overexpressed in lymphoma cells. Therefore, it is used as target for immunotherapy. However, upon binding of antibodies to CD30 ADAM10 is activated and cleaves CD30 from the cell surface. Soluble CD30 in turn binds to the ligand of CD30 that is expressed on non-target cells which are rendered as new but unwanted target for the therapeutic antibodies[159].

These examples emphasised how wide spread and influential ADAMs are in human pathology of diseases. It also highlights that the same ADAM can contribute to different diseases as ADAM17 does in rheumatoid arthritis, multiple sclerosis, diabetes and cancer.

1.3.3 ADAM15

1.3.3.1 ADAM15 splicing

ADAM15 has been implicated in various physiological as well as pathological conditions. These are achieved by processes such as ecotodomain shedding or through regulation of cell-cell interactions. Altered ADAM15 protein levels have been associated with arthritis[160], cardiac disease[161], atherosclerosis[162] and cancer[163,164]. In breast cancer it was shown that ADAM15 splice variants predict disease stage and outcome. Not only an aberrant alternative use of exons was found, but also an increased copy number of ADAM15[165]. The gene copy number was increased in cells derived from mammary tumours, but did not correlate with the mRNA levels. Although, in most cancer cell lines the mRNA levels of ADAM15 were slightly increased, the primary mechanism was alternatively spliced ADAM15. Alternative spliced ADAM15 isoforms were found in various combinations in cancer cell lines. Among these cell lines were breast cancer derived cell lines such as BT474, HCC1954,

SK-BR-3 and T47D and the prostate cancer cell line DU145[165]. However, mRNA levels were not increased. *In silico* analysis of RT-PCR products demonstrated that the isoform patterns of ADAM15 were non random. In fact sets of various breast cancer cell lines had preferred splice variants that were expressed.

In order to gain more knowledge about regulation of ADAM15 Kleino et al[166] characterised the genomic organisation of regulatory elements and the use of alternative ADAM15 exons in human tissue. The ADAM15 gene is flanked by FLJ32785/DCST1 and ephrin-A4 genes and spans 11.4 kb from the from point of translation initiation to the polyadenylation signal. The gene contains 23 exons and 22 introns and has several transcriptional start sites within a TATAless, CAATless and GC-rich promoter. Four CpG islands are found within the gene. The first and longest extends from the last intron of FLJ32785/DCST1 to the first intron of ADAM15. Two islands are located within intron 1, while the fourth is found in exon 22 and spans past the polyadenylation site[166]. In all examined ADAM15 transcripts the exons 18, 22, and 23 were found, suggesting they are used constitutively. In normal human tissue the majority of variants were found arising from the alternative use of exons 19, 20a/b and 21a/b. This leads to different combinations of regulatory interaction motifs in the cytoplasmic domain.

Not much is known about the splice factors that are responsible for the alternative use of exons in the ADAM15 gene. In intron 1 and 2 highly conserved regions with clusters of regulatory motifs were found, which may contribute to transcriptional regulation[166]. Normally, constitutive human exons contain three to seven rescue exonic splice enhancer (ESE) motifs[167]. However, exons 19, 20a/b and 21a contain one, one and three ESE motifs and zero, zero and six putative ESE motifs, respectively. An overview of this distribution is shown in table 1.3. ESE motifs are sequences within exons and promote constitutive and regulated splicing. Regulation functions by networks formed with other ESE motifs, with small nuclear ribonucleoprotein particles (such as spliceosome subunits) and SR-related proteins[168]. The conserved family of SR proteins is involved in constitutive pre-mRNA splicing and are important regulators of alternative splicing. They also participate in post-splicing events such as mRNA nuclear export, mRNA translation and nonsense-mediated mRNA decay. Its name is composed of the one-letter-codes for the amino acids serine (S) and arginine (R). Both amino acids are found as long repeats in a part of the protein which was accordingly named RS domain and is required for protein-protein interactions with other RS domains. Apart from this region, SR-proteins also contain a RNA-recognition-motif (RRM) domain for sequence-specific RNA binding[169]. The predicted number of SR-protein binding motifs is about 30% lower than the average in constitutive ADAM15 exons[166]. Three SR-protein binding motifs were only found in alternative exons which suggests that the splicing of alternative ADAM15

exons is less enhanced than the splicing of constitutive exons by ESEs.

Table 1.3: Summary of the presence of exonic splice enhancers (ESE) and putative ESE in the alternatively used ADAM15 exons 19, 20a/b and 21a. Normally three to six rescue-ESE clusters are found in constitutive human exons[167].

	ESE	**Putative ESE**
Exon 19	1	0
Exon 20a/b	1	0
Exon 21a	3	6

Exons 19, 20a/b and 21a also lack exonic splice silencer (ESS)/putative ESS and heterogeneous nuclear ribonucleoprotein (hnRNP) binding motifs. ESS suppress splice-site selection and often work alongside ESE. However, ESE sequences are dominant over ESS[168]. HnRNPs are complexes consisting of RNA and proteins binding to pre-mRNA. They prevent the premature export into the cytoplasm. Also a lower number of exonic splice-regulatory sequences (ESR) are found. Exons 19, 20a/b and 21a only contain seven, eight and three ESRs while constitutive ADAM15 exons possess approximately 13. The function of ESRs is controversial. They are believed to function either as ESS or ESE, depending on their relative exonic location[170]. In contrast, exon 21b contains several ESRs, ESE, putative ESE, ESS as well as SR-protein and hnRNP binding motifs.
Contrary to the alternative exons, the alternative introns are rich in ESEs and ESSs, SR-protein and hnRNP binding motifs. Additionally many intronic splice enhancers (ISE) are dispersed throughout the introns. Concomitantly, different alternative splice regulation-associated motifs are found in the alternatively spliced intronic regions of ADAM15. Within these motifs, a recognition sequence for Fox-family alternative splice regulator proteins was found[166,171].
In the intronic region of intron 18, 19 and 20, binding motifs for the neuronal splice-enhancer Nova1/2 were found[166]. Nova1 is considered as "master regulator" in splicing since knockdown of Nova1 altered the splicing of almost 5000 transcripts. The affected genes are involved in apoptosis, exocytosis, splicing, transcription and insulin receptor signalling[172]. Intron 19 contains three while exon 19 possesses only one binding motif for CELF/BrunoL family proteins[166]. The CELF/BrunoL family comprises six members of which a few are involved in post-transcriptional regulatory processes. These events are alternative splicing and the control of stability and translation of target mRNAs[173]. Muscleblind-like protein 1 (MBNL1) binding motifs were observed in exon 20 as well as in intron 20 and 21[166]. MBNL1 regulates alternative splicing by binding specifically to CUG and CCUG repeats[174,175]. In intron 18, 19 and 21 exon skipping-associated C- or G-rich motifs (ESACG-motif)

are located[176]. To this day, two patterns of C and G repeats where identified causing skipping of an exon. The sequence repeats CTCC or CCTCCC and AGGG where found adjacent to exons in an intronic region[176]. It is believed that base pairing interactions underlie a mechanism which involves the secondary structure to control exon skipping[176]. An overview of the alternative splicing-associated elements are found in table 1.4. Two-third of the motifs are conserved in either mouse or rat.

ADAM15 contains numerous splice recognition sites, their regulatory role has not been tested experimentally. So far, only ESRP1 and ESRP2 splice factors have been validated experimentally to be regulating in ADAM15 splicing. ESRPs enhance the use of exon 20 and 21. Three splice forms were identified which enable the inclusion of on or the other exons or both. Knockdown of the ESRPs led to decrease of the isoforms[177]. Based on the results of this study the detected isoforms were ADAM15 B (inclusion of exon 20a), ADAM15 C (inclusion of exon 20a and 21) and ADAM15 E (inclusion of exon 21). ESPR1 and ESPR2 are highly conserved paralogs possessing three RRM domains. Both were found by inducing EMT in a mammary gland epithelial cell line which resulted in downregulation of both ESPRs. ESPRs not only regulate splicing of ADAM15, but also FGFR2, CD44, ENAH and p120-catenin splicing[178].

Table 1.4: Summary of alternative splicing-associated elements found in exonic and intronc regions of ADAM15. MBNL: Muscleblind-like protein 1; ESACG: Exon skipping-associated C- or G-rich motif

	Fox	**Nova1/2**	**CELF/ BrunoL**	**MBNL1**	**ESACG**
Exon			19	20	
Intron	18, 19, 20, 21	18, 19, 20	19	20, 21	18, 19, 21

The ECD of ADAM15 is conserved, hence it is similar in all isoforms. The ECD of the variants investigated in this thesis are identical. However, differences occur in the ICD. Due to differential splicing a total of 13 variants have been discovered[166]. The present work focuses on five isoforms: ADAM15 A, B, C, D and E. An overview of ADAM15 isoforms with its corresponding numbers of amino acid and proline-rich regions is depicted in table 1.5. Schematic representation of the ADAM15 ICD organisation in the studied five isoforms is represented in figure 1.10.

Table 1.5: Detailed information about ADAM15 splice variants

ADAM15 isoform	Gene Bank variant	AN.[1] DNA sequence	AN.[1] Protein sequence	Amino acids	Proline-rich regions
ADAM15 A	2	NM_003815.4	NP_003806.3	814	3
ADAM15 B	3	NM_207194.2	NP_997077.1	839	4
ADAM15 C	5	NM_207196.2	NP_997079.1	862	5
ADAM15 D	1	NM_207191.2	NP_997074.1	772	0
ADAM15 E	4	NM_207195.2	NP_997078.1	838	4

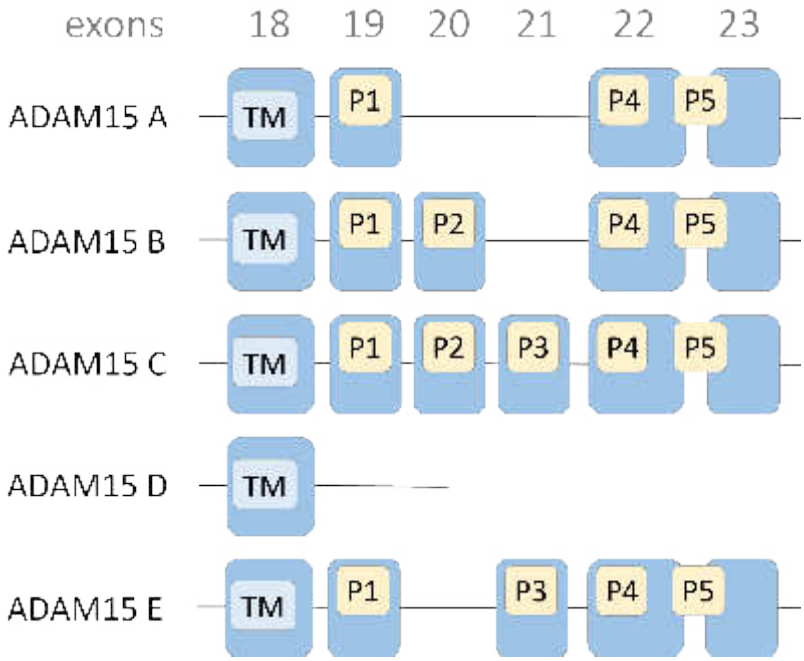

Figure 1.10: Schematic organisation of proline-rich regions in the ICD of ADAM15 isoforms. Exon 18, 22 and 23 are the continuous expressed exons which transcribe the transmembrane domain (TM) and two proline-rich regions (P4 and P5). Exon 19, 20 and 21 are alternatively spliced and provide one additional proline-rich region (P1, P2 and P3) each. Depending on inclusion of the exons the affinity towards SH3 domain containing proteins vary.

1.3.3.2 ADAM15 ICD interaction partners.

A diagram illustrating the organisation of the ICD in ADAM15 isoforms is presented in figure 1.11. ADAM15 isoforms have common, as well as distinct, interaction partners. Table 1.6 summarises the known interaction partners with ADAM15 isoforms identified predominantly by *in vitro* assays. However, characterisation of

[1] Accession number

changes in cellular behaviour of these isoforms are still elusive. In MDA-MB-435, we have previously shown that expression of ADAM15 A, B and C had differential effects on morphology, adhesion, migration and invasion[179]. However, further work is necessary to characterise potential isoform-specific, as well as catalytic function dependent effects of ADAM15 on cancer cell behaviour. Thus in this project we aimed to generate a set of isogenic ADAM15 A-E WT and catalytically inactive isoform expressing MDA-MB-231 cells to enable us to carry out detailed comparative analysis of ADAM15 isoform-specific effects.

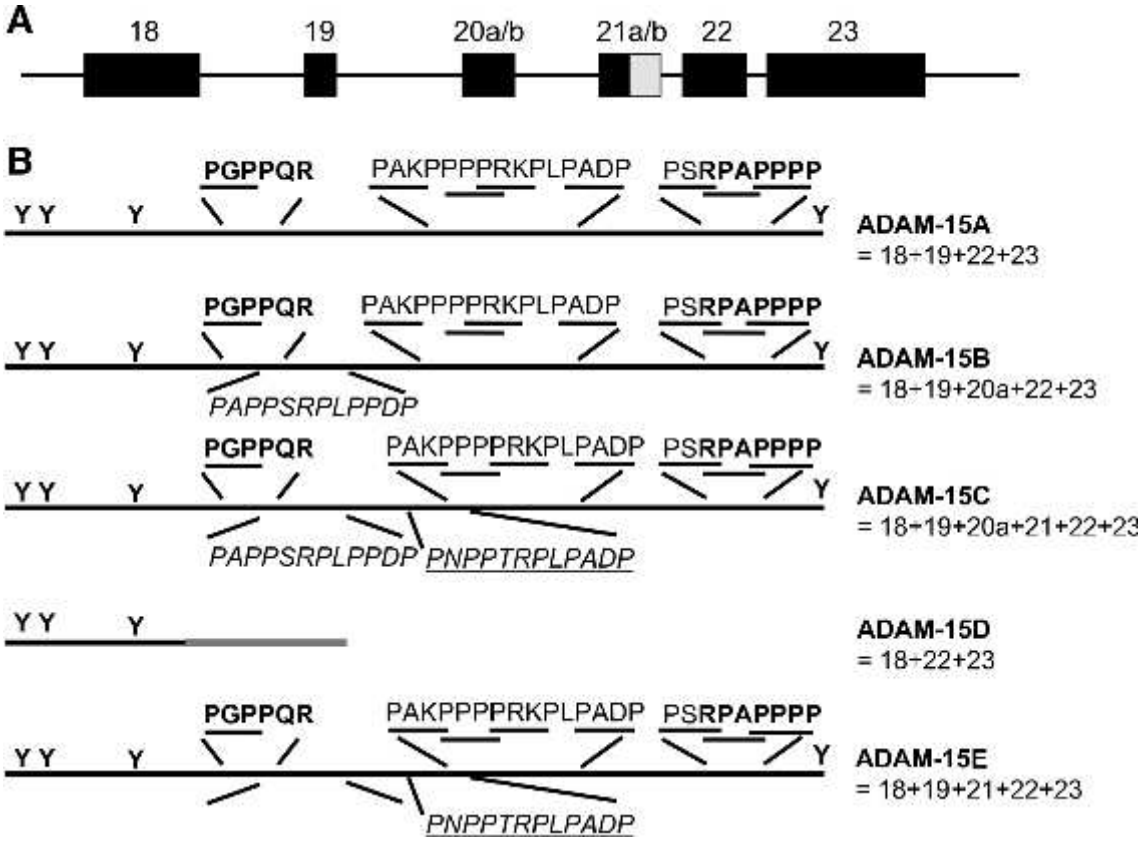

Figure 1.11: Organisation of the ICD and its translational sequence differences. **(A)** Schematic view of the cytoplasmic exon organisation depicted as black rectangles. Exon 20a and 20b have a size difference of one amino acid[166]. Exon 21a and 21b are two different splice regulatory sites[166]. **(B)** Representation of the ADAM15 splice variant ICDs. PXXP motifs are underlined. The two Src family RTK binding consensus class I (RXXPXXP) and class II (PXXPXR) sequences are showed in boldface. ADAM15 A represents the first identified, widely expressed and most commonly researched ADAM15. ADAM15 B contains an additional 75 bp insert adding another proline-rich region (*italic*). ADAM15 C does have the same 75 bp insert plus another 72 bp sequence (*underlined italic*) increasing the proline rich region to five. ADAM15 D introduces a frameshift mutation leading to a premature stop codon. ADAM15 E is lacking the 75 bp insert, but possesses the 72 bp sequence. The figure is adapted and modified from Zhong et al.[179]

In order to generate a table (table 1.6) combining all known interactions between ADAM15 and other proteins several approaches were combined. Interactions were categorised into four groups: - = no or very weak; + = weak; ++ = medium; +++ = strong interaction. If no data to a particular isoform was not available the interaction was stated as N/A. Pull-downs and IPs were judged according to the intensity of the

Western blot band. No bands were categorised as no interaction while weak bands were grouped into weak interaction. Strongly over-saturated bands were indicated as strong interaction while everything in between was judged as medium interaction. Since Klein et al.**??** displayed their results as heat map the different shades of grey was grouped into the same categories as Pull-downs and IPs. White indicates no/weak interaction, while black shows very strong interaction. Approximately 14 different shades could be visually identified. White, followed by two darker shades, are considered as no/weak interaction. Black is shown as strong interaction. The remaining 10 shades were separated: The weaker half was considered as weak interaction while the more intense half was treated as medium interaction.

Table 1.6: Interaction of different proteins with the ICD of ADAM15 isoforms. Association is done via SH3 domain if not stated otherwise. The table is based on work of Kleino[180,181], Poghosyan[182] and Zhong[179]. - = no or very weak; + = weak; ++ = medium; +++ = strong interaction. N/A = Data not available.
AHI1: Abelson helper integration site 1; Btk: Bruton's tyrosine kinase; CIP4: Cdc42 interacting protein 4; Eps8L: Epidermal growth factor receptor kinase substrate 8-like protein; FBP17: Formin-binding protein 17; Grb2: Growth factor receptor-bound protein 2; Itk: Interleukin-2-inducible T-cell kinase; MAD2: Mitotic arrest deficient 2; NFC1: Neutrophil cytosolic factor 1; OSTF1: Osteoclast stimulating factor 1; PTK6: Protein-tyrosine kinase 6; RIMBP: Regulating synaptic membrane exocytosis protein (RIM)-binding protein Src: sarcoma; SNX: Sorting nexin; TOCA1: Transducer of Cdc42-dependent actin assembly protein 1;

	A15 A	**A15 B**	**A15 C**	**A15 D**	**A15 E**
AHI1	+	++	++	-	+
Btk	+++	+++	+++	-	+++
CIP4	++	++	++	-	++
FBP17	++	++	++	-	++
Fyn	++	++	++	-	++
Grb2 (I)	++	+++	+++	-	++
Grb2 (II)	++	+++	+++	-	++
Hck[2]	++	++	++	-	++
Intersectin 1 (III)	+	++	++	-	+
Intersectin 2 (III)	++	++	++	-	++
Itk	+++	+++	+++	-	+++
Lck	++	+++	+++	-	++
Lyn	++	++	++	-	++
MAD2[3]	++	++	++	-	++
NCF1/p47phox	++	+++	+++	-	++
Nck1 (I)	-	++	++	-	+
Nephrocystin	++	+++	+++	-	++

[2]Binding also via SH2 domain[182]

[3]Binding not via proline-rich regions due to absence of SH3 domain

Table 1.6 Continued: Interaction of different proteins with the ICD of ADAM15 isoform.

	A15 A	A15 B	A15 C	A15 D	A15 E
OSTF1	++	+++	+++	-	++
p85α	++	++	++	-	++
pErk1/2[2]	+	+	+	-	N/A
PTK6/Brk	++	++	-	-	N/A
RIMBP1	++	++	++	-	++
RIMBP2	+	+	++	-	++
RIMBP3	+++	+++	+++	-	+++
Src	++	++	++	-	++
SNX9	+++	+++	+++	-	+++
SNX18	++	++	++	-	++
SNX33	+++	+++	+++	-	+++
Tec	++	+++	+++	-	++
Tks5 (I)	++	+++	+++	-	++
Tks5 (V)	++	+++	+++	-	++
TOCA1	++	++	++	-	++

1.3.3.3 ADAM15 in pathological conditions

A common way to elucidate the function of genes is to inactivate them in research animals. The resulting changes in either phenotype or physiology offer insights into their natural function(s). ADAM15 double knockout mice (ADAM15$^{-/-}$) have been generated in the lab of Carl Blobel[183]. They could not observe any morphological changes in examined tissues compared to age-matched wildtype (WT) adult animals. This suggests either functional redundancy with other ADAMs or ADAM15 does not play an essential role in tissue development. However, in vascular cells an extraordinary high level of ADAM15 was found which indicates a role in pathological neovascularisation. To investigate the role of ADAM15 in neovascularisation ADAM15$^{-/-}$ and WT mice were subjected to the retinopathy of prematurity (ROP) model in which young mice are exposed to high oxygen levels (75%) for 5 days, and then returned to normoxic air. The decline in oxygen concentration induces a strong angiogenic stimulus, which leads to pathological neovascularisation in the retina. The result was ADAM15$^{-/-}$ mice showed 64% less angiogenesis compared to their WT controls. In western blot analysis they observed an increase in ADAM15 expression from WT ROP treated animals in the retina. Therefore, they concluded that ADAM15 plays a role in pathological neovascularisation, but is not required for normal angiogenic development.

Böhm and colleagues hypothesised that ADAM15 promotes pathological extracellular matrix (ECM) remodelling, based on the finding of increased ADAM15 expression in human neoplastic cartilage and osteoarthritic spicimens[184]. In ADAM15$^{-/-}$ mice histopathological examination of knee joints revealed accelerated development of osteoarthritic lesions[185]. They found mild hyperplasia of synovial membrane and proteoglycan loss from cartilage matrix. However, more pronounced changes were found as well. Severe cartilage erosions in various degrees could be observed lasting from superficial changes, deep fissures, necrotic or complete loss of cartilage[185]. Cartilage derived detritus was found incorporated into synovial membrane resulting in inflammation. This irreversible damage was only observed in ADAM15$^{-/-}$ mice (7 of 12), but not in WT controls[185]. Based on these findings they concluded that ADAM15 does not have a destructive, rather a homoeostatic role in joint integrity and cartilage remodelling.

Another area in which ADAM15 has been implicated is the regulation of permeability in epithelial and endothelial cells. In endothelial cells semi-permeable barriers regulate the transport of fluids, solutes as well as cells across the wall of blood vessels. Barrier dysfunction, due to hyperpermeability, is a key event in the development of vascular diseases associated with inflammation. This includes atherosclerosis[162], diabetic complications[186], sepsis[187] as well as cancer inflammation and metastases[188]. In human umbilical vein endothelial cells (HUVECs) depletion of ADAM15 attenuated thrombin-induced barrier dysfunction[189]. Thrombin is a common used stimuli to induce barrier dysfunction due to redistribution of vascular endothelial-cadherin (VE-cadherin) and associated catenins[190]. Concomitantly, it was observed that ADAM15 knockdown also decreased endothelial permeability and overexpression led to hyperpermeability independent of its catalytic function[189]. Neutrophil transendothelial migration was also observed being dependent on ADAM15 expression since knockdown led to inhibition while overexpression increased migration[189]. These events are mediated via Src/Erk1/2-pathway and are independent of VE-cadherin shedding[189]. Later the same group was able to show in mouse model, that ADAM15 contributes to atherosclerosis by regulation of endothelial barrier dysfunction involving c-Src and c-Yes[162]. In a mouse model with lipopolysaccharide (LPS) induced acute lung injury, upregulation of ADAM15 was observed in association with neutrophil infiltration and pulmonary oedema[191]. In ADAM15$^{-/-}$ mice LPS induced inflammatory injury was attenuated and reduced neutrophil infiltration[191]. This data suggests that increased ADAM15 expression promotes inflammatory lung injury by increasing endothelial cell permeability and neutrophil transmigration. To further add evidence of ADAM15 beeing involved in regulating endothelial permeability a micro RNA (miRNA), miR-147b, was identified which decreased total and surface expression of ADAM15 in endothelial cells. In the same cells LPS induced

barrier dysfunction was attenuated when treated with miR-147b. An antagomir to miR-147b induced hyperpermeability of the endothelial cells with a similar effect as LPS[192].

According to literature ADAM15 has a high impact in cancer. Within the last decade scientists found elevated expression of ADAM15 in a variety of cancers, such as lung[193,194], aggressive breast[164], prostate[164] and pancreatic cancer[195].

In 2005, the first paper was published demonstrating the expression of ADAM15 in lung carcinomas[193]. ADAM15 is also upregulated in the lungs upon inflammation. LPS induced inflammation promotes ADAM15 overexpression facilitating neutrophil infiltration and plasma leakage which leads to pulmonary oedema[191]. In ADAM15$^{-/-}$ mice the inflammatory injury was greatly attenuated. To support this finding *in vitro* experiments demonstrated that ADAM15 deficiency diminished permeability and neutrophil transmigration within endothelium[191]. These observations provide evidence that ADAM15 contributes to acute lung inflammation by disrupting endothelial barrier integrity promoting hyperpermeability response. The function of ADAM15 in non-small cell lung cancer (NSCLC) is still not known. A recent publication by Dong et al. attempts to shed light on this[194]. They found that overall and relapse free survival (RFS) of NSCLC patients correlate with high expression of ADAM15. Upon shRNA-mediated knockdown of ADAM15, invasiveness and cell migration were reduced. In the epithelial lung carcinoma cell line A549 ADAM15 overexpression led to increased invasion. They also demonstrated ADAM15 upregulated the matrix metalloproteinase 9 (MMP9) via the MAPK pathway.

1.3.3.4 ADAM15 as a sheddase

In section 1.3.2.1 the shedding activity of ADAMs in general was desribed. This section focuses on ADAM15 and its proteolytic activity. Due to its clinical importance research for ADAM15 is increasing. So far only ten substrates have been identified: Collagen IV[196], CD23[145], pro-amphiregulin[197], pro-transforming growth factor α (pro-TGFα)[197], pro-heparin-binding EGF-like growth factor (pro-HB-EGF)[198], E-cadherin[199], Fibroblast growth factor receptor-2IIIb (FGFR2IIIb)[200], ADAM10[201], pro-MMP9[194] and major histocompatibility complex (MHC) class I polypeptide-related sequence B (MICB)[195]. These substrates are summarised in table 1.7.

The first substrate for ADAM15 was identified by Martin et al. in 2002. They hypothesised that ADAM15 MP is actively involved in human mesangial cell (HMC) migration. Gelatinolytic activity of ADAM15 was confirmed by zymography. To further substantiate the observation collagen IV was incubated with purified ADAM15 from HMCs. The result was that ADAM15 degraded collagen IV in a dose-dependent manner. To confirm that ADAM15 was actively involved, the epxeriment was re-

peated with either the addition of ethylenediaminetetraacetic acid (EDTA), leupeptin or phenylmethanesulfonyl fluoride (PMSF) to HMC purified ADAM15. The samples were subjected to western blotting and probed for collagen IV. Only EDTA reduced the degradation of collagen IV while ADAM15 was not inhibited by leupeptin or PMSF.

The first signalling related substrate for ADAM15, CD23, was identified by Fourie et al. and published 2003[145]. Earlier, Bonnefoy and et al. discovered that CD23 (FcεRII), a low affinity receptor for IgE, is proteolytically released by an unknown metalloprotease. CD23 upregulates IgE production and induction of inflammatory cytokines[202]. Together with ADAM15, ADAM8 and ADAM28 were also identified as CD23 sheddase.

A year later Schäfer et al. demonstrated that cleavage of pro-TGFα is dependent on ADAM15 in the human urinary bladder cancer cell line TCCSUP[197]. In the same publication they also showed the dependency of ADAM15 in proteolytic processing of pro-amphiregulin in another human urinary bladder cancer cell line 5637C[197]. Dominant-negative mutants of ADAM15, lacking pro-and MP-domain were stably transfected. Those mutants blocked the EGFR transactivation signal induced by lysophosphatidic acid (LPA), which induces EGFR tyrosine phosphorylation.

Hart and co-workers discovered ADAM15 as pro-HB-EGF sheddase. When endogenous ADAM15 was inhibited by short interference RNA (siRNA) the thrombin-induced EGFR tyrosine phosphorylation was reduced. To confirm this finding, they chose the same approach as Schäfer et al. Dominant-negative ADAM15 mutants were transfected into MDA-MB-231 and MCF-7 cells, in which thrombin-induced EGFR tyrosine phosphorylation was again reduced[198].

In 2008, Najy and colleagues revealed E-cadherin as substrate for ADAM15[199]. The first observation was that the overexpression of ADAM15 in MCF-7 cells correlated with elevated amounts of soluble E-cadherin in conditioned media. On the other hand, stable downregulation of ADAM15 by shRNA in these cells led to less soluble E-cadherin in the media. To further confirm, *in vitro* cleavage analysis was performed in which isolated E-cadherin and ADAM15 were co-incubated in equal ratios. A dose-dependent increase in soluble E-cadherin was observed. To ascertain that E-cadherin is an ADAM15 substrate, they added the broad spectrum MMP inhibitor 1,10-phenanthroline which reduced ADAM15 mediated E-cadherin cleavage *in vitro*.

Duan et al. demonstated that ADAM15 is involved in shedding of MICB[195]. MICB is a polymorphic, glycosylated, non-classical MHC class I protein anchored in the cell membrane. It is stress-induced and upregulated in lung, kidney, prostate, breast and colon cancer, although is it considered to be restricted to the gastrointestinal tract[195]. A study showed that soluble MICB, released by shedding, correlates with

high tumour stage and poor differentiation in pancreatic cancer[203]. Cleaving MICB from the tumour cell reduces immunogenicity[204] while shedding of MICB induces internalisation and degredation of one of its ligands (NKG2D) which is normally expressed under stress by infected or transformed cells to initiate cytotoxic response[205]. They found a correlation between ADAM15 and MICB in pancreatic ductal adenocarcinoma (PDAC) patients. Thus they suggest ADAM15 as therapeutic target for MICB shedding.

ADAM15 substrates exist also within the same family. ADAM10 is subjected to RIPing[201]. Tousseyn et al. could detect four bands in western blot experiments. A 85 kDa (pro-protein), a 65 kDa (mature form), a 10 kDa band which can only be detected with a C-terminus specific antibody, and 55 kDa fragment from the supernatant, that is only immunoreactive with N-terminal antibodies. The last fragment is considered as soluble ADAM10. From this they concluded ADAM10 must be processed by an unknown protein. To identify potential sheddases of ADAM10 a panel of inhibitors was screened. Those inhibiting ADAMs and MMPs showed accumulation of the soluble form while the C-terminal fragment (CTF) was reduced. This suggested the candidate belongs to the family of metalloproteinases. In ADAM9/15/19 null and ADAM9/15 null cells reduction of the CTF was observed suggesting those three ADAMs are involved. However, ADAM19$^{-/-}$ MEFs did not confirm the assumption. To further substantiate that ADAM9 and 15 are involved in ADAM10 shedding, COS cells, which express low levels of ADAM10, were transiently transfected with ADMA10. In contrast to WT COS cells, a strong double band and soluble ADAM10 were detected. Co-overexpression of increasing amounts of WT, but not catalytically inactive ADAM15, resulted in stronger bands of the CTF and soluble ADAM10. The same was observed with ADAM9. This confirms the hypothesis that ADAM15 and ADAM9 are involved in shedding ADAM10.

Maretzky et al. revealed FGFR2IIIb as substrate for ADAM15. So far the cleavage of ADAM15 substrates was based on research with isoform A. However, they were the first group to show that shedding activity can be splice form-dependent in ADAM15[200]. They were able to show that ADAM15 B, with an additional proline-rich region (figure 1.10), has increased shedding activity compared to ADAM15 A overexpressing cells. An additional proline-rich insert adds a binding site for Src. No difference in in the catalytic activity of ADAN15 A or B could be observed in Src$^{-/-}$ mouse embryonic fibroblasts (MEFs). However, stable transfection of wild-type Src rescued the singificantly higher activity in ADAM15 B, but not in ADAM15 A overexpressing cells. This emphasises that research needs to target also the other splice variants of ADAM15. In 2015, a study announced another substrate for ADAM15[194]. *In vivo* experiments showed interaction of ADAM15 with MMP9. *In vitro* they could demonstrate that ADAM15 was able to cleave pro-MMP9 and ac-

tivates it. This suggests that pro-MMP9 is bearing a target sequence for ADAM15 MP, but it remains to be elucidated if this happens *in vivo* as well.

Table 1.7: Overview of substrates shed by ADAM15

Substrate	Category	Reference
Collagen IV	ECM	Martin et al[196]
E-cadherin	Transmembrane protein	Najy et al[199]
Pro-Amphiregulin	Growth factor	Schäfer et al[206]
Pro-HB-EGF	Growth factor	Hart et al[198]
Pro-TGFα	Growth factor	Schäfer et al[206]
CD23	Receptor	Fourie et al[145]
FGFR2IIIb	Receptor	Maretzky et al[207]
ADAM10	Metalloproteinase	Tousseyn et al[201]
Pro-MMP9	Matrix metalloproteinase	Dong et al[194]
MICB	Stress-induced ligand for NKG2D	Duan et al[195]

1.4 Cell proliferation

Cell proliferation describes the increase in cell number due to cellular growth and division. It is not only essential for physiological events such as cell growth and normal tissue function but also for pathological mechanism such as tumourigenesis. Deregulation of proliferation is caused by the perturbation of various mechanisms and signalling pathways within the cell. A series of events in which various pathways are involved is the cell cycle in which the DNA is replicated and the cell mass increases. Two major phases during cell cycles occur: S-phase in which chromosomes duplicate and M-phase in which chromosomes are segregated and the cell divides (cytokinesis). Since cells need more time to increase there mass than doubling the chromosome, the cell cycle has also gap-phases. G_1-phase between M- and S-phase, and a G_2-phase between S-phase and mitosis (figure 1.12 a). The gap phases provide not only time for cell growth, but also time to monitor the environment. This ensures to have appropriate conditions and preparations completed prior to cell cycle progression. If conditions appear unfavourable such as G_1-delays the cell can enter a specialised resting phase named G_0.

To avoid malfunction of cell cycle events, such as partial initiation of chromosome condensation or breakdown of the nuclear envelope, the cells have a cell cycle control system consisting of various biochemical switches. A central component are the

cyclin-dependent kinases (CDKs). The activity of CDKs is alternating throughout the cell cycle. This leads to changes in phosphorylation states of intracellular proteins controlling different events. As the name CDK implies the most important protein regulating their activity belongs to the group of cyclins. The kinase activity of CDKs is only activated if bound tightly to cyclins. CDKs have preferred interaction partners, some exclusively interact with only one cyclin (figure 1.12 b). For example CDK1 preferably binds to cyclin B, but is also able to bind to cyclin A, D and E. Contrary, CDK4 can only interact with cyclin D. Complex formation of both proteins triggers cell cycle events.

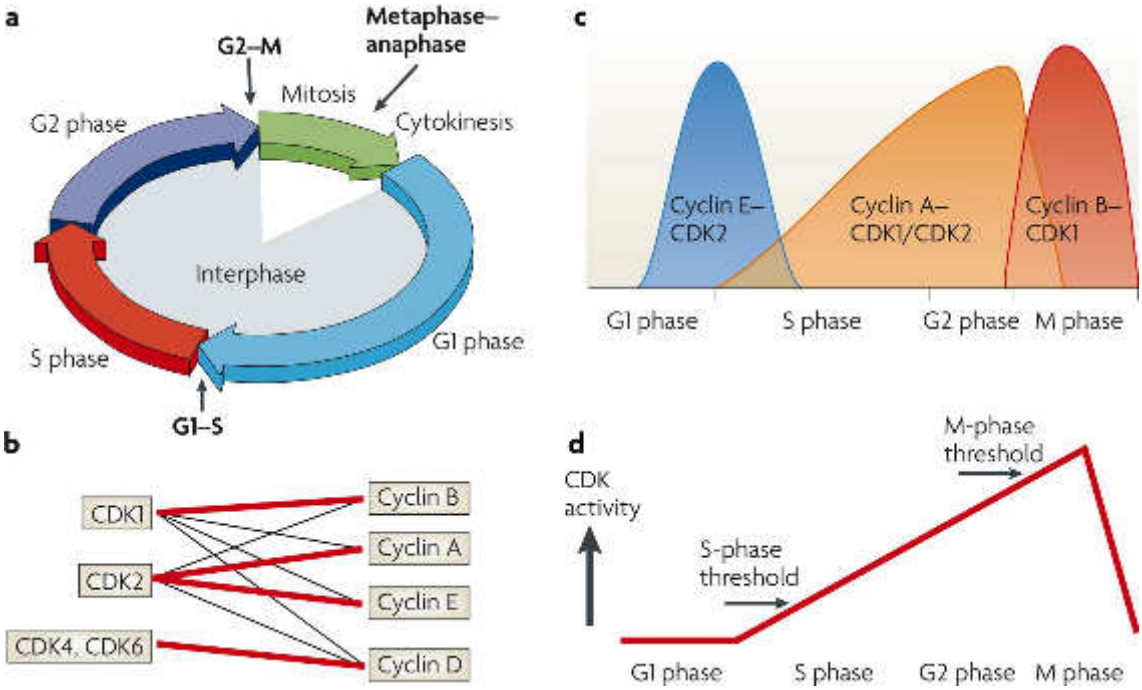

Figure 1.12: Model of cell cycle with active cyclins and CDKs. **(a)** Three major transition phases have to be passed by dividing cells: G_1/S-phase transition in which is the beginnning of DNA replication, G_2/M-phase transition which is marked by the onset of nuclear envelope breakdown and chromosome condensation. The third phase is the meta-to-anaphase transition in which the segregation of sister chromatids occurs. **(b)** Interaction of CDKs can be separated into two groups. CDK1 and 2 bind cyclin A, B, C and D whereas CDK 4 and 6 only interact with cyclin D. Thick red lines indicate the preferred interaction partners. **(c)** Early G_1-phase is regulated by D-type cyclins and CDK4 or CDK6 (not shown) whereas cyclin E/CDK2 induces S-phase transition. Late S-phase is regulated by cyclin A-CDK1/CDK2 wheras cyclin B-CDK1 drive mitosis. **(d)** Next to the classical cell-cycle control model, a minimal threshold model has emerged based on CDK-knockout studies. This suggests it is sufficient to control the interphase if either CDK1 or CDK2 is bound to cyclin A. In contrast, cyclin B-CDK1 is important for mitosis. The differences are likely to be based on localisation of the molecules. The image was taken from Hochegger, Takeda & Hunt in *Cyclin-dependent kinases and cell-cycle transitions: does one fit all?*, Nature reviews. Molecular cell biology, 2008[208]

In general, cyclins are grouped in four classes as illustrated in figure 1.12 c. In vertebrates, G_1/S-cyclins (type E cyclins) activate CDK2 in late G_1-phase and induce entry into cell cycle. Cyclin E levels decrease in S-phase. S-cyclins (type A cyclins) interact with either CDK1 or CDK2 and induce chromosome duplication.

Cyclin A levels remain high until mitosis is triggered. M-cyclins (type B cyclins) stimulate entry into mitosis by interacting with CDK1. The last group belongs to G_1-cyclins (type D cyclins) which assist cyclin E in controlling entry into S-phase. This type D cyclins are able to interact with CDK4 and CDK6. The cellular events which happen during cell cycle progression are versatile. Cyclins do not only activate its partner CDK, but direct it to and activate a different set of substrate proteins. Full activation of the cyclin-CDK complex is achieved by phosphorylation of an amino acid close to the active site of a CDK. This is mediated by the group of CDK-activating kinases (CAK). Phosphorylation causes a conformational change enhancing in turn phosphorylation of their target proteins. This processes are tightly regulated. CDKs possess also another phosphorylation site which leads to inactivation upon phosphorylation of Wee1. In contrast, dephosphorylation by Cdc25 causes increased CDK activity. Other regulatory mechanisms are known, but not further described. One are the group of CDK inhibitor proteins (CKIs). The mode of action lies on a conformational change of the CDKs active site rendering inactive.

1.5 Cell migration

Cell migration, as illustrated in figure 1.13, is crucial for the development of multicellular organisms. In mammals during embryogenesis a proportion of cells migrate over long distances. Neural crest cells, a highly migratory multipotent cell population migrates throughout the embryo to eventually differentiate into multiple cell types such as neurons, smooth muscle cells and adipocytes[209]. However, migration is not only restricted to physiological events, it also contributes to disease progression. In solid cancer types, cells enter blood vessel or lymph nodes to form distant metastases[210].

The way how cells migrate can be changed rapidly. They are highly flexible and the mode of migration can be altered between single cell and collective cell migration[211]. Motility also depends on the composition and stiffness of the environment including surrounding cells and the ECM[212]. The interaction with other cells affect and regulate the migration too. Upon cell-cell interaction cells undergo contact inhibition in which the migrating cell stalls. Consecutively, it leads to cell-cell adhesion or a change of direction. In many cancer cells this contact inhibition is defective[213].

Migration of the cell requires several molecular mechanisms. The initial step is to adhere to a cell surface such as other cells or ECM. Adhesion thereby serves two functions: One is to generate traction via interaction of the actin filaments to the extracellular substratum. The second function is to organise migration regulating signalling networks which also control gene expression, cell proliferation and sur-

vival[214].

Activated integrins bind to ECM components such as fibronectin or vitronectin. This can lead to clutering of the integrin receptors and/or a conformation change which leads to recruitment of intracellular signalling components such as FAK or vinculin. A more detailed introduction in focal adhesion dynamics is presented in chapter 5. Nascent adhesions, the precursor of focal adhesions are formed in the lamellipodium of migrating cells. Its formation depends on the rate of actin polymerisation as well as its inhibition. Within the lamellipodium FAK and vinculin bind to Arp2/3[215,216] regulating lamellipodia dynamics.

The morphological changes a cell needs to undergo in order to migrate is a highly dynamic process. This process is driven by actin polymerisation which begins with the formation of new actin filaments. It is regulated by three classes of nucleating proteins including the Arp2/3 complex, tandem-monomer-binding nucleators and formins[217]. The Arp2/3 complex is unique since it branches off new actin filaments from an exisiting strands at an angle of $70 \pm 7^{\circ}$[218] It consists of seven members including Arp2 and Arp3 which have similar structure to monomeric actin. In order to function, the complex needs also nucleation promoting factors (NPF). Arp2/3 mediated nucleation is regulated by many proteins, the most promiment family of NPFs are the family of Wiskott-Aldrich syndrome proteins (WASP) such as WAVE and WASH. Nucleation occurs at the pointed end and does not affect the assembly rate at the barbed end[217].

The two other existing families of nucleation factors produce linear filaments. The family of tandem-monomer-binding nucleators includes proteins such as spire, leiomodin and cordon-bleu. They bind at least three actin monomers forming a stable trimer. Tandem-monomer-binding nucleators bind to the pointed end of the actin filament and leave the barbed end free, similar to the Arp2/3 complex[219]. Formins represent the other family of linear nucleating factors which stabilise spontaneously formed actin trimer. Members of the formin family comprise proteins such as mDia1 and 2 which associated with the rapid growing barbed end of an actin filament and regulate its elongation[220]. Formins have conserved actin polymerisation domains of which one binds to actin monomers while the other interacts with profilin-actin complexes and promotes the addition of the monomeric actin[217].

Actin polymerisation leads to stress fibre formation which are mediated by Rho GTPases. This mechanism is crucial in moving cells forward. This induces contractile forces which, together with retrogade actin movement, build up tension to pull the trailing edge forward.

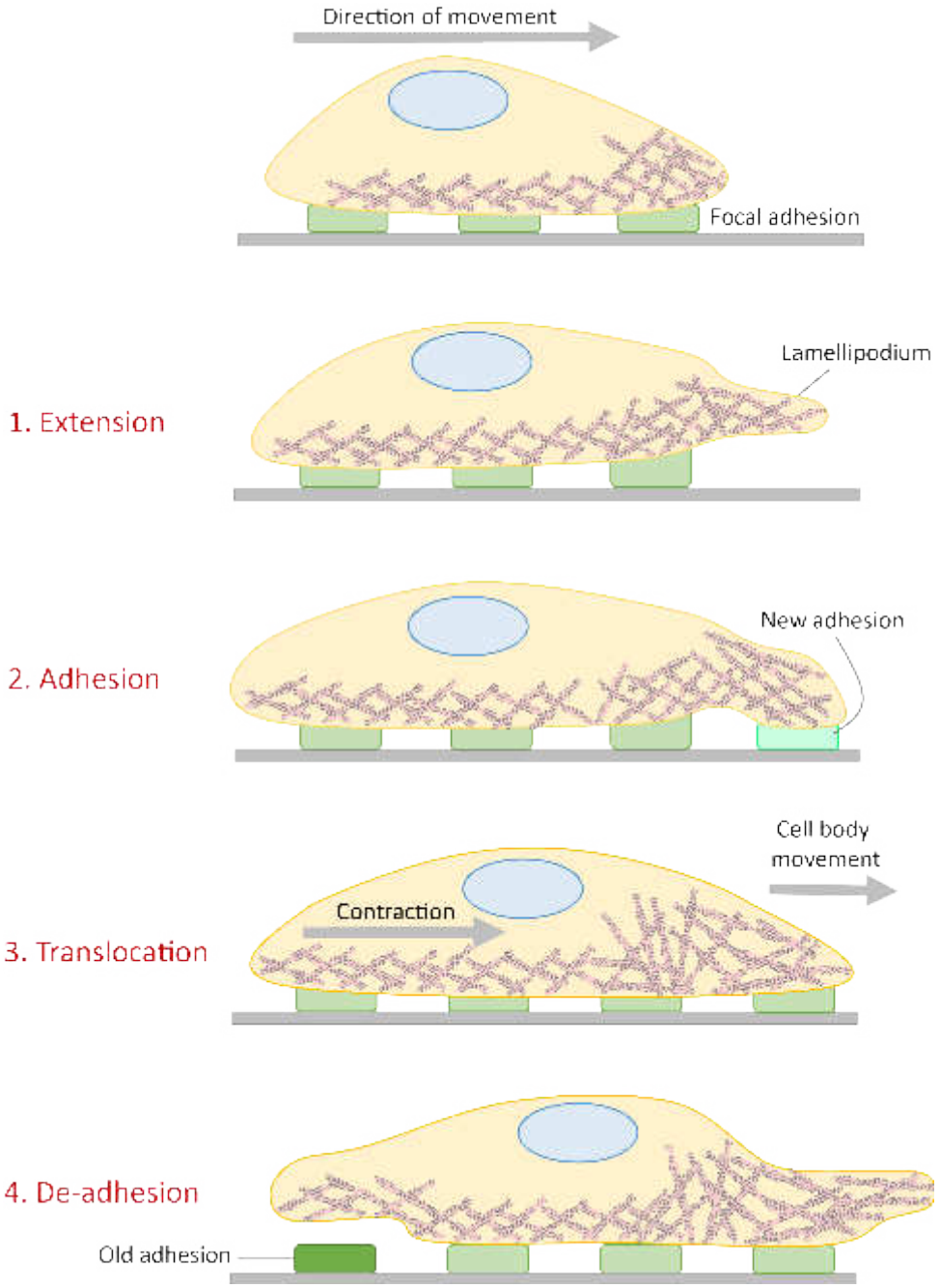

Figure 1.13: The four stages of 2D cell migration upon attachment. Focal adhesions are formed (green). **1. Extension:** Actin rapidly polymerises (red) and pushes the leading edge to the front resulting in lamellipodium formation. **2. Adhesion:** The lamelipodium adheres to the substratum forming a focal contact/new adhesion (neon green). **3. Translocation:** Actin stress fibre formation induces contractile forces. Together with retrogade actin movement tension is build up which pulls the trailing edge forward. **4: De-adhesion:** Focal adhesion disassembly occurs in the back removing cell attachment (dark green). Image was adapted from *Fibroblasts and the Ground They Walk On* by Tschumperlin, D. J., Physiology, 2013[221].

This tension, together with other factors, lead to disassembly of adhesions on both ends likely to be regulated in different ways. While the disassembly of the adhesion at the leading edge is mediated by FAK-Src signalling through paxillin, Erk and myosin light-chain kinase occurs[222], is the release of the trailing edge less well understood. However it seems it involves a weakening or separation of the integrin-ECM linkages or integrin-cytoskeletal interaction. This is at least partially driven by contractile forces. This results in severing of the integrins form the actin cytoskeleton which remain on the substratum. Components associated with the cytoskeleton translocate towards the direction of the cell body[214]. However, integrin recycling as well as endocytosis seem to be involved as well[223].

1.5.1 ADAM15 in migration

Various lines of evidence suggest that ADAM15 plays a role in cell migration. First experiments were performed by overexpressing ADAM15 in NIH3T3 cells[224]. Overexpression led to reduced migration on fibronectin due to increased cell-adhesion. The inihbitory effect of ADAM15 in cell migration on fibronectin was confirmed in CHO cells. Furthermore, it was shown that adhesion is enhanced by increase of α5-integrin expression at the cell surface mediated via Erk1/2 inactivation[225]. Further evidence that ADAM15 negatively influences cell migration was demonstrated by experiments overexpressing the disintegrin domain of ADAM15 in a hepatoma cell line. Overexpression led to decreased migration accompanied by reduced proliferation[226]. Contrary, in prostate cancer 3 (PC3) cells inhibition of ADAM15 reduced cell migration as well as adhesion to laminin, fibronectin and vitronectin[227]. That ADAM15 can also have the opposite effect in cell migration was further confirmed. In a rat model of rheumatoid arthritis knockdown of ADAM15 decreased migration of fibroblast-like synoviocytes[228].
These examples show that ADAM15 can either promote or inhibit cell migration depending on the cellular context. How individual ADAM15 isoforms will affect migration has not been investigated yet.

1.6 Epithelial-mesenchymal transition

Epithelial to mesenchymal transition (EMT) describes the process in which cells lose their cell polarity and cell-cell junctions which are necessary to keep contact with neighbouring cells. Cells which undergo EMT gain mesenchymal properties, such as fibroblastoid morphology, changes in gene expression (an overview of epithelial and mesenchymal expression markers is listed in figure 1.14), increased motility, ability to invade the basal membrane, enhanced migration, loss of polarity, el-

evated resistance to apoptosis and increased production of ECM components[229–231].

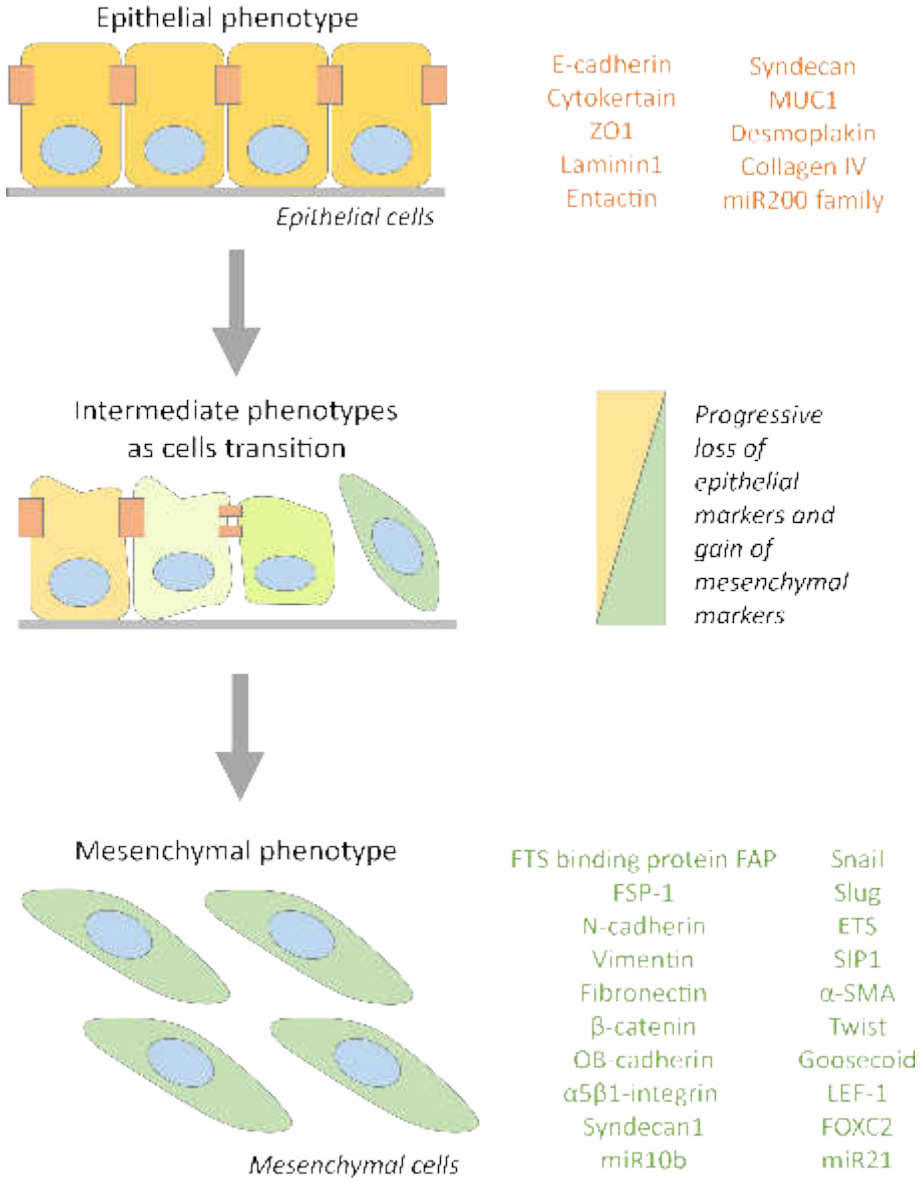

Figure 1.14: Illustration of cells undergoing EMT with corresponding specific markers. Epithelial cells lose their polarity and cobblestone-like morphology. Mesenchymal cells are non polarised and appear fibroblastoid. Commonly used markers are listed next to the characteristic phenotype. Coexpression of markers from epithelial and mesenchymal cells define an intermediate state of EMT. Image was adapted from Kalluri & Weinberg in *Review series The basics of epithelial-mesenchymal transition*, Journal of Clinical Investigation, 2009[230].

An important transitional process is the loss of epithelial-cadherin (E-cadherin). During EMT the expression of E-cadherin is switched to neural cadherin (N-cadherin). N-cadherin is mostly expressed among mesenchymal cells, whereas E-cadherin is a marker for epithelium. E-cadherin is crucial for the cell shape since it connects the α- and β-catenin to the actin cytoskeleton. This helps to sustain cell shape and polarity. EMT initiation and execution is caused by several transcription factors and miRNAs. Transcription factors involved in inhibiting

E-cadherin directly comprises zinc finger proteins of the SNAIL superfamily, such as snail or slug, zinc finger and E-box binding proteins of the ZEB family, such as ZEB1 or ZEB2 or TWIST proteins. Examples for indirect inhibition are the homeobox proteins goosecoid and SIX1 or the forkhead-box protein FOXC2[232].

1.7 Cell junctions

Epithelial and endothelial cells have the important role to assemble barriers to separate tissue. Their function is to regulate the exchange of ions and different sized molecules. The two main players in junctional organisation are adherens junctions (AJ) and tight junctions (TJ). Junctional proteins are classified in three groups: The first are structural transmembrane proteins, which facilitate contact between membranes of adjacent cells. The second group comprises plaque proteins which associate with the cytoskeleton. The last group are signalling proteins which enable cell-cell communication. Apart from AJs and TJs, cell-cell junctions also contain desmosomes and gap junctions. Desmosomes are adhesive spot-like junctions which connect the intermediate filaments of adjacent cells via desmosomal cadherins. Beside stabilisation of tissue architecture desmosomes also contribute to cellular signalling of neighbouring cells[233]. Unlike AJ's,TJs' and desmosomes, gap junctions do not contribute to the structural integrity of cell-cell junctions. They form intercellular channels which facilitates the exchange of ions and other larger cytoplasmic solutes[234]. Therefore, they are important in cell-cell communications.
Since AJs and TJs contribute most to cell-cell contacts the following subsections focus on those only.

1.7.1 Adherens junctions

AJs are located immediately below tight junctions. AJs are composed of two complexes, the cadherin-catenin and nectin-afadin complex. An illustration of both is shown in figure 1.15. The name cadherins is originated from their requirement of calcium ions (calcium-adhering).
The classical cadherin-catenin complex consists of α–, β– and p120-catenin. E-, P- and N-cadherins contain five N-terminal cadherin repeats which are necessary for the Ca^{2+}-interaction as well as the cadherin-mediated adhesion. It is followed by a transmembrane domain and a C-terminal ICD. The cadherin ICDs bind to the armadillo repeats (not shown) of p120- and β-catenins. α-catenin associates with either β-catenin or its close relative γ-catenin. Cells are opposed with a distance of about 10-20 nm between their plasma membranes[235].

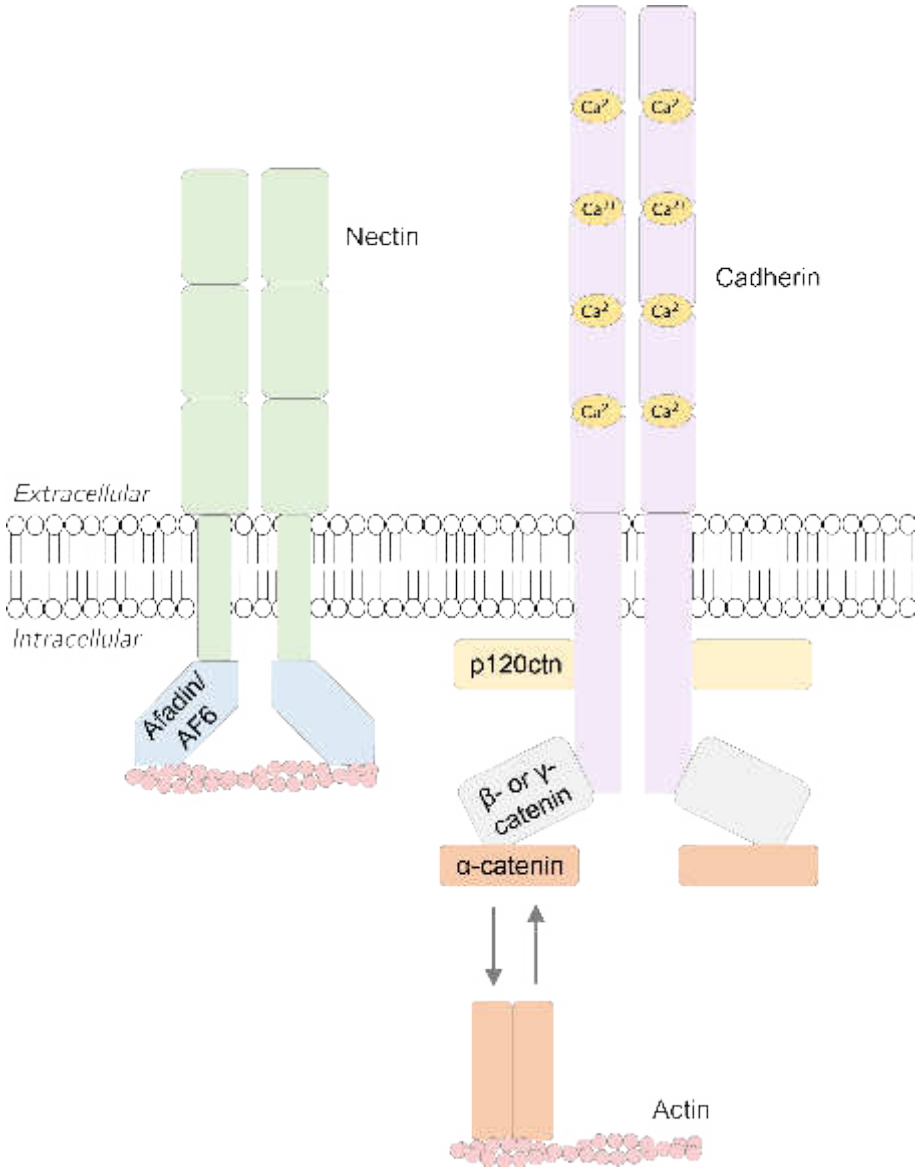

Figure 1.15: Illustration of an adherens junction. The nectin-afadin complex (left) consists of a homodimeric receptor of either nectin-1, 2, 3 or 4 which associate with the actin binding protein afadin. Nectins possess an ECD which has three IgG-like loops, a transmembrane region and an ICD with a C-terminal PDZ binding motif (not shown). Afadin serves as adapter protein and establishes the connection between the nectins and actin. The classical cadherin-catenin complex (right) consists of α, –β– and p120 catenin. E-, P- and N-cadherins contain five N-terminal cadherin repeats which can bind Ca^{2+}. It is followed by a transmembrane domain and a C-terminal ICD. The cadherin ICDs bind to the armadillo repeats (not shown) of p120- and β-catenins. α-catenin associate with either β-catenin or its close relative γ-catenin. Depending on its constitution α-catenin binds either to cadherin/catenin or actin. The figure was adapted from Niessen in *Tight junctions/adherens junctions: basic structure and function*, The Journal of investigative dermatology, 2007[236].

The calcium binding sequences of the ECD of the cadherins are crucial to establish the connection among neighbouring cells. In fact, the interaction of calcium ions with the sequences dictate the conformation of the ECD[237]. Upon association with calcium the ECD of cadherins bind to opposing cadherins via a homophillic interaction[235].
It has been shown that the cadherin-p120 catenin interaction is important to maintain cell-surface stability[238]. Also, p120-catenin is a major regulator of Rho GTPase signalling[239]. For a long time it was believed that α-catenin connects β-catenin to the actin cytoskeleton. However, it seems that α-catenin binds either to cadherin or actin filaments. It is reported that α-catenin is a monomer or homodimer. Depending on its form its affinity is stronger toward cadherin/catenin (monomer) or to actin (homodimer)[240]. The nectin-afadin complex consists of a homodimeric receptor of either nectin-1, 2, 3 or 4 which associate with the actin binding protein afadin (AF6). The nectins enable the complex to employ a homophilic as well as heterophilic adhesion with either other nectins or nectin-like receptor molecules. Nectins possess an ECD which has three IgG-like loops, a transmembrane region and an ICD with a C-terminal PDZ binding motif[241]. Afadin serves as adapter protein and establishes the connection between the nectins and actin. Afadin consists of a PDZ-, a dilute-, a forkhead associated (FHA)- and two Ras-associating domains[129]. The PDZ domain of afadin associates with the nectins and is thus responsible for the interaction. Within the nectin-afadin complex it seems that the dilute domain is involved in stress fibre formation[242]. The role of the FHA domain is to bind phosphopeptide and thus has a regulatory function. At least one of the Ras associated domains is able to bind to Rap1A, a small GTPase and member of the Ras superfamily[243].
Studies with CHO cells showed that co-expression of ADAM15 and vascular endothelial-cadherin (VE-cadherin) led to translocation of ADAM15 to the cell periphery[244]. Cell-cell contacts in these cells are established by VE-cadherin mediated AJ formation. Co-expression of ADAM15 not only resulted in translocation, but also to co-localisation with VE-cadherin. This proposed that ADAM15 may be a component of AJ in endothelial cells. Experiments in HUVEC cells demonstrated that VE-cadherin is not a substrate for ADAM15[189].

1.7.2 Tight junctions

TJs are the most apical structure of cell-cell junctions forming the border between basolateral and apical membrane (figure 1.16). Their function is not only to provide structural integrity, they are also a site for signalling, polarity cues and binding site for intracellular vesicles. Three major TJ protein families mediate cell-cell adhesion.

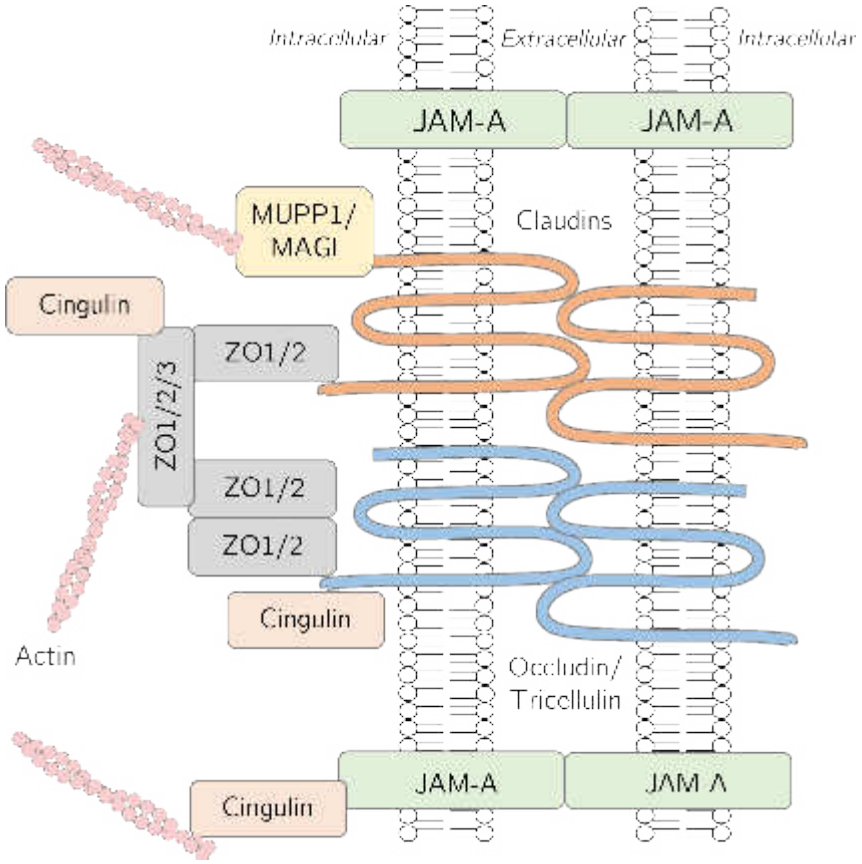

Figure 1.16: Illustration of a tight junction. TJs are the most apical structure of cell-cell junctions forming the border between basolateral and apical membrane. Their function is to provide structural integrity, they are a site for signalling, polarity cues and binding site for intracellular vesicles. The three major TJ proteins mediating cell adhesion are claudins, occludins and JAMs. Tricellulin is found in tricellular TJ. Cingulin forms a complex with JAM-A and interacts with actin filaments as well as myosin II and several TJ proteins including paracingulin, occludin, ZO1, ZO2 and ZO3. ZO proteins function as scaffold proteins and provide structural integrity supporting the assembly of multiprotein complexes. The figure was adapted from Niessen in *Tight junctions/adherens junctions: basic structure and function*, The Journal of investigative dermatology, 2007[236].

These structural transmembrane proteins are claudins, occludins and junctional adhesion molecules (JAMs). Occludins are transmembrane proteins. They contain three extracellular loops which are flanked by four transmembrane domains. Hence Occludin passes the plasma membrane four times with the N- and C-terminus localised in the cytoplasm. In cancer occludin plays an important role, due to its role in barrier formation. An important step in cancer progression is the formation of metastases by gaining the ability to invade vascular endothelium. Therefore, TJs need to be overcome first and loss would facilitate invasion. Thus the loss of occludin correlates with increased invasion. A protein which has structural similarities with occludin is tricellulin. It is predominantly localised in tricellular junctions of epithelia. Its function is to contribute to barrier formation[245]. Cingulin interacts with actin filaments as well as myosin II and several TJ proteins including paracingulin, occludin, ZO1, ZO2 and ZO3. It was also found to be in a complex with JAM-A[246].

A schematic representation of occludin, claudin1, JAM-A, ZO1, ZO2 and ZO3 is shown in figure 1.17. Unlike occludins JAMs have only one transmembrane domain. The cytoplasmic tails bind to PDZ domain-containing proteins such as ZO1 or afadin[247]. Within their ECD two Ig-like domains can be found[248]. Those are not only important for tight junction assembly, but are also involved in reovirus binding, platelet aggregation and leukocyte migration. Blocking the IgG-like domains results in reduced barrier function. This is caused by the inhibition of JAM homodimer formation[249]. ZO proteins function as scaffolding molecules and provide structural integrity supporting the assembly of multiprotein complexes in intercellular junctions. They link the filamentous cytoskeleton to the integral proteins. ZO proteins also appear to participate in cell growth and proliferation[250]. Due to the possession of a guanylate kinase (GuK) domain they belong to the family of membrane-associated guanylate kinase (MAGUK)-like proteins. Molecular studies demonstrated that ZO proteins contain conserved nuclear export and localisation motifs[251,252]. Tight junction are also the target and site of several diseases such as infectious diseases, vitamin D mediated malabsorption of Ca^{2+} ions and cancer.
Often microorganisms target tight junction such as *Clostridium perfringens*. Its enterotoxin is a common cause of food poisoning which uses claudin3 and 4 as receptors[253,254]. Upon binding of *C.perfringens* enterotoxin to claudin3 or 4 the new complex is internalised causing distortions in the functions of TJs[255]. The bacterium *Vibrio cholerae* causes severe diarrhoea by digesting occludin via a combination of several toxins[256]. It was also found that reorganisation of the actin cytoskeleton occured by targeting ZO1[256].
Calcium plays an essential role in several physiological functions, such as blood coagulation, neuromuscular transmission, bone mineralisation, cell-cell adhesion, muscle contraction and intracellular signalling. Since claudins have a major role in cell permeability they are also involved in uptake of calcium. Mice, deficient for vitamin D receptor showed decreased expression of claudin2 and 12[257].
Cancer cells also undergo changes in their composition of TJ. They lose their polarity and specific functions with reduced development of TJ. It was observed that well differentiated colorectal and endometrial adenocarcinomas expressed occludin. Further de-differentiation led to loss of occludin and tight junctions[258,259].
These were just a few examples how diverse the TJ mediated cause of dieases can be. More detailed information about pathological implications involving claudins are dicussed below.

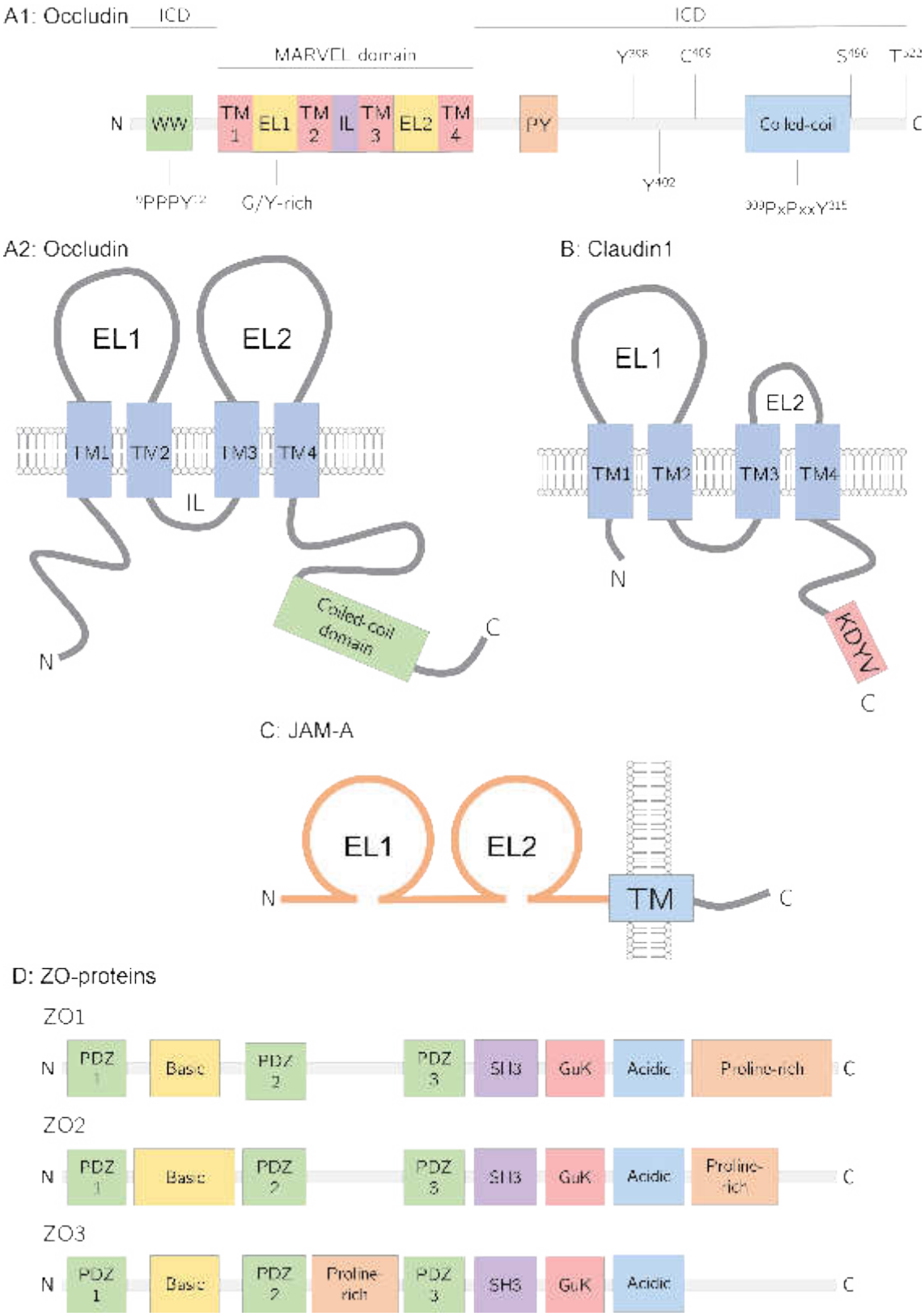

Figure 1.17: Illustration of the structure of tight junction proteins. **A1:** Occludin, drawn as linear structure. WW-motif (Itch binding domain); TM1-4 (transmembrane domains); EC1-2 (Extracellular loops 1 & 2) are rich in Glycine (G) and Tyrosine (Y); IL (Intracellular loop); PY (Nedd4-2-binding domain); Occludin can be phosphorylated at indicated positions: Y (Tyrosine), C (Cysteine), S (Serine), T (Threonine), **A2:** Depiction of occludins natural organisation. **B** Illustration of claudin1 in its natural organisation. *KDYV*-motif serves as PDZ-interaction motif. **C:** Picture of the natural organisation of JAM-A. **D:** Illustration of ZO-proteins. PDZ (PSD95-Dlg1-ZO1-domain), SH3 (Src homology 3 domain), GuK (guanylate kinase domain). The figure was adapted from Cummins[260], Krause et al.[261], Ebnet et al.[262] and Bazzoni & Dejana[263].

1.7.3 Claudins

The claudin family consists of 24 members which are distributed differently within tissues and organs. Localised on 12 different chromosomes they are encoded by at least 17 human genes and their size varies from 22 to 27 kDa depending on the type of expressed claudin[264]. One of the major functions of claudins is to regulate intercellular permeability of ions[265]. This depends on the type of claudin present, as the amino acid charge of the extracellular loops varies. It was demonstrated that altering the charges lead to changes in ion specificity of the barriers[266]. Claudins can be separated into two groups: Pore-forming or barrier-forming proteins. Typical member of tight epithelia are claudin 1, 3 and 4. These are commonly found in organs in which a tight epithelium is crucial for its natural function such as the gall bladder[267] or prostate[268]. On the other hand, claudins can increase the permeability. This is in particular important for organs or tissues, which require diffusion of ions. Diffusion of ions is an important prerequisite of homoeostasis. Claudin2 and 16 are examples of the claudin family which increase the ion permeability. Claudin2 is typically found in the crypts of small and large intestine[269]. Intestinal crypts are known to be responible for resorption of digested nutrients. Another organ which requires the exchange of ions is the kidney. Claudin16 is found in the thick ascending limb of the henle's loop, which is known for its high paracellular cation permeability[270]. It was found that especially the first extracellular loop is important for the regulation of paracellular ion permability[271].

1.7.3.1 Claudin1

Claudin1 is normally found in tissues and organs which rely on functional barriers to keep compartments separated. For example, claudin1 is found in brain endothelial cells which are characterised by a high, TJ induced, transepithelial electrical resistance and decreased paracellular permeability[272]. Another common location is in mammalian breast duct cells, where it is normally distributed across the membrane[273]. In contrast, claudin1 is normally absent in mesenchymal tissues and haematopoietic cells since these do not take part in separating tissue compartments or in forming cellular layers[274].

First experiments which demonstrated the importance of claudin1 in barrier formation were conducted by Furuse et al.[275] They generated knockout mice which lack claudin1 expression. The mice were born normally, but died within a day. The animals failed to generate TJs in the epidermis which resulted in a loss of water by evaporation. Although, the organisation of keratinocytes appeared normal, they were not able to prevent the dehydration. In control wildtype mice close examination of healthy epidermis revealed continues TJs in the stratum granulosum in which

claudin1 is concentrated. Experiments with subcutaneously applied tracer demonstrated that the dye is not able to pass through the epidermis in healthy animals. In contrast, claudin1 deficient epidermis was not able to hold the tracer back and diffused through the skin[275].

Mutations in the gene of claudin1 have been found. Affected people suffer from neonatal ichthyosis and sclerosing cholangitis (NISCH) syndrome[276]. Other symptoms include oligodontia, sclerosing cholangitis, enamel dysplasia, scaling alopecia and leukocyte vacuolisation. Only four patients with this disease have been discribed which were two inbred kindreds of Moroccan origin[277]. The affected gene was mapped to chromosome 3q27-28 which encodes claudin1. A homozygous deletion in exon 1 (position 200-201) of two nucleotides (TT) resulted in a frameshift mutation leading to a premature stop codon at amino acid 67[276]. Later a different mutation in a Swiss family was found also leading to a premature stop codon, but at a difference amino acid (on position 120)[278]. No claudin1 expression was found in the liver of these patients[276]. It appears that the predominant syndromes, ichthyosis and sclerosing cholangitis, occur due to lack of claudin1 in skin and liver[275,279]. Claudin1 is expressed in the bile canaliculi of the liver. The function of it is to transport the bile acid into the bile duct[279]. The syndrome of ichthyosis is likely due to the same reasons as in the claudin1$^{-/-}$ mice. Due to the lack of proper functioning TJs, water cannot be retained which leads to the phenotype of this disease. This highlights once more how crucial claudin1 is for barrier formation.

Scientific evidence is available to highlight that claudin1 is a key player in cell clustering. *In vitro* experiments show that claudin null cells establish cell-cell contact upon introduction of claudin1. Fibroblasts transfected with claudin1 formed strands of TJ in which claudin1 is localised[280].

Several signalling pathways have been implicated in regulating claudin1 expression. It has been demonstrated that claudin1 expression is regulated by PKC in rat choroid plexus cells[281]. Leotlela et al.[281] demonstrated in melanoma cells a direct correlation of PKC activity and claudin1 expression. They also showed that in endogenous cells lacking claudin1, phorbol myristic acid (PMA) treatment induced PKC mediated upregulation of claudin1 expression. Concomitantly, inhibition of PKC led to reduced claudin1 expression. In intestinal epithelial cells, stimulation by TNFα increased claudin1 expression[282]. It was also found that HIF1β mediates intestinal epithelial TJ integrity by regulation of claudin1[283].

For a long time it was believed that the C-terminal PDZ-binding motif of claudin1 is responsible for membrane localisation. However, Rüffer and Gerke[284] demonstrated that C-terminal deletion mutants (ΔKDYV) continued to localise at the apical TJs. Removal of the entire C-terminal domain led to mislocalisation in the cytoplasm. This suggests that the residues C-terminal to the last transmembrane domain are

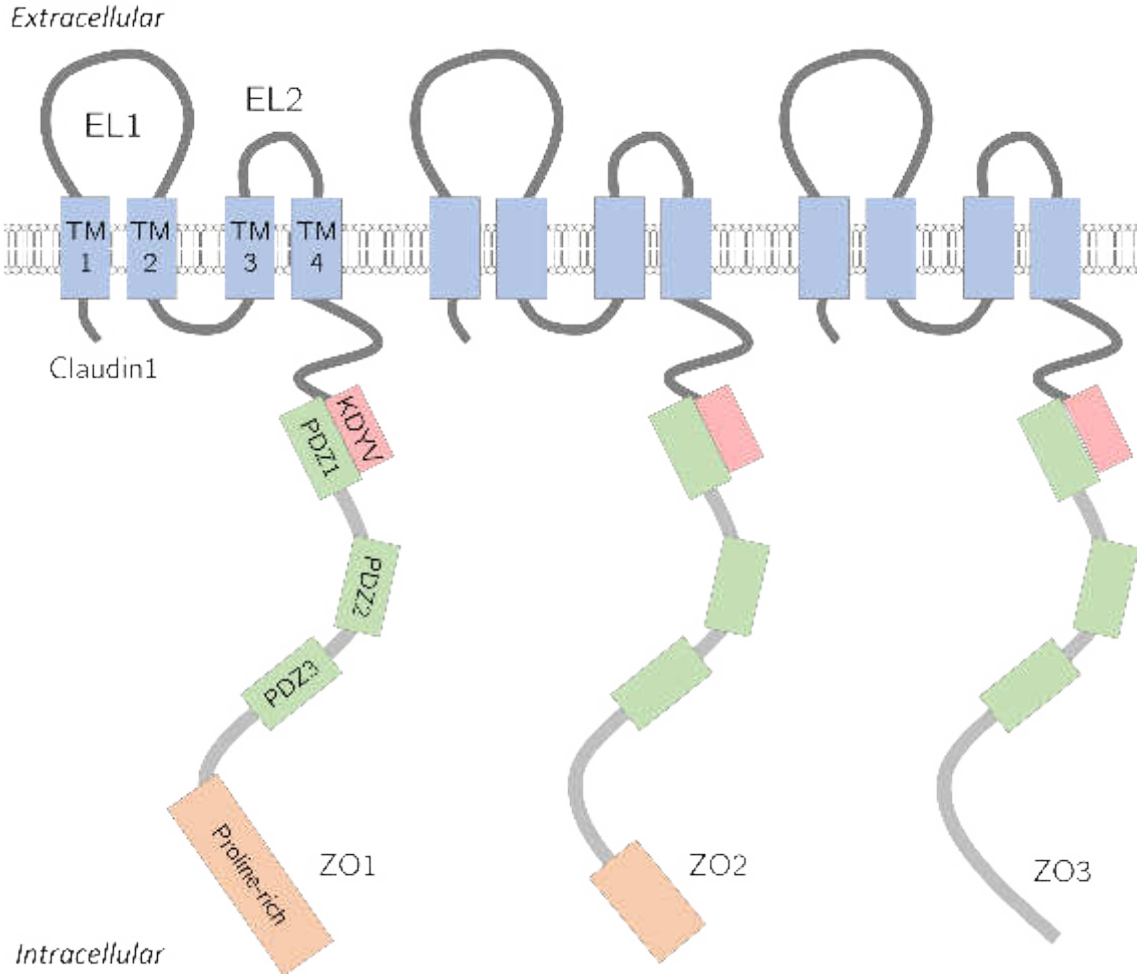

Figure 1.18: Illustration of the interaction between claudin1 and ZO1. Claudin1 is a transmembrane protein with two extracellular loops. The C-terminal KDYV-domain of claudin1 interacts with the N-terminal PDZ (PDZ1) domain of the ZO1/ZO2/ZO3[291]. The latter are obligate intracellular proteins and connect the TJ proteins to the actin cytoskeleton. EL1-2 (Extracellular loops 1 & 2) are rich in Glycine (G) and Tyrosine (Y); TM1-4 (Transmembrane domain 1-4); PDZ (PSD95-Dlg1-ZO1-domain); KDYV (Lysine-Aspartic acid-Tyrosine-Valine, binds to PDZ domain).

crucial for membrane homing. Besides, the C-terminal tail contains Ser/Thr/Tyr phosphorylation sites[285]. Phosphorylation of claudin1 by MAPK[286] or PKC[287] promotes barrier function in TJs.

All interaction partners of claudin1 bind via their PDZ-domains to the KDYV-motif. An illustration of three proteins, ZO1, ZO2 and ZO3 is shown in figure 1.18. The ZO proteins possess three PDZ domains, but the interaction with claudin1 is mediated by the N-terminal PDZ1 domain[262]. The ZO proteins connect claudin1, and other TJ proteins, to the actin cytoskeleton. Another claudin1 binding partner is the multi-PDZ domain protein 1 (MUPP1)[262], it is involved in opioid tolerance and opioid-induced hyperalgesia[288] and the regulation of olfactory sensory neurons[289]. It has also been reported that claudin1 forms a complex with CD81, a member of the tetraspanin family, so serve as a co-receptor for HCV entry[290].

As previously mentioned the first extracellular loop of claudin1 has a particular

importance regulating ion permeability. However, it is not only important for homoeostasis, but it also serves as viral receptor for Dengue[292] and Hepatitis C virus (HCV)[293]. Since claudin1 appears to be essential for many physiological processes, dysregulation has drastic effects in pathology.

Dysregulation of claudin1 is observed in many diseases. It is one of the few claudins which are expressed continuously throughout the intestine[294]. Thus it was found that several diseases affecting the intestine show abnormal expression of claudin1. In ulcerative colitis the expression of claudin1 is elevated[282,295]. The rate of inflammation plays a role in rate of expression. Severely inflamed tissues obtained at biopsy showed higher claudin1 expression compared to slightly inflamed samples[295]. On the other hand, in irritable bowel syndrome (IBS) claudin1 expression is decreased[296]. In correlation with reduced claudin1 expression, the intestinal permeability was increased. Compared to healthy biopsies, claudin1 localisation shifted towards the cytoplasm in colonic mucosa tissue in IBS[296]. This emphasises that not only the expression, but also localisation of claudin1 is important in disease progression. The most dysregulation of claudin1 has been observed in cancer. Loss and gain has been associated with several types of cancer. Claudin1 upregulation was observed in thyroid[297], pancreatic[298], colorectal[299] and gastric cancer[300]. Contrary, downregulation has been observed in liver[301,302], lung[303] and breast cancer[304].

It has been hypothesised that claudin1 acts as a tumour suppressor in invasive human breast cancer. First evidence was demonstrated by the reexpression of claudin1 in breast cancer spheroids, which induces apoptosis[305]. MDA-MB-361 cells were transduced with claudin1 leading to to prominent membrane localisation correlated with the rate of apoptosis. In parallel, it was observed that the paracellular diffusion rate was reduced[306]. Together this suggests that loss of claudin1 membrane localisation contributes to tumour progression. The importance of claudin1 seems to be the limitation of the influx of nutrients and growth factors in breast cancer cells. In normal epithelial breast cells loss of claudin1 led to neoplastic transformation[307]. Interestingly, this was found by deletion of the mitochondrial DNA (mtDNA) which suggest claudin1 regulation is downstream of the oxidative phosphorylation chain. A study with patients observed a correlation of decreased claudin1 expression and recurrent disease[308]. The immunohistochemical expression of claudin1 in 83 patients was observed. 26 patients with recurring breast cancer showed significantly lower expression of claudin1 compared to the group of non-recurrent disease. Decreased expression correlated with short RFS. The expression pattern was also significantly lower in node positive patients. Therefore claudin1 expression correlates with the status of recurrence and the malignant potential of breast cancer[308]. Later, a larger study using tissue microarray found differential claudin1 expression in ER+ve and -ve samples. Significantly more ER+ve tumours express claudin1 compared to ER-

ve ones[56]. Considering ER-ve cancer is more aggressive than ER+ve, it supports the hypothesis of claudin1 beeing a tumour suppressor. Although less common, loss in ER+ve occurs. Experiments about the mechanisms have been conducted. One study was searching for mutations in the promoter and coding regions of CLDN1, but none were found[304]. Recent work suggests that methylation of CpG islands in the promoter region of claudin1 is associated with low expression of claudin1[309]. Another mechanism regulating claudin1 expression involves miRNAs. In ovarian cancer cells miR-155 was found to decrease claudin1 levels at mRNA and protein level[310]. Concomitantly, miR-155 mediated suppression of claudin1 reduced proliferation and invasion of these cells[310]. On the other hand, elevated levels of miR-155 were found in blood samples of breast cancer patients were it is associated with cancer progression[311,312]. Thus, in breast cancer miR-155 might play a role in downregulating claudin1.

Apart from the previously discussed subtypes of breast cancer a novel subset was proposed which is characterised by the high levels of claudin1 and reviewed by Myal et al.[264]. Over- and underexpression of claudin1 in breast cancer has been reported which emphasises how complex its role in cancer pathology is. Despite supporting evidence that claudin1 functions as a tumour suppressor there is also proof for otherwise. It was found that ER-ve breast cancers had frequently more claudin1 positive tumours than ER+ve cancers[56]. The same group could also show that claudin1 positivity is associated with BLBC[56]. Myal et al. have proposed that during tumourigenesis claudin1 expression is not lost in all tumour cells. Furthermore they suggest that cells retaining claudin1 expression are predetermined to become ER-ve BLBC. In these cells claudin1 would not take the role of a tumour suppressor, but a tumour promoter. In order to explain the evolution of breast cancer two hypothetical models were proposed: A linear model in which different subtypes originate from the same cell which means these subtypes are acquired by genetic and epigentics. The non linear model suggests the different subtypes originate from different cells such as stem or progenitor cells[313]. Believing in the linear model would question whether the increased frequency of claudin1 in ER-ve cancer[56] occurred due to re-expression of claudin1. This turns the tumour suppressor properties into tumour enhancing. The causes of re-expression would be caused by genetic mutation or epigenetic modification of the claudin1 gene. In hereditary and sporadic breast cancer sequence analysis of of the CLDN1 coding region did not identify any significant changes[304]. Myal et al. suggest that accumulation of claudin1 may be due to a defective interaction with claudin1 binding partners. It may accumulate in the cytoplasm if the transportation to the membrane is distorted where it may escape downregulation by other molecules. In addition, it is thought that the strength of tight junctions is determined by the exact combination of expressed claudins[314].

Therefore, a consequence of accumulation of claudin1 in ER-ve breast cancer could be due to an altered composition of TJ proteins. Taken together claudin1 is a fascinating protein and the evidence on both functioning as tumour suppressor and enhancer makes it even more interesting.

It has been demonstrated the claudin1 is also involved in EMT. Claudin1 induced MAPK/Erk-pathway mediated EMT in human liver cells through activation of Slug and ZEB1[315]. In colon cancer, claudin1 upregulates ZEB1 via PI3K/Akt-pathway which results in reduced E-cadherin expression[316]. In breast cancer, claudin1 up-[317] and downregulation[59] have also been shown to modulate the expression of several EMT related genes[317]. In contrast to colon cancer, overexpression of claudin1 downregulates ZEB1 in MCF7 cells[317]. This shows that claudin1 has an effect on EMT, but is cancer type dependent. It has also been demonstrated that claudin1 is regulated by EMT markers. Slug and snail, which are able to repress transcription of claudin1 by binding to the E boxes within the promoter[318].

In cancer it was observed that claudin1 deregulates certain MMPs which results in increased motility and invasiveness[319,320]. In breast cancer, direct interaction of claudin1 and MMPs have been shown. The interaction is crucial for MMP1 and proMMP2 activation[319]. This suggests that claudin1 may play a role in matrix degradation during cell invasion.

Due to the natural functions of claudin1 it is believed that it also plays a role in collective cell migration. Cancer cell migration is generally distinguished by two characteristics: Single cell or collective cell migration. During single cell migration one cell detaches from the tumour and re-localises to distant tissue or organs where it starts to metastasise. Gain of mesenchymal characteristics and/or loss of polarity facilitate this progress[321]. Contrary, collective cell migration is characterised by the movement of whole cell clusters. They maintain cell-cell junctions, form protrusions, use cell-matrix adhesion receptors, form focal adhesions, utilise proteolytic breakdown of ECM components and use the actin-myosin machinery for cell movement[321].

There is scientific evidence that claudin1 is involved in collective cell migration. It has been demonstrated that loss of keratin 8 and 18 leads to EMT marker independent upregulation of claudin1. Concomitantly, cells increase collective cell migration and invasiveness[322]. Keratin 8 and 18 are proteins of epithelial cell-specific intermediate filaments. Their loss during EMT is associated with tumour chemoresistance and metastasis. Keratin depleted cells showed hyperactivation of the PI3K/Akt/NFκB signalling pathway as well as increased MMP2 and 9 expression[322].

Immunohistochemical analysis of ductal carcinoma cells showed either complete loss of claudin1 or a scattered distribution among these cells[273]. Contrary, in apocrine

metaplasia, a benign cystic breast disorder, claudin1 membrane localisation was frequently observed[273]. In colon cancer, particularly in metastatic lesions, claudin1 is upregulated and frequently mislocalised from the cell membrane to the cytoplasm and nucleus[301]. Majority of human colorectal carcinomas possess a mutation in the gene of adenomatous polyposis coli (APC), a negative regulator controlling β-catenin expression[323]. Interestingly, those cell lines with APC mutations upregulate claudin1 expression. This confirms the fact that claudin1 is a probably target of β-catein/Tcf signalling[299]. However, it was found that some cell lines with wildtype APC do not have detecable levels of claudin1, even with a mutation which stabilises β-catenin[301]. This suggests the involvement of other mechanisms underlying claudin1 modulation. Active β-catein/Tcf is not sufficient to activate claudin1 expression. Due to the clinical implications of claudin1 it is suggested as tumour marker and potential therapeutic target. Treatment of anti-claudin antibodies inhibited cell growth of metastatic colorectal cancer xenograft in mice[324]. Increased levels in MCF7 breast cancer cells decreased survival and rendered these cells more susceptible to several anti cancer drugs[317]. Soini[274] proposed to use claudins as marker for tumours. The expression profile of claudin1, together with claudin2, 3, 4, 5 and 7 can be used to distinguish melanocytic lesions, as well as lymphoid and soft tissue tumours. Apart from cancer, claudin1 is involved in viral diseases, especially in the uptake of HCV. Also for viral diseases claudin1 should be considered to be a therapeutic target, because the uptake of HCV can be blocked by a monoclonal antibody against the EL1 of claudin1[325].

1.8 The PI3K/Akt/mTOR pathway

The phosphatidylinositol-3-kinase (PI3K)/Akt/Mechanistic target of rapamycin (mTOR) pathway is involved in various processes such as cellular metabolism, growth, proliferation, metastasis and cytoskeletal reorganisation[326].

PI3K is a heterodimeric kinase consisting of a regulatory p85 and a catalytic p110 subunit. An illustration of the two subunits is depicted in figure 1.19. The catalytic subunit consists of an N-terminal p85-binding motif, a Ras-binding motif, a C2 domain, a helical domain followed by the catalytical domain[327]. The function of C2 domains are to target the protein to the cell membrane[328]. The helical domain acts as scaffold[329]. p85 contains an SH3 domain, a BH (B-cell lymphoma 2 (Bcl2) homology) domain which is flanked by proline-rich regions at each end, and a p110-binding domain flanked by two SH2 domains. The SH3 domain interacts with PXXP-motifs[330] while the SH2 domains bind to phosphotyrosines within the YXXM-motif[331]. The BH domain interacts with the Rho family proteins Cdc42 and Rac1[332,333]. Two of the major kinases in this pathway are Akt and the Ser/Thr

kinase phosphoinositide-dependent kinase 1 (PDK1). The schematic representation is also shown in figure 1.19. The pleckstrin homology (PH) domains of PDK1 and Akt are the binding motifs for $PIP_{2/3}$. interaction[334].

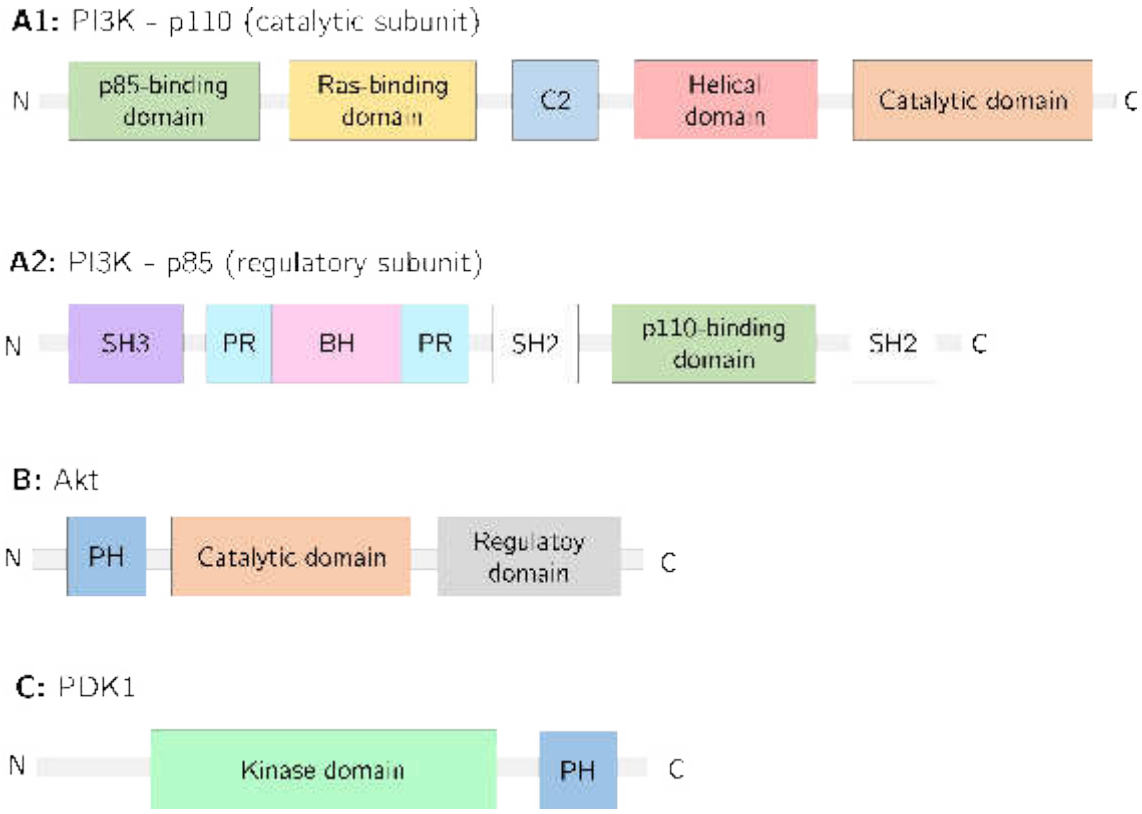

Figure 1.19: Illustration of PI3K and its activator Akt. **A1:** Schematic of p110 - the catalytic subunit. It consists of a p85-binding- , a Ras-binding-, a C2-, a helical- and catalytic domain. **A2:** The regulator subunit p85 contains an SH3 motif, a BH-domain flanked by proline-rich regions (PR) and a p110-binding domain flanked by SH2 motifs. **B:** Scheme of Akt which comprises a pleckstrin homology (PH)-. followed by a catalytic-, and regulatory domain. **C:** PDK1 consists of a kinase- and PH-domain. The image is adapted from Vanhaesebroeck et al. in *The emerging mechanisms of isoform-specific PI3K signalling*, Nature reviews: Molecular cell biology, 2010[335]

mTOR is a multidomain Serine/Threonine kinase which belongs to the PI3K-related kinase (PIKK) family[336]. It is highly conserved in various species[336,337]. The mTOR was identified after the drug rapamycin had been discovered. Section 2.8.2 describes rapamycin and other drugs in more detail. mTOR is the catalytic subunit of two distinct protein complexes: mTORC1 and mTORC2. A simplified scheme is shown in figure 1.20. The mTOR complexes are defined by their association with the scaffold proteins regulatory-associated protein of mTOR (Raptor) and rapamycin-insensitive companion of mTOR (Rictor). Raptor only associates with mTORC1 whereas Rictor associates with mTORC2. There are also additional components which are exclusive to individual complexes. mTORC1 associates with proline-rich Akt substrate 40 kDa (PRAS40) whereas mTORC2 contains mammalian stress-activated protein kinase-interacting protein 1 (mSIN1) and protein observed with Rictor (Protor). Both complexes also share common

regulatory components such as mammalian lethal with SEC13 protein 8 (mLST8) and DEP domain-containing mTOR-interacting protein (DEPTOR)[338].

Raptor is a 150 kDa adaptor protein for mTOR and constitutively bound to mTORC1. It is crucial for its activity and essential in regulating mTORC1. Upon stimulation of insulin or other upstream activators mTOR phosphorylates Raptor at Ser863[339]. PRAS40 is a 40 kDa substrate of Akt. It has proline-rich regions and is a negative regulator of mTORC1. In unphosphorylated state it binds to mTORC1 and blocks the interaction of Rheb GTPase. Upon insulin stimulation Akt phosphorylates PRAS40 which disassociates from mTORC1 allowing its activation[339].

Deptor is an 48 kDa endogenous inhibitor of mTOR. mTOR can directly interact with Deptor which expression is negatively regulated by mTORC1 and mTORC2[340]. Suppression of Deptor leads to reduced mTORC activity. In multiple myeloma disease Deptor is overexpressed and crucial for the survival of the myeloma cells, because downregulations induces apoptosis. *In vitro* activity of 4E-BP1 and S6K1 is reduced upon depletion of Deptor[340].

mLST8 is a 36 kDa regulator protein. It can directly interact with mTOR. The full kinase activity of mTOR is only achieved by binding mLST8. However, the interaction is only essential for mTORC2 since the knockdown of mLST8 caused disruption of the mTOR/Rictor complex, but did not affect the mTOR/Raptor interaction[341].

mSIN1 acts as scaffolding protein since ablation of SIN1 disrupts mTOR-Rictor interaction in yeast[342]. It is also required for mTORC2 mediated Akt phosphorylation at Ser473[342,343]. The FRB binding site of mTOR is a specific binding site for FKBP12, a protein which belongs to the family of peptidylprolyl isomerases[344]. Beside the function as isomerase FKBP12 also functions as chaperone[345].

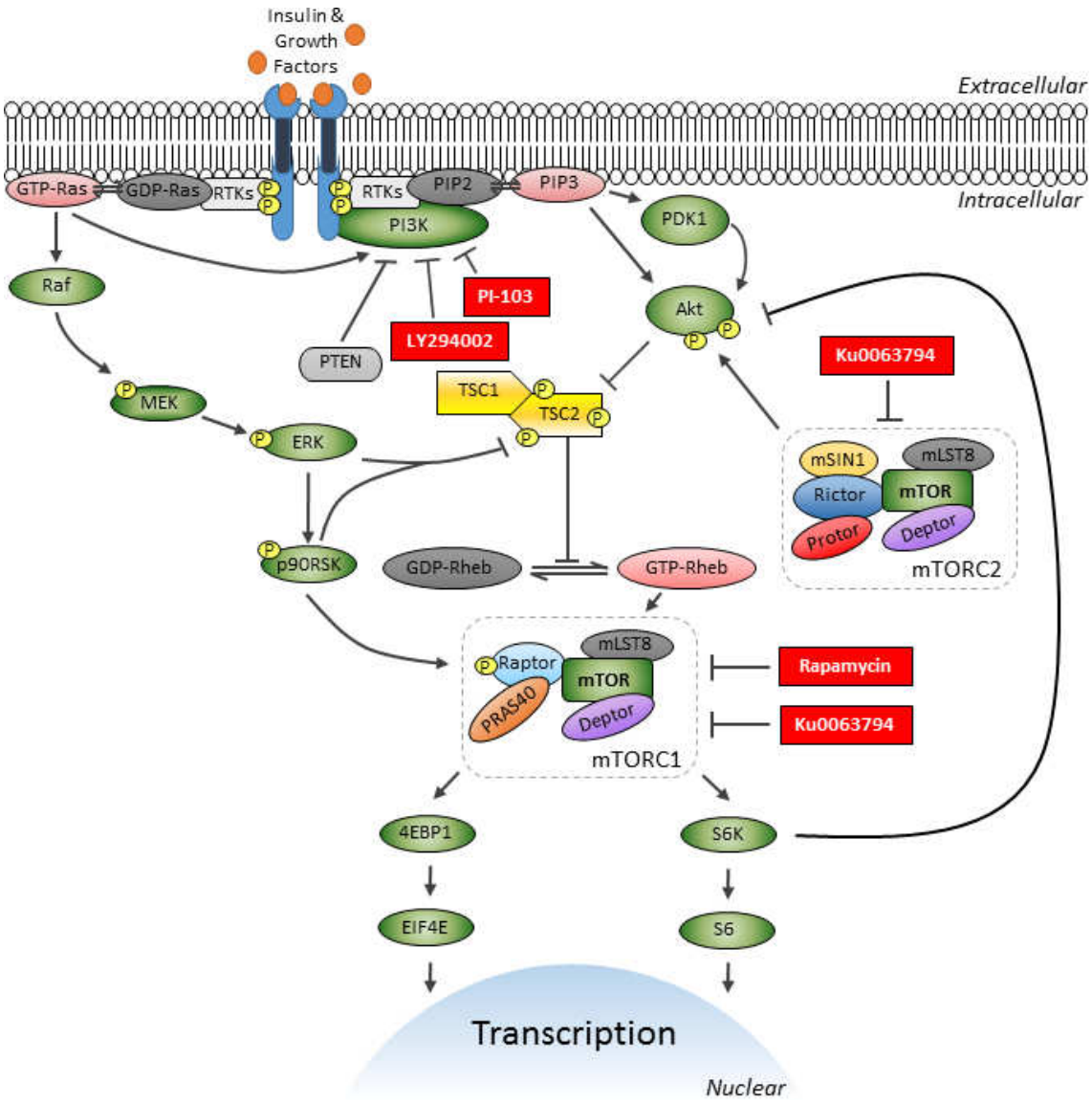

Figure 1.20: Schematic representation of the PI3K/mTOR pathway. Pharmacologcial inhibitors are displayed as a red squared box. Arrows indicate the activation or phosphorylation (P) of a downstream molecule. Lines with horizontal bar indicated inhibition of downstream target.

The PI3K/mTOR pathway is activated downstream of RTKs such as Erb family receptors, FGFR and IGF-1R[346,347]. PI3K is also stimulated by the catalytic domain of the small GTPase RAS[348]. An illustration of the pathway is depicted in figure 1.20. Activated PI3K translocates to the plasma membrane and phosphorylates phosphatidylinositol 4,5-bisphosphate (PIP_2) to phosphatidylinositol 3,4,5-triphosphate (PIP3)[329]. PIP_3 activates PDK1[334] as well as Akt. Partial activation of Akt is also done by PDK1 on Thr308[349], but full activation of Akt is mediated by mTORC2 at Ser473[350]. Activated Akt phosphorylates tuberous sclerosis complex 2 (TSC2) which causes the disruption of the TSC1/TSC2 complex. This complex serves as GAP for Ras homologue enriched in brain (RHEB) GTPase, because TSC1/TSC2 interaction causes hydrolysis of Rheb which remains in its in-

active GDP bound state[351]. Upon inactivation of TSC1/TSC2 complex GTP-Rheb phosphorylates mTORC1 which leads to its activation. Active mTORC1 leads to elevated protein synthesis by eukaryotic initiation factor 4E (EIF4E)-binding proteins (4E-BP1) and ribosomal protein S6 kinase.
Termination of PI3K signalling is achieved by different mechanisms. The most common mechanism is interference with PIP_2/PIP_3 conversion or the dephosphorylation of Akt. The SH2-containing phosphatases (SHIP1 and SHIP2) can bind to the 5th position of the inositol ring of PIP_3. Dephosphorylation leads to PIP_2 which renders it inactive again[349]. Also the conversion of PIP_2 to PIP_3 can be antagonised by the phosphatase and tensin homolog (PTEN) which dephosphorylates PIP_3 to PIP_2[352]. Therefore, the loss of PTEN activates both mTORC1 an 2[340]. The other mechanism comprises direct interaction with Akt. Dephosphorylation of Akt at Thr308 by PP2A[353] and at Ser473 by PH domain leucine-rich repeat protein phosphatase 1 and 2 (PHLPP1/2). A schematic representation of mTOR is depicted below (figure 1.21).

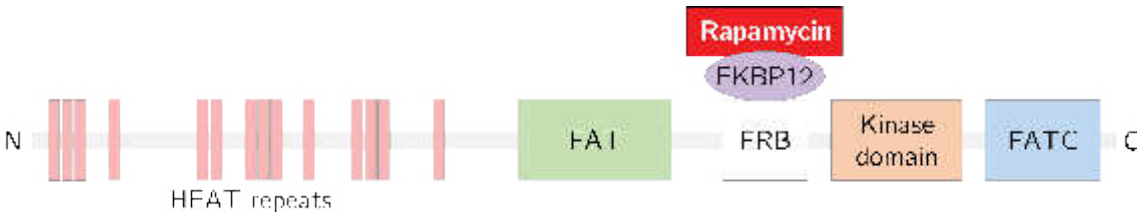

Figure 1.21: Schematic overview of mTOR. Several HEAT repeats cand be found followed by a FAT domain. The FRB is the specific binding site for FKBP12. FKBP12 is the target of Rapamycin. The kinase domain lies adjacent priot to the c-terminal FAT domain (FATC). The illustration is adapted from Cargnello et al., *The expanding role of mTOR in cancer cell growth and proliferation*, Mutagenesis, 2015[338].

In intestinal porcine epithelial cells (IPEC) L-Tryptophan induced mRNA upregulation of tight junction proteins via mTOR activation[354]. Upregulation of occludin, claudin1, ZO1 and ZO2 were observed, but expression of claudin1 and ZO3 were unaffected. A new paper from 2016 demonstrated that in IPEC cells glucagon-like peptide-2 (GLP-2) promotes claudin1, ZO1 and occludin expression via the PI3K/mTOR pathway[355]. GLP-2 is an intestinotrophic growth hormone that facilitates the biological function of the intestines.

1.9 Integrins - cellular bridges

Integrins are heterodimeric transmembrane receptors mediating cell attachment to the ECM. They consist of non-covalently bound α- and β-subunits. To date, 18 α- and 8 β-subunits are known. In mammals 24 different integrin heterodimers exist.

Both subunits are single transmembrane glycoproteins with a short C-terminal ICD (about 50 amino acids) and large N-terminal ECD (over 700 amino acids). The familiy of integrins comprises many cell surface receptors which interact with several ECM components such as collagens, fibronectin (FN), laminins and vitronectin (VN) via their extracellular portion[356]. Almost all integrin heterodimers associate via their β-chain with the cytosolic talin. The ICD binds to different cytoplasmic proteins which establish interaction to the actin cytoskeleton. Unlike kinases, which are activated via phosphorylation, integrin activation is mediated via a conformational change. Integrins can be in a folded (inactive) or unfolded (active) state. During the inactive state, both α- and β-chains are in close proximity and adhere to each other. Upon unfolding of the ECD the contact is abolished and the transmembrane domain and ICD move apart. This exposes the binding site for talin. Binding of talin induces actin assembly at the ICD complex of the integrin as well as a sequence of intracellular signalling events such as Src and focal adhesion kinase (FAK) phosphorylation. The process when integrins activate intracellular signalling events, induced by extracellular matrix ligation, are referred to as "outside-in signalling". Talin competes with the α-subunit for β-chain interaction. When talin binds to the β-subunit the heterodimer separates. The extracellular portion extends and goes into active confirmation which allows ligand interaction. This process is referred to as "inside-out signalling". However, "inside-out signalling" can also be induced via external regulators. One example is the signalling molecule phosphatidylinositol 4,5-bisphosphate (PIP_2) which is expressed in response to receptor activation. PIP_2 activation can be induced by G-protein coupled receptors (GPCRs) or RTKs[357]. The affinity and ligand specificity of integrins can be influenced by the divalent-cation-binding domain, present in both α– and β-chain. Therefore, extracellular concentration of Mg^{2+} and Ca^{2+} affect integrin activity. Integrin-induced adhesion signalling pathways can activate cytoskeletal reorganisation and alter gene expression by outside-in or inside-out activation[358].
Since its is known that ADAM15 interacts via its RGD motif with α5β1[114] and αvβ3[114,115] as well as RGD-independently to α9β1[359], I will focus on the functions of the subunits involved in this interaction.

1.9.1 Integrin subunits

1.9.1.1 α5

Loss of function mutations that occur in the murine α5 gene caused embryonic death if present on both alleles. This was observed after interbreeding of mice which were heterozygous for the α5 mutation. From 120 liveborn progenies none were homozygous for α5 mutation. Embryos homozygous for the mutation were identified by

southern blot analysis. All of them showed deformations from day 8.5 to 10.5. At day 10.5 the number of homozygous mutated embryos was reduced and displayed deterioration. At day 11.5 to 12.5 no homozygous mutated embryos were found which suggested that they die around day 11.[360]. Examination of histological specimens revealed that posterior trunk regions have defects in neural tube and the mesoderm. Also defects of vascularisation were observed since the formation of blood vessels was impaired.
The only known integrin heterodimer containing an α5 subunit is α5β1 that specifically interacts with the RGD motif in FN. The fact that the mutant embryos die that early in development points out how important α5β1 is for embryogenesis, even when there are several other integrins mediating adhesion to FN. This suggests α5β1 has unique functions other than FN binding. Indeed, tissue sections from α5-null embryos showed expression of FN and the FN-matrix pattern was indistinguishable. Additionally, no differences were observed in FA formation when analysed by vinculin and talin analysis. It seems the function of α5 is essential in some processes such as embryogenesis in which other integrins fail to compensate the loss. Contrary, in other events as assembly of FN matrices or formation of focal adhesions (FA) the lack of α5 can be compensated.

1.9.1.2 α9

The α9 subunit only associates with β1 to form the α9β1 integrin receptor. This heterodimer interacts with the ECM proteins osteopontin and tenacsin C as well as vascular cell adhesion molecule-1 (VCAM1). Expression of the receptor was observed in hepatocytes, smooth muscle cells and some epithelia.
Mice which are deficient in α9 were born alive, but showed signs of respiratory distress between 6 and 12 days of age. Within 2 days after onset of this symptom the mice died. The reason of death was found to be chylothorax, an obstruction of the thoracic duct. This causes the space between chest wall and lung to be filled with milky fluid high in triglycerides. In addition a high concentration of cholesterol and a high number of lymphocytes were found. Histological analysis of the chest wall revealed accumulation of inflammatory cells accompanied with oedema.
These results suggest that α9 integrin is crucial for development of the lymphatic system including the thoracic duct.[361]

1.9.1.3 αv

αv-subunits are widely expressed. They are expressed in neural crest cells, glia cells, muscle cells, osteoclasts, epithelia, blood vessels during development and in angiogenic tumours[362].

In 80% of the mice αv ablation is lethal. However, all embryos develop normally to stage E9.5, and only 20% were born alive, but died at the day of birth. By E10.5 the majority of embryos exhibited pericardial oedema and deteriorated at E11.5. While the vascularisation of the yolk sac was normal, abnormalities of the placenta were observed. Specifically, αv-null placenta had reduced labyrinthine zones. The proportion of born progenies suffered from intestinal and intracerebral haemorrhages. This condition became more serious with increasing age. No other organs showed haemorrhage and were well vascularised. Additionally, postnatal mice exhibit cleft palates[362].

1.9.1.4 β1

The β1 subunit associates with at least ten different α-chains and is the largest integrin subfamily. β1 family integrins are considered as particularly important in embryogenesis where they mediate adhesion and provide positional information for morphogenesis.
This is confirmed by the generation of β1-null mice since deficiency caused lethality shortly after implantation of the embryo[363]. In order to determine whether the β1 gene is essential for early embryonic development (until E3.5) blastocysts of heterozygous females, which were mated with heterozygous males, were isolated. About a fifth of the blastocysts were homozygous for β1 mutation. This suggests that the β1 gene is not crucial in the very early stage of embryogenesis[363]. In another experiment chimeric β1-deficient mice were generated from two independent β1-null embryonic stem cells (ES cells). Histological examination of E8.5 embryos found labeled ES cells in all germ layers suggesting that cells differentiate and migrate normally[363]. β1-deficient cells were found in all analysed regions, suggesting that migration of neuronal cells can occur in the absence of β1 containing integrins.
Separately, Stephens et al. demonstrated that absence of β1 is lethal during early postimplantation development[364]. *In vitro*, β1-null embryos were able to form blastocysts which outgrew normal trophoblasts. They were indistinguishable to the wildtype and heterozygous embryos. However, during the experiment the inner cell mass of the blastocyst was smaller and disorganised compared to the control embryos. These experiments further confirmed the importance of β1-chains in normal embryogenic development.

1.9.1.5 β3

The β3-subfamily comprises αvβ3 and αIIbβ3 which have been implicated in a variety of functions. This includes thrombosis and platelet aggregation for αIIbβ3 integrin. For αvβ3 integrin it includes implantation, placentation, bone remodeling, angiogen-

esis and tumour progression.
β3-deficient mice are viable and fertile. However, they show all symptoms of the Glanzmann thrombasthenia - the human bleeding disorder. Their symptoms comprise clot retraction and platelet aggregation, prolonged bleeding as well as cutaneous and gastrointestinal bleeding[365]. Implantation of the embryo appears independent of β3, but placental defects occurred which lead to foetal mortality. As a consequence of the haemorrhaging anaemia lead to reduced postnatal survival. It has been reported that retinal neovascularisation of newborn mice is inhibited by peptides which block αvβ3 function[366]. However, this observation could not be confirmed since the pattern of the neovascularised vessel of the β3-null mice did not show differences to the control mice. This suggests that this mechanism is independent of the β3-chains. β3-integrins are involved in locomotion, shape, cell signalling and cell cycle regulation.

1.9.2 Integrin endocytosis

The presence of integrins on the membrane is crucial for various cell functions. Thus the control of availability at this compartment is important. Internalisation is a crucial mechanism in which integrins are withdrawn from the membrane. In general endocytosis is separated into two groups: Clathrin-dependent and clathrin-independent endocytosis. Both will be discussed in detail below. Clathrin-coated vesicles (CCV) are crucial for membrane trafficking in cells and do not only transport integrins. Clathrin forms a triskelion shape which is composed of three 190 kDa heavy and three 25 kDa light chains as illustrated in figure 1.22 a. The heavy chains provide a structural backbone whereas the light chains regulate assembly and disassembly of the lattice. Each arm consists of the following parts, starting from the centre: Proximal segment, knee, distal segment, ankle, linker and terminal domain. Interaction of triskelia leads to formation of a polyhedral lattice which surrounds the vesicle. The triskelia can form different structures as illustrated in 1.22 b. The mini-coat is made up of 28 triskelia and has a tetrahedral symmetry. The hexagonal barrel structures contain 36 triskelia with D6 (six-sided dice) symmetry. The soccer ball structure comprises 60 triskelia with icosahedral symmetry[367].

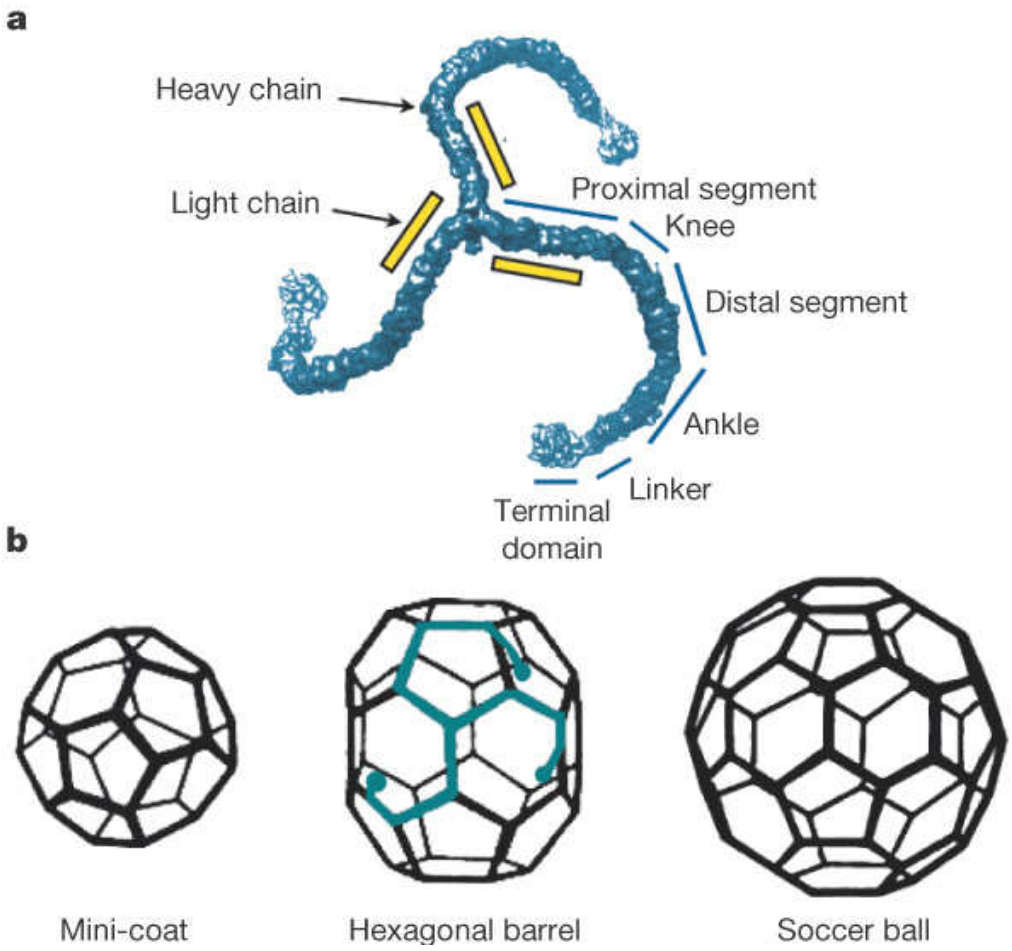

Figure 1.22: Illustration of the clathrin triskelion including examples of different lattices. **a)** Triskelion with labeled segements of the heavy chain (blue). Order from N- to C-terminus towards the vertex: Terminal domain, linker, ankle, distal segment, knee, proximal segment. The schematic positions of the light chains is indicated in yellow. **b)** Assembled structures of clathrin formed *in vitro*. Mini-coats show a tetrahedral symmetry; Hexagonal barrel show a D6 symmetry; Soccer ball show a icosahedral symmetry. A triskelion is highlighted in blue in the hexagonal barrel. the image was taken from Fotin et al, *Molecular model for a complete clathrin lattice from electron cryomicroscopy*, Nature, 2004[367].

1.9.2.1 Clathrin-dependent endocytosis

In general, the clathrin-dependant integrin internalisation mechanism is better understood and characterised when compared with the clathrin-independent mechanism. The ICD of integrin β-chains contain NXXY-motifs. This motif recruits transmembrane receptors to CCV through interaction with adaptor proteins such as AP2 adaptor complex[368]. Other adaptor proteins such as disabled (Dab) and protein numb homologue contain phosphotyrosine-binding (PTB) domains which can bind to to NPXY-motifs[369]. Both contribute to the endocytosis of integrins. Numb can associate directly with β1- and β3-integrins. Knockdown of numb inhibits internalisation of α5β1 and αvβ3 by modulation of proteinase-activated receptor 3 (PAR3)-protein kinase C ζ (PKCζ) signalling. Studies found another adaptor protein, disabled homologue 2 (Dab2), involved in clathrin-dependent β1 endocyto-

sis[370]. Quantitative proteomic analysis showed that β1-integrins are the preferred cargo of Dab2-mediated endocytosis since these were the main proteins depleted from the cell membrane[371]. β1-integrins are recruited to Dab2-rich clathrin-coated structures (CCS) were they get internalised. Clathrin, Dab2 and AP2 are recruited to the adhesion sites, followed by integrin endocytosis into CCS[370]. Experiments with conformation-specific antibodies showed that only active β1-integrins are endocytosed during FA disassembly[370]. Neuropilin 1 (Nrp1) directly associates and protmotes α5β1-mediated endothelial cell adhesion to FN at adhesion sites. Nrp1 is a transmembrane glycoprotein that is expressed on endothelial cells, neurons, different types of tumours and tumour-derived cell lines. In Ras-related protein (Rab) 5-positive early endosomes, the serine-glutamic acid-alanin (SEA)-motif of Nrp1 binds to the homomultimeric endocytic adaptor Gα interacting protein (GAIP)-interacting C terminus, member 1 (GIPC1) which selectively stimulates the internalisation of active α5β1[372]. Nrp1 dependent internalisation of integrins occur along fibrillar adhesions. Fibrillar adhesions are highly matured and not generally seen in migrating cells. They are characterised by large stress fibers and underlying fibrillar FN. Internalisation of α5β1-NRP1 complexes also require the recruitment of myosinVI. It links GIPC1 to the SEA-motif of Nrp1. This bridges the myosin motor to the integrin and assists in the formation and transportation of endocytic vesicles across actin filaments[372].

It was believed that the integrin levels on the membrane dictate the speed of migration. However it was found that the internal pool of integrins is responsible and not the cell surface level[371]. A reason could be that the internal pool might get recycled and contribute to new focal contacts at the leading edge. It still needs to be investigated at which cellular location clathrin-dependent endocytosis occurs. It has been reported that it occurs only near FA[373], at the apical surface[374] or at the entire cell surface[371].

1.9.2.2 Clathrin-independent endocytosis

Both, α5β1 and αvβ3 are endocytosed via CCS, but internalisation can also occur via different routes. It has been shown that α5β1 can be endocytosed independently of the NXXY-motif and clathrin by upregulating Rab21[375]. Clathrin and NXXY-motif independent endocytosis seems to occur via cholesterol-sensitive caveolar routes which can be activated by Rab21[376]. In myofibroblasts and endothelial cells, α5β1 and αvβ3 localise to caveolae, cholesterol-containing membrane structures. Despite the fact that these integrins have been shown to be internalised by CCV it has also been demosntrated that β1-integrin is endocytosed via a clathrin-independent, but caveolin1 mediated route[377]. Another route which has long been known to regulate integrin endocytosis is via the direct interaction of PKCα and the ICD of

β1-integrin[378]. Prior to internalisation, the β1-chain is trafficked to an endosomal compartment via a Ca^{2+}/PI3K/dynamin1-dependent route. It is assumed that this happens through prolonged clustering of integrins, demonstrated with α2β1. Antibody-induced clustering of this integrin induced a lateral movement along actin filaments on the cell surface. Small clusters are fused together during this lateral movement and were subsequently internalised into caveosome-like perinuclear structures mediated via PKCα activity[379]. In primary neutrophils, it has been shown that αLβ2-integrin is internalised via a clathrin-independent and cholesterol-sensitive pathway[380].

1.9.3 ADAM15 and integrins

ADAM15 contains a disintegrin domain which has been shown to interact with integrins. Experiments with a recombinant disintegrin domain or ECD of ADAM15 were used to reveal its function. The first experiments with recombinant disintegrin domain of ADAM15 were carried out by Zhang et al. They expressed the disintegrin domain as a fusion protein with GST and used the pull-down approach to identify binding partners. They were the first who discovered that αvβ3 binds to the disintegrin domain in an RGD-dependent manner[115]. One year later Nath et al.[114] demonstrated the interaction between ADAM15 and αvβ3 and also α5β1 in haemopoietic cells using the recombinant ADAM15 ECD. The interaction of ADAM15 with αvβ3 was further confirmed with recombinant human ADAM15 disintegrin domain using a phage display[381]. The recombinant ADAM15 disintegrin domain inhibited the binding of αvβ3 to vitronectin in a dose-dependent manner. Subsequently, similar results were observed for αIIbβ3 on fibrinogen[382]. Jeon et al. showed that altering the amino acid residues proximal to the RGD sequence (RPTRGD and NWKRGD) increase the affinity of αIIbβ3 towards the disintegrin domain of ADAM15.

Hou et al. demonstrated that the recombinant human disintegrin domain of ADAM15 reduces migration and proliferation of Bel-7402 cells in a liver cancer model. This was as a result of a partial G_2/S arrest with concomitant increase in activity of the initiation caspases 8 and 9 as well as the executioner caspase 3[226]. In the same study they used a zebrafish as a model for tumour xenografts of Bel-7402 cells and as model for apoptosis induction. They demonstrated that 1 pM recombinant disintegrin domain led to reduced growth of metastasis while a ten times lower dose induced severe cell death in somatic cells of the zebrafish[226].
Eto et al.[113] confirmed that αvβ3 binds ADAM15 via its RGD-motif. They also showed that α9β1 interacts with ADAM15 independently of the RGD motif. The interaction required Arg481 and the Asp-Leu-Pro-Glu-Phe residues (488-492).

Chen et al. demonstrated that overexpression of ADAM15 in CHO cells, expressing endogenous α5β1, led to decreased migration and enhanced adhesion on FN, which was the consequence of ADAM15-driven cell surface expression of α5β1. Using IP and immunofluorescence analysis they confirmed no interaction between ADAM15 and α5β1-integrin. Instead, overexpression of ADAM15 decreased Erk1/2 phosphorylation. Pharmacological inhibition of Erk1/2 phosphorylation enhanced α5 expression on the cell surface[225]. This experiments revealed a novel mechanism in which ADAM15 regulated migration and adhesion via Erk1/2.
ADAM15 is also found in exosomes which are released by PMA stimulation[383]. ADAM15-positive exosomes show enhanced binding to αvβ3-integrin in an RGD-dependent manner. ADAM15 containing exosomes suppressed FN- and VN-induced growth, cell adhesion, migration and *in vivo* tumour growth. This experiments suggest that ADAM15 may function as a tumour suppressor in an exosome-mediated way by interacting with integrins.
It has been demonstrated that ADAM15 isoforms interact with Nck, but with varying affinity[179]. Under genotoxic stress ADAM15 enhanced FAK and Src phosphorylation[384,385]. Crosstalk between ADAM15 and integrins was also found in inflammatory diseases as well as in different types of cancers. In the crypt abcesses of inflammatory bowel disease α5β1 positive leukocytes were found in close contact with ADAM15 positive epithelial cells. In regenerative areas, α5β1- and αvβ3-positive pericryptic myofibroblasts were in close contact with ADAM15-positive epithelial cells[386]. Histological analysis of primary colon tumour samples showed downregulation of ADAM15 in poorly differentiated carcinomas. This downregulation was statistically significant with increased localisation of α5β1-integrin at the cell membrane. In immunofluorescence stainings it was observed that normal epithelial colon cells express ADAM15 at their basolateral membrane, but do not express α5β1. Contrary, in carcinoma cells with downregulated ADAM15 expression, α5β1 was found at the basolateral membrane[387]. This suggests an ADAM15-to-α5β1 switch. Another observation which was made by the same group was that downregulation of ADAM15 in the tissue sample correlated with downregulation of α3β1. Regulation of α3β1 by ADAM15 has not been shown before. More studies need to be carried out to address this novel finding. Direct correlation of ADAM15 expression and αv membrane localisation has been observed in prostate cancer 3 (PC3) cells. Knockdown of ADAM15 resulted in a decreased localisation of αv at the cell surface[227]. In ovarian cancer cells overexpressed ADAM15 significantly reduced αvβ3-mediated adhesion to vitronectin[388] which could be due to higher affinity of the integrin to the RGD motif of ADAM15. Co-localisation of ADAM15 and αvβ3 is often observed in lung cancer cell lines[193].
While there is substantial evidence on integrin and ADAM15 interactions, and po-

tential implications for normal cell biology as well as pathological conditions, the work carried out to date reflects only what happens between specific integrins and ADAM15 A isoform. Whether the other ADAM15 isoforms affect integrin biology differently is currently unknown and requires further research.

1.9.4 Ras homologue (Rho) GTPases are key players in cytoskeleton rearrangement

Migration is a process which requires the communication between two opposing ends of the cell. Not only coordination of protrusions in the leading front and retraction at the rear are important, also shape, organisation and polarity that are driven by the cytoskeleton. In respect of locomotion three distinct activities are involved to move a cell forward: 1) Protrusions in the front of cell structures, rich in actin, are pushed out. 2) Attachment, in which the cell membrane is connected to the substratum by the actin cytoskeleton. 3) Traction in the rear. The trailing cytoplasm is drawn forward. These cytoskeletal rearrangements are governed by the Rho protein family: Rho, Ras-related C3 botulinum toxin substrate (Rac) and cell division control protein 42 homologue (Cdc42). The function of Rho is to regulate actin stress fibre assembly, whereas Rac regulates membrane ruffles and lamellipodia formation at the cell periphery, while Cdc42 is responsible for filopodia formation[389].

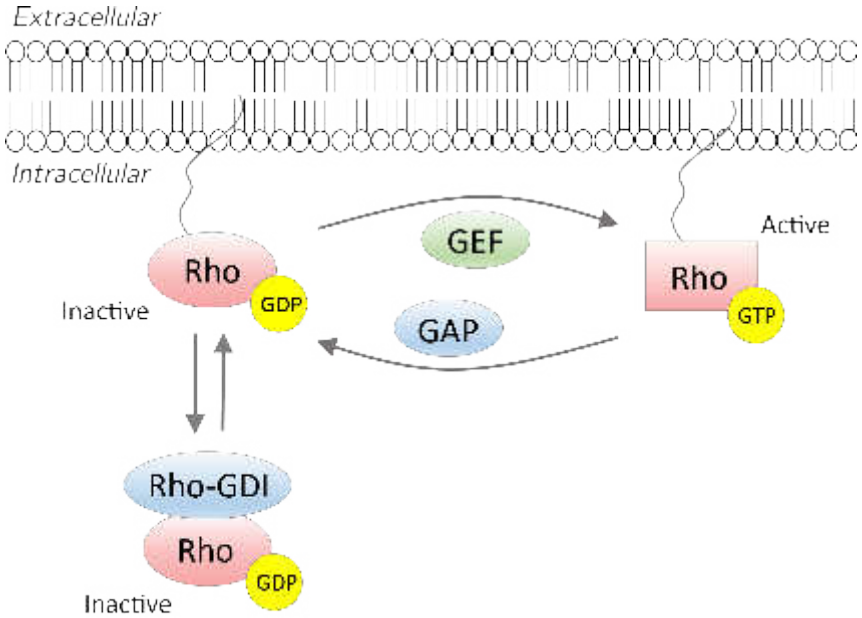

Figure 1.23: Illustration of Rho-GTPase activation. Rho-GDIs release inactive Rho-GTPases in the cytoplasm. Sequestered Rho-GTPases are targeted to the cell membrane. GEFs mediate their activation by binding to GTP. GAPs promote their inactivation by binding to GDP. The image is adapted from Huveneers and Danen, *Adhesion signaling - crosstalk between integrins, Src and Rho*, Journal of Cell Science, 2009[390].

Within the cytoplasm GTPases are bound by Rho-GDP dissociation inhibitors (Rho-GDI) as shown in figure 1.23. Sequestered Rho-GTPase from Rho-GDIs are targeted to the plasma membrane. GTPase switches between an active GTP-bound and an inactive GDP-bound state. Guanine nucleotide exchange factors (GEFs) promote activation of GTPase through the catalytic removal of GDP and enabling GTP binding whereas GTPase-activating proteins (GAPs) show the opposite effect, causing down regulation of GTPase activity.

The initiation of cell adhesion and spreading occurs in parallel with inhibition of RhoA and activation of Rac1 and Cdc42. This increases actin-mediated protrusion formation and suppresses actomyosin contractility. Later, the activities of Rac1 and Cdc42 decline while RhoA activity increases which leads to FA and stress fibre formation. The reason of this mutually exclusive behaviour is that RhoA suppresses the activity of Rac1 and *vice versa*. Rac1 inhibits low-molecular-weight protein tyrosine phosphatases by induction of reactive oxygen species (ROS) production. This leads to an increase in tyrosine phosphorylation and activation of p190RhoGAP which inhibits RhoA activity[391]. In contrast, RhoA inactivates Rac1 by promoting Rho-associated coiled-coil containing kinases (ROCK)-mediated phosphorylation of FilGAP[392]. FilGAP is a filamin A-binding RhoGTPase-activating protein. It functions as a GAP for Rac1, localising to sites of membrane protrusions.

Integrins are the major regulators of RhoGTPases largely via the FAK-Src complex. A simplified illustration of integrin-mediated RhoGTPse activation is shown in figure 1.24. Upon binding of an integrin to a ligand the cytoplasmic domain unfolds and various FA initiation proteins are recruited to the the membrane such as talin and FAK. Recruitment of FAK causes its autophosphorylation at Y397 which serves as binding site for the SH2 domain of Src. This leads to transphosphorylation of FAK within the kinase domain activation loop at Y576 and Y577 as well as C-terminal domain at Y861 and Y925[393]. This phosphorylation events serve two purposes: They maximise the kinase activity of FAK and generate new binding sites for other proteins. The active FAK/Src complex recruits and phosphorylates the scaffolding protein p130Cas[394]. Active p130Cas associates with the adaptor protein v-crk sarcoma virus CT10 oncogene homologue (Crk) thereby recruiting engulfment and motility 1 (ELMO1) and dedicator of cytokinesis-180 kDa (Dock180). The Dock180-ELMO1 complex promotes the formation of membrane protrusions by functioning as an unconventional GEF for Rac1[395]. Apart from activating p130Cas the FAK/Src complex also phosphorylates paxillin that subsequently recruits the ArfGAP paxillin-kinase linker (PKL) as well as the mutual GEF for Rac1 and Cdc42, Pak-interacting exchange factor-β (β-PIX). Rac1 is recruited and activated by β-PIX via direct interaction[396]. A proline-rich region of Rac1 binds to the SH3 domain of β-PIX[396].

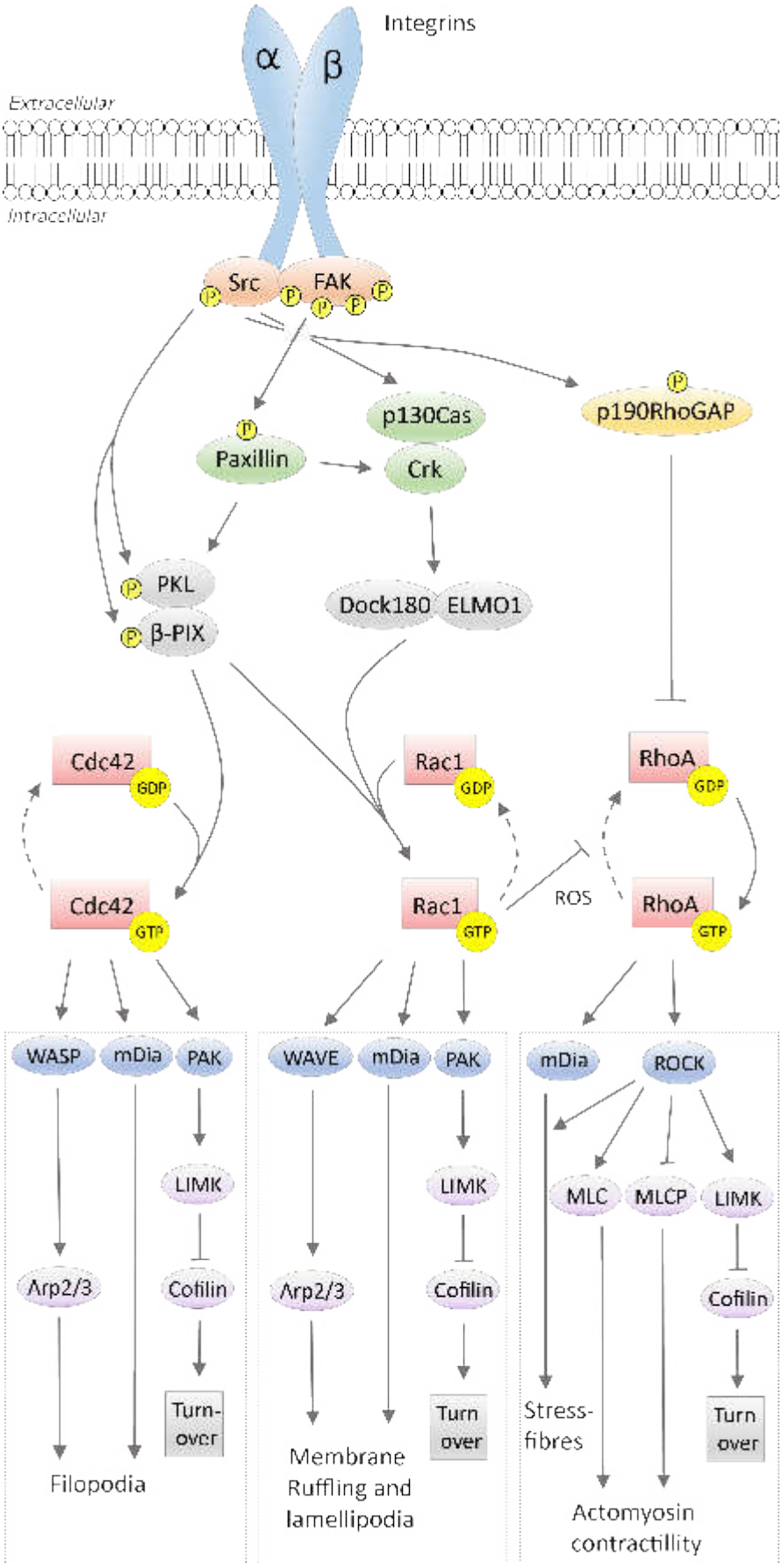

Figure 1.24: Simplified illustration of integrin induced regulation of Rho-GTPases. At the site of integrin activation Src and FAK are recruited and form a complex. This complex modulates Cdc42, Rac1 and RhoA activity via several pathways. The image is adapted from Huveneers and Danen[390] and Dráber, Sulimenko and Dráberová[397].

It has been demonstrated that PKL can be directly phosphorylated by Src and/or FAK[398] while β-PIX is activated by Src[399]. Furthermore, Src mediates the transient inhibition of RhoA through regulation of p190RhoGAP[400].
There are multiple downstream targets of RhoGTPases with direct effects on actin cytoskeleton rearrangements. This includes formins, kinases and members of the Wiskott-Aldrich syndrome protein (WASP) family and other scaffolding proteins. The most prominent contributors are the mammalian Diaphanous formin (mDia), proteins of WASP and Wiskott-Aldrich syndrome protein-family verprolin homologous protein (WAVE), ROCK and p21-activated kinase (PAK). Cdc42 and Rac1 activate PAK which promotes LIM-motif containing kinase (LIMK) activity. Both, Cdc42 and Rac1, activate the Arp2/3 complex, Cdc42 through WASP while Rac1 stimulates it via WAVE[401]. Cdc42-mediated Arp2/3 activation leads to filopodia formation while Rac1-regulated Arp2/3 stimulation leads to membrane ruffling and lamelipodia formation. Interestingly, the ADAM15 adaptor protein Grb2 is an alternative activator of WASP, stimulating actin polymerisation. Cdc42 and Grb2 elicit a synergistic effect by simultaneous binding to N-WASP which increases its activity[402].
RhoA promotes stress fibre formation via activation of mDia and ROCK. Besides, ROCK also mediates actomyosin contractility via phosphorylation of myosin II light chain (MLC) and myosin light chain phosphatase (MLCP). Activation of LIMK by ROCK leads to phosphorylation of cofilin. This leads to inhibition of cofilin which is associated with actin-filament turnover[403].
RhoGTPase-mediated mDia activation has a promoting effect on cytoskeleton rearrangement by stabilising microtubules[404].

In addition to integrins, GPCRs and RTKs have the ability to activate RhoGTPases[405,406]. Furthermore, GPCRs can also activate G-protein subunits such as G 12/13 regulating RhoGEFs[407]. These subunits modulate the turnover of membrane ruffles upon growth factor induction[408]. The Swiss 3T3 cell line has shown stress fibre formation and FA assembly prior to G 12/13 stimulation via the RhoGTPase pathway. Overexpression of β1-integrin enhances Rac activity and lamellipodia formation whereas the overexpression of β3-integrins showed an increase in Rho activity and stress fibre formation[409]. More than half of the 58 known RTKs activate at least one Rho family member. Several RTKs are able to activate the same Rho GEFs, but it is also possible that a single RTK activates different Rho GEFs (16 in total) which increases the complexity of RTK signalling.

1.9.5 Focal adhesions and their turnover

Migration is dependent on the generation of short-term self-assembling complexe named focal adhesions (FA). FA assemble around the cytoplasmic domains of integrins that connect the ECM to the cytoskeleton and other intracellular molecules. FA are made of from a variety of proteins with wide ranging functions. They comprise not only integrins as ECM adhesion receptors, but also kinases like Src and FAK, and adaptor proteins such as paxillin which contributes to intracellular complex formation. Together they orchestrate the rearrangement of the actin cytokeleton with effects on cellular behaviour such as migration and locomotion. A simplified illustration of a FA complex is shown in figure 1.25. FA dynamics are mainly regulated by phosphorylation events and changes in actomyosin-generated tension[410].

The assembly of FA is mostly introduced by outside activation mediated by integrins. A key molecule regulating integrin activation is talin. The function of it is to provide a link between the cytoplasmic tail of integrins and actin[411]. Moreover, upon binding of talin to the cytoplasmic tail of the β-subunit talin triggers a conformational rearrangement of the integrin ECD enhancing their affinity[412]. In a specialised domain of talin a phosphotyrosine-binding motif was found which was able to activate αIIbβ3 integrin[412]. This phosphotyrosine-binding motif is also found in other proteins which interact with integrins. However, this is not sufficient for integrin activation highlighting the crucial role for talin. The talin-binding site in β-integrin tails overlap with a filamin-binding site[413]. Filmanins are actin cross-linking proteins connecting the cytoskeleton to cell membrane receptors (not shown in figure 1.25).

Another interacting protein found to bind the ICD of β1-integrin is the integrin-linked kinase (ILK)[414]. It is found in a multiprotein complex and functions as a scaffolding-protein. The localisation of ILK to FAs is regulated by particularly interesting cysteine- and histidine-rich protein (PINCH)[415]. ILK also interacts with the actin-binding proteins α-parvin (affixin)[416], β-parvin (CH-ILKBP)[417] and the adaptor protein paxillin[418]. The interaction with paxillin regulates the localisation of ILK to FAs[418]. The kinase activity of ILK is negatively controlled by the Ser/Thr phosphatase ILK-associated phosphatase (ILKAP)[419]. ILK is positively regulated in a PI3K dependent manner since it was bound and activated by PIP_3[420]. Activated ILK in turn phosphorylates the downstream targets of PI3K Akt and glycogen synthase kinase-3 (GSK3). In contrast, PIP_3 inhibition by PTEN decreased the activity of ILK[421]. Biochemical experiments demonstrated that ILK is able to form a PINCH mediated complex with Nck-2 which co-localised with α5β1-integrin in periperhal ruffles[415].

FAK is a cytosolic protein kinase and a key regulator of FA that functions as signalling molecule and adaptor protein. FAK binds to HDRK-motifs in β1- and β5-subunits and to adjacent sequences[422]. Autophosphorylation of FAK at Y397 leads to recruitment of Src, which in turn phosphorylates Y576/577 and Y925 residues in FAK. FAK is then able to recruit various signalling molecules regulating FA assembly and disassembly[222,423]. It can also recruit talin to nascent adhesions independently of talin-β1-interaction[424]. FAK signalling also stimulates the association with talin and promotes PIP_2 production at FA[425]. Another member of the FAK family is the proline-rich tyrosine kinase 2 (Pyk2). Its activation is similar to FAK since it is phosphorylated at a tyrosine (Y402). Upon phosphorylation a binding site for the SH2 domain of Src is exposed[426]. Despite their common way of activation the response to α5β1 mediated fibronectin binding is different. Pyk2 is only activated weakly while FAK is stimulated strongly[426].

Src is a non-receptor tyrosine kinase. It is an important signalling molecule since FAK phosphorylation by Src is essential for FA turnover[423]. In Src-deficient fibroblasts cell-spreading on VN, but not on FN is inhibited[427]. Co-localisation of Src with the αv-subunit was found, but not with the β1-chain[427]. The C-terminal Src kinase (Csk) (not shown in figure 1.25) is a cytosolic tyrosine kinase which negatively regulates Src activity by phosphorylating the regulatory tyrosine residue Y527, which is conserved in all Src family kinases[428–430]. Csk translocates to FAs when Src kinases are activated[431]. Fibroblasts expressing FA-targeted Csk lost integrin-mediated adhesion due to reduced Src activity[430].

The deleted in liver cancer 1 (DLC1) is a potential tumour suppressor gene encoding a RhoGAP which co-localises with vinculin and tensin2 at FA[432]. It negatively controls the Rho/ROCK/MLC pathway and its presence in FA was demonstrated in many cell types[433].

Tensins belong to the family of FA proteins and are able to bind to the ICD of the integrin β-chains via its PTB domain[434]. It also contains a SH2 domain at the C-terminus and share sequence homology with PTEN. Tensins contribute not only to FA assembly and to actin cytoskeleon organisation[435,436], but also play a role in signal transduction, for example by activating the JNK and p38 pathway[437].

Paxillin is a multi-domain scaffolding protein playing an essential role in FA dynamics. Upon growth factor response or adhesion stimuli, paxillin becomes phosphorylated by several kinases. This generates further bindings sites for other FA proteins. Thus it controls, together with other structural and regulatory proteins, gene expression, cytoskeletal reorganisation and cell adhesion[438].

Caveolins are the primary structural proteins of caveolae. Caveolae are invaginations in the cell membrane participating in signal transduction and cellular transport[439]. The caveolin family comprises three members Caveolin1 (Cav1), Cav2 and Cav3

whereas Cav1 was found in FAs where it serves as scaffolding protein. Rac1 drives the accumulation of Cav1 to FAs while its translocation requires phosphorylation at Y14 by Src[440,441].

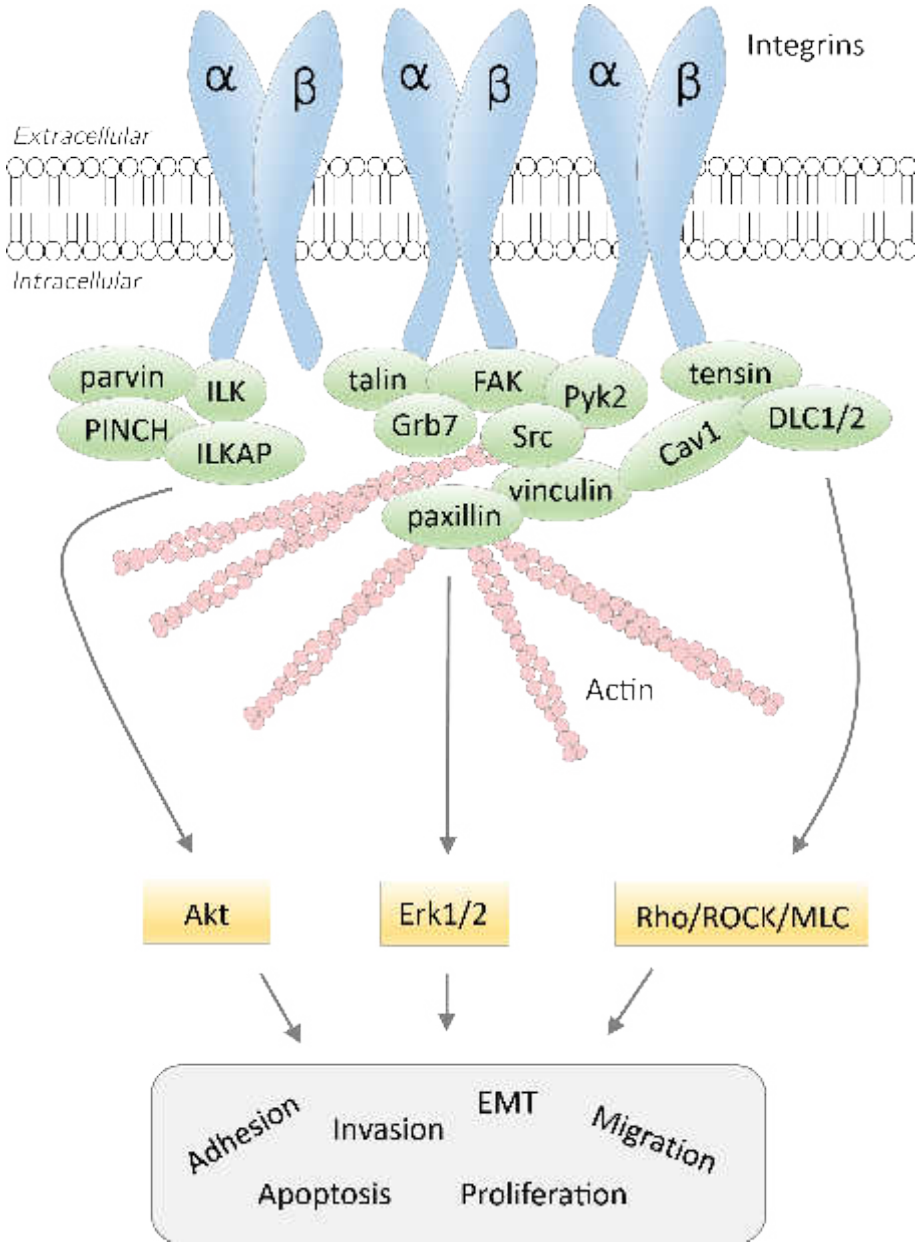

Figure 1.25: Illustration of a focal adhesion complex. FA complexes are formed in which heterodimerc integrins link the ECM to cytoplasmic proteins. Cascades of phosphorylation and dephosphorylation events regulate cellular processes. Adapted from Yam et al., *Role and significance of focal adhesion proteins in hepatocellular carcinoma*, Journal of Gastroenterology and Hepatology, 2009.

FA are generally short lived, and their continuous assembly and disassembly is necessary to assure cell movement. Nocodazole-induced microtubule-depolimerisation is a common way to address FA turnover. It is an anti-mitotic drug inhibiting microtuble assembly by binding to the heterodimer tubulin. The

affinity of nocodazole to interact with tubulin varies, depending to which isotype of tubulin it binds to[373]. Serum-starved cells possess only few focal adhesions. Nocodazole treatment induces stress fibre formation and FA assembly via activation of Rho GTPase[442]. The regrowth of microtubles after washing out nocodazole lead to disassembly of FA which is independent of Rho and Rac, but depending on dynamin and FAK[443]. This shows that FA disassembly is not just the reversal of FA formation, but an independent complex mechanism. Later it was found that this mechanism is also dependent on clathrin.

1.10 Rationale, hypothesis and aims of the project

Previous research on ADAM15 has predominantly focused on the most abundant and ubiquitously expressed isoform, ADAM15 A, demonstrating the importance of ADAM15 in a variety of processes that regulate cell behaviour in normal, as well as pathological conditions. However, recent findings show that ADAM15 is subjected to alternative splicing that regulates the presence of specific protein-protein interaction motifs within the ADAM15 ICD. The expression of specific ADAM15 isoforms correlates with differential prognosis in breast cancer survival, suggesting that these isoform-specific intracellular interactions regulate ADAM15 functions. This was illustrated by the interplay of ADAM15 B and Src tyrosine kinase, where Src associates with ADAM15 B ICD, phosphorylates a critical tyrosine within the ICD, leading to enhanced shedding of transmembrane receptor FGFR2IIIb by ADAM15 B. Hence, the principal hypothesis we wanted to test was the following: ADAM15 isoforms have similar, as well as distinct functions that may affect multiple aspects of cell behaviour in isoform-specific unique ways. To test the hypothesis, the project consisted of the following major aims:

1. To generate and characterise an isogenic cell panel expressing individual wild type and corresponding catalytically inactive ADAM15 isoforms.

2. To compare and contrast the role of individual ADAM15 isoforms in regulating cell-cell adhesion.

3. To compare and contrast the role of individual ADAM15 isoforms in regulating cell-ECM interactions.

Chapter 2

General Methodology

2.1 Statistical analysis

Throughout this thesis the significance for various experiments is calculated with GraphPad Prism 6.01. If not stated otherwise one- or two-way analysis of variance (ANOVA) were performed. Confidence intervals are as follows: $* = p \leqq 0.05; ** = p \leqq 0.01; *** = p \leqq 0.001; **** = p \leqq 0.0001$. The error bars in bar charts indicate the standard deviation.

2.2 Cell Culture

2.2.1 Cancer cell lines

The work in this project is based on cancer cell lines, primarily on MDA-MB-231. Throughout the thesis other cell lines appear which were used as controls. In the following subsections they are briefly described.

2.2.1.1 MDA-MB-231

MDA-MB-231 is a breast cancer cell line derived from a 51 year old Caucasian woman suffering from an adenocarcinoma. MDA-MB-231 are of epithelial origin and were derived from pleural effusion (metastatic site). Although they are derived from epithelial tissue they demonstrate mesenchymal morphology which is due to epithelial-mesenchymal-transition (EMT) . The tumour origin was the mammary gland. Karyotyping shows aneuploidity with 52 to 68 chromosomes (modal number = 64), but lack chromosome 8 and 15[444,445]. MDA-MB-231 cells are triple-negative, which means they are lacking the expression of ER, PR and Her2/Neu. MDA-MB-231 cells are highly invasive[446] and tumourigenic[447].

2.2.1.2 T47D

T47D were used as a control cell line in some experiments due to their naturally high expression of ADAM15 and claudin1 and their propensity to form tight junctions. They were removed from a metastatic site, the pleural effusion. They have been derived from a 54 year old Caucasian female suffering from ductal carcinoma. T47D are true epithelial cells expressing high amounts of E-cadherin. They have a modal chromosome number of 65 while lacking chromosome 7,9 and 10. Contrary, chromosome 11 is generally present in 4 copies[444]. T47D cells express ER and PR, but lack HER2/Neu[446].

2.2.1.3 A431

A431 were also used as a control cell line due to its high expression of epithelial markers. These cells were derived from a 85 year old female suffering from epidermoid carcinoma. The cell line was extracted from the skin and shows clear epithelial morphology. They have a modal chromosome number of 74[444].

2.2.2 Generation of an isogenic cell panel expressing ADAM15 WT and E349A isoforms in MDA-MB-231 cells

The construction of pcDNA5/FRT/ADAM15 isoform plasmids and the generation of all cell lines were performed by Dr Zaruhi Poghosyan.

The generation of a isogenic cell panel expressing ADAM15 isoforms, as described in table 1.5 and figure 1.10, was achieved by using the Invitrogen Flp-In™ system. An adapted scheme of the transfection strategy is depicted in figure 2.1. The *ScaI* linearised pFRT/lacZeo plasmid was introduced first into original MDA-MB-231 cells, according to manufcaturer's protocol, using Lipofectamine 2000. The pFRT/lacZeo vector introduces the Flp recombination target (FRT) site and a Zeocin resistance gene. Zeocin-resistant clones were isolated and expanded followed by screening for single integration sites (see section 3.2 for detailed validation). A validated clone was used to co-transfect pOG44, expressing Flp recombinase, and pcDNA5/FRT/ADAM15 constructs. Clones were picked, selected and expanded in Hygromycin B (450 µg/mL) containing growth medium.

In order to generate proteolytic inactive variants the zinc-binding sequence HEXGHXXGXXHD-sequence was mutated as shown by Maretzky et al.[200]. Mutations are introduced to change the acidic glutamic acid (E), which is negatively charged, to an aliphatic alanine of neutral charge. The conversion of the amino acids prevents zinc-binding leading to a non-functioning MP-domain.

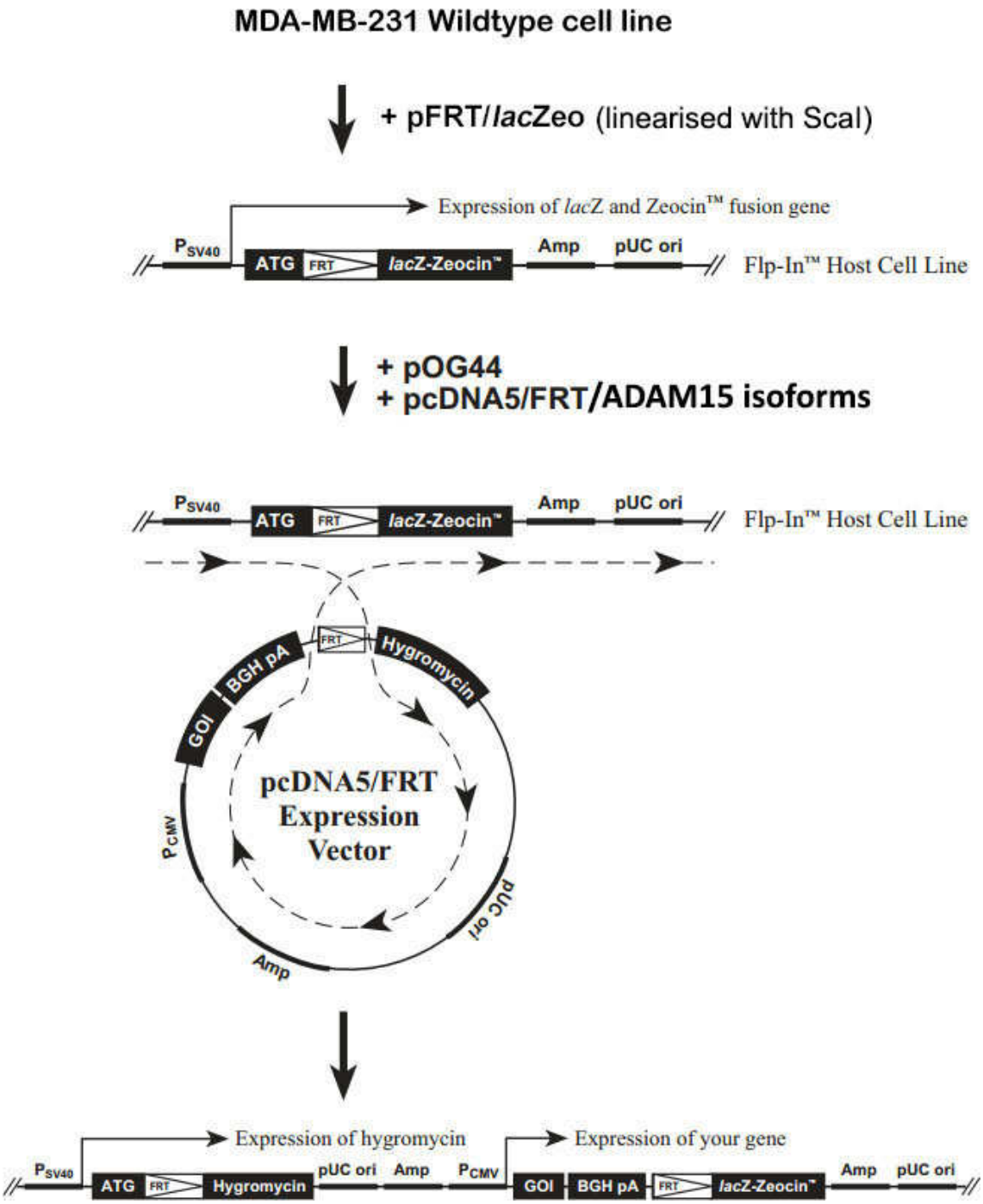

Figure 2.1: Generation of isogenic constitutive ADAM15 isoform expressing MDA-MB-231 breast cancer cells using the Invitrogen Flp-In™ system as described in table 1.5 and figure 1.10. Image was taken and modified from Invitrogen.

2.2.3 Maintaining cell lines in culture

All cell lines were kept in Dulbecco's modified eagle medium (DMEM) supplemented with 10% (v/v) fetal bovine serum (FBS), 100 units/mL Penicillin, 100 µg/mL Streptomycin and 2 mM L-Glutamine (L-Glu). In other sections the term "normal or complete growth medium" is used to refer to this media composition. Cells were maintained in a humidified incubator at 37°C with 5% CO_2. MDA-MB-

231/FRT cells were cultured with additionally 100 µg/mL Zeocin, MDA-MB-231 with expressing ADAM15 WT or E349A constructs were grown with 450 µg/mL Hygromycin. Short hairpin RNA (shRNA) expressing cell lines were maintained in 1 µg/mL Puromycin which is added to their normal media composition. Cells were passaged regularly, usually twice a week. Depending on the cell line, confluent dishes were split with ratios between 1 : 10 and 1 : 4.

2.2.4 Freezing and thawing of human cell lines

Cells were expanded in either T75 (75cm^2 surface area) or T175 (175cm^2 surface flasks). As soon as they were confluent cells were trypsinised and spun down. Afterwards they were resuspended in medium and mixed 1:1 with freezing medium. The suspension was then immediately distributed to cryo vials with 1 mL of total volume. A confluent T75 flask was split between four cryo vials whereas a T175 was split into ten vials. Subsequently the vials were cooled down in a Mr. Frosty freezing container at -80°C. The freezing container is the preferred method since it allows optimal cool down rate of -1°C/min. For long term storage the cryo vials were kept in liquid nitrogen.
Frozen cells were thawed by immersing them halfway in 37°C warm water bath to assure rapid thawing. As soon as the suspension was liquefied cells were transferred into a falcon tube with 10 mL of medium to dilute the DMSO, reducing the toxicity to the cells. The cells were centrifuged for 5 minutes (500 x g) and resuspended in fresh medium (including selection antibiotic if required) and cultured in a T25 flask.

2.3 MTS proliferation assay

Cell lines were seeded into 96-well plates with 3x10^3 cells per well in 100 µL volume. They were plated as triplicates into four plates, one for each time point (24h, 48h, 72h and 96h). After each time point 20 µL of CellTiter 96®AQueous One Solution was added to each well and incubated for 4h at 37°C. After incubation the absorbance was immediately measured at 450 nm.
For analysis the blank was subtracted from the reading of the samples. The measurement after 24h was considered as 1.

2.4 Determination of cell size

2.4.1 Microscopic determination of cell size

In order to quantify the area which is covered by the cell, phase-contrast images were taken at 200 x magnification and quantified with ImageJ. An image of a corner square of the Neubauer counting chamber was used to set the scale since the dimension are known (250 μm^2). For each cell line five images, during exponential growth phase, of random positions were taken using an EVOS XL core imaging system (ThermoScientific). This was done for three different passages to achieve 15 images. For each picture ten representative cells were chosen and the cell area was outlined and measured. This led to 150 measured cells for each cell line. For statistical analysis Bartlett's test for equal variances was used to determine the significance. As follow-up test Dunnett's multiple comparison test was used. The results are presented as a box-and-whiskers plot.

2.4.2 Flow cytometric analysis of cell size

The forward scatter (FSC) of flow cytometrical analysis gives an indication about the size of cells. Analysis was performed using an Accuri C6 flow cytometre.
A fraction of trypsinised and resuspended cells was stained with propidium iodide (PI) at a final concentration of 10 µg/mL, to exclude dead cells, and measured subsequently.
For analysis FlowJo 10.0.7 R2 was used. The FSC-A (Area) was plotted against the FSC-H (Height) to discriminate doublets. The subpopulation was then used in a histogram with PI to distinguish live and dead cells. The fluorescence intensity of dead cells is usually 50-fold greater compared to living cells, thus the peak of the living population is gated. The new gate was then used in another histogram with FSC-A to determine the cell size. An example of the gating strategy is shown in figure 2.2.
The median was automatically calculated by FlowJo. For comparison, a scatter plot was generated and one-way ANOVA was performed.

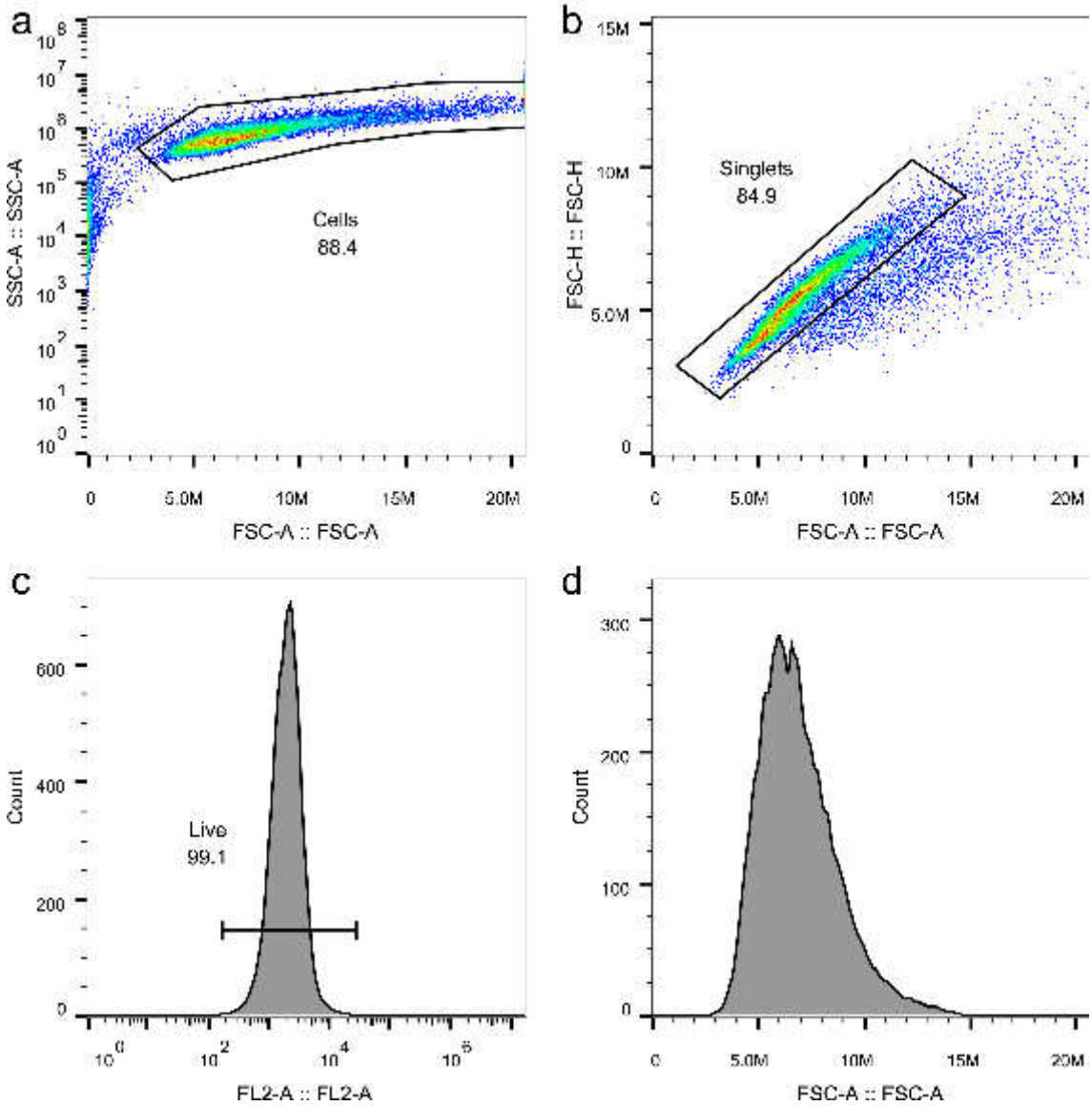

Figure 2.2: Gating strategy for determination of the cell size using flow cyotmetry. **(a)** The SSC area was plotted against the FSC area to exclude cell debris. **(b)** To discriminate doublets the subpopulation was used. The FSC height was plotted against the FSC area **(c)** The resulting subpopulation was then displayed as a histogram showing PI staining on the x-axis. Autofluorescent cells show up around 10^3 whereas dead cells display at 10^6. **(d)** The live population is than plotted as FSC-A-Histogram in which FlowJo can automatically determine the median value.

2.5 Demethylation assay

4 x 10^6 cells were seeded into 35 mm dishes using medium supplemented with FBS, P/S and L-Glu. On the following day two dishes per cell line were treated with 33.3 µM Decitabine (5-aza-2'-deoxycytidine). After 24h Decitabine was replaced with a higher concentration of 50 µM. On the following morning the treatment was repeated with 50 µM Decitabine. In the evening, one dish containing Decitabine was replaced with fresh Decitabine in combination with 500 nM Trichostatin A (TSA) . After overnight incubation the cells were processed as described in section 2.7. The

western blot was probed with V5 to visualise ADAM15 isoform expression.

2.6 Wound healing assay

Cells were seeded into 6 cm dishes in normal growth medium and grown until confluence. Seven parallel wounds were introduced with a white tip (0.5 µL - 10 µL). Detached cells were removed by swirling followed by aspiration. The medium was temporarily replaced by OptiMEM during the acquisition of the images at time point 0h. The pictures were taken with 100 x magnification. Afterwards the cells were fed with normal growth medium and consecutive images were acquired after 8, 24, 32 and 48h using an EVOS XL core cell imaging system (ThermoScientific).
Analyis was carried out with a modified version of the *MRI wound healing tool* in ImageJ. The tool only works with 8-bit images which need to be manually converted. The modification was done by adding the appropriate command line to automatise this step. Three wounds with 640,000 ± 75,000 μm^2 were used for further analysis. The 0h time points were normalised to 100% and the wound closure was calculated using Microsoft Excel. Statistical analysis was carried out with 2-way ANOVA and Bonferroni post-test in GraphPad Prism 5.01. ADAM15 isoform expressing cells were compared to to the parental cell line MDA-MB-231/FRT.

2.7 Protein analysis

2.7.1 Subcellular fractionation

Cells were grown until confluence and harvested by trypsinisation, followed by inactivation with complete growth medium. The cells were counted using the Neubauer counting chamber and adjusted to 2.5 x 10^6 (which equals a packed volume of 20 µL in a 1.5 mL tube). Cells were centrifuged and resuspended in ice cold PBS. One vial with 2.5 x 10^6 cells was lysed with radioimmunoprecipitation assay (RIPA) buffer as described in section 2.7.2. The vial for subcellular fractionation was processed according to the manufacturer's protocol. However, following changes were made to achieve cleaner separation: Incubation times were doubled and the pellets were washed twice with ice cold PBS after transferring the extract, before adding the consecutive compartment lysis buffer.
Fractions were subsequently stored in -80°C until further processing. Prior to western blot analysis samples were quantified according to the manufacturer's protocol of the GLISA kit to balance deviation in protein concentration during extraction. For western blot analysis 10 µg of total lysate as well as cytoplasmic and membrane extract were loaded. The amount of used nuclear fraction was 5 µg. Samples were

diluted with RIPA buffer prior to the addition of 6 x loading dye. As controls, antibodies against heat shock protein 90 (HSP90) were used as cytoplasmic control. Antibodies against R-cadherin were used as membrane control and antibodies against Lamin A/C were used as nuclear control.

2.7.2 Lysate preparation

Cells were grown in various sized petri-dishes and harvested at different stages of confluences depending on the experiment. After seeding cells were cultured for at least 48h prior to collection. Dishes were placed on ice and washed twice with PBS. Snippets of filter paper were used to drain surplus washing buffer. An appropriate volume of RIPA lysis buffer (table 2.1) was applied to the dish and incubated for 5 min on ice. A rubber policeman was used to scrape the cells from the surface. The cell suspension was transferred to a new pre-chilled tube and incubated another 10 min on ice. Subsequently, the lysate was sonicated three times for 10 sec each with 30 sec of cooling-down phase between pulses. Sonicated samples were store at -80°C until further processing.

200 mM Phenanthroline

- 901.05 mg 1,10-Phenanthroline

Adjust to 2 mL with Methanol
Store aliquots of 1 mL at -20°C

20x Phosphatase inhibitor

- 2 tablets PhosSTOP per 1 mL MilliQ water

Store aliquots of 200 µL at -20°C

25x Proteinase inhibitor

- 1 tablet cOmplete proteinase inhibitor per 2 mL MilliQ water

Store aliquots of 200 µL at -20°C

Lysis buffer

- RIPA buffer (purchased)
- 1:20 Phosphotase inhibitor
- 1:20 Phenanthroline (10 mM)
- 1:25 Proteinase inhibitor

Table 2.1: Volumes of lysis buffer in different dishes and confluence

Confluence	35 mm	60 mm	100 mm	150 mm
50%	50 µL	150 µL	200 µL	500 µL
70%	100 µL	200 µL	300 µL	750 µL
100%	150 µL	250 µL	350 µL	1000 µL
150%	200 µL	300 µL	400 µL	1200 µL

2.7.3 Protein quantification

To enable comparison of protein samples, it is crucial to determine the protein concentration. For this purpose the bicinchoninic acid (BCA) protein assay kit was used (Pierce). Lysates were thawed on ice and spun down for 15 minutes at full speed (21,100 x g) at 4°C to remove cell debris. The supernatant was then transferred into pre-chilled 1.5 mL tubes. The quantification was carried out in a 96-well plate according to the manufacturer's manual. The bovine serum albumine (BSA) standards were diluted 1 : 10 in the lysis buffer. In total nine standards (0-2 mg/mL) were used in duplicates. Samples were used in triplicates to minimise minor deviation through pipetting. The plate was incubated for 2 h in the incubator. The ideal wavelength to measure the absorbance of the BCA assay is at 562 nm.

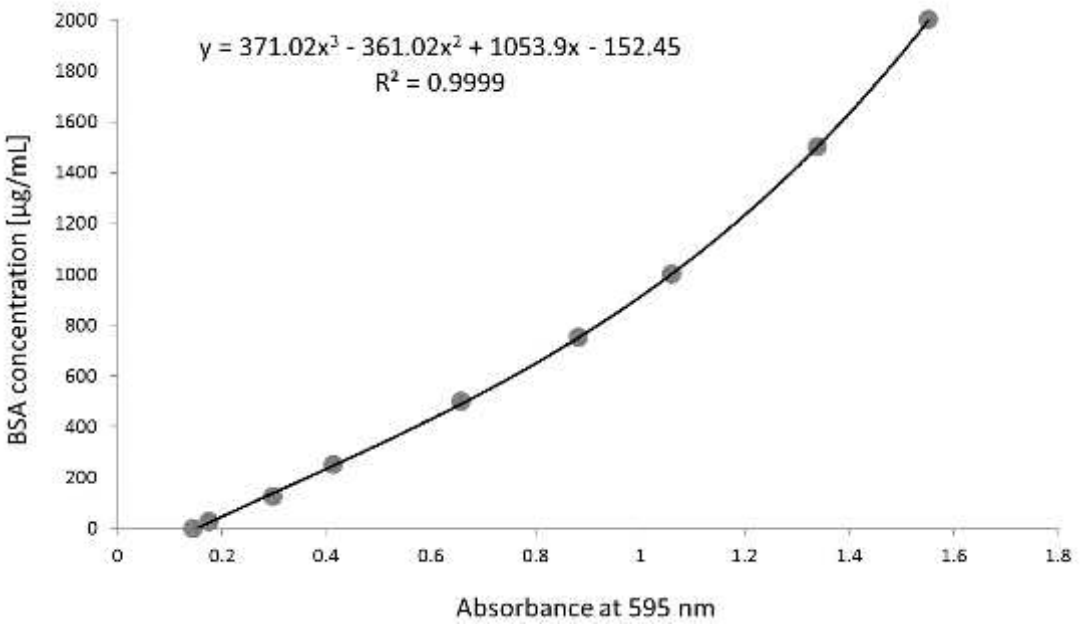

Figure 2.3: Almost ideal result of a standard curve for the determination of protein concentrations

However, the plate reader did not have the correct filter thus it was measured at 595 nm. According to the manufacturer this does not cause a problem if the incubation time is increased to 2h (compared to 30 min normally). A standard curve was plotted using cubic regression ($ax^3 + bx^2 + cx + d$). The sample concentration

was calculated accordingly. Using a polynomial of degree three the formula can give a very precise standard curve as seen in figure 2.3 which results in a more accurate determination of protein concentration. This should contribute to the quality of further processed experiments such as sodium dodecyl suldate polyacrylamid gel electrophoresis (SDS-PAGE) which is described in section 2.7.6.

2.7.4 Immunoprecipitation (IP)

Cells were seeded in either 10 cm or 15 cm dishes using complete growth medium and grown until they were confluent. Lysis and quantification were done as described in sections 2.7.2 and 2.7.3. Depending on the IP either Sepharose G beads or α-V5 affinity gel was used. For Sepharose G 20 µL of slurry per IP was transferred into a new tube and washed thrice with PBS followed by 1 min centrifugation with 500 x g. Between 500-1,000 µg protein was diluted to a volume of 500 µL. 10 µL of the washed slurry was added to the diluted protein and incubated for 1h at 4°C on a rotary wheel to pre-clear the lysate. The remaining beads were resuspended in 3% (w/v) BSA/PBS to block unspecific binding. After incubation the vials were spun down for 1 min at 500 x g. The pre-cleared supernatant was transferred into a new tube. The BSA/PBS was aspirated from the remaining beads, resuspended in RIPA buffer and shared between the supernatants (equivalent of 10 µL slurry per IP). The antibody of interest was then added. All tubes were sealed with parafilm and incubated overnight on the rotary wheel at 4°C. After incubation, the IPs were centrifuged for 1 min at 500 x g and the supernatant was aspirated. The beads were washed thrice with RIPA lysis buffer. After the last washing step approximately 25 µL of bed volume was left behind and 5 µL 6x loading dye was added. All IPs were boiled at 95°C for 5 min followed by SDS-PAGE as described in subsection 2.7.6.
For V5 IPs α-V5 affinity gel was used which is directly conjugted to V5 antibodies. Therefore, pre-clearing and blocking steps are omitted. Due to the smaller size of the beads centrifugation steps were carried out at full speed (21,100 x g). All other steps remained constant.

2.7.5 Preparation of Polyacrylamide (PAA) gels

PAA gels were prepared with buffers described in section 2.7.5.1 and reagents listed in section 9.3.2. First, a running gel was prepared from the recipe in table 2.2 and topped up with isopropanol. After 30 min the isopropanol was removed and the stacking gel solution was applied (table 2.3). PAA gels were prepared one day in advance and stored for up to a week, wrapped in moist tissue and cling film, at 4°C.

Table 2.2: Recipe for polyacrylamide running gels

	7%	**8%**	**10%**	**12%**	**17%**
H_2O	5.75 mL	5.5 mL	5.0 mL	4.5 mL	3.2 mL
1.5 M Tris pH 8.8	2.5 mL	2.5 mL	2.5 mL	2.5 mL	2.5 mL
40% Acryl:Bis 29:1	1.75 mL	2.0 mL	2.5 mL	3.0 mL	4.3 mL
10% SDS	100 µL	100 µL	100 µL	100 µL	100 µL
10% APS	100 µL	100 µL	100 µL	100 µL	100 µL
TEMED	10 µL	10 µL	10 µL	10 µL	10 µL

Table 2.3: Recipe for polyacrylamide stacking gel

	4%
H_2O	6.5 mL
0.5 M Tris pH 6.8	2.5 mL
40% Acryl:Bis 29:1	1.0 mL
10% SDS	100 µL
10% APS	100 µL
TEMED	10 µL

2.7.5.1 Reagents for Polyacrylamide gels

This subsection lists all reagents used to make PAA gels.

0.5 M Tris pH 6.8

– 30.29 g Tris-base

Adjust pH to 6.8 with HCl
Adjust to 500 mL with MilliQ water
Store aliquots of 50 mL at -20°C

1.5 M Tris pH 8.8

– 90.86 g Tris-base

Adjust pH to 8.8 with HCl
Adjust to 500 mL with MilliQ water
Store aliquots of 50 mL at -20°C

10% (w/v) APS

– 5 g Ammonium persulfate

Adjust to 50 mL with MilliQ water
Store aliquots of 1 mL at -20°C

10% (v/v) SDS solution

– 50 mL of 20% SDS solution

Add 50 mL of MilliQ water
Store at room temperature

2.7.6 SDS-PAGE

Quantified protein lysates were adjusted to 2 µg/µL with lysis buffer and 6 x loading dye and boiled at 95°C for 5 min. Samples were then mixed by flicking and centrifuged with full speed (21,100 x g) at RT for 1 min. 10 µL of the protein mixture (20 µg) was loaded onto a PAA gel filled with 1 x SDS running buffer and run at 90 volts (V) until the separation within the running gels started. The voltage was then increased to 130 V and stopped as soon as the running front reached the bottom of the gel. The gel was subsequently transferred onto polyvinylidene fluoride (PVDF) membrane as described in section 2.7.7.

2.7.6.1 SDS-PAGE buffers and solutions

This subsection lists all buffers and solution which were used for SDS-PAGE.

6x Protein loading dye

- 300 mM of 0.5 M Tris pH 6.8 (6 mL)
- 0.05% (v/v) of 1% (w/v) Bromophenol blue solution (500 µL)
- 20% (v/v) of 99% Glycerol (2 mL)
- 1.5% (v/v) of 10% (v/v) SDS solution (1.5 mL)
- 625 µL β-Mercaptoethanol

Store aliquots of 300 µL at -20°C

10x SDS-PAGE Running buffer

- 250 mM Tris-Base (30.28 g)
- 1.92 M Glycine (144.13 g)
- 1% (v/v) of 20% (v/v) SDS solution (50 mL)

Adjust to 1 L with MilliQ water

1x SDS-PAGE Running buffer

- 100 mL 10x SDS-PAGE running buffer
- 900 mL MilliQ water

2.7.7 Western blot

PVDF membranes were activated in methanol, rinsed with MilliQ water and equilibrated in anode I buffer for at least 20 min. PAA gels were rinsed in cathode buffer. The blotting sandwich was assembled as follows (from bottom to top): three sheets of filter paper soaked with anode II buffer, three sheets of filter paper soaked

with anode I buffer, equilibrated membrane, PAA gel and six sheets of filter paper soaked with cathode buffer. The lid of the Turboblot bay was closed carefully and run at 25 V and 1 A for 30 min. The membrane was blocked in either 5% (w/v) semi-skimmed milk or 5% BSA (w/v), if phospho-antibodies were used, in tris buffered saline with 0.1% (v/v) Tween-20 (TBST) at RT for 1h. Since primary antibodies were always diluted in 5% BSA (w/v) in TBST, milk blocked membranes were rinsed several times in TBST, whereas BSA blocked membranes were not prior to primary antibody incubation.

A list of all antibodies used for western blots in this project are shown in table 2.4.

2.7.7.1 Western blot buffers and solutions

This subsection lists all buffers and solution which were used for western blotting.

Anode I buffer

- 25 mM Tris-Base (3.03 g)
- 20% (v/v) Methanol (200 mL)

Adjust to 1 L with MilliQ water

Anode II buffer

- 300 mM Tris-Base (36.34 g)
- 20% Methanol (200 mL)

Adjust to 1 L with MilliQ water

Cathode buffer

- 25 mM Tris-Base (3.03 g)
- 25 mM 6-Aminohexanoic acid (5.24 g)
- 5% Methanol (50 mL)
- 0.05% SDS (2.5 mL of 10% SDS solution)

Adjust to 1 L with MilliQ water

10x TBS

- 200 mM Tris-Base (24.2 g)
- 150 mM NaCl (88.0 g)

Adjust pH to 7.6 with HCl and fill up to 1 L with MilliQ water

1x TBST

- 10% (v/v) 10x TBS (100 mL)
- 90% (v/v) MilliQ water (900 mL)
- 0.1% (v/v) Tween-20 (1 mL)

2.7.7.2 Antibodies for western blot

Table 2.4: Detailed information about antibodies used for western blotting

Antibody	Supplier	Catalogue number	Source	Detected band(s)	Primary antibody dilution	Secondary antibody dilution
Actin	Sigma	A2066	Rabbit	42 kDa	1:4,000	1:5,000
ADAM15 (ICD)	Abcam	ab39159	Rabbit	115 kDa	1:2,000	1:8,000
β1-Integrin	Abcam	ab52971	Rabbit	140 kDa	1:10,000	1:10,000
β3-Integrin	Santa Cruz	sc-14009	Rabbit	125 kDa	1:1,000	1:4,000
Claudin1	Invitrogen	37-4900	Mouse	22 kDa	1:1,000	1:5,000
E-cadherin	CST	#3195	Rabbit	135 kDa	1:1.000	1:4.000
FAM190A	Santa Cruz	sc-246676	Goat	100 kDa 74 kDa	1:500	1:2,000
Lamin A/C	CST	#4777	Mouse	74 kDa 63 kDa	1:10,000	1:10,000
HSP90	CST	#4874	Rabbit	90 kDa	1:1,000	1:4,000
V5	Sigma	46-0705	Mouse	115 kDa	1:10,000	1:10,000
OB-cadherin	CST	#4442	Rabbit	120 kDa	1:1,000	1:4,000
Occludin	Invitrogen	71-1500	Rabbit	79 kDa 65 kDa	1:3,000	1:8,000
pS6 (S235/236)	CST	#2211	Rabbit	32 kDa	1:1,000	1:2,000
R-cadherin	GeneTex	GTX62825	Rabbit	100 kDa	1:50,000	1:10,000

Table 2.4 Continued: Detailed information about antibodies used for western blotting

Antibody	**Supplier**	**Catalogue number**	**Source**	**Detected band(s)**	**Primary antibody dilution**	**Secondary antibody dilution**
Slug	CST	#9585	Rabbit	30 kDa	1:1,000	1:5,000
V5	Invitrogen	46-0705	Mouse	115 kDa (ADAM15 isoforms)	1:10,000	1:10,000
Vimentin	CST	#5741	Rabbit	57 kDa	1:5,000	1:15,000
ZO1	CST	#8193	Rabbit	220 kDa	1:1,000	1:4,000
ZO2	CST	#2847	Rabbit	150 kDa	1:1,000	1:5,000
Goat	Santa Cruz	sc-2020	Donkey	-	-	-
Mouse	GE Healthcare	NA-931	Sheep	-	-	-
Rabbit	GE Healthcare	NA-934	Donkey	-	-	-

2.7.7.3 Densitometry for western blot analysis

The films of developed membranes were scanned at 600 dpi. ImageJ was used to carry out densitometrical analysis. Each band was outlined with the *rectangular selection tool*. The first band was set as first lane (*Analyze* → *Gels* → *Select First Lane*). The rectangular selection box is then dragged over the second band and set as next lane (*Analyze* → *Gels* → *Select Next Lane*). As soon as all bands are marked with boxes the peaks could be plotted (*Analyze* → *Gels* → *Plot Lanes*). The baseline under the peak was then continued with the *straight line tool* to close the peak area. The *wand (tracing) tool* is used to select the inside of the peak which displays the area in the regions of interest (ROI) manager in square pixel. The bands of the protein of interest was then normalised to the actin control and compared.

2.8 Inhibitor treatments

2.8.1 Treatments

Cells were seeded into 6 cm dishes in duplicates. After 72h, at approximately 50% confluence, cells were treated with the corresponding inhibitors. Dilutions were made in OptiMEM if not stated otherwise. Total volume of the medium was 2 mL for incubation overnight. The application volume of the inhibitors was equalised to 2 µL per dish. If not stated otherwise, the reconstitution reagent was DMSO. An untreated and vehicle control were included.

2.8.2 Inhibitors of various pathway

In this section a variety of inhibitors (table 2.5) were used targeting several pathways. The aim was to perturb the expression of claudin1 to identify which pathway(s) are involved in ADAM15-mediated upregulation. The origin and mode of action will be explained for those inhibitors which helped identifying the underlying pathway of claudin1 regulation.

Table 2.5: Inhibitors used in this project.

Inhibitor	Company	Cat. no.	Stock conc.	Final conc.	Target
Bim1	Millipore	203290	1 mM	1 µM	Novel and classical PKC
FLLL31	Sigma	F9057	5 mM	5 µM	STAT3
Gefitinib	see footnote[1]		500 µM	500 nM	EGFR

[1]Kind gift from Stephen Hiscox

Table 2.5 Continued: Inhibitors used in this project.

Inhibitor	Company	Cat. no.	Stock conc.	Final conc.	Target
Gö6976	Merck/ Millipore	365250	1 mM	1 μM	Ca^{2+} – dependent PKCα and β
Ku0063794	Sigma	SML0382	1 mM	1 μM	mTOR
LY294002	CST	#9901	50 mM	50 μM	PI3K
PD98059	Sigma	P215	10 mM	10 μM	MAPK
PI-103	Selleckchem	S1038	1 mM	1 μM	PI3K
PP2	Sigma	P0042	100 μM	100 nM	Src family kinase
Rapamycin	Merck/ Millipore	553210	100 μM	100 nM	mTOR
Rottlerin	Merck/ Millipore	557370	5 mM	5 μM	PKCδ
SB203580	Sigma	S8307	10 mM	10 μM	p38MAPK

In the following section I am going to elaborate on the inhibitors which were of particular interest.

2.8.2.1 PI3K inhibitors

In this chapter two inhibitors were used to target the PI3K pathway - LY294002 and PI-103.

LY294002 was, along wortmannin, one of the first PI3K inhibitors. Since it binds to all class I variants it belongs to the category of "pan-inhibitors". It is a synthetic compound based on the flavonoid quercetin[448]. LY294002 is widely used, due to its higher specificity and stability in solution, compared to wortmannin[448]. Although, both mode of action is to target the ATP binding pocket within the catalytic domain of PI3K, LY294002 is a reversible inhibitor while wortmannin is not.

LY294002 and wortmannin cannot be used in therapeutics, since they do not distinguish between isoforms. Studies show that PI3K isoforms possess non redundant functions downstream of different receptors[449]. Therefore, there is still ongoing need for inhibitors which specifically inhibit each isoform.

One of the newer and more selective inhibitors is the synthetic pyridinylfuranopyrimidine based inhibitor PI-103. It selectively inhibits the p110/α/β/γ/δ subunits in varying concentrations[450]. As LY294002 and wortmannin, PI-103 also competes for ATP and interacts with the ATP binding pocket of the p110 subunit[451].

2.8.2.2 Mammalian target of Rapamycin (mTOR) inhibitors

In this chapter two inhibitors were used to target the mTOR pathway - Rapamycin and Ku0063794.
Rapamycin was the first drug identified which targets mTOR. That is the reason why mTOR is named *the mammalian target of rapamycin*. Rapamycin was discovered in soil samples from the island of Rapa Nui[452] (Easter Islands) and is produced by the bacterium *Streptomyces hygroscopicus*. It belongs to the group of macrolides and has a immunosuppressant mode of action. Its inhibitory behaviour results from the ability to bind FK506-binding protein 12 (FKBP12), a small protein which specifically associates with mTOR close to the kinase domain. Upon binding a complex is formed thus ceasing its activity[337,453,454].
Another and rather recent inhibitor against mTOR is Ku0063794. It is small molecule which inhibits both mTORC1 and mTOR2[455]. The half maximal inhibitory concentration (IC_{50}) is approximately 10 nM. It is highly specific, since the activity of 76 other kinases as well as 7 lipid kinases is not affected even with 10^3-fold higher concentration[455]. Importantly, class 1 PI3Ks are not affected either. Ku0063794 can permeate the cell membrane and suppresses phosphorylation of Akt and S6K. Experiments show that Ku0063794 induces G_1-cell-cycle arrest and suppress cell growth.

2.9 Immunofluorescence

2.9.1 Pretreating of coverslips

If not stated otherwise, 3 x 16 mm glass cover slips were transferred into a 35 mm plastic dish and covered with growth medium without any antibiotic. The cover slips were incubated for at least 24h at 37°C and 5% CO_2.

2.9.2 Plating of cells

Before cells were seeded onto the coated cover slips the medium was changed corresponding to the cell line described in subsection 2.2. Depending on the cell line between approximately 5 x 10^4 and 1.5 x 10^5 were seeded and grown at least 72h to assure a natural growth pattern.

2.9.3 Staining of IF slides

Cover slips were fixed in 4% (v/v) formaldehyde (FAH) for 20 min at RT, then washed once in PBS. After that the cells were permeabilised with 0.1% (w/v) saponin

in PBS at RT for 2 min. The cover slips were washed in PBS and blocked in 1% (w/v) BSA at RT for 30 min. The primary antibody probing was done in blocking buffer overnight at 4°C. A list of used antibodies is shown in table 2.6. Following overnight incubation the cover slips were washed three times in blocking buffer and then incubated with AlexaFluor (AF) secondary antibody at RT for 1h in the dark. Coverslips were then washed three times with PBS and mounted on a microscope slide using Prolong mounting media (with DAPI). The slides were dried in the dark overnight at RT.

Table 2.6: Detailed information about antibodies used for Immunofluoerescence

Antibody	**Supplier**	**Catalogue number**	**Source**	**Dilution**
ADAM15 (ECD)	R&D	MAB935	Mouse	1:100
AF488 (α-mouse)	Invitrogen	A11001	Goat	1:1,000
AF488 (α-rabbit)	Invitrogen	A11008	Goat	1:1,000
AF568 (α-mouse)	Invitrogen	A11031	Goat	1:1,000
AF568 (α-rabbit)	Invitrogen	A11011	Goat	1:1,000
Claudin1	Invitrogen	37-4900	Mouse	1:100
Claudin1	Invitrogen	51-9000	Rabbit	1:100
Paxillin	Abcam	ab32084	Rabbit	1:250
Phalloidin[1]	Invitrogen	A12379	*Amanita phalloides*	1:40
V5	Invitrogen	46-0705	Mouse	1:500
Vinculin	Santa Cruz	sc-73614	Mouse	1:100
ZO1	CST	#8193	Rabbit	1:200

2.9.4 Examination of IF slides

Coverslips were examined using a Leica SP5 confocal microscope. For AlexaFluor-488 fluorescent dyes an argon laser with 488 nm excitation wavelength was used. For AlexaFluor-568 fluorescent dyes a helium-neon laser with 543 nm excitation wavelength was used. DAPI was examined with a 405 nm diode laser. If not stated otherwise acquisition of the images was performed at 400 Hertz scan speed with a resolution of 1024 x 1024 pixel.

[1]Toxin; directly conjugated to AlexaFluor-488

2.10 shRNA knockdowns

The production of lentiviral particles and generation of the knockdown cell lines were performed by Dr Zaruhi Poghosyan.

2.10.1 Production of lentiviral particles

293FT cells were cultured in DMEM medium supplemented with 10% FBS, 100 units/mL Penicillin, 100 µg/mL Streptomycin, 4 mM L-Glu, 1 mM MEM sodium pyruvate, 0.1 mM MEM non-essential amino acids (NEAA) and 500 µg/mL Geneticin. Cells were maintained in a humidified incubator at 37°C with 5% CO_2. A day prior to transfection 293FT cells were seeded into 10 cm dishes with 5 x 10^6 cells using growth medium without antibiotics which will be referred to as transfection medium. On the day of transfection the medium was replaced with Opti-MEM. Transfection was done according to manufucaturer's protocol using Lipofectamine 2000 and ViralPower^{TM} packaging mix containing plP1, plP2, plP/VSVG and pLKO.1 expression constructs. An overview of the used plasmids is shown in table 2.7. A day after transfection the medium was replaced with transfection medium. After 48h the supernatants were collected and snap frozen in aliquots. Lentiviral particles were stored at -80°C until transduction.

Table 2.7: shRNAs used for stable knock down cell lines

Supplier	Catalogue number	Target	Description
Sigma	NM_003815.3-1890s21c15	ADAM15	Mission shRNA
Sigma	NM_003815.3-1361s21c1	ADAM15	Mission shRNA
Sigma	NM_003815.3-1736s21c1	ADAM15	Mission shRNA
Sigma	NM_003815.2-497s1c1	ADAM15	Mission shRNA
Sigma	NM_003815.2-1076s1c1	ADAM15	Mission shRNA
Sigma	NM_021101.3-902	CLDN1	Mission shRNA
Sigma	NM_021101.3-402	CLDN1	Mission shRNA
Sigma	NM_021101.3-305	CLDN1	Mission shRNA
Sigma	NM_021101.3-626	CLDN1	Mission shRNA
Sigma	NM_021101.3-627	CLDN1	Mission shRNA

2.10.2 Generation of stable knock down cells using shRNA

T47D or MDA-MB-231/ADAM15 A expressing cells were seeded into 35 mm dish with 2.5 x 10^5 cells each in complete growth medium without antibiotics. The following day, shClaudin1 or shADAM15 containing lentiviral particles were added to

the cells. 8 µg/mL of Polybrene® (hexadimethrine bromide) was added to enhance transduction. A day after infection the medium was replaced with fresh transfection medium. On the following day the medium was replaced with complete growth medium containing 1 µg/mL Puromycin for selection. Cells got expanded and knockdown efficiency determined by western blot analysis as described in section 2.7.

2.11 mRNA analysis

2.11.1 RNA extraction

RNA extraction was done according to the manufacturer's protocol using Qiagen QIAshredder and RNeasy Kit. The elution step was done twice with 25 µL water.

2.11.2 RNA quantification

RNA was quantified using a NanoDrop® ND-1000. The measurement was done in duplicate and the averaged concentration was used for further analysis.

2.11.3 Reverse transcription

1 µg RNA was mixed with 500 nM random hexamers, 400 nM dNTP mix and RNase/DNase free water to achieve a total volume of 12 µL. All upcoming incubation steps were done in a thermo cycler. The mix was heated up to 65°C for 5 min and quickly chilled on ice. 4 µL of 5 x first-strand buffer and 400 µM Dithiothreitol (DTT) were added and incubated at 25°C for 2 min. After that 200 units of Superscript II reverse trascriptase were added and following temperature profile was applied: 25°C for 10 min, 42°C for 50 min, 70°C for 15 min and then cooled at 4°C infinitely. The ready products were then either stored temporarily at 4°C until further processing or at -80°C for long term storage.

2.11.4 PCR

Following the reverse transcription claudin1 and glyceraldehyde-3-phosphate dehydrogenase (GAPDH) were amplified from the complementary DNA (cDNA) with primers displayed in table 2.8. The master mix was prepared according to the manufacturer's protocol. Ingredients, volumes and concentrations are shown in table 2.9. The settings for the thermal cycler are displayed in table 2.10.

Table 2.8: PCR primer sequences

Gene	Direction	Sequence
Claudin1	Forward	5'-ccaacgcggggctgcagctgttg-3'
Claudin1	Reverse	5'-ggatagggccttggtgttgggtaag-3'
GAPDH	Forward	5'-cgtcaaggctgagaacgggaagcttgtcatcaatgg-3'
GAPDH	Reverse	5'-catgccagtgagcttcccgttcagctcagggatg-3'

Table 2.9: Protocol for KAPA PCR master mix. Final volume per reaction was 12.5 µL

Component	Volume	Final concentration
PCR-grade water	3 µL	-
2x KAPA Taq ReadyMix	6.25 µL	1x
10 µL forward primer	0.625 µL	0.5 µM
10 µL reverse primer	0.625 µL	0.5 µM
cDNA	2 µL	-

Table 2.10: PCR cycle protocol. [a)] Claudin1; [b)] GAPDH

	Temperature	Duration	Cycles
Initial denaturation	95°C	3 min	1
Denaturation	95°C	30 sec	25
Annealing	[a)] 60°C / [b)] 66°C	30 sec	
Extension	72°C	1 min	
Final extension	72°C	10 min	1
Hold	4°C	∞	1

2.11.5 Agarose gel electrophoresis

Samples were separated on 1% agarose gels (in 1 x Tris-acetate-EDTA (TAE) buffer, purchased). The total volume for a midi-gel was 120 mL and mini-gel 50 mL. The gels were run at 100 V. GelRed was used as non toxic alternative for ethidium bromide.

2.12 Focal adhesion dissassembly assay

2.12.1 Treatment with nocodazole

Cells were plated on glass coverslips as described in section 2.9 and grown for 72h in complete media, then serum starved overnight. Afterwards the medium was replaced with 10 µM nocodazole (in serum free DMEM) and incubated for 4h at 37°C. The nocodazole was then washed off twice with serum free DMEM and incubated for 15, 30, 45, 60 and 120 min to allow FA disassembly. Cells were fixed as described in section 2.9.3.

2.12.2 Immunofluorescence staining

IF staining was performed as described in section 2.9.3.

2.12.3 Exmaination of slides

The examination of slides was described in section 2.9.4. For this experiments a digital zoom factor of 3 was applied to acquire all the images.

2.12.4 Semi-automated image analysis

The images retrieved from the confocal microscope are packed as Leica image file (.lif) and need to be extracted using the software *LAS AF Lite*. Exported pictures are potentially cropped to achieve single cell images, which are analysed by ImageJ. For total cell area the phalloidin staining was used (green channel). Example images of each processing step are shown in figure 2.4. The picture was loaded into ImageJ and converted into a 16 bit image to allow further conversion. It is then subjected to *mean dark* threshold in black & white (B&W) mode. This makes the stained cells uniformly black coloured. The binary colour values were set to 4 (black) and 255 (white) followed by analysing the particles with *size=1000-Infinity* and *circularity=0.05-1.00* to avoid noise and artefacts. The area was exported in a tab-separated values file (.tsv) to allow to transfer the measurement into Excel. Separately, a joint photographic experts group (.jpeg) file was generated with the image seen in figure 2.4 c to allow manual examination of the analysed cell. This eliminates wrongly measured cells from the evaluation. The macro code written for this analysis is displayed in listing 2.1.

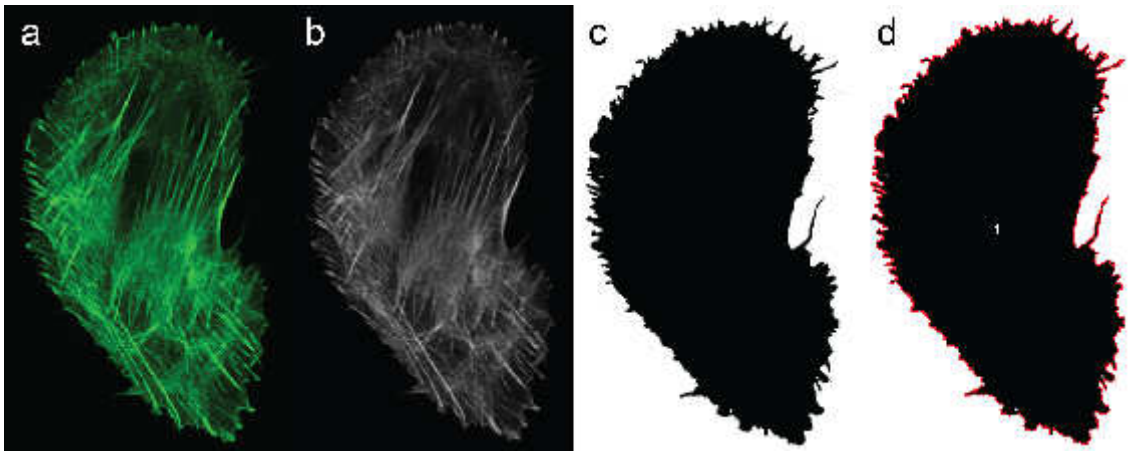

Figure 2.4: Measurement of total cell area. **(a)** The green channel with phalloidin was taken and **(b)** converted into an 16 bit image. **(c)** The *mean dark* threshold is applied to convert the cell into a filled binary image. **(d)** The area of the cell is measured using *Analyze particles* option.

Listing 2.1: Macro code used to determine cell area of phalloidin stained cells during focal adhesion analysis

```
macro "Cell area analysis" {
dir = getDirectory("Choose a Directory ");
list = getFileList(dir);
setBatchMode(true);
for (i=0; i<list.length; i++) {
path = dir+list[i];
open(path);

 run("16-bit");
 setAutoThreshold("Mean dark");
 //run("Threshold...");
 //setThreshold(4, 255);
 run("Convert to Mask");
 run("Analyze Particles...", "size=1000-Infinity
 circularity=0.05-1.00 clear add");

path2 = dir+File.nameWithoutExtension;
saveAs("JPEG", path2+"-bin.jpeg"); close();
saveAs("results", path2+"-results.tsv");
roiManager("reset");

 }
}
```

For analysis of FA the vinculin staining (red channel) was used. Example images of each processing step are shown in figure 2.5. The picture was opened in ImageJ and converted into a 16 bit image. The background was subtracted using a rolling ball radius of 10 pixels and the sliding paraboloid algorithm to decrease the likelihood of artefacts being amplified later. Next the contrast was increased using the *Contrast Limited Adaptive Histogram Equalization* (CLAHE)[456,457] plugin with following settings: *blocksize=50 histogram=256 maximum slope=6* to include weaker FA staining. To further enhance FA structures, especially with noisy background, the Laplacian of Gaussian 3D (LoG3D)[458] filter was applied. The LoG filter size was defined as σ_x=5 and σ_y=5 followed by *Yen*[459,460] thresholding in B&W mode. The binary areas were quantified by *analyze particles* with following settings: *size=1-Infinity* and *circularity=0.05-1.00*.

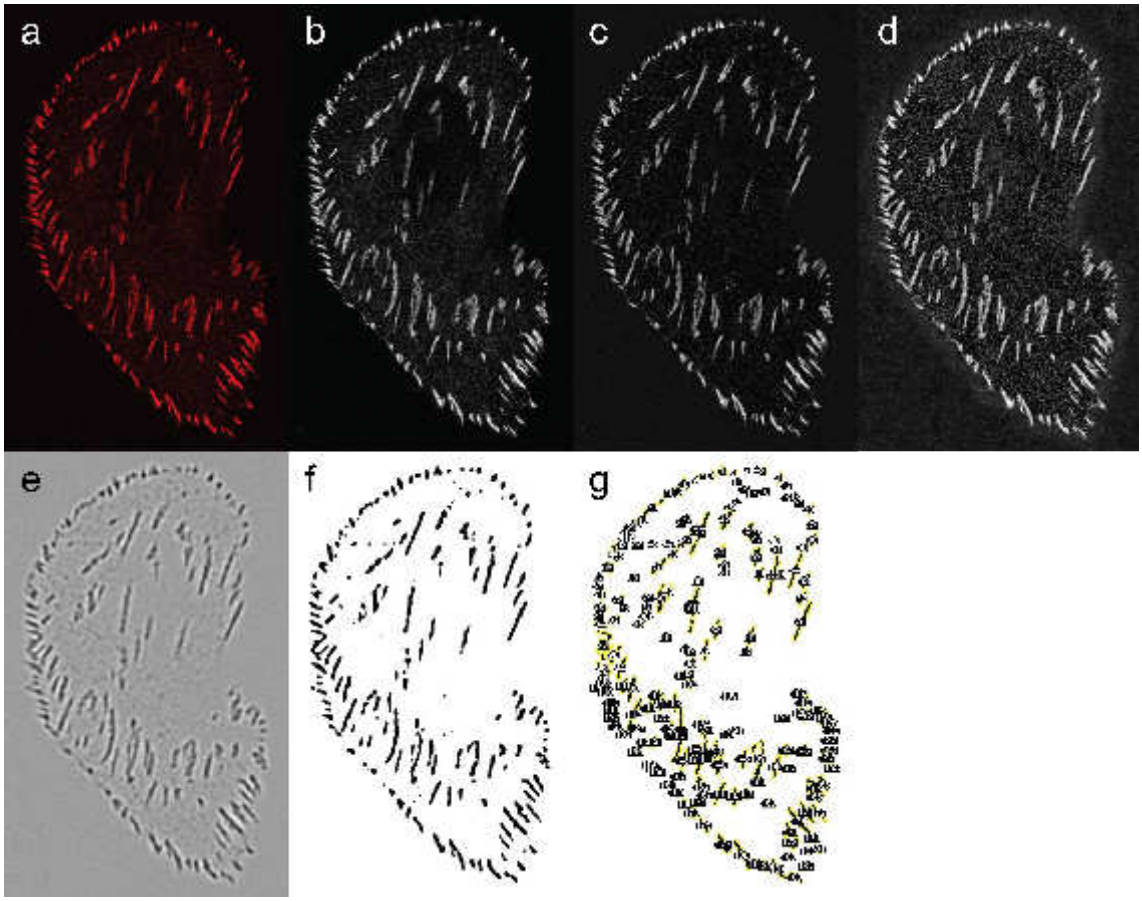

Figure 2.5: Analysis of FA. **(a)** The red channel with vinculin staining was taken and **(b)** converted into an 16 bit image. **(c)** Background was subtracted and **(d)** contrast increased using the CLAHE plugin **(e)** The LoG3D is applied to further enhance the focal adhesions. **(f)** To achieve a binary image a threshold is applied using the *Yen* method. **(g)** The particles are analysed to obtain the borders of the focal adhesions.

The macro code (listing 2.2) for the quantification of FA is similar to the one used for measuring the cell area. The function to select the folder, batch mode and the output is the same.

Listing 2.2: Macro code used to analyse area and intensity of focal adhesions

```
macro "Focal adhesion analysis" {
dir = getDirectory("Choose a Directory ");
list = getFileList(dir);
setBatchMode(true);
for (i=0; i<list.length; i++) {
path = dir+list[i];
open(path);

 run("16-bit");
 run("Subtract Background...", "rolling=10 sliding");
 run("CLAHE ", "blocksize=50 histogram=256 maximum=6");
 title = getTitle;
 run("LoG 3D", "sigmax=5 sigmay=5");
 selectWindow("LoG of "+title);
 setAutoThreshold("Yen");
 run("Analyze Particles...", "size=1-Infinity
 circularity=0.05-1.00 clear summarize add");

path2 = dir+File.nameWithoutExtension;
saveAs("JPEG", path2+"-bin.jpeg");
selectWindow(title);
run("Revert");
roiManager("Measure");
saveAs("results", path2+"-results.tsv");
selectWindow("Summary");
saveAs("results", path2+"Summary.tsv");
roiManager("reset");
close();

 }
}
```

2.13 Quantification of cell spreading plated on ECM components

Adhesion and motility of cells highly depend on interaction between ECM substrates and the cell. Furthermore, adhesion is a key event in generating cell shape and tissue organisation. Determine whether ADAM15 isoforms adhere differently to ECM substrates could give indication if integrin trafficking is affected by ADAM15. Quantification of cell spreading is done by measuring the area a cell spans on the surface. This gives an impression about the degree of cell spreading.

2.13.1 Cell plated on ECM components

Glass cover slips were coated with either complete growth medium or an ECM substrate (table 2.11) for 1h at 37°C. After a wash with PBS cells were plated in OptiMEM 1:12.5 from a confluent T25 flask. After 45 min and 105 min a cover slip of each coating was fixed in 4% FAH for 15 min and stained according to the procedure described in section 2.9.3.

Table 2.11: Detailed information about antibodies used for focal adhesion disassembly assay

Coating	Supplier	Cat. No.	Stock	Final	Dilution
Medium	Gibco	11960-085	-	-	-
Fibronectin	Sigma	F1141	1 mg/mL	10 µg/mL	1:100
Vitronectin	Invitrogen	Phe0011	1 mg/mL	10 µg/mL	1:100

2.13.2 Analysis of cell spreading

Cells were examined at 630x magnification. In total, ten images of random positions were acquired. Analysis was performed by ImageJ.
In ImageJ the scale was adjusted by using the scale set by the Leica AS AF Lite software. The *analyze particles*-function was set to *exclude on edges* to omit any cells touching the image margin. This avoids the inclusion of incomplete captured cells. Potential gaps within the cells, due to the used algorithm, were compensated with the *include holes*-function to avoid falsified measurements.
The picture was loaded into ImageJ and converted into a 16 bit image to allow further conversion. It is then subjected to *triangle dark* threshold in B&W mode. This makes the stained cells uniformly black coloured. The binary colour values were set to 12 (black) and 255 (white) followed by analysing the particles with *size=50-Infinity* and *circularity=0.05-1.00* to avoid noise and artefacts. The area was exported in a tsv-file to allow to transfer the measurement into Excel.

Separately, a jpeg file was generated with the image seen in figure 2.6 b to allow manual examination of the quantified cell. This eliminates wrongly measured cells from the evaluation. The macro code written for this analysis is displayed in listing 2.3.

Listing 2.3: Macro code used to analyse cell spreading

```
macro "ECM spreading" {
dir = getDirectory("Choose a Directory ");
list = getFileList(dir);
setBatchMode(true);
for (i=0; i<list.length; i++) {
path = dir+list[i];
open(path);

        run("16-bit");
        setAutoThreshold("Triangle dark");
        //run("Threshold...");
        //setThreshold(12, 255);
        run("Convert to Mask");
        run("Analyze Particles...", "size=50-Infinity
        circularity=0.05-1.00
        display exclude clear include add");

path2 = dir+File.nameWithoutExtension;
saveAs("JPEG", path2+"-bin.jpeg");

close();
saveAs("results", path2+"-results.tsv");
roiManager("reset");

  }
}
```

After analysis the outcome was manually checked for errors such as cells which could not be told apart by ImageJ. An example image is shown in figure 2.6. In order to count the number of cells the corrected table of measurements was subjected to cell count by Excel using the *count*-function (=COUNT(xy:xz)). Cells at the edge

of the images are excluded as well as clusters.

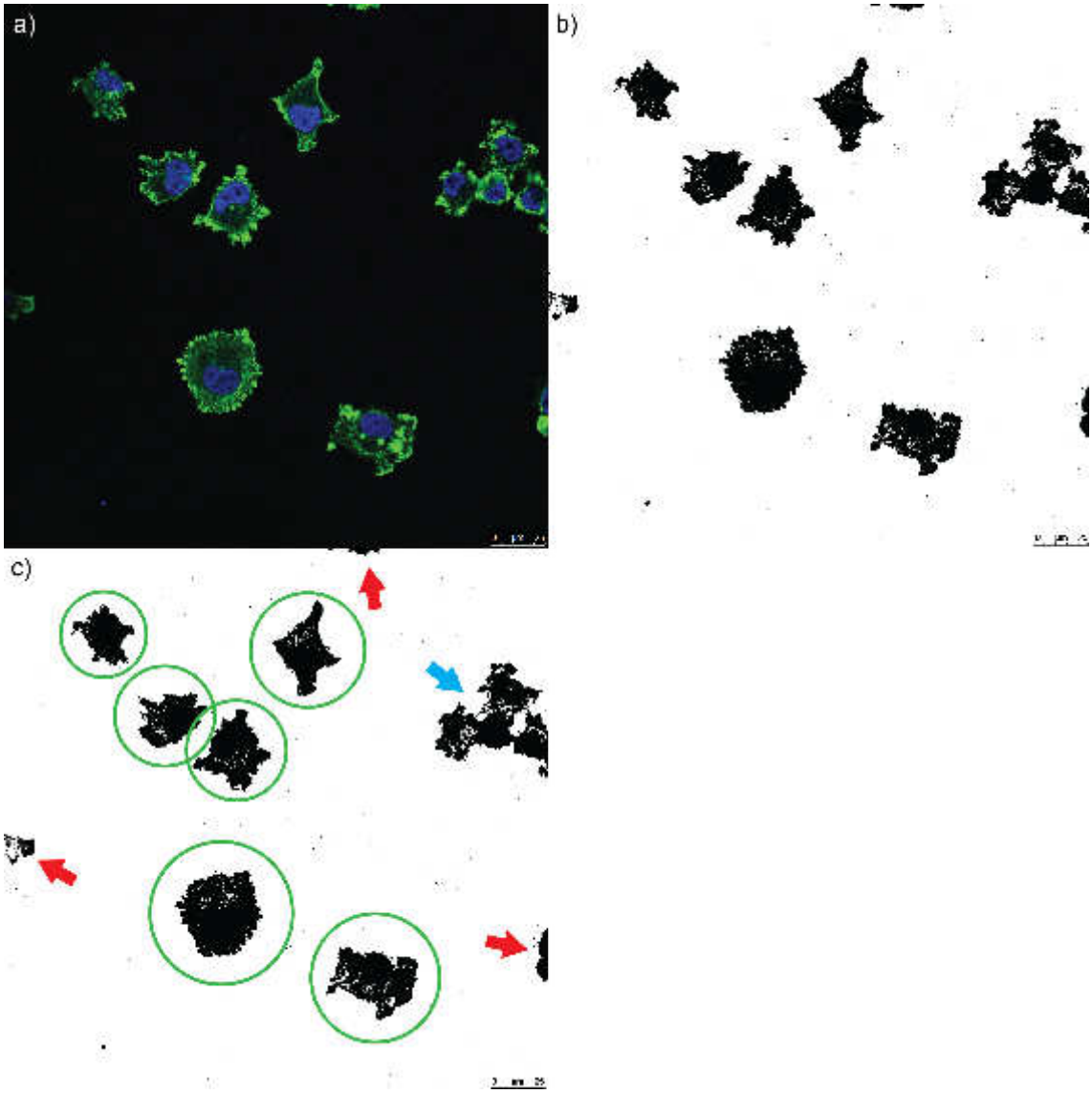

Figure 2.6: Example image of cell spread on ECM components. The image shows an example of MDA/ADAM15 A expressing cells plated on VN for 105 min. **a)** Image as it was acquired by confocal microscopy. **b)** Jpeg of analysed image from the ImageJ automated script for manual verification. **c)** The same jpeg image, but with highlighted events. The red arrows indicate cells on edge which are automatically excluded by the script. The blue arrow indicates a cluster of cells which could not be told apart by ImageJ. Since the right cell of the cluster is touching the frame of the image ImageJ excluded it as cell on edge. Cluster in the centre of the image were not automatically removed for the measurement, but manually afterwards. Cells within the green circle were valid to measure the cell area. Scale bar = 25 µm

2.14 GTPase-linked Immunosorbent Assay (GLISA)

Cells were seeded with a ratio of 1:5 from confluent T25 flasks in 10 cm dishes and grown for 72h. Dishes were then placed on ice, the medium was aspirated and the

plate was washed once with PBS. PBS was aspirated and the plate tilted, whatman paper was used to remove surplus liquid. 250 µL GLISA lysis buffer was added, scraped, transferred to a pre-chilled tube and incubated for 5 mins on ice. The samples were centrifuged for 1 min at full speed (14,800 x g). 30 µL cell suspension was transferred into a new pre-chilled screw cap tube for quantification. The remaining lysate was shared between two tubes. All were snap frozen in liquid nitrogen. Sample preparation did not exceed 10 min. Quantification was done according to manufacturer's protocol. The samples were equalised to the one with the lowest concentration within an experiment. In three independent experiments the range was between 970 and 1000 ng/µL detecting active Rho and Rac GTPase. The assay was performed in duplicates according to manufacturer's protocol. Incubations using the orbital shaker were done at 300 rpm. The incubation time for HRP detection was 15 min. Absorbance was measured at 492 nm. The average of both readings was taken and the blank subtracted from the samples including positive control. The parental cell line was normalised to 1 and the fold difference calculated by dividing ADAM15 A-E WT expressing cells by the parental cell line. The results are plotted as bar chart.

Chapter 3

Characterisation of ADAM15 isoform expressing cells

3.1 Introduction

3.1.1 Aims of the chapter

1. Generation of a cell panel which can be used to observe changes to cell behaviour induced by ADAM15-isoforms
2. Characterisation of changes in morphology
3. Characterisation of changes in proliferation
4. Characterisation of changes in migration

3.2 Results

The main aim of this chapter was to create isogenic cell lines overexpressing proteolytically active and inactive ADAM15 splice variants in order to determine their role in breast cancer. Our group had previously linked ADAM15 splice variant expression to differential outcome in breast cancer[179]. Therefore, these cells provide an excellent *in vitro* model to investigate if and how ADAM15 isoforms may affect various aspects of cell biology differently, to be able to elucidate potential functions of these isoforms in breast cancer. MDA-MB-231 cells express predominantly ADAM15 A and very little ADAM15 B or E (unpublished data). Analysis with isoform-specific primers needs to be conducted as both spliceforms differ only by one amino acid in size (table 1.5).

3.2.1 Validation of parental MDA-MB-231/FRT cell line

The Invitrogen Flp-In^{TM}system allows the integration of a gene of interest at a specific genomic location in mammalian cells. A recombination site is inserted into the genome of cells, which allows the insertion of the genes of interest in a specific recombination site.

An MDA-MB-231/FRT cell line had previously been created by Dr. Zaruhi Poghosyan by transfecting linearised pFRT/lacZeo vector into MDA-MB-231 cells. Using southern blotting a single integration site had been identified for a clone lacking obvious cellular phenotype changes (figure 3.1 a). This cell line showed identical growth rate when compared to unstransfected MDA-MB-231 cell (figure 3.1 b). Therefore we selected these cells for further validation and subjected them to next generation sequencing (NGS) .

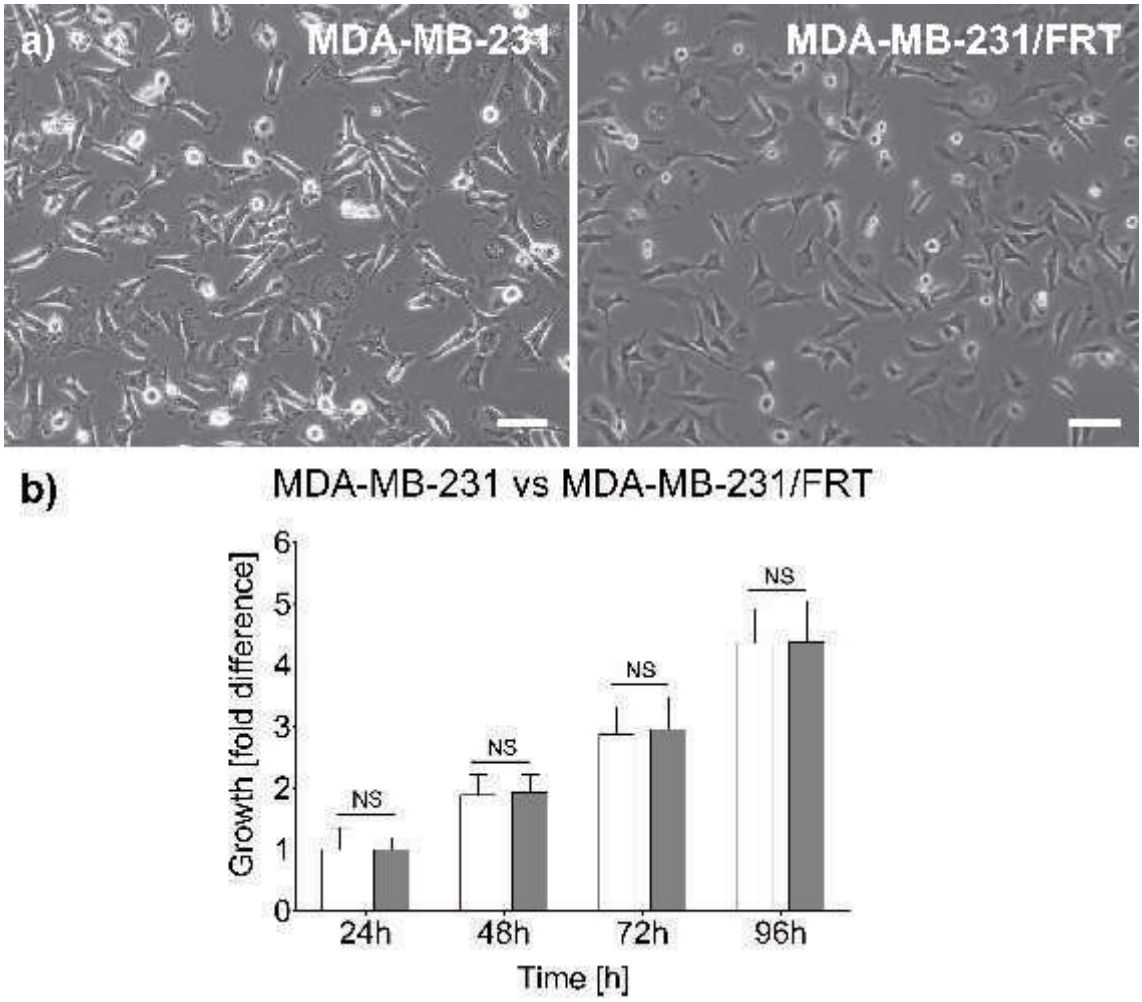

Figure 3.1: Characterisation of MDA-MB-231 and MDA-MB-231/FRT. **(a)** Phase-contrast images of MDA-MB-231 and MDA-MB-231/FRT cells. Scale bar = 100 µm **(b)** MTS assay of MDA-MB-231 and MDA-MB-231/FRT. Cells were seeded in 96-well format with 3 x 10^3 cells per well. After 24, 48, 72 and 96h MTS solution was applied and incubated for 4h at 37°C. Plates were measured at 450 nm. Values got normalised to 1 at 24h. Statistical significance was assessed with two-way ANOVA and Bonferroni post-test. MDA-MB-231/FRT (grey) were compared to MDA-MB-231 (white) at each time point. Confidence intervals are as follows: $* = p \leq 0.05, ** = p \leq 0.01, *** = p \leq 0.001$. n=3

Low-coverage whole genome sequencing (LCWGS) was performed and the pFRT/lacZeo vector integration site mapped in the human genome. Bioinformatic analysis of the sequencing was done by Dr Kevin Ashelford, Cardiff University. The results showed that the vector was integrated on chromosome 4 at position 91,481,550 - 91,481,600 which can be seen in figure 3.2. Alignment of the sequence to the human genome with *Basic Local Alignment Search Tool* (BLAST) confirmed that the vector was integrated in an intronic region (between exon 5 and 6) of the gene for FAM190A.

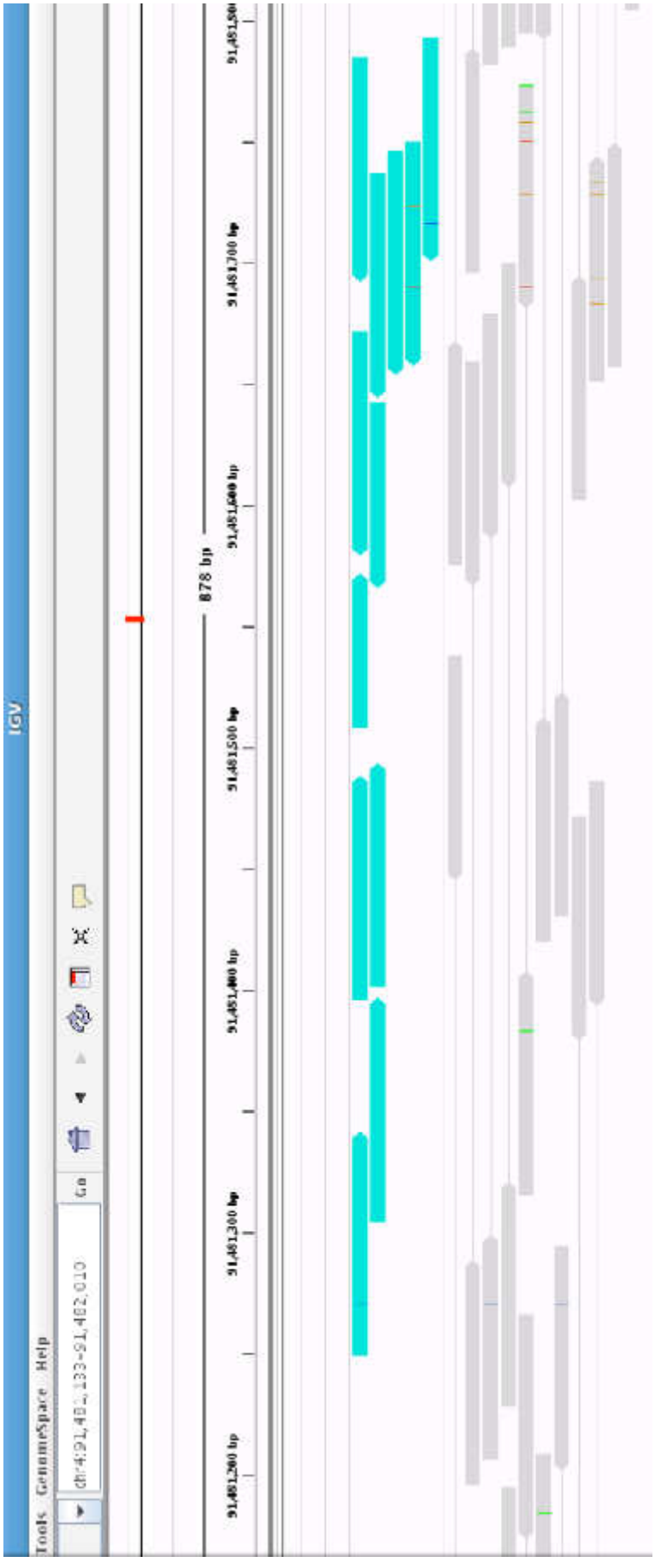

Figure 3.2: A screenshot of the software *Integrative Genomics Viewer* (IGV) visualising the integration site of the pFRT/lacZeo vector in the genome of MDA-MB-231 cells. Based on analysis of the low-coverage sequencing the vector is integrated at position 91,481,550 - 91,481,600 on chromosome 4. n=1

A cell panel was generated by co-transfecting ADAM15 splice variant expression plasmid with pOG-44 recombinase expression plasmid into MDA/FRT cells and subsequent selection with hygromycin to generate stable cell lines. ADAM15 variant expression was verified by western blot analysis using the V5-epitope tag encoded by each respective expression plasmid (figure 3.3). The molecular mass of the ADAM15 variants corresponds to about 115 kDa with variant D being considerably smaller, due to its shorter cytoplasmic tail. ADAM15 A and B showed the highest expression, while ADAM15 C and D were expressed the least. ADAM15 E expression was lower than the one of ADAM15 A and B, but more than ADAM15 C and D expression. The protein levels of the ADAM15 E349A variants were comparable to ADAM15 E WT and similar for all inactive mutants. To confirm that phenotypic changes in our cell panel were due to ADAM15 expression and not due to changes in FAM190A expression we tested whether FAM190A expression was affected by over expression of the ADAM15 transgenes by western blotting. Figure 3.4 shows identical expression of FAM190A across the whole ADAM15 splice variant cell panel which were comparable to levels in parental MDA-MB-231 cells.

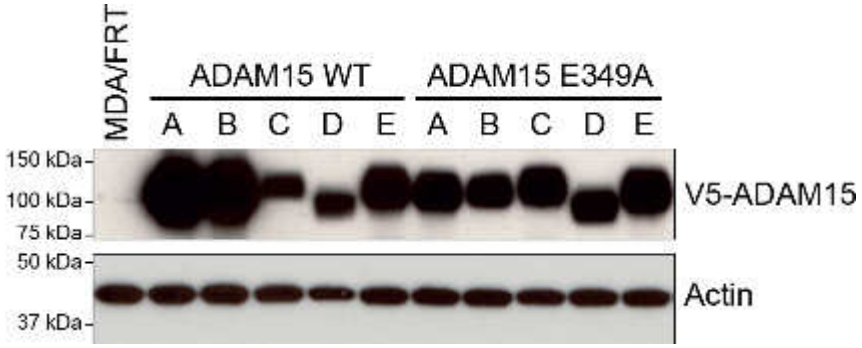

Figure 3.3: Western blot analysis of cell lysates for ADAM15 isoform expression detected via its V5-tag in MDA-MB-231 cells. n=14

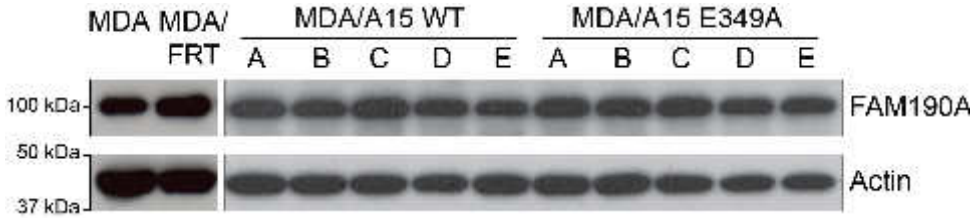

Figure 3.4: Protein expression analysis of FAM190A in MDA/ADAM15 WT and E349A expressing cells. The recombination site is integrated within an intronic region of FAM190A gene. Equal expression suggests the translation is not negatively influenced by integration. n=2

In order to understand whether ADAM15 C and D expression levels were due to epigenetic silencing cells were treated with decitabine (5-aza-2'-deoxycytidine) or in combination with TSA (figure 3.5). Decitabine hypomethylates DNA by inhibition of DNA methyltransferase and TSA inhibits deacetylation. The blot shows, that

expression of variant C and D is upregulated by decitabine/TSA treatment. However, decitabine is more effective in MDA/ADAM15 C than D expressing cells. We conclude that hypermetyhlation is a cause of downregulating ADAM15, but other mechanism regulating gene transcription may be involved as well.

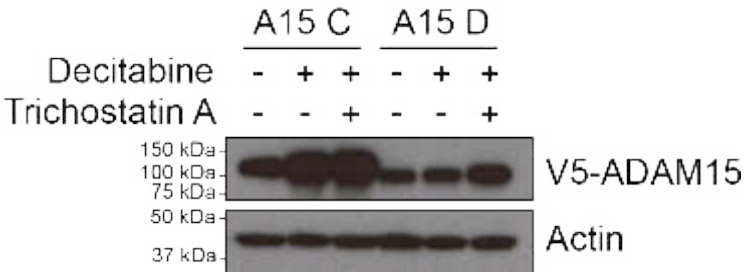

Figure 3.5: MDA/ADAM15 C and D expressing cells treated either with medium, decitabine (33.3 µM & 50 µM) and decitabine in combination with TSA (500 nM). n=2

3.2.2 ADAM15 isoform expression differentially affects cell morphology

Upon successful expansion of the cell lines it was noticeable that cell morphology was changed dependent on the splice variant expressed. Figure 3.6 shows that cells are more prone to cluster formation, especially in ADAM15 A, C and D expressing cells. They possess a cobblestone-like appearance compared to normal MDA-MB-231 cells, which grow scattered and are more elongated. Additionally, I compared the cell morphology of the WT ADAM15 expressing cells with cells expressing the inactive E349A mutants (see A E349A for the ADAM15 A splice variant). The cellular cluster formation was not as prominent as in WT cells, but can be noticed in A E349A, D E349A and E E349A expressing cells.

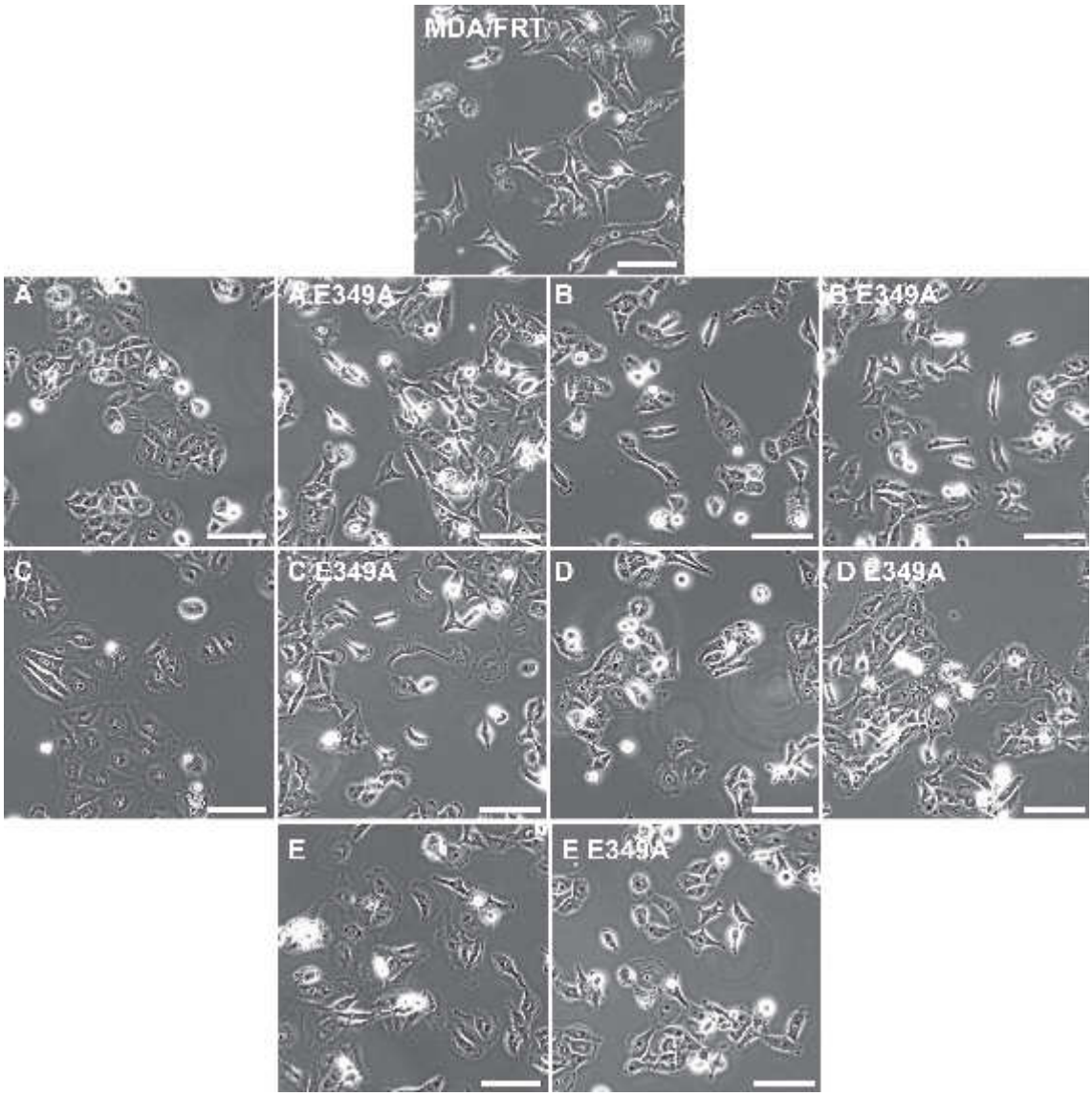

Figure 3.6: Representative phase-contrast images of MDA/FRT, MDA/ADAM15 WT and E349A isoform expressing cells. Scale bar = 100 µm.

To address whether the morphological changes depend directly on ADAM15 we generated stable knockdown cell lines targeting the coding region of ADAM15. Lentiviral particles were made as described in section 2.10. MDA/ADAM15 A expressing cells were seeded into 35 mm dishes with cell number of 5 x 10^5 and grown overnight. Polybrene was added to the supernatant containing lentiviral particles with either incorporated shRNA targeting ADAM15 or non-target (nt) shRNA. The medium on the seeded cells was replaced with the lentiviral supernatant and incubated overnight at 37°C. One day after infection the supernatant was replaced by fresh transfection medium. The next day, the medium was replaced by complete growth medium containing puromycin for selection. Surviving cells were expanded and cell lysates analysed for ADAM15 expression by western blotting (figure 3.7 a). Analysis of ADAM15 expression showed, that MDA/FRT contain little ADAM15.

MDA cells overexpressing ADAM15 A have a much higher protein level of ADAM15. Knockdown by shRNA decreased ADAM15 expression to a level which is below the level of ADAM15 in MDA/FRT cells.

As shown in phase-contrast images MDA/FRT cells grow as single cells with spindle-like morphology (figure 3.7 b). MDA cells overexpressing ADAM15 A grew in cobblestone-like structures (figure 3.7 c). MDA/ADAM15 A shADAM15 expressing cells reversed to the original phenotype of MDA-MB-231 cells (3.7 d). This indicates that the changes in morphology depend on the overexpression of ADAM15 A.

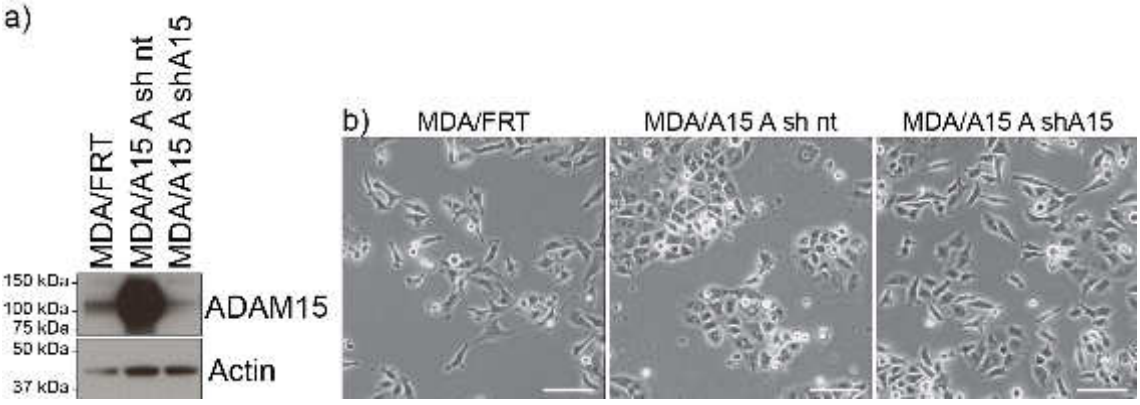

Figure 3.7: Epithelial morphology is directly dependent on ADAM15 A overexpression. **a)** Western blot analysis of MDA/FRT, MDA/ADAM15 A and MDA/ADAM15 A shADAM15 expressing cells. **b)** Phase-contrast images of the parental MDA/FRT cell line, MDA/ADAM15 A expressing and MDA/ADAM15 A shADAM15 cells. Scale bar = 100 µm

3.2.3 ADAM15 isoform expression affect cell size

Analysis of phase-contrast microscopy images indicated that cell size may be affected by ADAM15 overexpression. Five random images were acquired from MDA-MB-231 and ADAM15 WT expressing cells at 200x magnification. In each image ten representative cells were measured. This was repeated twice more (with one week in between) making a total of 150 cells per cell line. Surface area of the cells growing on TC plastic area was determined for each cell line and compared to the parental MDA/FRT cells. The results are displayed in figure 3.8 and statistical analysis performed to evaluate changes in comparison to the parental cell line. ADAM15 C and E expressing cells were significantly larger than MDA-MB-231. ADAM15 D cells were larger as well, but to a lesser degree. In contrast, cells overexpressing the ADAM15 B variant were significantly smaller. The ADAM15 A spliceform did not change the cell size.

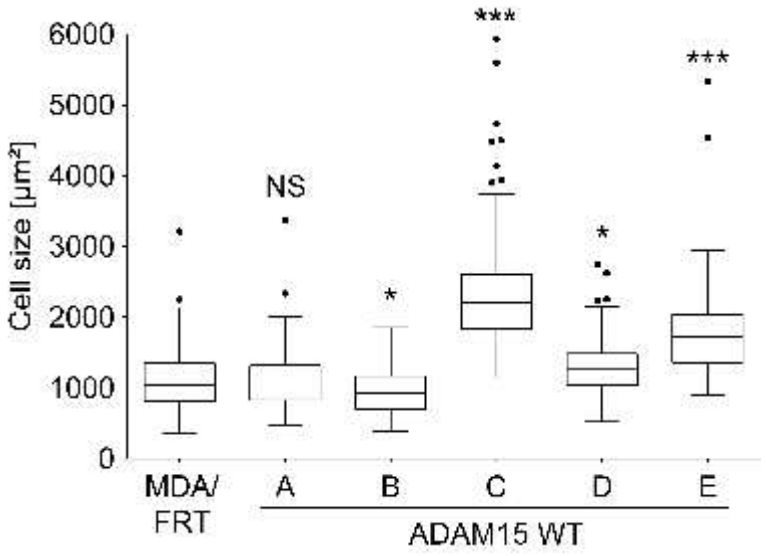

Figure 3.8: Measurement of cell spreading of MDA/ADAM15 isoform expressing cells. Five images of exponential growing cells were randomly taken and ten representative cells per picture were measured. Statistical significance was assessed with Dunnet's multiple comparison test. MDA/ADAM15 WT expressing cells were compared to the 231/FRT control. MDA/ADAM15 A-E WT expressing cells were compared to the MDA/FRT control cell line. Confidence intervals are as follows: $* = p \leq 0.05, ** = p \leq 0.01, *** = p \leq 0.001, **** = p \leq 0.0001$. The measurement was repeated in three independent biological experiments. n=150

To confirm change in cell size an additional experiment was performed using forward scatter (FSC) analysis. An indication of cell size or volume is given by the FSC measured in flow cytometry[461–463].

Scattering of light occurs when a cell or particle deflects or refracts light of the laser beam. This depends on the physical properties of the passing object, the size and its internal complexity. A flow cytometre contains several detectors, one is in the front of the light beam (FSC) while several other detectors are at the site of it measuring the side scatter (SSC). The FSC is proportional to the cell-surface area or size of the particle or cell. It measures primarily the diffracted light close to the axis of the incoming light of the photo diode. The SSC is proportional to the internal complexity or cell granularity and measures primarily reflected and refracted light. It is collected at approximately 90° to the leaser beam. Since only the FSC is a measure of cell size the SSC was not used.

Cells were trypsinised, washed and stained with propidium iodide (PI) and analysed with a flow cytometre. After discriminating debris, doublets and dead cells the FSC-Area (FSC-A) was measured. The median of three independent experiments was plotted as box-and-whiskers plot as shown in figure 3.9. FSC-A analysis confirms that MDA/ADAM15 C and E expressing cells are significantly larger than their parental cell line, while MDA/ADAM15 C expressing cells increase cell size the most. Interestingly, FSC-A analyses showed that MDA/ADAM15 A expressing cells were significantly larger as well, but smaller than MDA/ADAM15 C and E

expressing cells.

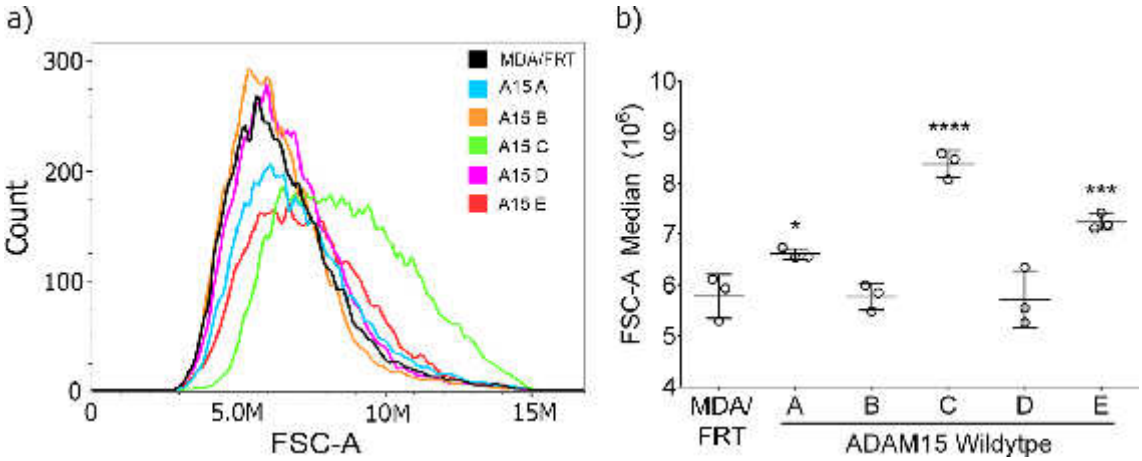

Figure 3.9: Measurement of cell size of MDA/ADAM15 isoform expressing cells. 20,000 events were counted and the median of three independent experiments compared. **(a)** Number of events plotted against the FSC-A: black = MDA/FRT; blue = ADAM15 A; orange = ADAM15 B; green = ADAM15 C; pink = ADAM15 D; red = ADAM15 E. **(b)** Scatter plot comparing the median of all experiments. Statistical significance was assessed with Dunnet's multiple comparison test. MDA/ADAM15 A-E WT expressing cells were compared to the MDA/FRT control cell line. Confidence intervals are as follows: $* = p \leq 0.05, ** = p \leq 0.01, *** = p \leq 0.001, **** = p \leq 0.0001$. n=3

As mentioned earlier, the expression of ADAM15 isoforms led to cell rounding and clustering to varying degree, with particularly ADAM15 A isoform expressing cells having cobblestone-like appearance, while the host cell line is elongated and mesenchymal. To quantify this the circularity was calculated from the cell outlines used to determine cell area of figure 3.8. All ADAM15 isoform expressing cells were more circular compared to the host cell line (figure 3.10). A perfect circle is represented by the value of 1.

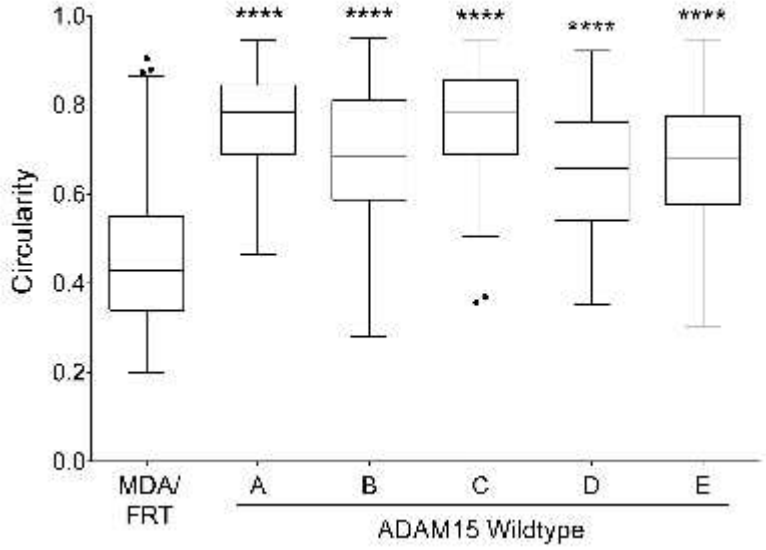

Figure 3.10: Circularity measurement of MDA/ADAM15 isoform expressing cells. five images of exponential growing cells were randomly taken and ten representative cells per picture were measured. Statistical significance was assessed with Dunnet's multiple comparison test. MDA/ADAM15 A-E WT expressing cells were compared to the MDA/FRT control cell line. Confidence intervals are as follows: $* = p \leq 0.05, ** = p \leq 0.01, *** = p \leq 0.001, **** = p \leq 0.0001$. This was repeated in three independent biological experiments. n=150

3.2.4 The expression of ADAM15 isoforms affects proliferation rate in MDA-MB-231 cells

Next we asked whether the growth rate is affected by ADAM15. Therefore the proliferation assay MTS was performed. Cells were seeded into 96-well plate which was measured every 24h. The 24h time point was normalised to 1 and the fold difference calculated. Apart from ADAM15 B expressing cells the expression of all other ADAM15 WT isoforms reduced growth rates to varying degree (figure 3.11). In MDA/ADAM15 A, D and E expressing cells the change in growth rate was independent of the catalytic function. Cells expressing the corresponding catalytically inactive mutants behaved in a similar fashion. However, the expression of ADAM15 C isoform reduced the growth rate of MDA cells the most, and this required its catalytic function, as the expression of ADAM15 C E349A did not affect growth rate.

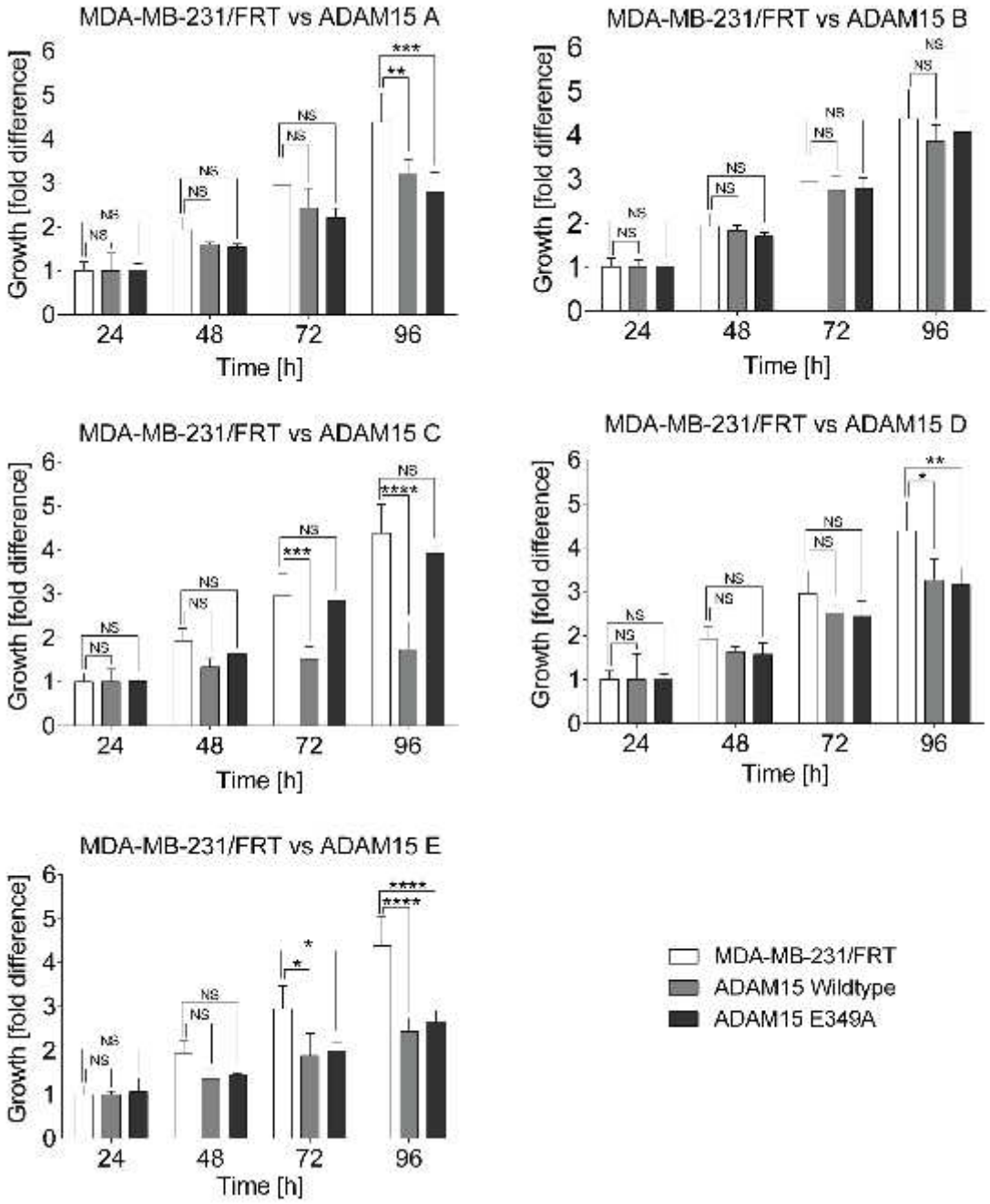

Figure 3.11: Cell proliferation assay with MDA/FRT, ADAM15 WT and E349A expressing cells. MDA-MB-231/FRT compared to ADAM15 A-E WT and E349A expressing cells. 96-well plates were seeded with 3 x 10^3 cells per well and measured every 24h for 96h in total. Results were equalised to 24h and converted to fold difference. Statistical significance was assessed with post-hoc Bonferroni's multiple comparison test after performing two-way ANOVA analysis. The individual ADAM15 WT and E349A isoform was compared to the MDA/FRT control cell line. Confidence intervals are as follows: $* = p \leq 0.05, ** = p \leq 0.01, *** = p \leq 0.001, **** = p \leq 0.0001$. n=3

3.2.5 ADAM15 splice variants alter cytoskeleton rearrangement

We have previously shown that overexpression of ADAM15 splice variants A and B alter actin rearrangement in MDA-MB-435 cells[179]. Here we compared cytoskeletal architecture of ADAM15 A-E WT in MDA-MB-231.

The host cell line and MDA/ADAM15 isoform expressing cells were seeded onto glass coverslips and grown for 72h. Afterwards they were fixed with FAH and stained with phalloidin-488 as described in section 2.9. The slides were examined with a confocal microscope. Representative images are shown in figure 3.12 and a summary of the results displayed in table 3.1

MDA/ADAM15 B expressing cells looked similar to the host cell line. Straight and curved actin bundles were found in the periphery. Some stress fibres, invadopodia-like structures and loose actin meshwork was observed within the cell. MDA/ADAM15 A expressing cells formed membrane ruffles. Some stress fibres and a large number of invadopodia-like structures were found within the cell. Only MDA/ADAM15 D expressing cells showed more invadopodia-like structures, but not ruffle formation and less stress fibres. They also showed curved and straight actin bundles at the periphery. MDA/ADAM15 C expressing cells showed primarily thick curved bundles of actin filaments at the cell periphery with reduced numbers of invadopodia-like structures and stress fibres. Finally, MDA/ADAM15 E expressing cells showed prominent stress fibres, with a reduced number of invadopodia-like structures.

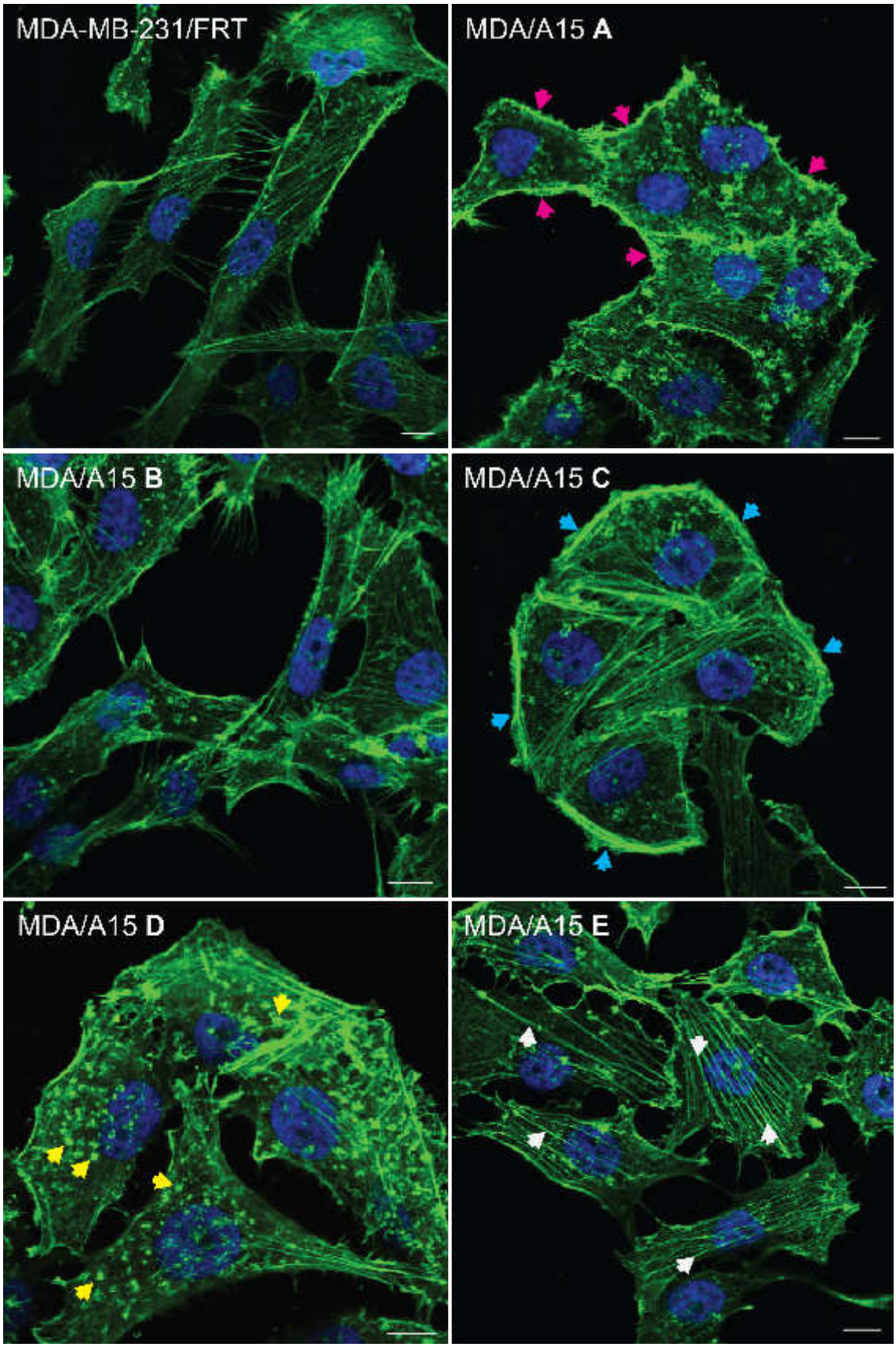

Figure 3.12: Immunofluorescence staining of the actin cytoskeleton in MDA/FRT and MDA/ADAM15 A-E WT expressing cells. Green: Actin cytoskeleton stained with phalloidin-488; Blue: Nucleus stained with DAPI. Scale bar = 10 μm. Actin structures summarised in table 3.1 are labelled with arrows in the image in which they are most abundant. Five examples of each are shown. Magenta arrow: Ruffles; Cyan arrow: Curved actin bundles; Yellow arrow: Invadopodia-like structures; White arrow: Stress fibres. n=6

Table 3.1: Subjective categorisation of observed actin structures and their abundance. "-" = not present, "o" present, "+" = prominent, "++" = abundant.

Cell line	Ruffles	Curved actin bundles	Invado-podia-like	Stress fibres
MDA/FRT	-	o	+	+
MDA/15 A	++	o	+	+
MDA/15 B	-	o	+	+
MDA/15 C	-	++	+	+
MDA/15 D	-	o	++	+
MDA/15 E	-	o	+	++

During examination of the actin cytoskeleton Invadopodia-like structures were observed. Co-staining with V5 revealed that ADAM15 is localised in the centre of these structures (figure 3.13). This was seen in MDA/ADAM15 B, C, D and E expressing cells. Despite possession of Invadopodia-like structures in MDA/ADAM15 A expressing cells, localisation of ADAM15 in this structures was not observed. Figure 3.13 a shows that the majority of ADAM15 is found in the intermediate Z-position. ADAM15 intensity was fading towards the basal and apical position. Figure 3.13 b shows the intermediate Z-position of MDA/ADAM15 C, D and E expressing cells. ADAM15-positive Invadopodia-like structures are marked with arrows.

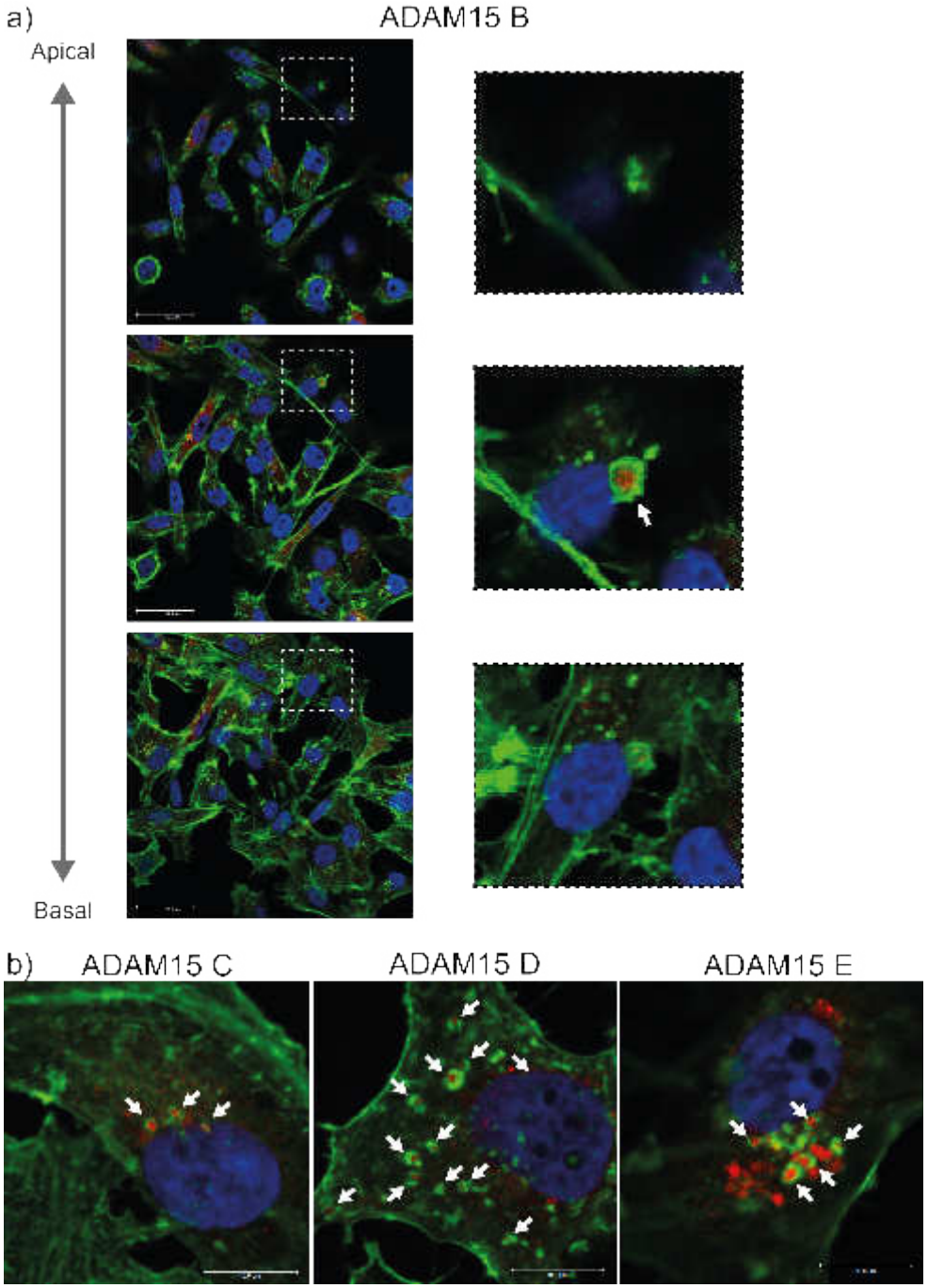

Figure 3.13: Immunofluorescence analysis detected ADAM15 in invadopodia-like structures in MDA/ADAM15 B, C, D and E expressing cells. Yet, we failed to detect co-localisation of ADAM15 A in invadopodia. Green = phalloidin; Red = V5-ADAM15; Blue = Dapi. Arrows indicate co-localisation of invadopodia and ADAM15. **a)** ADAM15 B expressing cells from different Z-positions. Top panel shows the apical position of acquisition. The middle panel shows the intermediate position while the lower panel shows the basal Z-position. **b)** ADAM15 C, D and E expressing cells showing invadopodia with co-localised ADAM15 indicated by arrows. ADAM15 D expressing cells demonstrate and increase number of invadopodia compared to the other cell lines. Scale bar = 10 μm. n=2

GTPases are major mediators of actin rearrangement. Since Rho activity correlates with stress fibre formation and Rac drives cortical actin production, we sought to determine whether their overall activities varied across our cell panel. Based on

the different actin structures present within each cell population, we would expect to see higher Rho activity in MDA/ADAM15 E expressing cells, and higher Rac activity in MDA/ADAM15 A and C expressing cells.

Cells were seeded into 10 cm dishes and lysed after 72h in GLISA kit lysis buffer. The harvesting was done within 10 min. The samples were aliquoted, snapfrozen and stored at -80°C until further processing.

The GTPase activity was analysed with the RhoA and Rac1 G-LISA activation assay kits according to the manufacturer. GTPase activity of MDA/ADAM15 expressing cells was compared to the parent control and the fold difference shown as bar graphs in figure 3.14. No significant changes in total Rho and Rac activity between cell lines were observed.

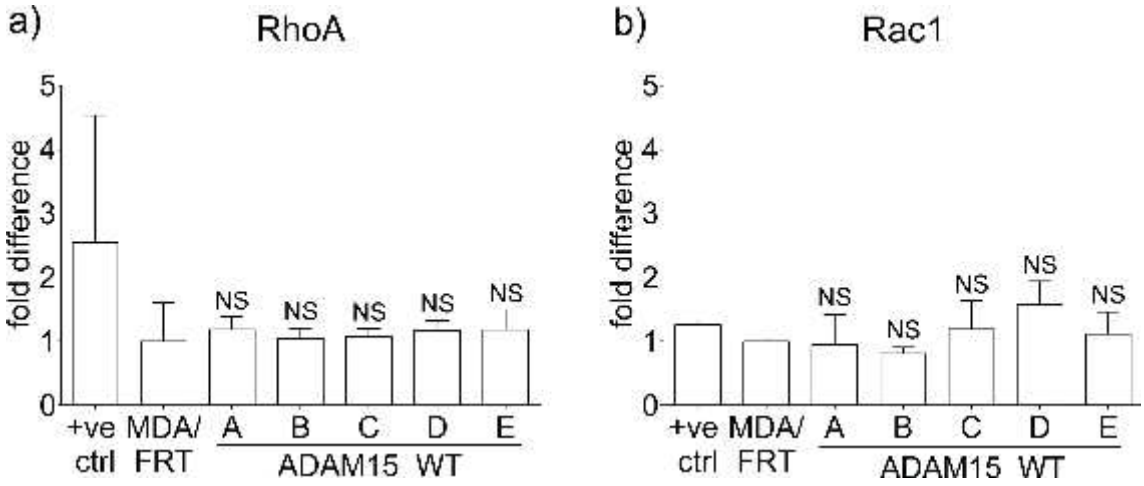

Figure 3.14: Determination of RhoA and Rac1 GTPase activity. **(a)** RhoA GLISA with MDA-MB-231/FRT and ADAM15 isoform expressing cells. **(b)** Matching Rac1 GLISA. Statistical significance was assessed with the post-hoc Dunnet's multiple comparison test after performing one-way ANOVA analysis. MDA/FRT was used as reference and the fold difference was set to 1. The MDA/ADAM15 A-E WT expressing cells were then compared to the MDA/FRT control cell line. Confidence intervals are as follows: $* = p \leq 0.05, ** = p \leq 0.01, *** = p \leq 0.001, **** = p \leq 0.0001$. n=3

3.2.6 ADAM15 isoforms differentially regulate cell migration

The vast majority of ADAM15-related research so far was carried out focusing on the most abundant isoform, ADAM15 A. Based on the literature the disintegrin domain of human ADAM15 is known to inhibit migration in human hepatoma cells[226]. Monolayers of Bel-7402 cells were wounded and different concentrations of recombinant human disintegrin of ADAM15 was administered resulting in a dose-dependent decrease of wound closure. The potential effect of individual ADAM15 isoforms on migration of MDA cells was analysed by using a 2D scratch-wound assay.

Cells were seeded and grown until confluent, scratch wounds were introduced and

analysed using phase-contrast microscopy at 8, 24, 32 and 48h intervals. The wound area at 0h timepoint was set to 100% and wound closure was analysed over time. The results are shown in figure 3.15. Parental cells showed complete wound closure after 48h. Decreased migration was observed in all cell lines apart from MDA/ADAM15 E expressing cells. MDA/ADAM15 A and B expressing cells close the wound to approximately 15% and 25%. while MDA/ADAM15 C and D expressing cells showed the slowest wound closure (about 50%.). The latter one did not close the wound after 96h (data not shown), whereas ADAM15 C expressing cells did.

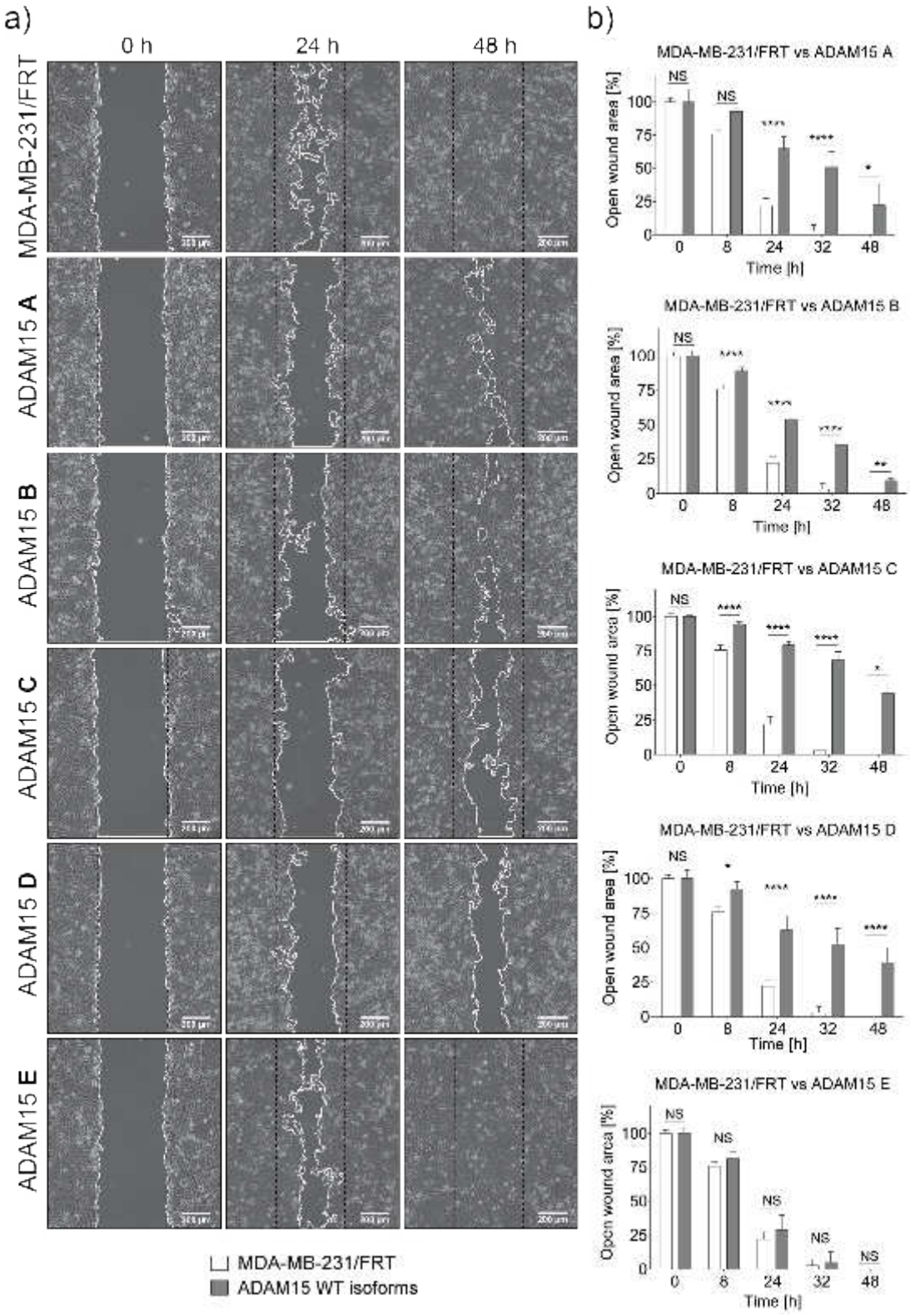

Figure 3.15: Wound healing assay of MDA/ADAM15 isoform expressing cells **a)** Example images of MDA-MB-231/FRT and ADAM15 WT isoform expressing cells right after wounding (0h), 24h and 48h. **(b)** Column charts comparing the parental cell lines against each ADAM15 WT expressing isoform. Images were analysed with ImageJ. Wound at 0h was considered as 100% and closure correspondingly calculated. Statistical significance was assessed with post-hoc Bonferroni's multiple comparison test after performing two-way ANOVA analysis. The individual ADAM15 WT isoform was compared to the MDA/FRT control cell line. Confidence intervals are as follows: $* = p \leq 0.05, ** = p \leq 0.01, *** = p \leq 0.001, **** = p \leq 0.0001$. n=3

3.3 Discussion

In this chapter I have characterised the isogenic cell panel expressing ADAM15 A-E WT and E349A expressing cells in MDA-MB-231 cell line. LCWGS revealed a single insertion of the FRT site within an intronic region of the gene FAM190A. Western blot analysis confirmed that insertion or recombination did not negatively influence the expression of FAM190A. I showed that the insertion of the recombination site did not change morphology or growth rate of the cells. Western blot analysis of the generated MDA/ADAM15 isoform expressing panel showed that ADAM15 A and B is slightly over- and C and D little underexpressed compared to ADAM15 E and their corresponding catalytically inactive mutants. Decitabine and TSA treatment indicated that the reduced expression of ADAM15 C and D is due to hypermethylation. Phase-contrast analysis showed that the cell morphology changed depending on the expressed ADAM15 isoform and catalytic activity. MDA/ADAM15 A WT expressing isoforms showed dense cobblestone-like appearance compared to MDA/ADAM15 A E349A. Downregulation of the induced ADAM15 A isoform rescued the original morphology. MDA/ADAM15 C and D expressing cells were significantly larger than parental or other isoform expressing cells. All cell lines expressing ADAM15 isoforms were less elongated and rounder. MDA/ADAM15 A, D and E expressing cells grew slower than MDA/FRT independent of their catalytic function. MDA/ADAM15 C expressing cells had the slowest proliferation rate which depended on the catalytic function. MDA/ADAM15 B expressing cells did not change the growth rate.
We have shown that the actin rearrangement is different in all MDA/ADAM15 WT isoform expressing cells. MDA/ADAM15 A expressing cells have a high number of invadopodia-like structures and membrane ruffles while MDA/ADAM15 B expressing cells are similar to MDA/FRT. MDA/ADAM15 C expressing cells have much more cortical actin while MDA/ADAM15 D expressing cells are rich in invadopodia-like structures too. MDA/ADAM15 E has very high number of stress fibres. To address whether this is caused by RhoA and Rac1 GTPase, major contributor to actin rearrangement, the cell panel was tested for RhoA and Rac1 activity using G-LISA. However, no significant changes compared to the parental cell line were observed. Migration was also affected by ADAM15 expression. Expression of ADAM15 A and B slowed the migration rate down by approximately 20% while ADAM15 C and D reduced it by 50%. ADAM15 E showed no changes.
The FRT integration site in MDA-MB-231 cells was validated by LCWGS. As the name implies, the coverage of this methods is rather low. The *1000 Genomes Project* had an average coverage of 3.6x in 179 analysed samples and let to the identification of approximately 15 million single nucleotide polymorphisms (SNPs)[464] . Since the aim was to identify the locus of a sequence with more than 8 kilobase pairs (kbp)

LGWGS seemed to be appropriate. However, there could be a possibility to get no coverage where the vector is integrated. This would only provide information on the copy number and not on the location. Mapping demonstrated that a coverage of 1x-5x was achieved. The adjacent sequences were identified as intronic region of FAM190A.

The WB analysis revealed that FAM190A expression is equal suggesting that no negative effects were induced since the insertion happened in a non-coding area. Equal levels could have also been achieved by rescuing the expression of FAM190A on the other chromosome, since insertion happened only once and genes are normally in doublets. Another indication of an integration without side effects is that no phenotypical changes were induced. According to its function, FAM190A is still uncharacterised, but evolutionary conserved in vertebrates[465]. Patel et al. showed that knock down of FAM190A by shRNA caused multinuclearity, cytokinesis defects and multipolar mitosis[466] suggesting it is involved in those events. Occasionally, multinuclear and giant cells were found which could suggest cytokinesis defects. However, multinuclear[94,467] and giant cells are also sometimes found in MDA-MB-231[94]. Thus, the host cell line was considered suitable to use for recombining in the ADAM15 sequences.

The recombination step into the same parental MDA/FRT clone was repeated twice more with ADAM15 isoforms, and in each case the expression levels of ADAM15 C and D were lower than the rest. Treatment with decitabine or in combination with TSA increased the levels of ADAM15 C and D. Decitabine is an inhibitor of DNA methyltransferase while TSA inhibits histone deacetylase (HDAC) class I and II[468]. DNA methylation, histone acetylation and deacetylation play a crucial role in regulating gene expression. Active transcriptional chromatin is linked to hyperacetylation via histone acetyltransferases (HATs), whereas silenced genes are associated with hypoacetylation induced by HDACs. Interestingly, the MDA/ADAM15 E349A splice variants show equal expression throughout. A reason could be that the active MP domain in WT cells is involved in signalling pathways that regulate factors which are harmful to the cell, thus gene silencing is used as means of cell protection. Alternatively, it might directly regulate HDACs and HATs by processing transcriptions factors. So far this was only observed in MDA-MB-231 cells since MCF-7, PC3 and LNCaP cells (unpublished data) allow equal expression.

We observed that, depending on expressed ADAM15 isoform, cell shape changed dramatically. Naturally, MDA-MB-231 cells grow spindle-shaped like fibroblasts. However, ADAM15 A isoform expressing cells grow as more epithelial-like cells which could indicate re-activated mechanism which leads to transformation into epithelial cells. This matter will be discussed in chapter 4 in which I will focus on identifying the reason for epithelial-like cell clustering.

Upon ADAM15 overexpression the spindle-like appearance switched to a rather round phenotype. Since cytoskeletal rearrangement is the major mechanism dictating cell shape[469] it is highly likely that ADAM15 introduces changes in assembly/disassembly of either actin, tubulin or microfilament dynamics.

Initial characterisation of the morphology of the cell panel revealed that MDA/ADAM15 C and E expressing cells are significantly larger than the other isoform expressing cells. One reason could be a that ADAM15 induces changes in key players of G_1/S-phase transition. During G_1-phase the cell acquires mass necessary for the transition to S-phase in which the DNA is replicated. During G_1-phase Retinoblastoma protein (pRB) is bound to E2F transcription factor and the release is induced by phosphorylation of pRB by the dimer cyclin-D/CDK4/6 as reviewed first by Weinberg[470]. One potential reason could be a reduced amount of pRB, other upstream signalling molecules or restricted phosphorylation. This would suggest that only the mass increases, but the nucleus/DNA amount is comparable to the non-enlarged isoforms. Defects in cytokinesis seem unlikely, because the majority of cells should be binucleated, which was not observed in immunofluorescence stainings. Additionally, it is possible that ADAM15 C and D upregulate specific signalling pathways, such as PI3K, that increase cell size. I will discuss the PI3K pathway in detail in chapter 4.

The results of the proliferation assay suggests that more than one mechanism is involved. Cells showing reduced growth mostly showed it is independent of the catalytic function (ADAM15 A, D and E). However, in MDA/ADAM15 C expressing cells it depends on an active MP domain. In MDA/ADAM15 B cells the proliferation rate was not affected unlike the others. This points out that the specific protein-protein interactions with individual ICDs have a role in regulating ADAM15 functions necessary for cell proliferation. There are several ways ADAM15 could contribute to proliferation such as shedding of cell surface receptors necessary for proliferative signals such as EGFR or IGFR. Also the interaction with integrins with the disintegrin domain or kinase/adaptor protein interactions with the ICD are likely do modulate cell growth.

Previously, we showed that overexpression of ADAM15 B in MDA-MB-435 cells introduced prominent changes to the actin cytoskeleton compared to the introduction of ADAM15 A. ADAM15 B expressing cells were less well spread, smaller, fewer and short actin stress fibres and stronger cortical actin staining[179]. This was not seen in the MDA-MB-231 cells which may suggest it depends on the cell type. This raised the question whether the activity of Rho family GTPases is altered by ADAM15 expression since these GTPases play an essential role in the reorganisation of the actin cytoskeleton[471]. ADAM15 may also mediate GTPase activity via activation of receptor tyrosine kinases such as EGFR. ADAM15 is able to activate HB-EGF

by shedding[198], which in turn is known to induce strong RhoA activation[472].
ADAM15 has also the potential to influence RhoGTPases via adaptor proteins or Src family kinases due to its binding motifs for SH2 and SH3 domains as well as phosphorylation site of the ICD. Assembly of protein complexes might induce downstream signalling resulting actin rearrangement. As described earlier, Src has essential functions in integrin-mediated Rho GTPase activation. ADAM15 isoforms with different affinities towards Src could affect this mechanism. ADAM15 isoform specific changes in actin rearrangement were found, but no differences in total RhoA and Rac1 activity was observed. During the experiment the lysates were prepared from exponential growing cells. The aim was to determine the GTPase activity in their natural growth phase. However, since they do not grow identically, it could have happened that the GTPase activity was balanced and thus no significant changes were observed. To overcome this issue cell lines could be serum starved and synchronised by addition of FBS. Alternatively, pull-down assays can be performed. Usually a fusion protein of a Rho GTPase binding domain and glutathione-S-transferase (GST) is made which binds to the active form of the specific Rho GTPase in a lysate. Several probes for monitoring GTPase activity are in use. They are all high-affinity domains of Rho-GTPase effectors. To pull down active RhoA commonly the RhoA binding domain of Rhotekin is used. For active Rac and Cdc42 the PAK-CRIB motifs of PAK1 is used. To investigate only active Cdc42 the CRIB domain of WASP is taken[473]. A pull-down is achieved by use of glutathione coated beads which have a high affinity to GST. Pulled down proteins are then analysed by western blotting.
Pull downs, or the used G-LISA kits, analyse the total GTPase activity in a cell population. However, the GTPase activity can differ within a cell, depending on its localisation. To overcome this problem, single cell based assays need to performed to specifically determine GTPase activity across the whole cell. The simplest approach would be to use IF anlysis, in which antibodies are used that specifically target active GTPases. A more quantitative approach can be done using fluorescence resonance energy transfer (FRET) which measures the energy transfer between to chromophores[474]. A similar approach is fluorescence-lifetime imaging microscopy (FLIM). While conventional confocal microscopy makes use of the fluorescence intensity, is FRET based on energy transfer and FLIM makes use of the exponential decay of fluorescent samples[475]. These approaches would help to reveal the distribution of Rho and Rac GTPases which are potentially affected by ADAM15. Beside the direct examination of Rho and Rac their downstream effectors ROCK (for RhoA) and PAK1 (for Rac) can be analysed for the activation. Apart from RhoA and Rac1 there are many other members of the GTPase family which are also known to regulate the actin cytoskeleton: For example Rac2 and 3[476], RhoB-G[476–478] and Cdc42[476]. Therefore, it is important to include other members of the GTPase fam-

ily into future experiments. Interestingly, RhoE is a unique GTPase since it lacks GTPase activity, but is able to bind GTP[479]. Thus it is believed that RhoE is constantly active. Nevertheless, it was demonstrated that RhoE controls the actin organisation under mechanical stress in human periodontal ligament cells[478]. This emphasises the need of including non classical Rho GTPases.

In MDA/ADAM15 B expressing cells the least amount stress fibres were observed. This could be due to increased activity of RhoE since it is demonstrated that it inhibits stress fibre formation[477]. MDA/ADAM15 C expressing cells could potentially have increased Cdc42 GTPase activity, since together with Rac GTPases, Cdc42 regulates the formation of cortical actin-associated structures mediated via Arp2/3 complex[480]. Stress fibres, as predominantly enriched in MDA/ADAM15 E expressing cells, are normally the result of high RhoA activity. Active RhoA activates ROCK kinase which nucleates and polymerises actin filaments. Concomitantly, ROCK phosphorylates LIM-kinase which in turn inactivates cofilin by phosphorylation. Inactivation of cofilin prevents degradation of the stress fibres[481]. Several scenarios may be theoretically possible without increase of RhoA activity. Firstly, ROCK is activated independently of RhoA. Second, LIM kinase is activated independently of Rho-ROCK or cofilin may be degraded/inactive independently of the classical upstream activation. It has been demonstrated that Src is able to bind and phosphorylate RhoGDI which decreases the ability to interact with Rho GTPases[482]. The release of RhoGTPases from RhoGDI complexes in the cytoplasm is a key event for RhoGTPase activity.

In order to investigate changes in the actin cytoskeleton, potentially affected by ADAM15, we stained our cell panel with phalloidin to visualise the actin cytoskeleton. We found an enhanced number of invadopodia-like structures[483] in ADAM15 A and D expressing cells. Invadopodia are actin-based dynamic protrusions of the cell membrane which are sites of attachment and degradation of the ECM. Indeed, ADAM15 has been affiliated with degradation of the ECM. ADAM15, extracted from renal glomerulus cells (mesangial cells), was found to degrade collagen IV and gelatin[196]. Additionally, we observed ADAM15 localised in the centre of these invadopodia-like structures (appendix, figure 3.13). ADAM15 localisation in invadopodia-like structures is somewhat expected, as ADAM15 ICD associates with TKS5, an adaptor protein that acts as a scaffold in invadopodia. In order to evaluate if ADAM15 isoforms, that localise to invadopodia, have specific ECM degrading capacity, a gelatin invadopodia assay is required. Cells are plated on a fluorescent-labeled gelatin matrix which can be fixed and co-stained for IF analysis. Invadopodia activity would be visualised by decreasing fluorescent signal at sites of degradation[484].

According to literature ADAM15 is involved in cell migration. In a rat model

of rheumatoid arthritis the knockout of ADAM15 caused reduced migration of fibroblast-like synoviocytes. It was observed that the expression of pro-inflammatory chemokines and cytokines was suppresed by ADAM15[228]. A previous study showed that the recombinant human disintegrin domain of ADAM15 slows down migration in hepatocellular carcinoma cells by inducing G_2/S arrest[226]. However, the mechanism must be more complex since the disintegrin domain remain constant throughout the isoforms and no difference in migration was observed in ADAM15 E expressing cells. This indicates that the ICD has an important role in migration. Experiments with HUVEC cells and peripheral blood cells showed that overexpression of ADAM15 promoted whereas inhibition reduced neutrophil transendothelial migration[189]. They identified the Src/Erk1/2-axis as pathway regulated by ADAM15 activity. In CHO cells, which express endogenous α5β1-integrin, overexpression of ADAM15 enhanced cell adhesion and reduced migration on fibronectin[225]. It was observed that the surface expression of α5 increased with ADAM15 expression while Erk1/2 phosphorylation was decreased. Experiments with ovarian cancer cells demonstrated that ADAM15 impairs motility via its ability to bind αvβ3-integrin via its RGD motif[388]. Vitronectin is the major ECM ligand for αvβ3. Rendering the RGD sequence inactive (RGD to SGA) increased the migration on vitronectin. This suggests that migration is impaired by the competition of ADAM15 and vitronectin for αvβ3. There is a lot of evidence in literature indicating the role of ADAM15 in cell migration. However, the proliferation rate might have influenced the wound closure of MDA/ADAM15 C expressing cells, as they are the slowest growing isoform. This however does not affect MDA/ADAM15 D expressing cells, as they have comparable growth rate with the other isoforms. Nevertheless, influence of proliferation cannot be ruled out. To overcome this issue the experiment can be repeated with pretreatment of Mitomycin C[485]. Mitomycin C prevents cell proliferation by crosslinking the DNA[486].

Charrier et al. carried out migration experiments, specifically with the shortest known isoform of ADAM15 most likely ADAM15 D[101]. Wound healing assays showed that overexpression of the shortest ADAM15 variant led to decreased wound closure. Especially the last examples identifying a close relationship with integrins and ADAM15 show that crosstalk between ADAM15 and integrins seems very important for adhesion and migration and may explain whether these interaction play a role in our used breast cancer model. Another key mediator of adhesion and migration in cells are focal adhesions which need to be closer investigated. Chapter 5 will focus on this.

Chapter 4

ADAM15 mediated upregulation of claudin1 expression

4.1 Introduction

4.1.1 Aim of this chapter

In the previous chapter I described the morphological changes influenced by the expression of specific ADAM15 isoforms. One of the prominent features was cell clustering, and cell-cell junction formation in some isoform expressing cells.

1. Identify the cause of cell clustering
2. Identify potential pathways involved in ADAM15-mediated cell clustering
3. Identify potential implications of ADAM15-mediated cell clustering

The main aim in this chapter was to investigate if and how ADAM15 isoforms are involved in regulating cell-cell junctions.

4.2 Results

4.2.1 MDA/ADAM15 isoform expressing cells do not undergo mesenchymal-epithelial transition (MET)

Original MDA-MB-231 cells grew as single cells with elongated spindle-like appearance indicating a mesenchymal phenotype. Stable expression of ADAM15 isoforms led to morphological changes of MDA-MB-231 cells. With exception of MDA/ADAM15 B expressing cells, the other cell lines formed clusters to varying degree. Especially ADAM15 A and C expressings cells showed cobblestone-like morphology (chapter 3 figure 3.6). We suspected that MDA cells underwent MET which is the reverse mechanism of EMT. EMT describes the phenomenon when epithelial cells lose their cell polarity and cell-cell adhesion property. This process can be reversed and described as reversal of EMT or MET. MDA-MB-231 cells lost their epithelial characteristics and are true mesenchymal cells. To evaluate whether the expression of ADAM15 isoforms triggered MET, the expression levels of epithelial and mesenchymal markers were analysed by western blotting (figure 4.1). E-cadherin, which is expressed in many epithelial, but not mesenchymal cells[487], was only detected in the control cell line A431. No changes in the expression levels of the mesenchymal markers slug[487] and vimentin[488] were observed in the ADAM15 variant expressing MDA panel. This suggests that the introduction of ADAM15 did not induce MET.

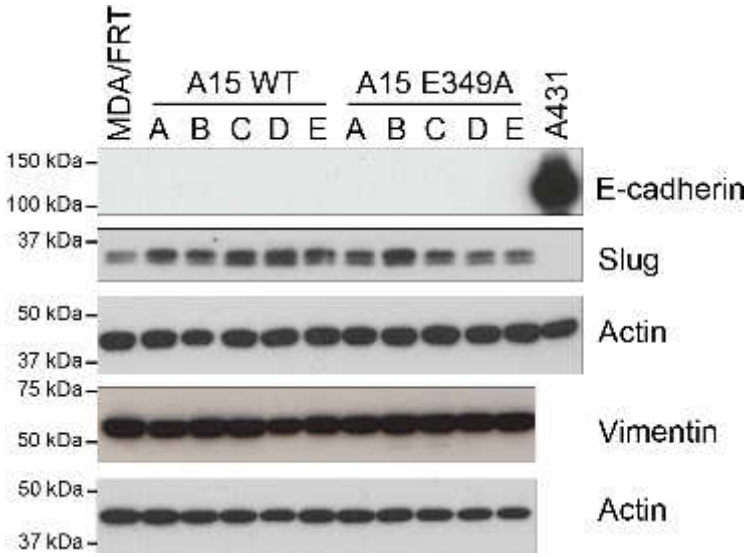

Figure 4.1: Expression of EMT/MET markers in the host cell line and MDA/ADAM15 isoform expressing cells. n=2

Another group of proteins responsible for cell-cell adhesion are tight junction proteins[487]. Different members of this group were screened for changes in expression (figure 4.2 a). ZO1 and ZO2 levels were unaltered across the cell line panel investigated. In contrast, occludin levels were variable across the cell panel as seen in figure 4.2 a. However, expression changes were not statistically significant. Occludin and ZO1 were found to be slightly different within independent samples. However, densitometry of MDA/ADAM15 isoform expressing cells showed no significantly altered expression (figure 4.2 b).

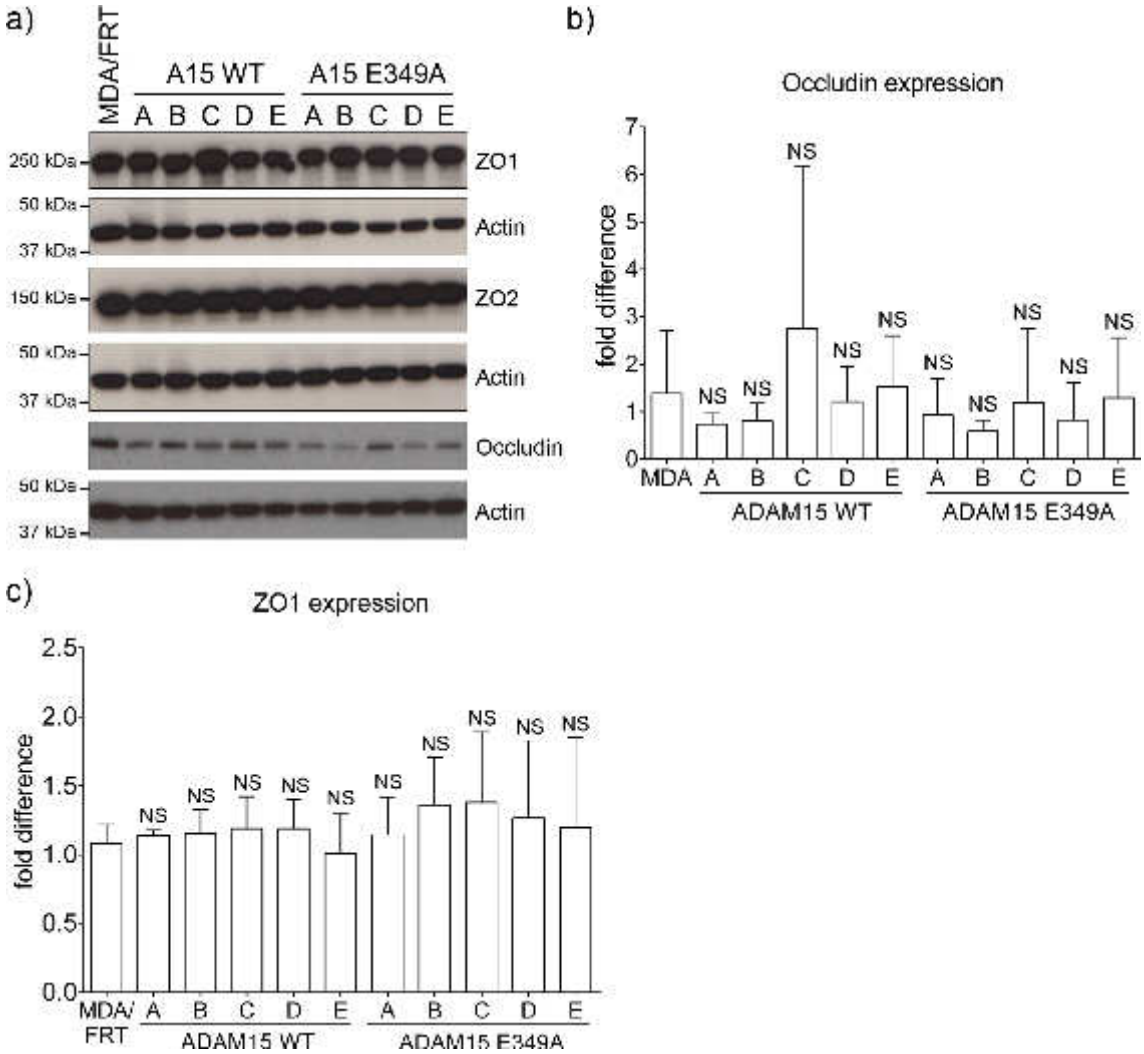

Figure 4.2: Unchanged expression of various tight junction proteins. **a)** The expression of ZO1 (n=3), ZO2 (n=1) and occludin (n=5) were not altered in MDA/FRT and MDA/ADAM15 isoform expressing cells. Occludin expression highly varied within experiments. **b)** Densitometry analysis of Occludin/Actin and **c)** ZO1/Actin expression. No significant changes were observed compared to the parental cell line. Kruskal-Wallis test was performed with Dunn's multiple comparison test. MDA/ADAM15 A-E WT and E349A expressing cells were compared to the MDA/FRT control cell line. Confidence intervals are as follows: $* = p \leq 0.05, ** = p \leq 0.01, *** = p \leq 0.001$. n=5

4.2.2 ADAM15 overexpression leads to claudin1 upregulation

Next we investigated whether claudin expression levels were affected by ADAM15 expression. Together with occludins, claudins are a family of TJ proteins which directly connect adjacent cells. The cell panel was seeded and harvested as soon the dishes were confluent. Western blot analysis was performed to analyse the expression of claudin1. Significant upregulation of claudin1 was found in MDA/ADAM15 A, C and E expressing cells (figure 4.3). Compared to the parental cell line, the claudin1 expression in MDA/ADAM15 A expressing cells was almost 7 fold higher. On average, the level of claudin1 was 3 fold higher in MDA/ADAM15 C and E than

in parental cells. In MDA/ADAM15 B and D expressing cells claudin1 was not upregulated. By western blot analysis weak bands of claudin1 in the catalytically inactive MDA/ADAM15 A, C and E E349A expressing cells could be observed. However, expression was not significantly increased. These results indicated that upregulation of claudin1 expression in response to ADAM15 A, C and E requires the proteolytic activity of ADAM15.

RNA analysis demonstrated that claudin1 expression is 3 fold higher in MDA/ADAM15 A expressing cells compared to MDA/FRT cells. MDA/ADAM15 C and E expressing cells showed 2.5 and 2 fold higher amounts of claudin1 RNA. The RNA levels of claudin1 in MDA/ADAM15 B and D, as well as in E349A expressing cells, were either equal or less compared to MDA/FRT cells.

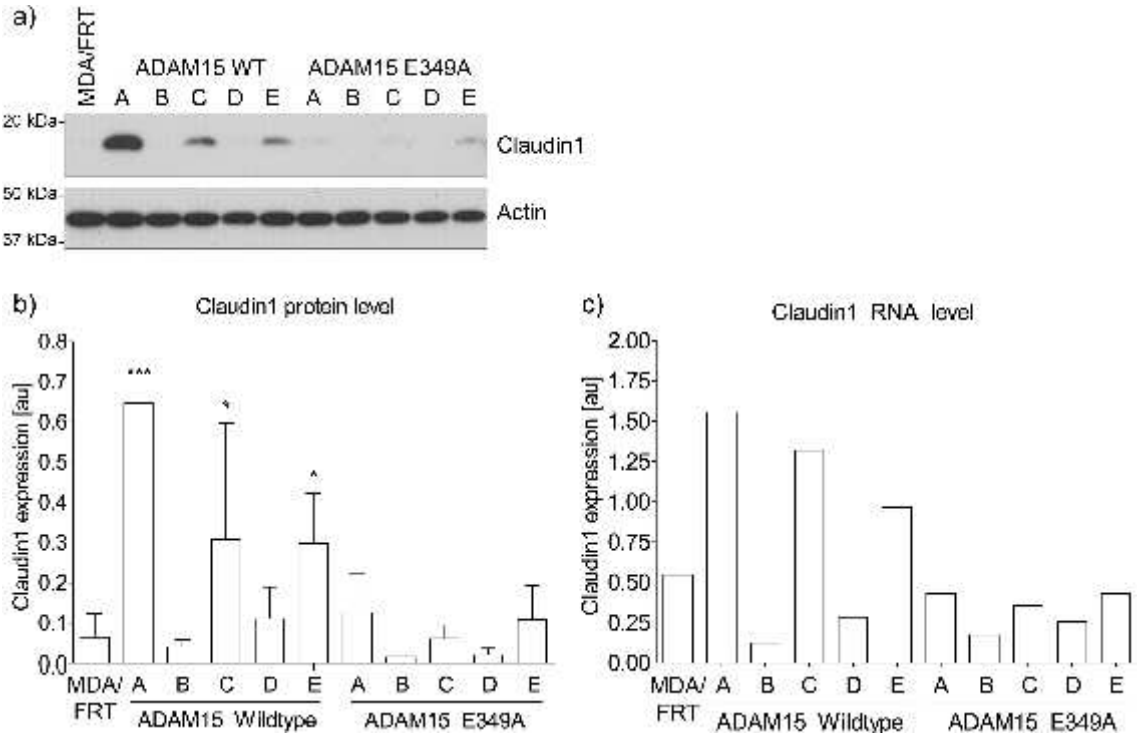

Figure 4.3: ADAM15 upregulates claudin1 in an isoform specific manner.**(a)** Representative western blot of claudin1 expression **(b)** Claudin expression at protein level. Densitometry was performed using ImageJ. Claudin1 expression was normalised to the actin control and displayed as arbitrary unit (au). Statistical significance was assessed with one way ANOVA and Dunnet's multiple comparison test. MDA/ADAM15 A-E WT and E349A expressing cells were compared to the MDA/FRT control cell line. Confidence intervals are as follows: $* = p \leq 0.05, ** = p \leq 0.01, *** = p \leq 0.001$. n=4 **(c)** Claudin1 expression at RNA level. n=1

Slightly elevated expression of claudin1 was also found in the E349A variant of MDA/ADAM15 A, C and E expressing cells, but the increase was insignificant. This finding was confirmed on both protein (figure 4.3 a and b) and RNA level (figure 4.3 c). MDA/ADAM15 isoform expressing cells were harvested from 10 cm dishes and RNA was extracted. The TaqMan analysis was carried out by the lab of Dylan

Edwards (University of East Anglia, Norwich, UK) in one experiment. In summary, claudin1 upregulation was significantly increased in MDA/ADAM15 A, C and E expressing cells.

As cells grow more confluent, tight junctions stabilise. This leads to accumulation of tight junction proteins. To confirm whether the newly expressed claudin1 behaves like a classical tight junction protein, identical numbers of MDA cells expressing ADAM15 isoforms were seeded in duplicates. The first set was harvested for protein analysis during exponential growth (50%), while the second set was harvested two days after the cells became confluent (>100%) (figure 4.4). Western blot analysis was performed for claudin1. In the parental cell line (MDA/FRT) weak bands for each density were observed. This indicates that MDA-MB-231 cells do express claudin1, but in an amount which is close to the detection threshold (figure 4.4). Claudin1 expression was detected in parental and MDA/ADAM15 D expressing cells, but no difference could be observed between both densities. In MDA/ADAM15 A, C and E expressing cells claudin1 expression increased at >100% confluence compared to 50%. In constrast, MDA/ADAM15 B expressing cells lacked the expression of claudin1 and a higher density did not change its level. In order to tell if the accumulation of claudin1 is significant in MDA/ADAM15 C and E expressing cells, a further repeat is necessary. Concomitantly, the membrane was also probed for V5-ADAM15. The protein levels of ADAM15 were independent of cell density.

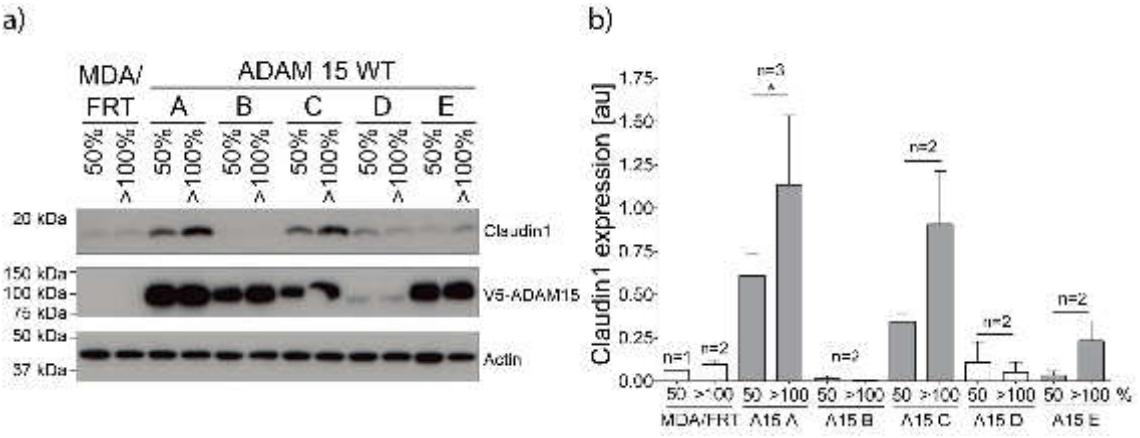

Figure 4.4: Claudin1 expression is dependent on cell density in MDA/ADAM15 A expressing cells. **a)** Western blot analysis of MDA/FRT and MDA/ADAM15 A-E WT expressing cells probed for claudin1 and V5-ADAM15. Actin was used as loading control. **b)** Results of densitometric analysis of claudin1 expression shown as column diagram. Densitometry was performed using ImageJ. Claudin1 expression was normalised to the actin control and displayed as arbitrary unit (au). Statistical significance was assessed with students T-test. The increase in claudin1 expression between 50 and >100% density was addressed. Statistical analysis was performed where applicable. MDA/ADAM15 WT was compared to the MDA/FRT control cell line. Confidence intervals are as follows: $* = p \leq 0.05, ** = p \leq 0.01, *** = p \leq 0.001$. The number of repeats is shown above the individuals bars.

4.2.3 ADAM15 co-localises with claudin1 in MDA-MB-231 cells

Aberrant expression and mislocalisation of claudin1 correlates with very aggressive basal-like beast cancer[59]. We identified that ADAM15 A cells did not undergo MET (section 4.2.1). We hypothesised that claudin1 might not necessarily be restricted to cell-cell junctions in these cells. It was sought to determine the localisation of claudin1 in MDA/ADAM15 A cells. These cells were chosen for subsequent experiments as they had the highest expression of claudin1.

Glass coverslips were coated with growth medium for at least 24h. Cells were seeded and incubated for 72h to reach a confluence of about 30% and to allow cell-cell junctions to form. Subsequently, IF staining was performed as described in section 2.9.

In MDA/ADAM15 A expressing cells co-localisation of both claudin1 and ADAM15 was observed in cell-cell junctions and in the periphery (figure 4.5). Some claudin1 was detected in the cytoplasm, but much more of ADAM15 was localised there. In the parental MDA/FRT cell line some claudin1 was detected across the cell, but neither in the membrane nor cell-cell junctions. The expressed amount was localised to the cytoplasm, but seemed close to the detection threshold. A431 cells showed a very strong localisation of claudin1 in cell-cell junctions and partially at the membrane and the cytoplasm. Since ADAM15 was detected with an anitbody against the V5-tag endogenous ADAM15 in MDA/FRT and A431 was not picked up.

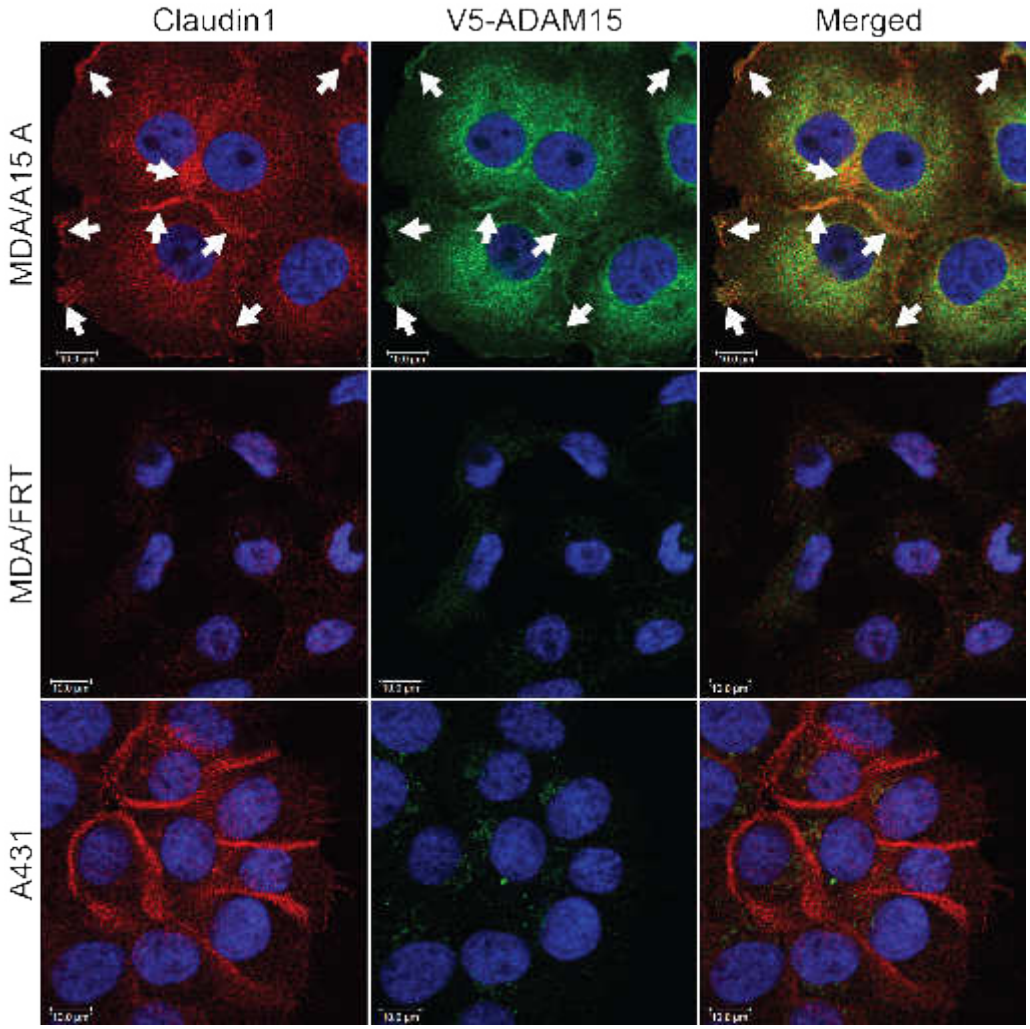

Figure 4.5: Co-localisation of overexpressed ADAM15 and claudin1 in MDA/ADAM15 A expressing cells. The left column shows expression and localisation of claudin1 in MDA/ADAM15 A, MDA/FRT and A431 cell lines. The middle column displays ADAM15 expression and localisation visualised with an antibody against its V5 tag. The right column shows the merged image. Arrows indicate the localisation of claudin1 and ADAM15 in cell-cell junctions and at the periphery. Scale bar = 10 μm. n=6

4.2.4 ZO1 and ZO2 - new ADAM15 interaction partners

The immunolocalisation analysis of claudin1 and ADAM15 raised the possibility that these proteins might form a complex. It is known that the only protein-protein interaction motifs in ADAM15 ICD are the tyrosines and proline-rich regions, that allow direct interactions with SH2 and SH3 domains of various proteins, respectively. However, claudin1 does not contain SH2 or SH3 domains, hence it is unlikely to interact with ADAM15 directly. Contrary, ZO1, a protein that directly binds to claudin1, has an SH3 domain[129] which could potentially link claudin1 and ADAM15. To address the hypothesis that ZO1 forms a complex with ADAM15 and claudin1 IFs were performed with MDA/ADAM15 A expressing cells (figure 4.6). In MDA/ADAM15 A, the analysis shows that ZO1 is primarily found in the mem-

brane and cell-cell junctions with a moderate expression in the cytoplasm. This also applies to ADAM15. The merged image demonstrated ADAM15 and ZO1 co-localisation along cell-cell junctions, as well as the cell periphery.

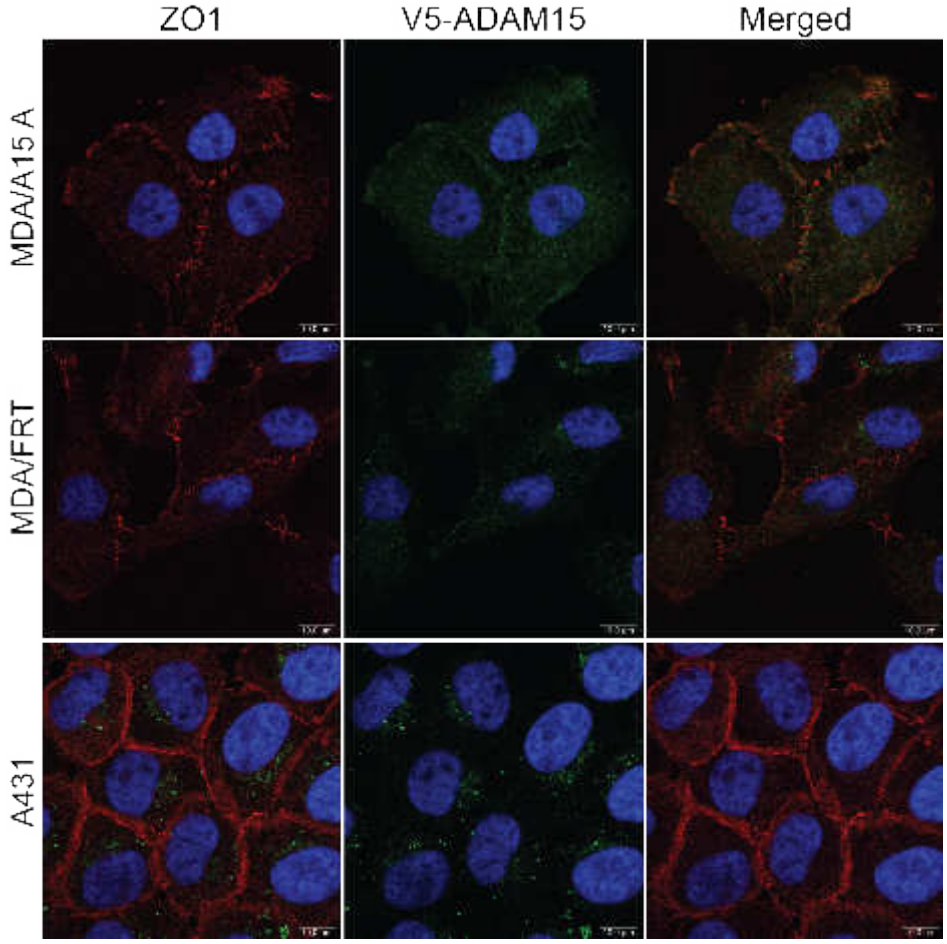

Figure 4.6: Co-localisation of overexpressed ADAM15 and ZO1 in MDA/ADAM15 A expressing cells. The left column shows expression and localisation of ZO1 in MDA/ADAM15 A, MDA/FRT and A431. The middle column displays ADAM15 expression and localisation visualised with an antibody against its V5 tag. The right column shows the merged image. MDA/FRT and A431 cells do not contain V5 tagged ADAM15 and serve as negative control. Scale bar = 10 μm. n=3

In the parental MDA cell line and A431 cells ZO1 was primarily found in cell-cell junctions. A moderate localisation was also observed in the membrane and cytoplasm. MDA/FRT and A431 cells do not express V5-tagged ADAM15. They serve as negative control for V5. However, some unspecific signal was observed. A431 were used as control since ZO1 is expressed in large quantities.
Additionally, to investigate whether endogenous ADAM15 co-localises with claudin1 and ZO1, I carried out IF analysis of T47D cells (figure 4.7). T47D are epithelial cells expressing high levels of claudin1 and ADAM15. IFs were performed with T47D cells and stained for claudin1 or ZO1 and co-stained for ADAM15 using an antibody against the ADAM15 ECD. Claudin1 and ADAM15 were primarily localised in cell-cell junctions and periphery. A moderate expression was also found in the cytoplasm.

Co-localisation of ZO1 and ADAM15 was also observed predominantly in cell-cell junctions and periphery.

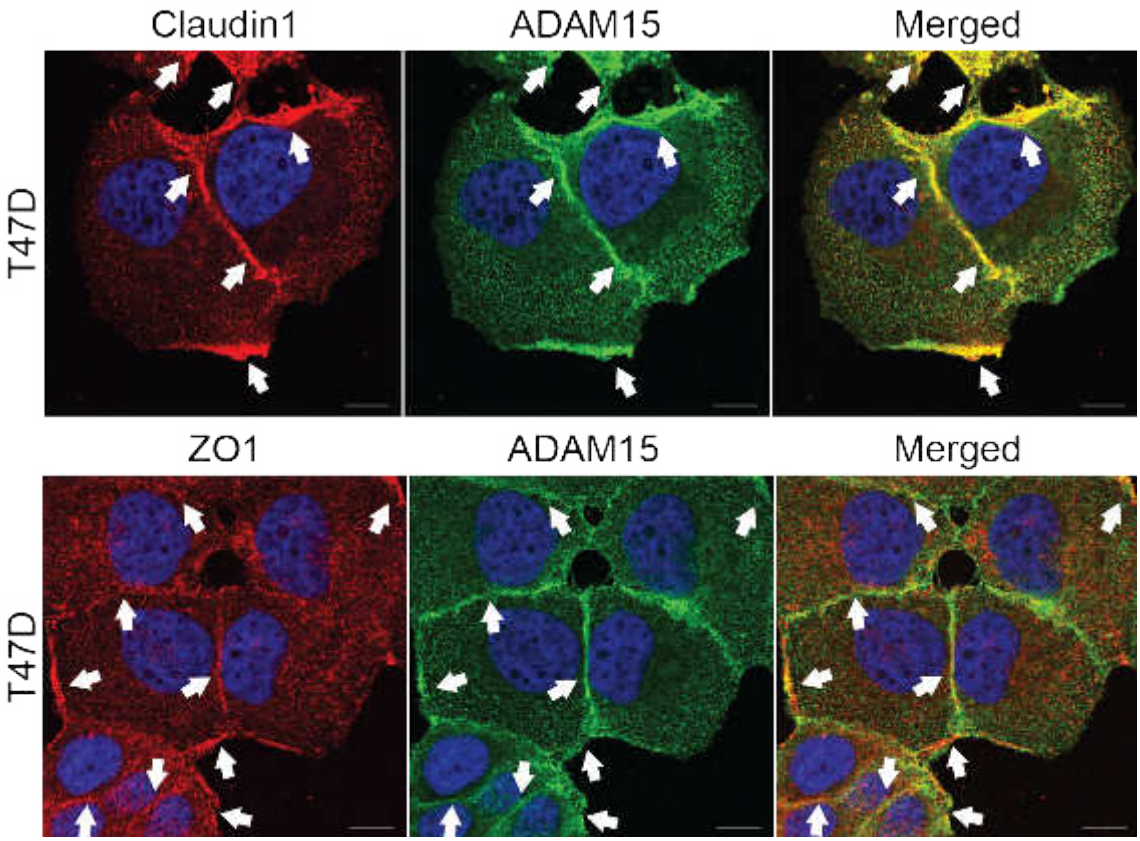

Figure 4.7: Co-localisation of ADAM15 and claudin1 in T47D cells. Areas of co-localisation are highlighted with an arrow. The top row shows T47D cell stained with claudin1 (left column, red) and ADAM15 (middle column, green). The right column presents the merged image of claudin1 and ADAM15. The bottom row shows T47D stained with ZO1 (left column, red) and ADAM15 (middle column, green). The right column presents the merged image of ZO1 and ADAM15. Scale bar = 10 μm. n=3

These results suggest that these proteins are likely to be in a complex. To confirm whether ZO1 and ADAM15 are indeed in a complex, immunoprecipitation analysis was performed. Parental MDA/FRT and MDA/ADAM15 A-E expressing cells were seeded into 10 cm dishes and grown until confluent. IPs were performed with 1 mg of total protein lysates from each cell line. ADAM15 isoforms were immunoprecipitated from MDA/ADAM15 isoform expressing cells with an anti-V5 antibody. Western blot analysis (figure 4.8) showed different levels of ADAM15 isoforms with the highest deviation in ADAM15 D isoform. This is likely to affect the IP results. In figure 4.8 a ZO1 was co-IPed with ADAM15 A, B, and C isoforms, but was not observed in ADAM15 D and E expressing cells. To confirm complex formation between ADAM15 isoforms and ZO1 reverse IPs were also performed. ZO1 was immunoprecipitated from lysates of MDA/FRT and MDA/ADAM15 A-E expressing cells. The western blots were probed with ZO1 to confirm successful precipitation. Antibodies against V5 were used to detect the coIPed ADAM15

isoforms (figure 4.8 b). ADAM15 was detected in ZO1 in MDA/ADAM15 A, B, C and E expressing isoform.

We questioned whether ZO2 would be in a complex with ADAM15, since it also contains an SH3 domain. ZO2 was immunoprecipitated from lysates of MDA/FRT and MDA/ADAM15 A-E expressing cells. The western blots were probed with ZO2 to confirm successful precipitation. Antibodies against V5 epitope were used to detect co-IPed ADAM15 isoforms. ADAM15 A, B, C and E isoforms precipitated equally with ZO2. We also detected some ADAM15 D in ZO2 IPs.

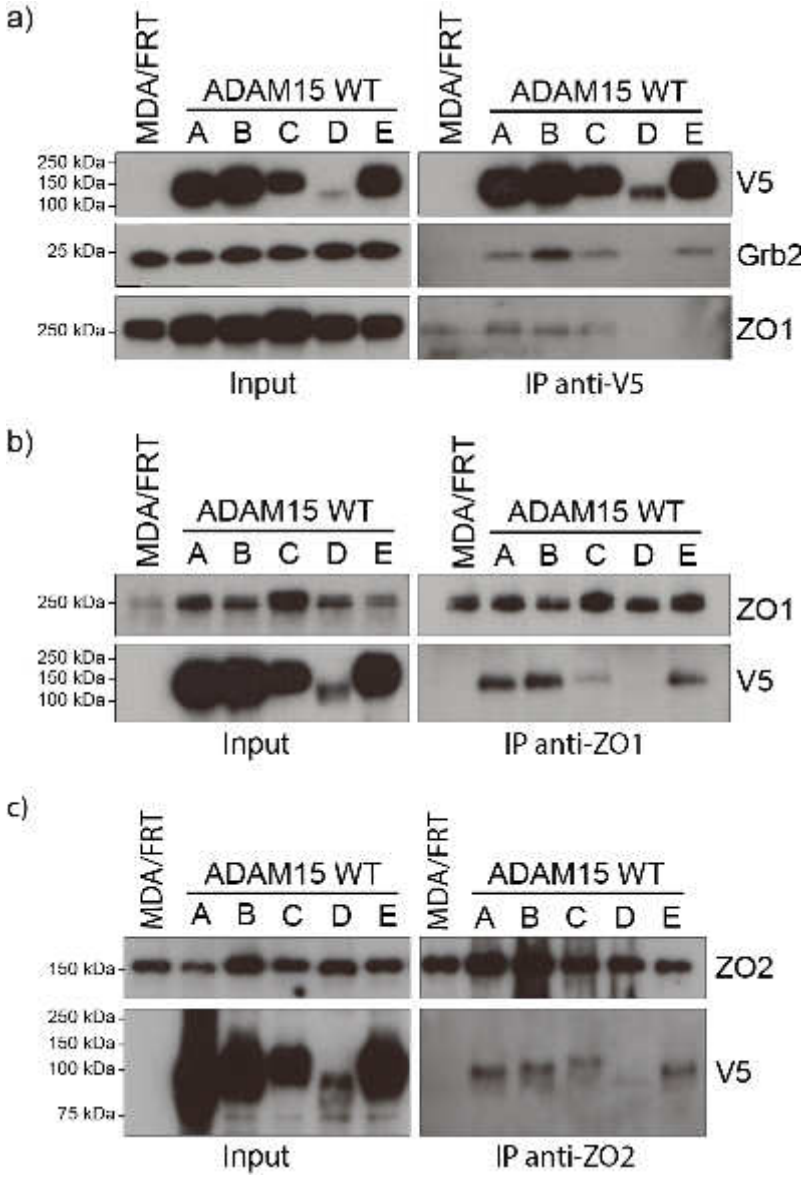

Figure 4.8: Co-IPs of ADAM15, ZO1 and ZO2 in MDA/FRT and MDA/ADAM15 A-E exoressing cells. **(a)** V5 IP probed with V5, Grb2 and ZO1. **(b)** ZO1 IP probed with ZO1 and V5. **(c)** ZO2 IP probed with ZO2 and V5. n=2

These data suggest that ADAM15 A, B, C and E isoforms are in a complex with ZO1 and ZO2 and that ZO1 and ZO2 are potential new ADAM15 interaction

partners.

To validate that we are able to detect co-IPed proteins, I performed IPs with α-V5 and probed for Grb2, a known interaction partner of ADAM15[179,181,182]. As expected, Grb2 co-IPed with all ADAM15 isoforms except D, which does not contain the Grb2 interaction motif.

To confirm the IP results, we carried out IF analysis for ADAM15 and ZO1 in ADAM15 isoform expressing cell lines. As we can see in figure 4.9, exogenously expressed ADAM15 localises to cell-cell junctions in ADAM15 A, B, C, and E expressing cells, where it co-localises with ZO1.

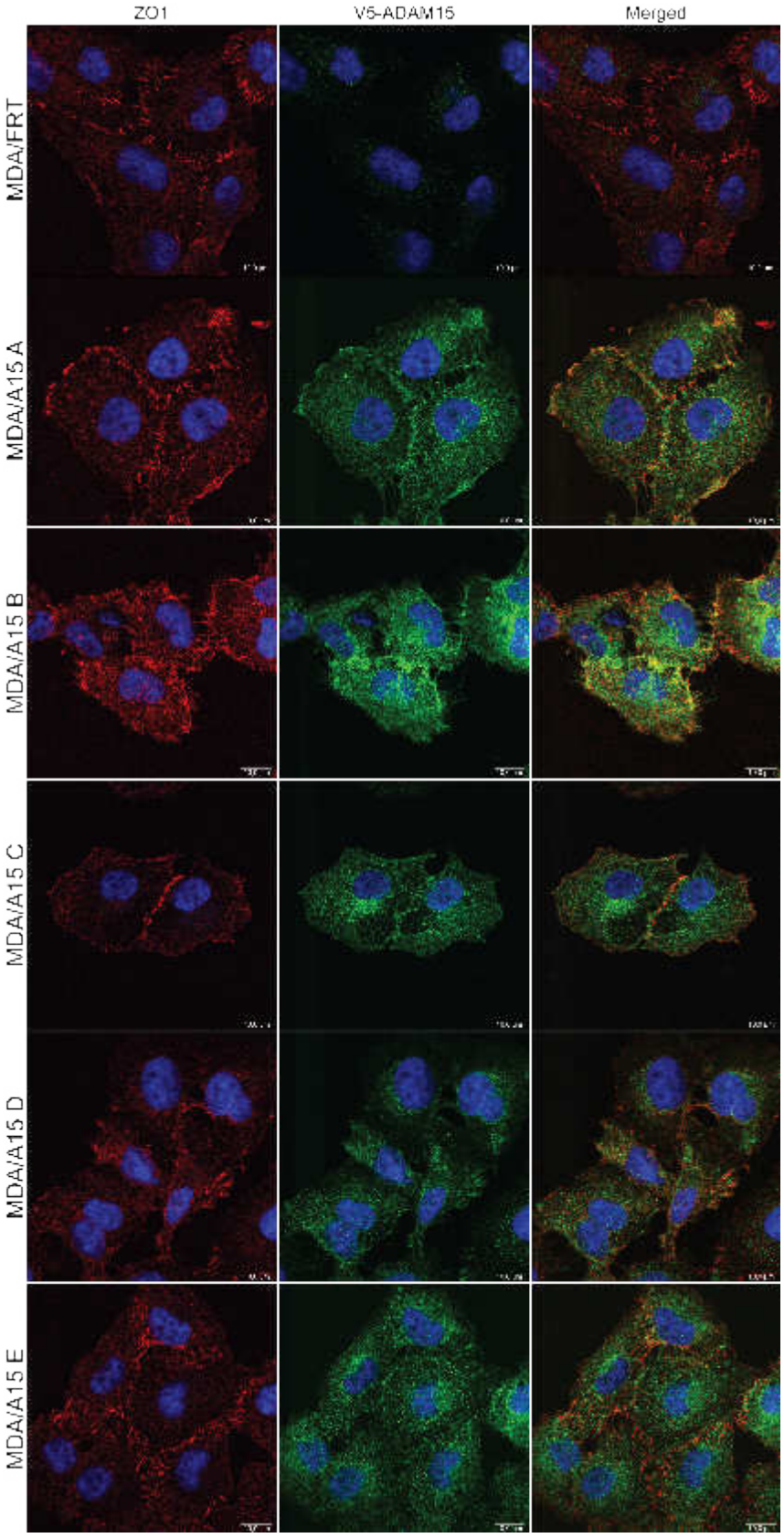

Figure 4.9: Co-staining of V5-ADAM15 and ZO1 in MDA/FRT as well as MDA/ADAM15 isoform expressing cells. The left columns shows ZO1 staining (red) while the middle column shows ADAM15, visualised via its V5 tag (green). The right columns shows the merged image. The nucleus is visualised with DAPI (blue). Scale bar = 10 µm. n=3

4.2.5 Claudin1 is localised in the nucleus of ADAM15 A expressing cells

In the course of claudin1 IF analysis a small proportion of MDA/ADAM15 A expressing cells showed positive staining for claudin1 in the nuclei as shown in figure 4.10.

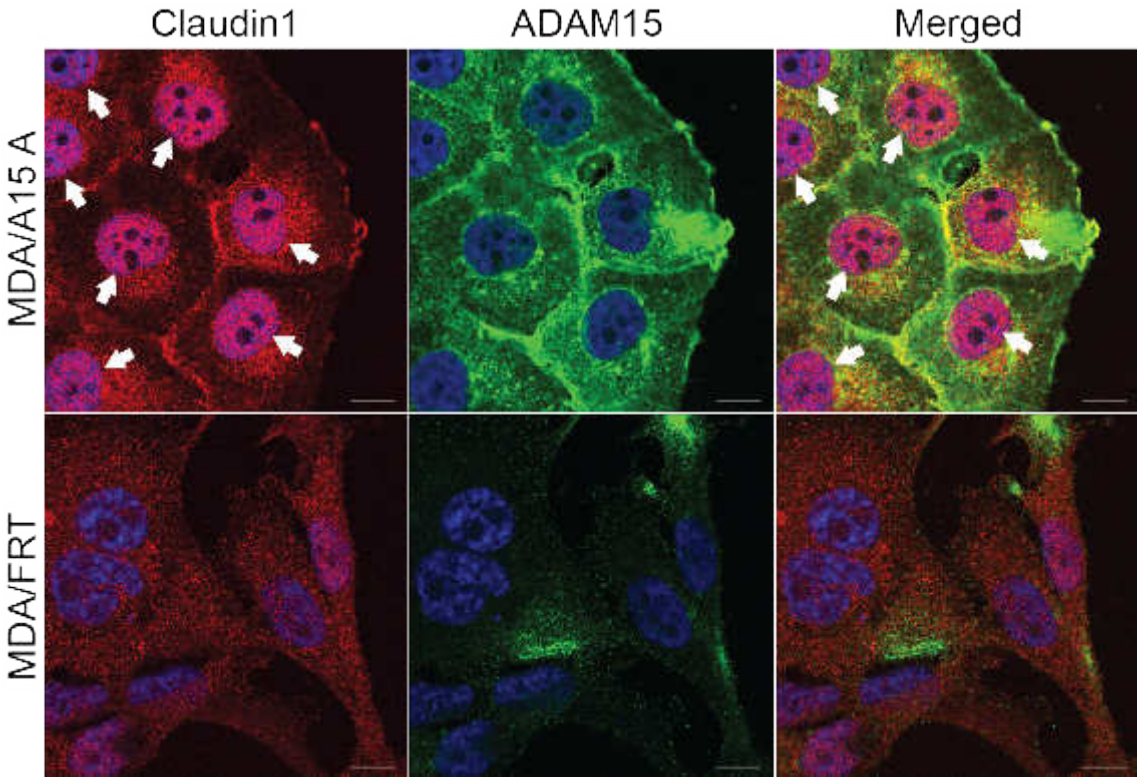

Figure 4.10: Co-localisation of ADAM15 and claudin1 in MDA/FRT and MDA/ADAM15 A expressing cells. MDA/FRT serve as negative control. The used ADAM15 antibody targets the ECD. Scale bar = 10 µm. n=3

To address whether this finding is specific claudin1 targeting shRNA was packaged into lentiviral particles and transduced into MDA/ADAM15 A expressing cells. Clones were selected in puromycin and expanded. The western blot method was used to identify successful downregulation (figure 4.11 b). MDA/ADAM15 A, MDA/ADAM15 A non-target, MDA/ADAM15 A shClaudin1 expressing cells were grown on medium coated glass coverslips until 50% confluent and subsequently stained as described in section 2.9. ADAM15 was stained with antibodies against the ECD. Both, MDA/ADAM15 A and MDA/ADAM15 non-target cells showed cytoplasmic and peripheral staining of ADAM15. Claudin1 was detected at the periphery, in the cytoplasm and in the nucleus of a small proportion of examined cells. As previously shown (figure 4.5) the IF analysis demonstrated ADAM15 and claudin1 co-localisation at the cell-cell junctions and cell periphery. MDA/ADAM15 A shClaudin1 expressing cells show much less staining throughout and considerably

less in the nuclei. ADAM15 staining remained unaltered in MDA/ADAM15 A shClaudin1 expressing cells.

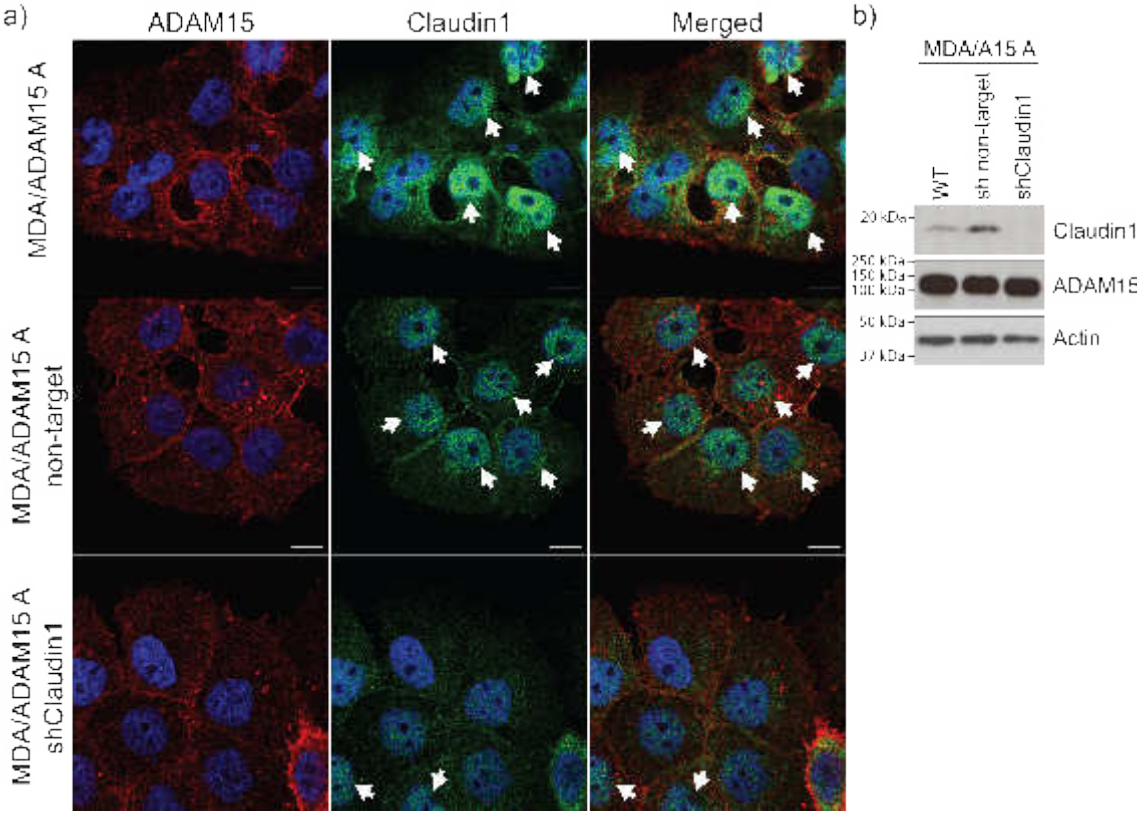

Figure 4.11: Immunofluorescence stainings and western blot validation of ADAM15 and claudin1 in MDA/ADAM15 A, MDA/ADAM15 A non-target and MDA/ADAM15 A shClaudin1 expressing cells. **a)** Representative IF images. Antibodies against the ECD of ADAM15 (red) were used and co-stained with claudin1 (green). DAPI was used to visualise the nucleus (blue). Scale bar = 10 µm. **b)** Western blot validation of used cells showing the expression of claudin1, ADAM15 and actin. n=2

Claudin1 nuclear staining was confirmed further by another claudin1 antibody. The primary anti-mouse (Invitrogen 37-4900) and anti-rabbit (Invitrogen 51-9000) antibodies were used to stain claudin1 in MDA/ADAM15 A non-target and MDA/ADAM15 A shClaudin1 expressing cells.
Cells were seeded on medium coated glass coverslips. These cells were grown for 72h and stained as described. The mounting was done with Prolong mounting media which is supplemented with DAPI. In figure 4.12 a summary of the examined slides is shown. The first two rows show MDA/ADAM15 A non-target expressing cells stained with 37-4900 and 51-9000. In both images claudin1 is stained in bright green. Staining can be found throughout the cytoplasm, some accumulation in cell-cell junctions and membrane as well as in the nucleus. There was not much difference in the fluorescence intensity between the antibodies.
To address whether the claudin1 signal is specific the staining was also done in MDA/ADAM15 A shClaudin1 expressing cells. Figure 4.11 b shows that the shRNA

knockdown was successful therefore expected to see less claudin1 expression in these cells. The central column shows that the lower panel, compared to the upper panel, had reduced expression of claudin1. However, weak expression was still observed in the cytoplasm, cell-cell junctions, membrane and nucleus.

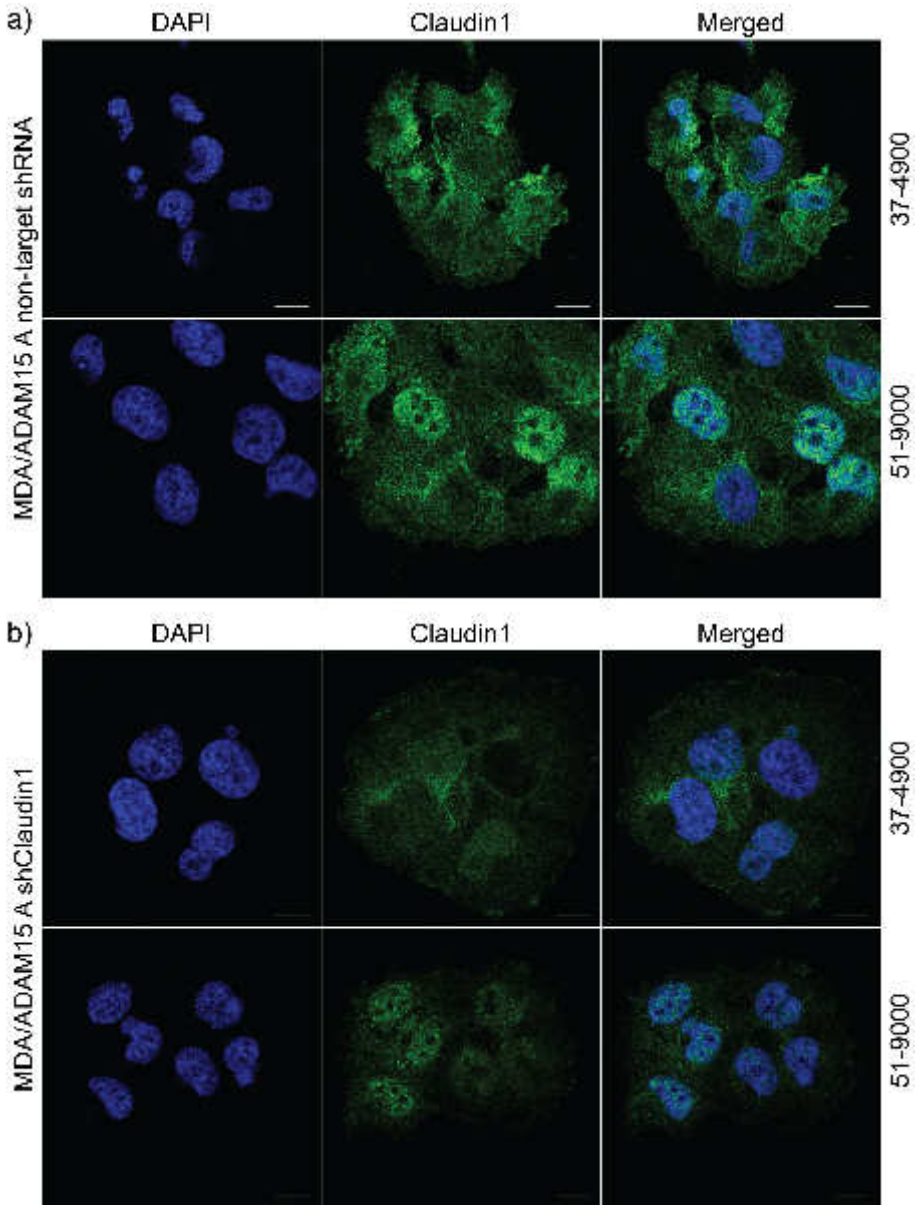

Figure 4.12: Validation of claudin1 antibodies for immunofluorescence staining. Both antibodies were purchased from Invitrogen. 37-4900 is a monoclonal mouse antibody and 51-9000 is a polyclonal rabbit antibody. The upper panel shows MDA/ADAM15 A non-target shRNA expressing cells. The lower panel shows MDA/ADAM15 A shClaudin1 expressing cells. The left column shows the DAPI staining of the tested cell lines. The middle panel shows the same cells stained with each of the claudin1 antibodies. The right panel shows a merged images of both. Scale bar = 10 µm

. n=1

Based on the results we could not see any changes between the antibodies. According to western blot analysis (figure4.11) b knockdown of claudin1 was highly efficient. However, in figure 4.12 b nuclear background staining was observed suggesting a degree of unspecific binding. To confirm that the nuclear localisation further fractionation experiments were performed from MDA/ADAM15 A expressing cells.

Cells were seeded into 10 cm dishes and grown until confluent. Confluent dishes were trypsinised and counted. 2.5 x 10^6 cells were lysed as described in section 2.7.2. The same cell number was subjected to fractionation as described in section 2.7.1. Following quantification, 10 µg of total cell extract (TE), cytoplasmic (CE) and membrane extract (ME) was used as well as 5 µg of nuclear extract (NE) to perform a protein analysis via western blot (figure 4.13).

HSP90 serves as cytoplasmic control while R-cadherin is used as membrane control. Lamin A/C was chosen as nuclear control. As detection control TE was used which was detected in all probings. Within the CE we detected claudin1 and ADAM15, but less compared to the TE. In the ME a prominent amount of claudin1 and ADAM15 was detected, comparable to the TE. This shows that this is the primary site of localisation. In the NE a weak band of claudin1 as well as ADAM15 was found. This data indicates that the membrane is the primary site of expression for claudin1 and ADAM15. However, both proteins also localise to the cytoplasm and nucleus.

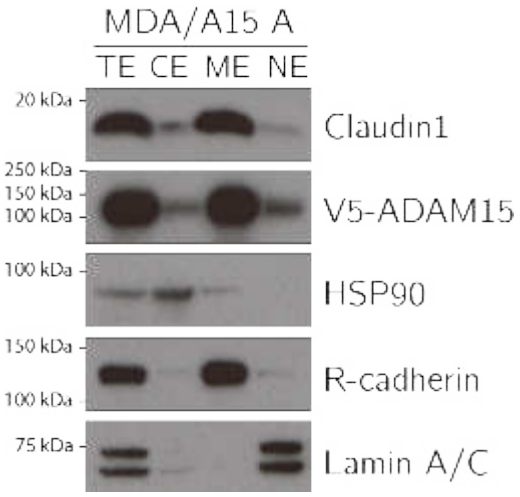

Figure 4.13: Localisation experiment of claudin1 in MDA/ADAM15 A expressing cells. Total cell lysate (TE) serves as control. Fractions of cytoplasm (CE), membrane (ME) and nucleus (NE) with corresponding compartment controls: HSP90, R-cadherin and Lamin A/C, respectively. n=3

4.2.6 ADAM15 ablation leads to downregulation of claudin1

Next, we asked whether claudin1 expression depends on continuous ADAM15 expression. We used the MDA/ADAM15 A shADAM15 expressing cells, described

in chapter 3, to investigate whether ADAM15 expression is necessary for claudin1 upregulation. ShRNA was introduced into lentiviral particles and transduced into MDA/ADAM15 A expressing cells. Emerging clones, during puromycin selection, were expanded and screened for successful knockdown. These knockdown cell lines were kept in puromycin selection to retain the stable knockdown and prevent outgrowth of clones without insert. Figure 4.14 shows a comparison of the generated cell lines. ADAM15 expression was analysed by western blot and detected with an antibody against ADAM15. Parental MDA/FRT cells served as control cell line with only moderate amounts of endogenous ADAM15 and no detectable claudin1. Non-target shRNA was introduced into MDA/ADAM15 A to ensure the infection did not alter ADAM15 expression. These cells express high levels of ADAM15 and detectable claudin1. The shRNA against ADAM15 in clones #22 and #71 showed successful suppression of expression of ADAM15. Interestingly, downregulation of ADAM15 expression led to a decrease in claudin1 levels. This suggests that ADAM15 expression is necessary for claudin1 upregulation.
To confirm this, the cell line T47D was used which has high endogenous levels of ADAM15 and claudin1. ShRNA against the 3' untranslated region (3'UTR) of ADAM15 was transduced into these cells. As before, the protein expression was analysed by western blot (figure 4.14 b). In both, T47D (WT) and T47D non-target shRNA, a high expression of endogenous ADAM15 as well as claudin1 was observed.

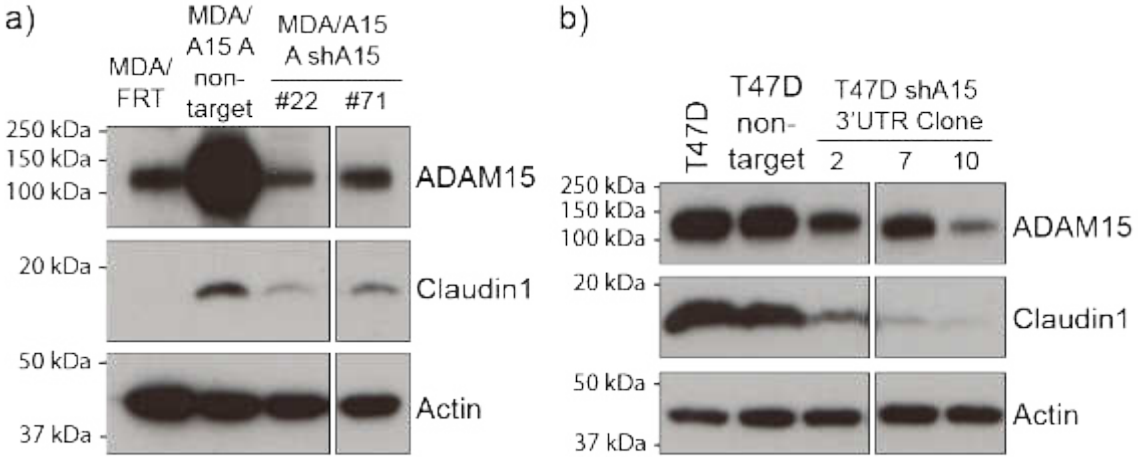

Figure 4.14: Knockdown of ADAM15 with shRNA in MDA/ADAM15 A expressing cells and T47D breast cancer cells analysed by western blot. **(a)** As shown in figure 4.3 a overexpression of ADAM15 A in MDA-MB-231 cells led to upregulation of claudin1. Upon downregulation of ADAM15 with shRNA claudin1 expression is concomitantly reduced. **(b)** Western blot analysis of T47D cells which have high endogenous levels of ADAM15 and claudin1. ShRNA against ADAM15 led to successful reduction in ADAM15 protein levels. Concomitantly, claudin1 expression is lowered as well.

As seen with MDA/ADAM15 expressing cells, downregulation of endogenous ADAM15 expression led to a significant decrease in claudin1 expression. This con-

firms that ADAM15 expression is necessary for claudin1 upregulation.. The phenotype of those cells did not change (figure 4.15).
In summary, shRNA targeting ADAM15 led to concomitant reduction in claudin1 levels in cells overexpressing ADAM15 and cells showing naturally high levels of ADAM15 and claudin1. Thus claudin1 expression depends on ADAM15 expression at least in breast cancer cells. In T47D cells ADAM15-mediated downregulation of claudin1 did not affect cell morphology (figure 4.15).

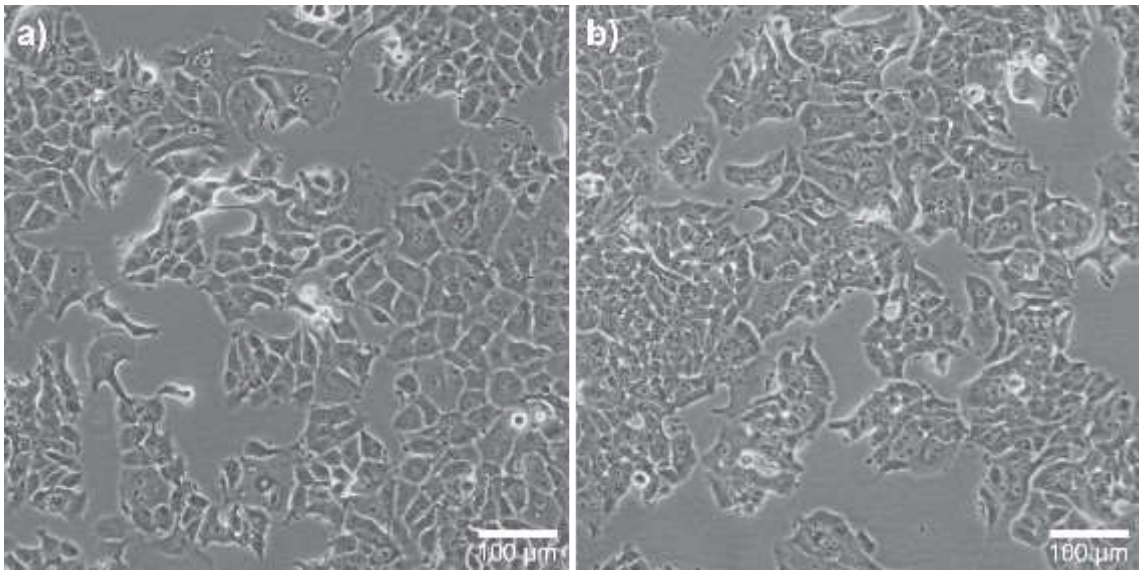

Figure 4.15: Phase-contrast images of T47D non-target and T47D shADAM15 expressing cells. **a)** T47D cells stably transfected with non-target shRNA. **b)** T47D cells stably transfected with shRNA targeting ADAM15. Scale bar = 100 µm.

4.2.7 Claudin1 upregulation is regulated via PI3K/mTOR pathway

In order to understand how claudin1 is upregulated various signalling pathways were analysed. The initial experiment screened a selected panel of inhibitors targeting several major pathways. This panel comprised p38MAPK (SB203580), MAPK (PD98059), PI3K (LY294002), EGFR (Geftinib), Signal transducer and activator of transcription 3 (STAT3) (FLLL31), novel and classical protein kinase C bisindolylmaleimide inhbitor 1 (Bim1), Ca^{2+}-dependent PKCα and β (Gö6976) and PKCδ inhibitor (Rottlerin). The p38MAPK, PI3K and PKC inhibitors were chosen, because claudin1 expression is regulated via these pathways in adult rat hepatocytes[489]. Gefitinib was chosen, because it was reported that EGF-induced EGFR activation increased claudin1 expression in Madin-Darby canine kidney (MDCK) II cells[490]. STAT3 inhibitor was used since it is reported that STAT3 regulates barrier function in intestinal epithelial cells[491]. The reason of choosing a MAPK inhibitor was that ADAM15 interacts with pErk1/2[179] and that claudin1 regulates intestinal epithelial

homoeostasis via Erk/Notch signalling[492]. Cells were seeded into 10 cm dishes and grown for 48h to establish potential tight junction formation. Cells were treated with recommended pharmacological doses for 24h, lysates taken and analysed by western blot and RNA for claudin1 expression.
Validation (only by western blot) of the used inhibitors Gefitinib, LY294002, PD98059 and PP2 is shown in figure 4.16. Additionally, the PKC inhibitors were provided and validated by Wanger et al.[493]. FLLL31 was provided and validated by Dodd et al.[494]. SB203580 was provided and validated by Davis et al.[495]. Rottlerin was validated by Stephens et al.[496].

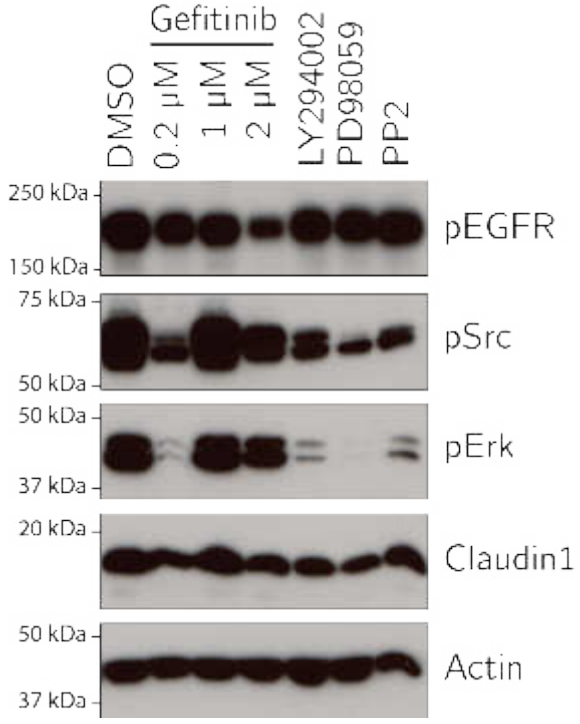

Figure 4.16: Validation of inhibitors used to determine the pathway involved in claudin1 upregulation. Gefitinib (EGFR inhibitor, 0.2/1/2 µM); LY294002 (PI3K inhibitor, 1 µM); PD98059 (MAPK inhibitor, 2.5 µM); PP2 (Src family kinase inihbitor, 100 nM). n=1

Only the inhibition of PI3K by LY294002 led to reduced claudin1 expression (figure 4.17 d). None of the other inhibitors changed claudin1 expression suggesting claudin1 upregulation is mediated by PI3K pathway. (figure 4.17 a-c)

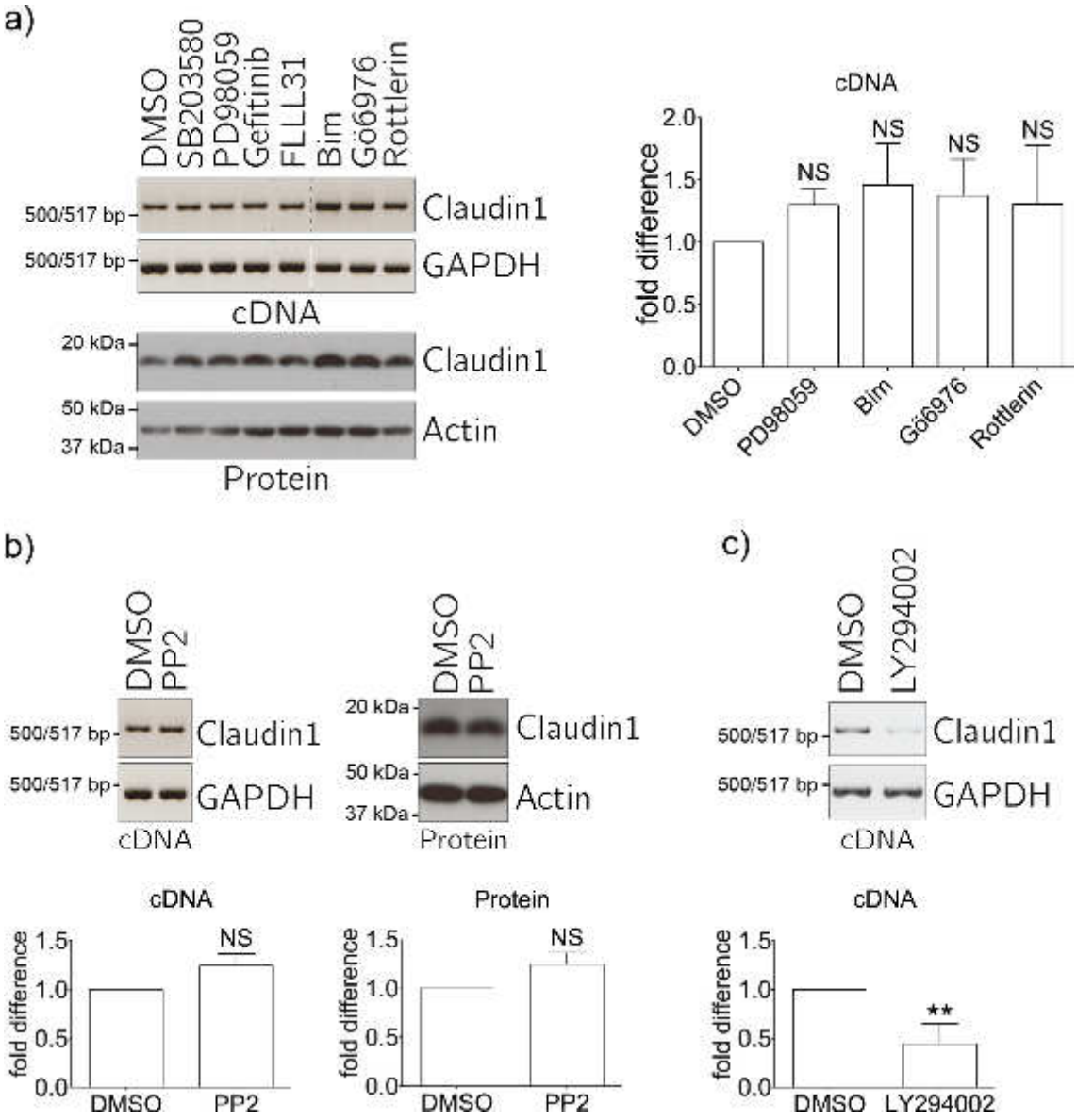

Figure 4.17: Screening for signalling pathways potentially involved in claudin1 upregulation in MDA/ADAM15 A expressing cells. Duration of treatment was 24h with following inhibitors: SB203580 (10 µM; n=1), PD98059 (10 µM; n=4), Gefitinib (0.5 µM; n=2), FLLL31 (5 µM; n=1), Bim (1 µM; n=3), Gö6976 (1 µM; n=3), Rottlerin (5 µM; n=3), PP2 (100 nM; n=3) and LY294002 (50 µM; n=5). Densitometry and analysis of the mRNA was performed using ImageJ. Claudin1/GAPDH ratio was normalised to the DMSO control. The result is shown as fold difference in bar graphs. To address statistical significance one-way ANOVA was performed. The inhibitor treated samples were compared to the vehicle control. Confidence intervals are as follows: $* = p \leqq 0.05; ** = p \leqq 0.01; *** = p \leqq 0.001$. **a)** Representative images and quantification of analysed mRNA and protein. GAPDH was used as control for mRNA analysis whereas actin was used as control for protein. The RNA was reverse transcribed to cDNA and amplified with claudin1 and GAPDH-specific primers followed by separation on a agarose gel. **b)** mRNA and protein analysis of Src family kinase inhibitor PP2 (100 nM). Claudin1/Actin ratio was normalised to the DMSO control. **c)** mRNA analysis of the PI3K inhibitor LY294002 (50 µM).

In order to confirm the role of PI3K pathway in ADAM15-dependent claudin1 upregulation, we used another PI3K inhibitor, PI-103 to confirm the findings. Additionally, mTOR is another major signalling pathway downstream of PI3K. Thus we also employed inhibitors to mTOR: Rapamycin, that inhibits mTORC1, and Ku0063794, which inhibits mTORC1 and mTORC2. Phase-contrast images of the cells were taken after 24h inhibitor treatment to observe morphological changes of MDA/ADAM15 A, C and E expressing cells. The phenotype of DMSO treated cells was unchanged compared to to untreated cells confirming that the solvent had no adverse effect on cell morphology. LY294002 treatment of the cells resulted in spindle-like morphology, which was mostly seen in MDA/ADAM15 A expressing cells (figure 4.18). This phenotype was mostly prominent in MDA/ADAM15 A expressing cells, to a lesser extent in MDA/ADAM15 C and least in MDA/ADAM15 E expressing cells. Objectively, PI-103, Rapamycin and Ku0063794 treatment did not affect the phenotype of all tested cells.

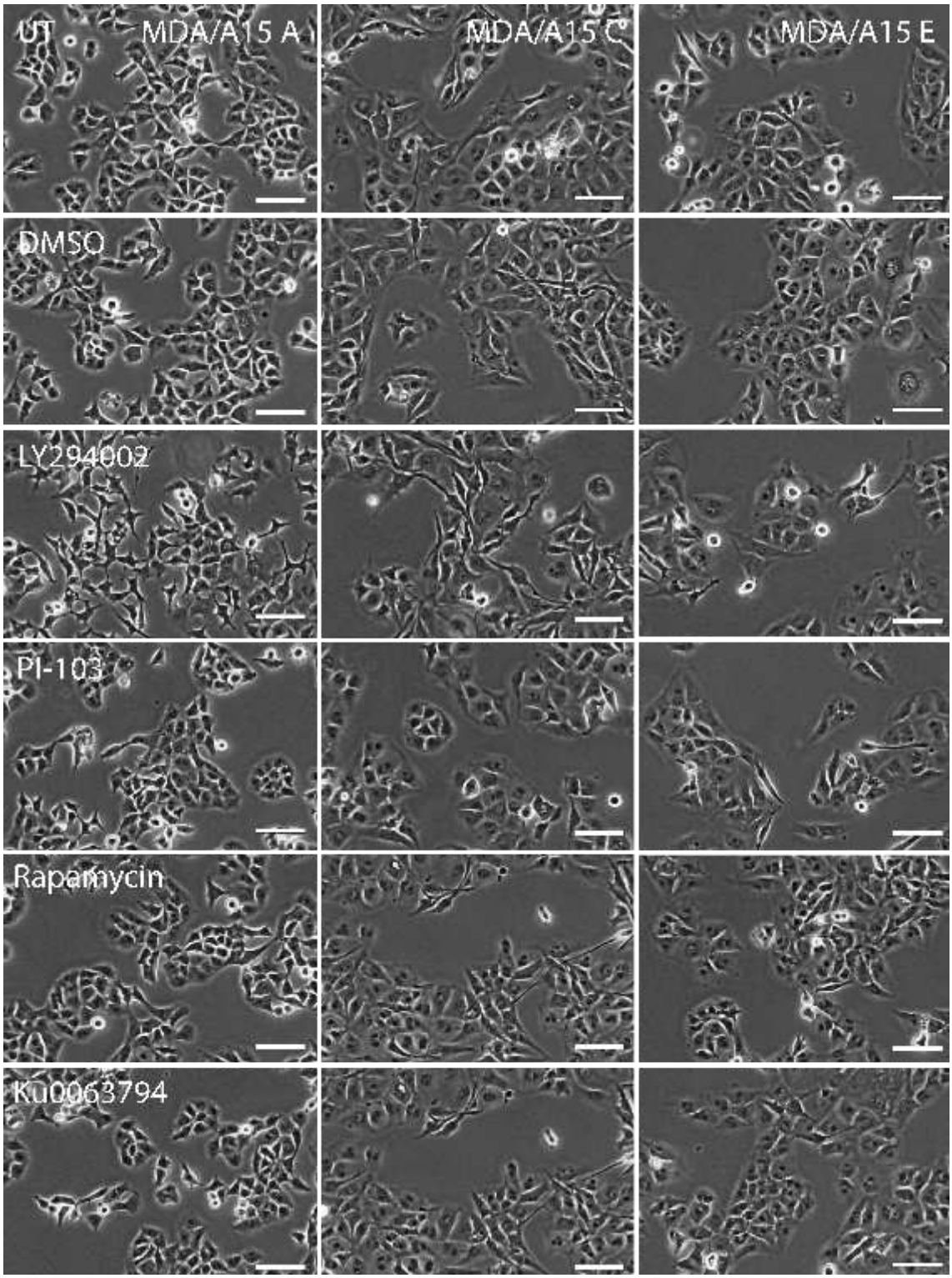

Figure 4.18: Representative phase-contrast images of MDA/ADAM15 A, C and E expressing cells after 24h of inhibitor treatment. The first column shows images of MDA/ADAM15 A, the second column MDA/ADAM15 C and third column MDA/ADAM15 E expressing cells. From top to bottom: UT, DMSO, LY294002 (50 μM), PI-103 (1 μM), Rapamycin (100 nM) and Ku0063794 (1 μM). Scale bar = 100 μm.

Western blot analysis (figure 4.19 a and b) demonstrated moderate, but significant claudin1 downregulation when cells were treated with LY294002. In contrast, PI-103 treatment did not reduce the expression of claudin1 in any of the tested cells (figure 4.19 a and c). Rapamycin treatment reduced the claudin1 levels significantly in MDA/ADAM15 A and C, but not in E expressing cells (figure 4.19 a and d). However, this inhibitor was less efficient then LY294002 when claudin1 levels were quantified using ImageJ (figure 4.19 b and d). Neither of these cells responded to Ku0063794 treatment (figure 4.19 a and d). To confirm that the inhibitors were effectively blocking the mTOR pathway, the western blots were probed with an antibody detecting phosphorylated S6, which is downstream of PI3K/mTOR pathway. All treatments resulted in reduction of pS6 phosphorylation.

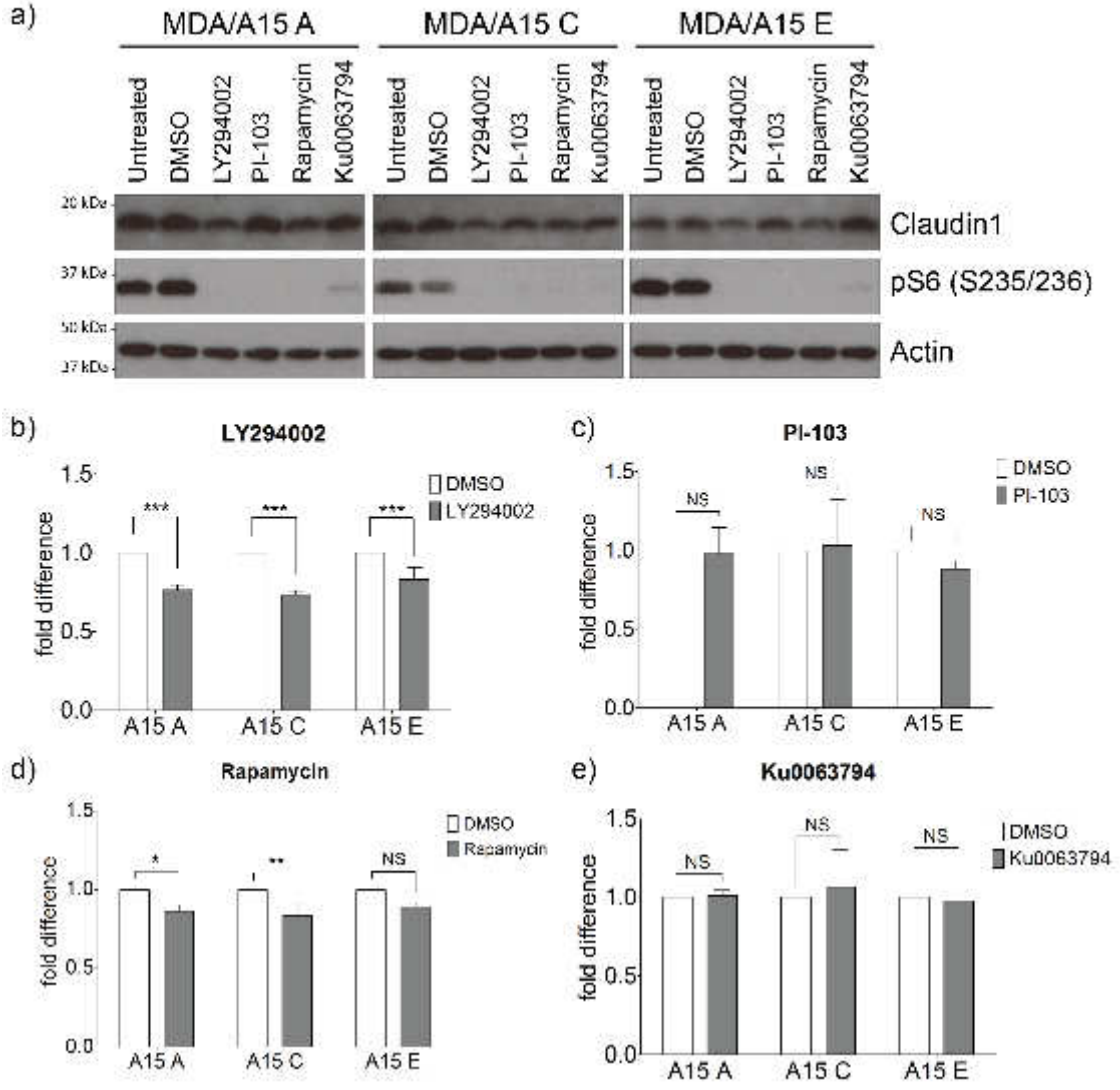

Figure 4.19: ADAM15 A, C and E expressing cells treated with PI3K and mTOR inhibitors. Densitometry on the bands was carried out using ImageJ. Claudin1 expression values were normalised to actin and then to the DMSO control of each isoform. The result is shown as fold difference using bar graphs. To address statistical significance two-way ANOVA was performed. The inhibitor treatment was compared to the vehicle control for MDA/ADAM15 A, C and E expressing isoform individually. Confidence intervals are as follows: $* = p \leqq 0.05; ** = p \leqq 0.01; *** = p \leqq 0.001$. n=3

The moderate decrease in claudin1 protein levels in response to PI3K/mTOR inhibitors led us to hypothesise that claudin1 might be very stable over the time period that inhibitor treatment was performed. To address that I treated ADAM15 A expressing cells with cycloheximide (CHX), a protein biosynthesis inhibitor. Western blot analysis demonstrated that claudin1 protein is stable over 24h period, and that claudin1 levels reduced after prolonged (48h) treatment with a high (10 µg/mL) dose of CHX (figure 4.20). Figure 4.20 c shows the total protein concentration of the used samples which served as positive control for protein synthesis inhibition. After 48h of growth the total protein concentration increased by approximately 50% in UT and DMSO treated samples. CHX treatment successfully inhibited protein synthesis since the protein concentrations were similar to the starting concentration prior to incubation/treatment.

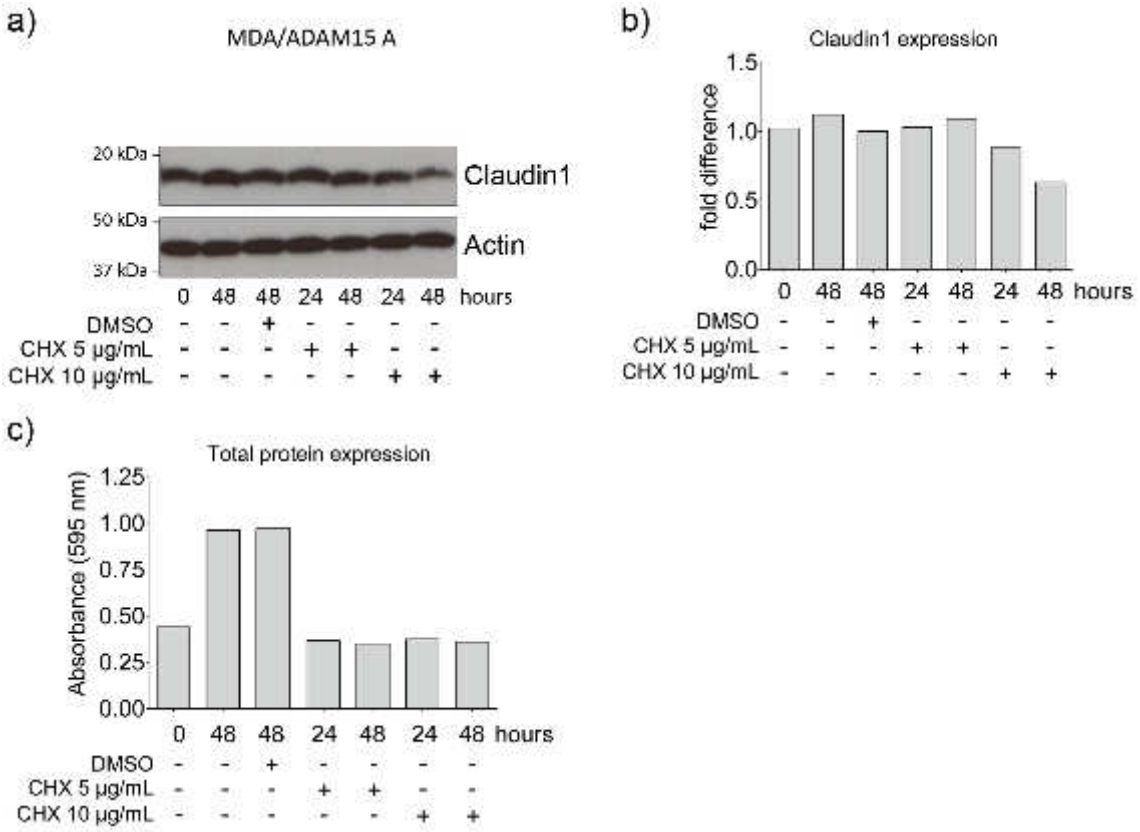

Figure 4.20: Claudin1 expression is stable for up to 48h in MDA/ADAM15 A expressing cells. MDA/ADAM15 A expressing cells were treated with either DMSO, 5 or 10 µg/mL CHX at 70% confluence. One dish was lysed immediately without treatment. Protein lysates were harvested after 24 or 48h of CHX treatment. **(a)** Protein analysis of claudin1 and actin. **(b)** The bands were quantified with ImageJ and the ratio of claudin1:actin normalised to the UT control at 0h. The result is shown in fold difference. **(c)** Absorbance of total protein concentration which serves as control of protein synthesis inhibition. n=1

As the CHX treatment confirmed that claudin1 protein is stable for at least 24h, we analysed claudin1 mRNA levels in response to PI3K/mTOR inhibition. The inhibitor treatments were repeated as described earlier, followed by RNA extrac-

tion. RT-PCR was performed with extracted RNA. The cDNA was in turn used for PCR, and products amplified with claudin1- and GAPDH-specfic primers. Upon treatment with LY294002 claudin1 mRNA was significantly reduced by over 70% in MDA/ADAM15 A, C and E expressing cells (figure 4.21). When cells are treated with PI-103 a reduction of claudin1 mRNA is observed in all tested cell lines. However, the reduction was only statistically significant in MDA/ADAM15 C expressing cells. Claudin1 mRNA levels were significantly downregulated in all cell lines in response to rapamycin. While Ku0063794 treatment reduced claudin1 mRNA levels in all cell lines, the reduction was statistically significant only in MDA/ADAM15 C expressing cells. To conclude, LY294002 and Rapmycin treatment suppressed claudin1 mRNA significantly in all cell lines tested. PI-103 and Ku0063794 treatment achieved statistically significant reduction of claudin1 mRNA levels only in MDA/ADAM15 C expressing cells.

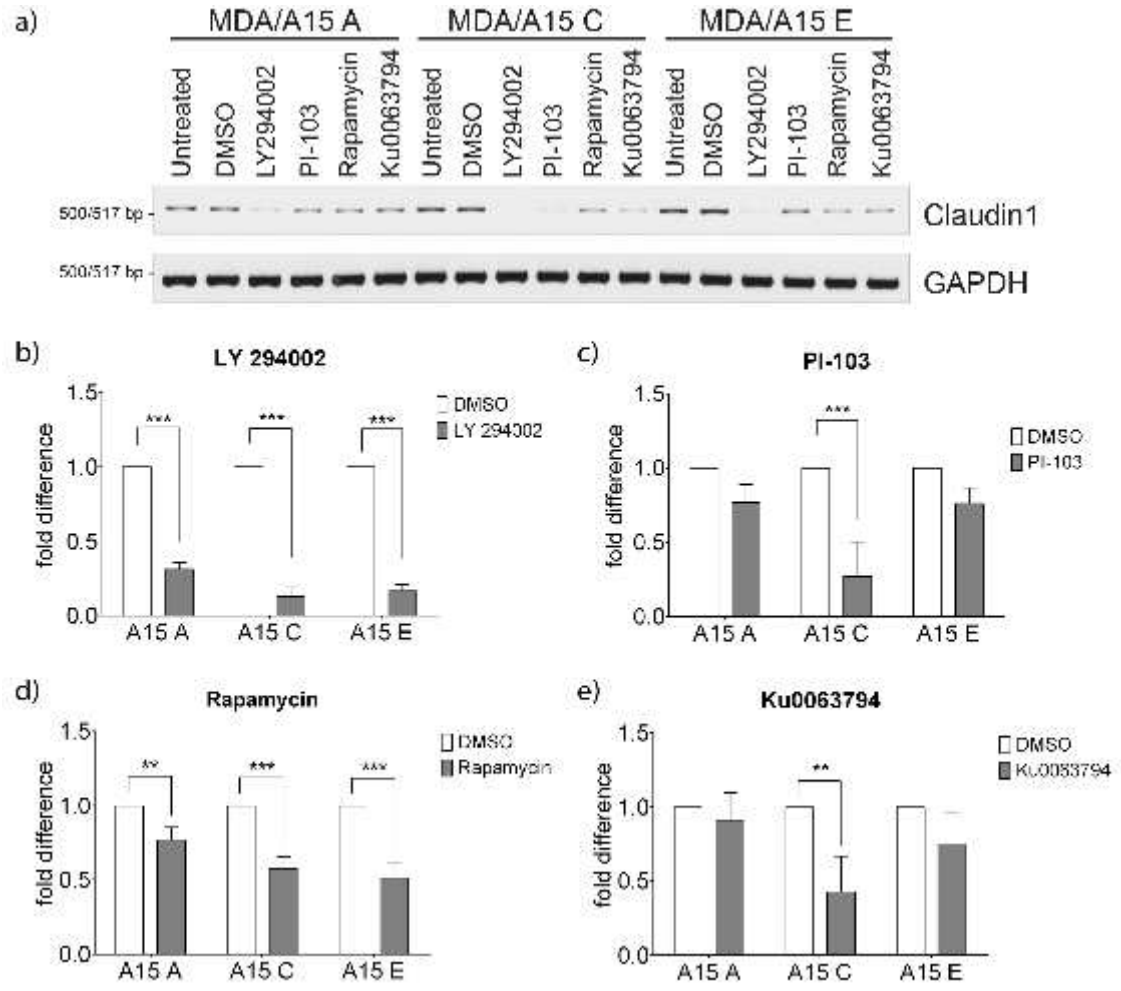

Figure 4.21: Amplified cDNA from extracted RNA of MDA/ADAM15 A, C and E expressing cells treated with PI3K and mTOR inhibitors for 24h. Extracted RNA was reverse transcribed to cDNA and amplified with claudin1 and GAPDH-specific primers followed by separation on a agarose gel. Bands were quantified using ImageJ. The ratio of claudin1:GAPDH was normalised to the DMSO control. **a)** Visualised cDNA bands of claudin1 and GAPDH on a 1.2% agarose gel with inverted colours. The results are depicted as line graphs for **b)** LY294002 (50 µM), **c)** PI-103 (1 µM), **d)** Rapamycin (100 nM) and **e)** Ku0063794 (1 µM). Statistical significance was addressed by two-way ANOVA. The inhibitor treatment was compared to the vehicle control for MDA/ADAM15 A, C and E expressing isoform individually. Confidence intervals are as follows: $* = p \leqq 0.05; ** = p \leqq 0.01; *** = p \leqq 0.001$. n=3

4.2.8 Claudin1 expression does not affect cell migration

In section 3.2.6 I demonstrated that overexpression of ADAM15 isoforms differentially affected scratch wound healing. As aberrant expression of claudin1 has been implicated in modulating cell motility, I determined whether claudin1 plays a role in mediating the defects in wound closure seen previously.

For this purpose MDA/ADAM15 A expressing cells with shRNA downregulation of claudin1 expression were generated and used in scratch wound assays (figure 4.22). Successful downregulation of claudin1 in MDA/ADAM15 A expressing cells is shown in figure 4.11 b. As previously shown MDA/ADAM15 A expressing cells were not closing the wound after 48h. MDA/ADAM15 A non-target sh expressing cells were not significantly different either. MDA/ADAM15 A shClaudin1 expressing cells did not change the rate of wound closure compared to both control cells. Therefore migration rates are independent of claudin1 expression level in ADAM15 A expressing MDA-MB-231 cells.

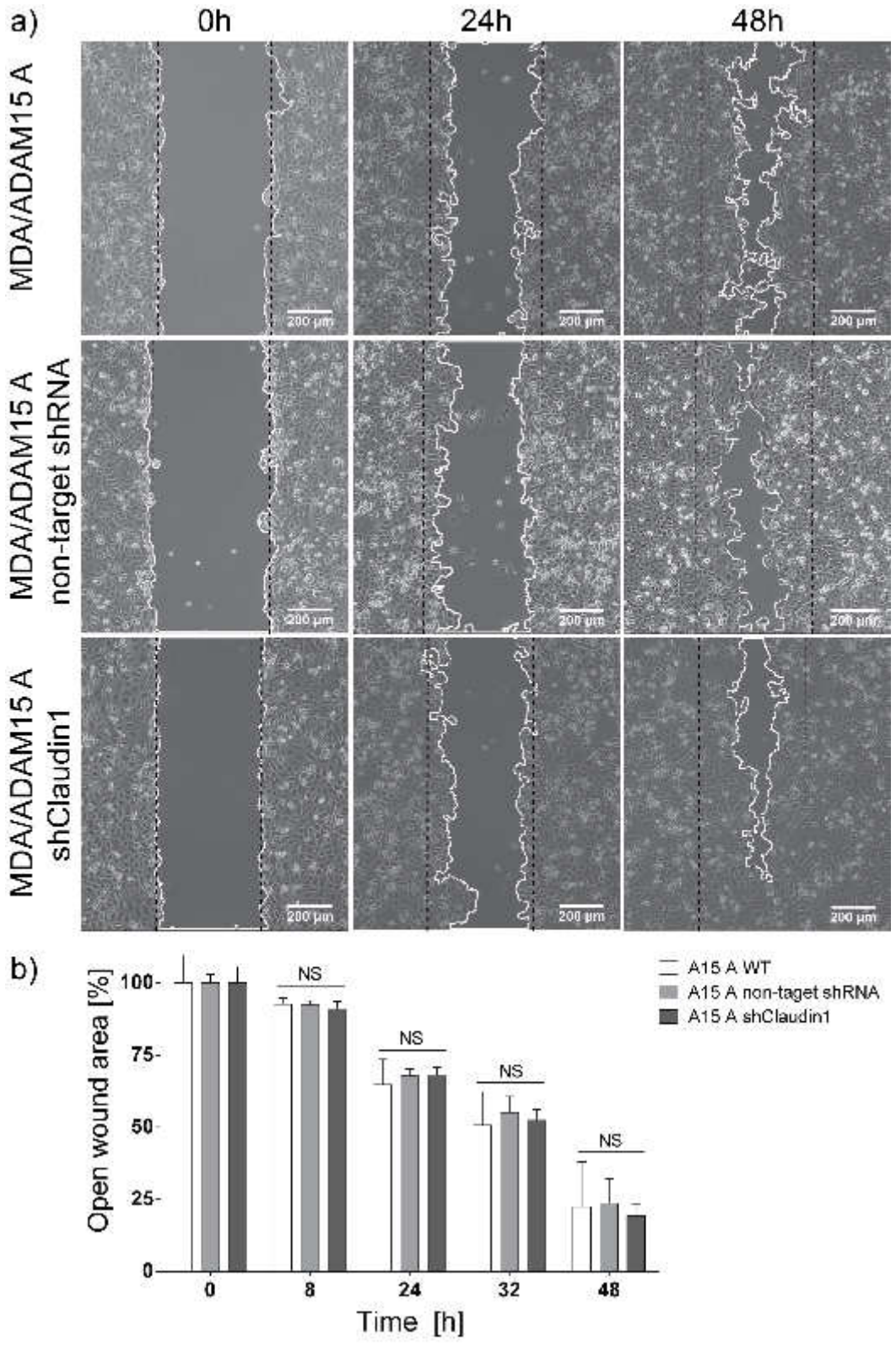

Figure 4.22: Wound healing assay of MDA/ADAM15 A, MDA/ADAM15 A non-target shRNA and MDA/ADAM15 A shClaudin1 expressing cells. **a)** Example images after wounding, 24h and 48h. Scale bar = 200 µm. **b)** Bar chart comparing the wound closure of the cell lines. Statistical significance was assessed with post-hoc Bonferroni's multiple comparison test after performing two-way ANOVA analysis. MDA/ADAM15 A non-target shRNA and MDA/ADAM15 A shClaudin1 expressing cells were compared to the MDA/ADAM15 A expressing control. Confidence intervals are as follows: $* = p \leqq 0.05; ** = p \leqq 0.01; *** = p \leqq 0.001$.n=3

4.3 Discussion

The most important finding in this chapter is ADAM15 isoform-dependent and catalytic function dependent upregulation of claudin1, as well as the identification of ZO1 and ZO2 as potential new interaction partners of ADAM15. Upregulation of claudin1 is not significantly increased in their E349A mutants. In MDA/ADAM15 A expressing cells claudin1 expression depends on cell density. Claudin1 co-localises with ADAM15 at cell-cell junctions and periphery in MDA/ADAM15 A expressing cells and in T47D. In a proportion of cells claudin1 is also localised in the nucleus. ZO1 co-localises with ADAM15 in MDA/ADAM15 isoform expressing cells and in T47D. ZO1 and ZO2 are found to be novel interactions partners of ADAM15. ADAM15 ablation leads to downregulation of claudin1. Claudin1 upregulation is regulated via the PI3K/mTOR pathway. In MDA/ADAM15 A expressing cells claudin1 does not mediate migration.

Screening of several EMT markers confirmed that ADAM15 expression did not cause MET. One of the most dominant markers of epithelial cells is E-cadherin[497,498]. Snail and slug, among other proteins, are able to bind to the E-cadherin promoter suppressing its transcription[499]. Slug has been detected in the whole cell panel and was only absent in the epithelial control whereas E-cadherin could only be detected in A431 cells. To further disprove MET the samples were analysed for vimentin which is only expressed in mesenchymal cells[500] and was detected, unchanged, in the host cell line as well as the ADAM15 isoform expressing cells. These observations confirmed that ADAM15 expression did not cause MET in this breast cancer cells. Since epithelial growth relies on cell-cell junction formation and MDA/ADAM15 A expressing cells show dense epithelial-like morphology we hypothesised whether differential regulation of tight junctions proteins are involved.

Tight junctions are important contributors in dense epithelial cells growth. The major protein families in cell-cell interaction are occludins and claudins. Both are integral proteins which are linked by ZO proteins to the actin cytoskeleton. Neither ZO1 nor ZO2 nor occludin showed altered expression, but claudin1 was significantly upregulated in ADAM15 A, C and E expressing cells.

Next it was observed that claudin1 is dependent on cell density. With advanced cell density claudin1 levels increased. It has been reported that the half-life and level of ZO1 expression increases with cell density[501] and overexpression of ZO1 inhibits proliferation in low-density cells[502]. Matter and Balda[503] proposed a working model in which accumulation of a TJ protein sensor for cell density. In non confluent cells the expression of TJ proteins is low and the inhibition of pathways reducing proliferation is weak. By increasing cell density expression levels of TJ increase and proteins stabilise at the forming TJs. This leads to recruitment of signalling pro-

teins such as ZO-1-associated nucleic-acid binding protein (ZONAB) and PTEN and therby inhibit proliferation. This may indicate that MDA/ADAM15 A expressing cells form tight junctions. Additionally, previously ADAM15 has been implicated in regulating epithelial and endothelial cell permeability[162,189,191,192,224], although this ADAM15 function has never been linked to claudin1 or any other tight junction related gene expression. Two classical and well established methods of addressing TJ permeability are transepithelial electrical resistance (TEER) measurement[504,505] and paracellular permeability assay[504,506]. TEER measures voltages which passes through a confluent layer of cells. This gives an indication about the resistance. The paracellular permeability assay makes use of differently sized dextran which is conjugated with a fluorescent dye. Smaller and larger sized conjugates are applied onto a confluent layer of cells grown on a porous membrane. Depending on the tightness of the TJ, varying amounts of the labelled dextran passes through. These experiments were performed by a colleague in the lab, and the results showed no difference in TEER and paracellular permeability between MDA/ADAM15 A non-target shRNA, MDA/ADAM15 A shADAM15 and MDA/ADAM15 A shClaudin1 expressing cells. This results suggest that claudin1 upregulation alone is not sufficient to form functional tight junctions. Claudin1 is a crucial component of TJs. Interference with the EL1 of claudin1 increased permeability[271]. However, it seems that more contributors are required to establish functional tight junctions. We have not investigated the expression and localisation of JAM proteins or the localisation of occludins or other claudin family members. It is likely that one or more are lacking in the cell-cell junctions of MDA/ADAM15 A expressing cells and thus cannot form functional TJ. RNA and protein analysis followed by confocal microscopy could answer this question. Claudin1 is a small transmembrane protein which function is to maintain the barrier function among epithelial cells. It regulates the paracellular diffusion of small ions across adjacent cells. Other functions comprise maintenance of cell polarity and epithelial cell homoeostasis. It has also been considered to be a tumour suppressor in human breast cancer. In TJs claudin1 binds ZO proteins via its C-terminal PDZ-binding motif. The interaction is established via the N-terminal PDZ domain of ZO1/ZO/ZO3. In MDA/ADAM15 A expressing cells claudin1 was primarily found in the cytoplasm, but also in the cell-cell junctions and periphery. A proportion of cells showed localised claudin1 in the nucleus. Co-localisation of claudin1 and ADAM15 was primarily observed in cell-cell junctions and periphery, but not in the nucleus. Concomitantly, ZO1 also co-localised with ADAM15 in cell-cell junctions and periphery. CoIP experiments revealed direct interaction of ADAM15 A, B, C and E expressing cells with ZO1. IPs with ZO2 showed coIP of V5 in MDA/ADAM15 A-E expressing cells. In ZO2 IPs we observed a ADAM15 D specific band. However, ADAM15 D is the truncated isoform which lacks the

proline-rich regions which interact with the SH3 domains as the ones in ZO2. Recent findings in our lab showed that ADAM15 D forms a dimer with ADAM15 A (unpublished data). Therefore we assume the anti-V5 antibody binds to V5-ADAM15 D in ADAM15 D expressing cells which dimerised with untagged endogenous ADAM15 A that in turn is bound by ZO2. Detection with anti-V5 antibody picks up ADAM15 D in western blot experiments but not the untagged ADAM15 A.

According to Uniprot[129] Claudin1 and ADAM15 are not able to interact due to the lack of interaction motifs. However, complex formation would be possible via ZO1. It has been shown that ZO1 (also ZO2 and ZO3) can interact with its PDZ domain and claudin1-8 via their COOH-terminal KDYV sequence[291]. ZO1 also has an SH3 domain[129] which is known to bind to proline-rich regions. ZO1 and ZO2 as interaction partners of ADAM15 raises the question about the benefit for the cell. It is known that ZO1 proteins link claudins and occludins to the actin cytoskeleton[262,507]. Complex formation of ADAM15 with ZO1 would assure localisation of ADAM15 to the tight junctions. A potential role for ADAM15 could be to increase microvascular permeability which is considered as a central hallmark of inflammation. It has been demonstrated that occludin is degraded by an unknown MMP to increase TJ permeability[508]. Recently, occludin was identified as substrate for MMP2[509]. Since ADAM15 is closely related to MMPs and possess catalytic activity there could be potential role as regulator of tight junctions.

Claudin1 was not only found in cell-cell junctions and plasma membrane, but also in the nuclear fractions of MDA/ADAM15 A expressing cells. Nuclear claudin1 has been found in benign nevi and early stage melanoma[510]. Nuclear localisation was also found in metastatic osteosarcoma KRIB cells[511], but the function remains unknown.

The major question is how ADAM15 upregulates claudin1. Inhibitor treatments showed that the PI3K/mTOR pathway is involved in upregulating claudin1 expression. Inhibition of both, PI3K and mTOR, led to reduced claudin1 expression. Western blot analysis showed that inhibition of PKCs upregulated claudin1. However, densitometry analysis of the western blot resulted in insignificant upregulation. It may still be that this method is not sensitive enough and should be repeated with a quantitative approach such as PKC activity assays. An explanation would involve the crosstalk of those pathways. LY294002 and PI-103 prevent indirectly phosphorylation of Akt since it is downstream of PI3K. Phosphorylation of Akt at S473 is necessary for its activation. It seems if this mechanism is inhibited claudin1 expression is reduced. In contrast, phosphorylation of Akt could lead to upregulation of claudin1. As this was observed upon treatment with different PKC inhibitors. In keratinocytes it was shown that inhibition of PKC increased insulin-like growth factor 1 (IGF-1)-incuded phosphorylation at S473 in Akt[512]. In contrast, stimulation

of PKC by an activator reduced Akt phosphorylation at S473[512]. Both observations suggest that PKC activation inhibits Akt activity. To confirm this hypothesis the treatments need to be repeated and claudin1 mRNA levels analysed.

It is not known how ADAM15 exactly drives claudin1 upregulation via PI3K/mTOR pathway. One possibility could be via Src kinase which interacts directly with the proline-rich regions of ADAM15 ICD via its SH3 domains[166,179]. The most plausible scenario would be that distinct intracellular protein-protein interactions with alternative ADAM15 ICDs modulate the extracellular MP function of ADAM15, leading to the shedding of specific substrates as illustrated in figure 4.23. These would then activate the corresponding receptors, followed by downstream PI3K/mTOR activation. This would be in line with our previous collaborative work showing ADAM15 B mediated shedding of FGFR2IIIb as a result of interacting with and being activated by Src tyrosine kinase[207]. It has been shown that Src is in a complex with PI3K[513] and also acts as a regulator[514]. In adult rat alveolar cells, Src is important in the activation of sodium-potassium adenosine triphosphatase (Na^+/K^+ – ATPase). Treatment of the thyroid hormone triiodothyronine (T3) induces expression of Na^+/K^+–ATPase via PI3K/Akt and MAPK/Erk1/2 pathways. Inhibition of Src blocked the activity of the Na^+/K^+–ATPase. Furthermore, T3 induced phosphorylation of both Erk1/2 and Akt was blocked. These findings suggest that Src regulates Na^+/K^+ – ATPase activity by both pathways. However, treatment of MDA/ADAM15 A expressing cells by PP2 (Src family kinase inhibitor) did not reduce claudin1 protein levels. This could be due to long half life of claudin1 which was shown in this chapter. Another reason could be that Src kinase functions alongside other mediators and inhibition upstream of PI3K can be rescued. On the contrary, Src and ADAM15 interaction might have no role in claudin1 upregulation. Considering that ADAM15 B has strong interaction with Src[181] and no upregulation of claudin1 was observed. It is known that p85α and ADAM15 ICD interact[181], but it can be excluded as a reason for claudin1 upregulation. Kleino et al. presented strong interaction of the SH3 domain of p85α and the proline-rich regions of ADAM15 isoforms. Especially ADAM15 B showed a strong interaction in the peptide array, together with ADAM15 C and E. However, our MDA/ADAM15 B expressing cells do not upregulate claudin1. Thus direct interaction of PI3K to ADAM15 may not activate the PI3K/mTOR signalling pathway.

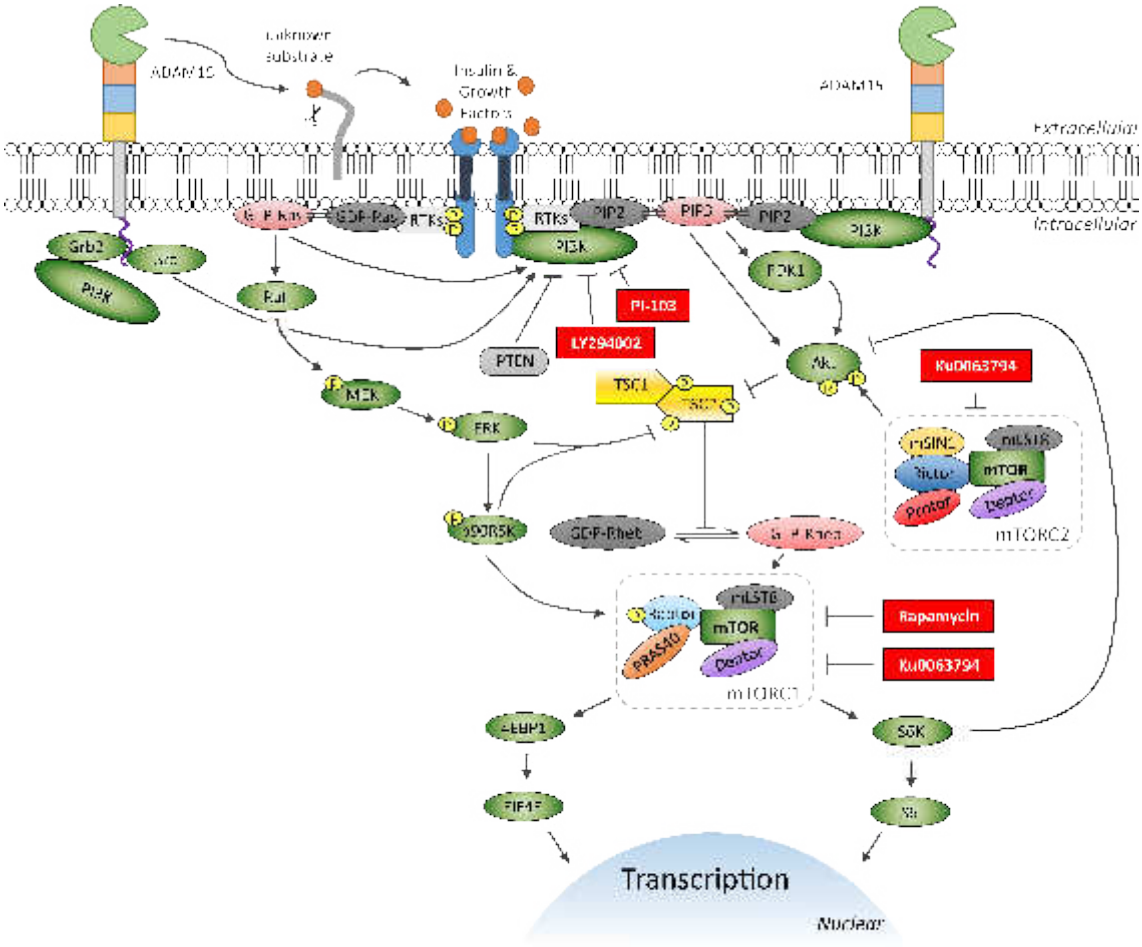

Figure 4.23: Schematic representation of the hypothesised ADAM15/PI3k/mTOR pathway. Pharmacological inhibitors are displayed as a red squared box. Arrows indicate the activation or phosphorylation (P) of a downstream molecule. Lines with horizontal bar indicated inhibition of downstream target.

Taken together, upregulation of claudin1 seems to be isoform specific and MP domain dependent. The ECD of ADAM15 isoforms are identical therefore something else dictates its function. The only difference between the cell lines are the length and number of proline-rich regions.

A hypothesis is that different intracellular interaction partners mediate claudin1 upregulation. The gain or loss of proline-rich regions could dictate the interaction with adaptor proteins or kinases. It is known that the cytoplasmic tail of ADAM15 spliceforms differentially associate with proteins[179,180,182]. As an example, In MDA/ADAM15 A expressing cells a protein could interact with one of the three available proline-rich regions which is necessary for claudin1 regulation. The fourth proline-rich region in MDA/ADAM15 B expressing cells might have a higher affinity to another adaptor which blocks the association of other proteins.

In order to address the pathways mediating claudin1 upregulation, LY294002 a

PI3K inhibitor was preferred over wortmannin due to its stability *in vitro*. The tested half life of wortmannin is between 8-13 min[515] which makes 24h treatments impossible. The prolonged incubation period was necessary due to the stability of the expressed claudin1. To confirm the findings with LY294002, the newer and more specific PI-103 inhibitor was used. However, the inhibition was not as striking as with LY294002. A reason could be the stability of the compound or the used concentration. Compared to LY294002, PI-103 already showed therapeutic potential *in vivo*, but it suffered from extensive metabolism[450]. Thus, it cannot be excluded that the cells *in vitro* also metabolise the inhibitor rapidly, since it is also used at a much lower concentration. In summary, it was demonstrated that ADAM15 upregulates the TJ protein claudin1 in an isoform specific and catalytically dependent manner. Upregulation is mediated via the PI3K/mTOR pathway. Claudin1 is directly regulated by ADAM15 in MDA-MB-231 and T47D cells, but it has no effect on cell migration. Claudin1 is localised primarily in the cell-cell junctions of MDA/ADAM15 A isoform expressing cells. However, claudin1 was also found in membrane, cytoplasm and, most interestingly, in the nucleus. This suggests a potential function as regulator of transcription. ADAM15 was found in a complex with ZO1 and ZO2 which suggests it is a potential regulator in tight junctions.

Several papers have been published describing the correlation of claudin1 expression and cell migration. One study showed that a stable knockdown of keratins 8 and 18 upregulated claudin1 via PI3K/Akt/NFκB pathway which led to increased collective cell migration and invasiveness of epithelial cancer[322]. Concomitantly, in mammary gland carcinoma cells (BT-20), claudin1 knockdown reduced cell migration[59]. In colorectal cancer tissue miR-155 was significantly upregulated[516]. It was observed that upregulation of miR-155 increased claudin1 expression which in turn enhanced cell migration and invasion. Many other studies confirm that claudin1 promotes migration in healthy cells as well as several types of cancer. The promotion of migration by claudin1 was observed in healthy liver cells[315], breast cancer[317], melanoma[281,510,517], hepatocellular carcinoma[315], gastric cancer[300,518] and lung cancer[519] (both mediated by TNFα). However, the opposite has also been reported. In MDCK and T47D cells, active Recepteur d'origine nantais (RON) reduced claudin1 expression and promoted cell migration[520]. RON belongs to the family of RTKs and regulates survival, growth, differentiation and migration. It is often overexpressed in several types of primary cancers[520]. Based on literature I was curious to see if claudin1 is also involved in the process of migration in MDA-MB-231 cells. In chapter 3 it was shown that MDA/ADAM15 A expressing cells significantly reduces cell migration compared to its parental control. Thus, I was interested to see whether claudin1 upregulation affects wound healing. Next, I performed scratch wound experiments on MDA/ADAM15 A expressing cells, MDA/ADAM15 with

non-target shRNA and also cells with shClaudin1 knockdown. The results showed that there is no significant difference between MDA/ADAM15 A non-target shRNA and shClaudin1. This means that in MDA-MB-231 cells the migration is independent of claudin1 expression. However, claudin1 can still contribute to collective cell migration as reported in different papers[322,519]. Collective cell migration has several implications which makes it crucial to understand the underlying mechanisms. One is that invasion is described as a similar collective behaviour of which cells established the development of protrusions, shape generation and interaction with the ECM[521]. On the first glance, it is paradox to have cells performing collective cell migration since the scientific dogma states that mesenchymal cells move single-celled while epithelial cells perform collective cell migration[522]. In this chapter it was confirmed that our cells did not undergo MET and remain mesenchymal. However, ADAM15 A overexpression makes them grow epithelial-like. In general, the benefit of collective migration is to retain a structure or tissue while remodelling it. Second, mobile cells drag immobile ones along. Third, movement as a collective ensures correct distribution of the cells and cell shaping. Fourth, it adds robustness to the collective. As an example, core cells are more protected from the immune system. Claudin1 could contribute to all mentioned benefits as a key player in maintaining the integrity of the motile cells. There are several experiments to perform to prove if MDA/ADAM15 A expressing cells migrate as a collective. Data from the wound healing assays suggest that cells perform sheet migration, which is a characteristic of epithelium. However, to investigate this process a better resolution and live imaging would be beneficial. A highly sophisticated approach to determine the kind of migration is force mapping[523]. The theory is that this experiment measures the dynamic traction forces which are exerted by epithelial cells which are combined with a multiple particle tracking. The sensors for measurement are a high-density array of microfabricated elastomeric pillars below the cells. Bending of the pillars give an estimate of the mechanical activity. This assay is a powerful tool to profile cell types. Different information such as degree of scattered cells, tractions force, the orientation of migration front can be measured. Another powerful tool is to observe the migration of cells embedded in matrigel. This 3D environment represents a more physiological system in which more complex movements such as sprouting or branching can be observed.

I conclude that claudin1 expression is mediated by catalytic active ADAM15 A, C and E isoform which shed an unknown substrate that in turn activates an unknown receptor. The activated receptor promotes claudin1 expression via the PI3K/mTOR pathway. Knockdown by shRNA targeting ADAM15 (shADAM15) as well as pharmacological inhibition of PI3K and mTOR inhibited claudin1 upregulation. An illustration of the hypothesised mechanism is displayed in figure 4.24.

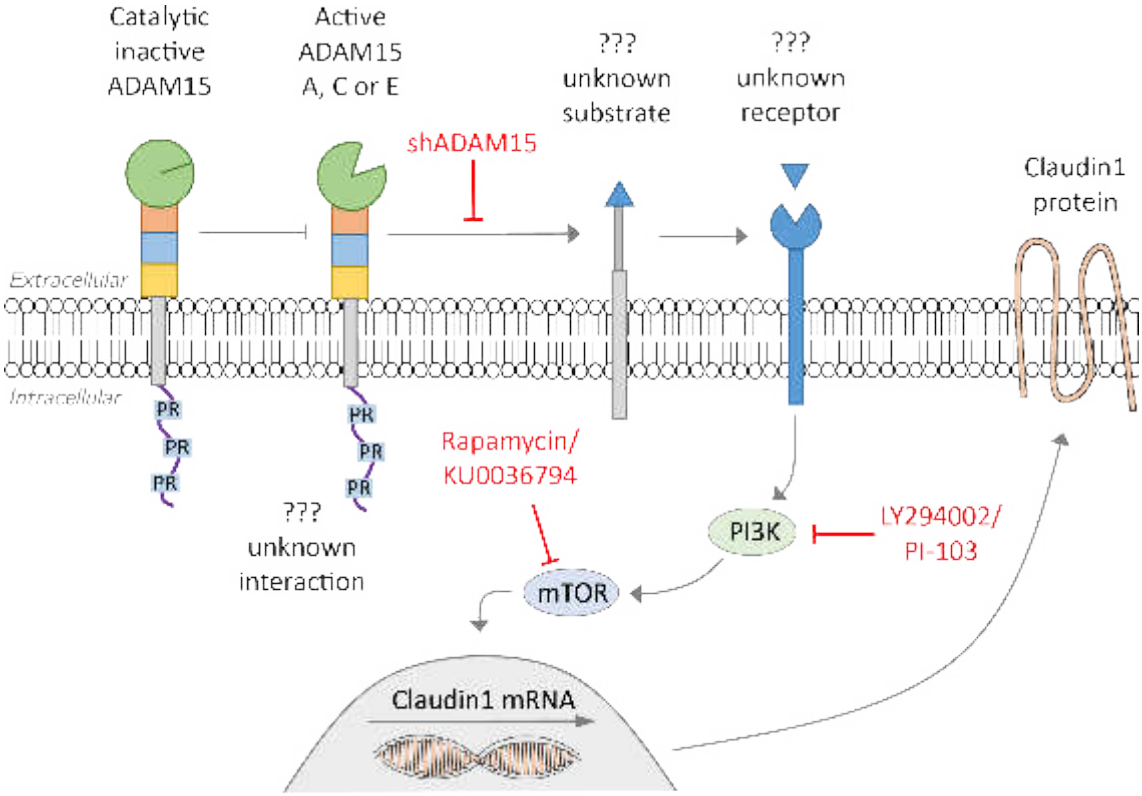

Figure 4.24: Regulation of claudin1 expression by catalytic active ADAM15 A, C and E requires PI3K and mTOR signalling. Catalytic active, but not inactive, ADAM15 A, C and E isoforms shed an unknown substrate which activates an unknown receptor. The activated receptor stimulates claudin1 expression via the PI3K/mTOR pathway. Knockdown by shRNA targeting ADAM15 (shADAM15) as well as pharmacological inhibition of PI3K (LY294002, PI-103) and mTOR (Rapamycin, Ku0036794) inhibited claudin1 upregulation.

Chapter 5

ADAM15 mediated changes in breast cancer cell adhesion

5.1 Introduction

5.1.1 Aim of the chapter

1. Investigate whether FA turnover may cause changes in cell migration
2. Investigate whether ECM spreading caused changes in cell migration

5.2 Results

5.2.1 Focal adhesion dynamics are differentially regulated by ADAM15 isoforms

FA are specialised cellular structures responsible for adhesion to a substrate which occurs in many cell types. Within these structures integrins on the plasma membrane interact with ECM components thereby establishing a link between the cell and its environment.

The wound healing assay (section 3.2.6) revealed that the expression of ADAM15 isoforms affects the migration rate of MDA-MB-231 cells. While the expression of ADAM15 E had no effect on the motility of these cells, the expression of all the other isoforms reduced the wound closure rate with ADAM15 D expression decreasing cell motility the most. This raised the question whether FA turnover is altered in ADAM15 expressing cells, since cell movement requires the assembling and disassembling of these structures. To assess the presence and distribution of FA in our cell panel I conducted a pilot IF analysis of paxillin/vinculin in resting cells. ADAM15 isoform expressing cells were seeded onto glass coverslips, allowed to grow for 72h, fixed and subjected to IF analysis. Figure 5.1 a shows representative images of immunostaining for paxillin and vinculin. As these cells were not synchronised, we would expect balanced and comparable FA distribution. However, the abundance as well as orientation of vinculin positive FA were strikingly different within the cell panel. In an attempt to quantify these differences 100 cells from each cell line in random fields were assessed and ordered in four groups based on the strength of vinculin staining (figure 5.1 b).

Cells which did not show any visible FA were categorised in one group (non). Cells with only a few FA were considered as “low”. In case FA cover the majority of the periphery or are “uncountable” due to their abundance FA were categorised as “high”. Cells which did not fit in the group “low” or “high” are considered as “medium”.

There were no major differences observed in the distribution and abundance of FA between ADAM15 A and E isoform expressing cells. Both contained similar cell

numbers with FAs of low (nascent adhesions), moderate (focal complexes), and high (FA) vinculin intensity. When compared with the parental cell line, they both contained more cells with high intensity vinculin staining. On the other hand, ADAM15 B and C isoform expressing cells were similar to each other, most of them possessed FAs of low vinculin intensity. In contrast to all the other cell lines, the vast majority of the analysed ADAM15 D expressing cells contained FAs with high vinculin intensity. The described differences indicated that the FA turnover may be affected by ADAM15 expression, where the expression of ADAM15 B and C isoforms prevented the formation of strong FA, and on the contrary, the expression of ADAM15 D isoform prevented the disassembly of mature FA.

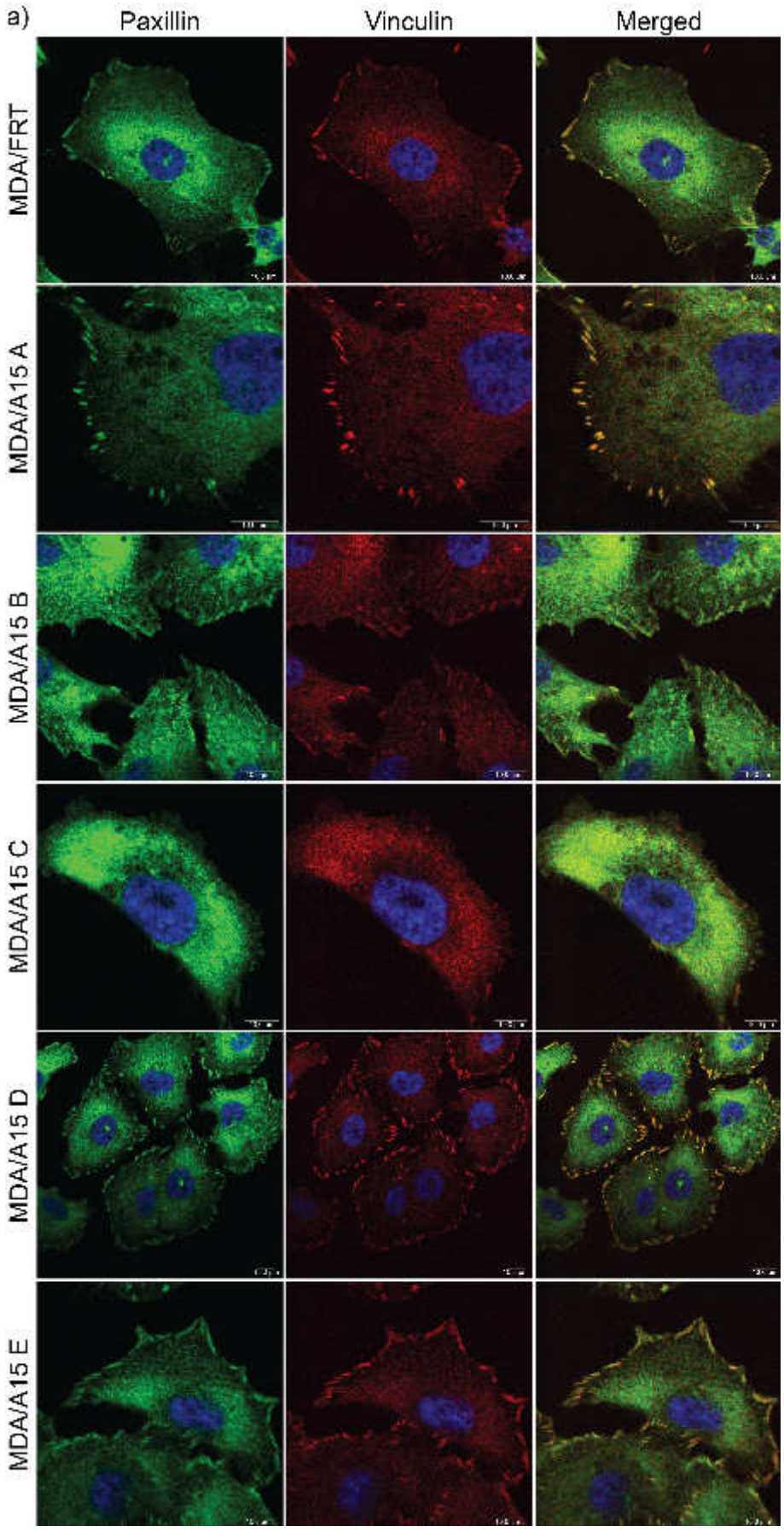

Figure 5.1: Continued on the next page

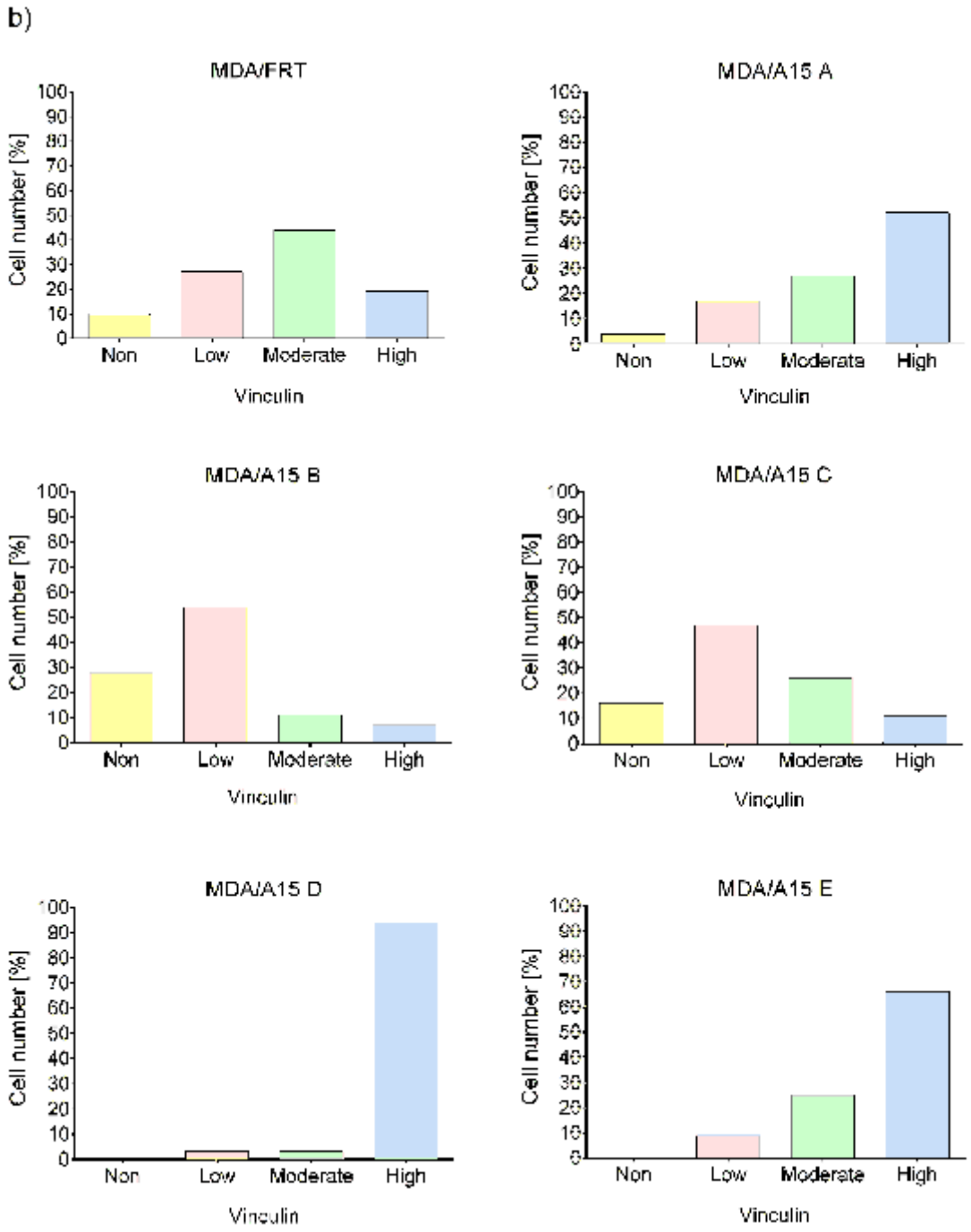

Figure 5.1: Assessment of FA in MDA/FRT and MDA/ADAM15 WT isoform expressing cells. **a)** IF analysis of the cell panel stained with the FA markers paxillin (green) and vinculin (red). The nucleus was visualised with DAPI (blue). Left column: Paxillin staining; Central column: Vinculin staining; Right column: Merged images. Scale bar = 10 µm. **b)** Quantification of the assessed FA by examining the vinculin staining. The slides were examined by a meander-shaped course while the first 100 cells were classified into one of four groups: No-, low-, moderate- or high vinculin. n=1

To address whether FA turnover is affected by the expression of ADAM15 isoforms, we conducted a FA disassembly assay using nocodazole as described by Ezratty et al[443] and Villari et al[524]. Nocodazole disrupts microtubule assembly by

binding to β-tubulin[373]. As microtubules are necessary for FA disassembly, nocodazole treatment stabilises FAs, allowing to evaluate if a cell is able to form FA, as well as the maximum potential coverage of FA in a cell. Once the nocodazole is washed out, microtubules begin to form, allowing FA to disassemble. The rate of the FA disassembly followed by recovery and formation can be monitored over time. In order to synchronise the FA turnover, cells were serum-starved overnight, followed by nocodazole treatment for 4h hours. Coverslips were fixed prior to nocodazole treatment, at the end of nocodazole treament, and after 15, 30, 45, 60 and 120 min post washout. Cells were stained with phalloidin and vinculin to visualise FAs. Ten representative images were acquired and analysed for the coverage of FA on the cell surface as a percentage of total cell area as well as the average feret diameter of FA as described in section 2.12. The number of analysed cells per cell line and timepoints are shown in table 6.1.

Table 5.1: Cell numbers analysed in focal adhesion disassembly assay.

	MDA/ FRT	**A15 A**	**A15 B**	**A15 C**	**A15 D**	**A15 E**
Nocodazole	50	48	62	30	56	52
Washout 15 min	27	35	37	33	29	38
Washout 30 min	43	45	39	34	41	48
Washout 45 min	36	39	47	38	34	33
Washout 60 min	44	48	53	35	37	45
Washout 120 min	31	48	41	25	34	36

Nocodazole treatment demonstrated (figure 5.2) that all cell lines have the capacity to form mature FA irrespective of the expressed ADAM15 isoform. There were no obvious differences between the cell lines: The FAs covered 8-10% of the total cell area, with an average feret diameter of 19-22 μm. Once the nocodazole was washed out, within 15 min in all cell lines, with the exception of ADAM15 D expressing cells, the FA successfully disassembled, as measured by the reduction of FA coverage down to below 1% of the total cell area, and the feret diameter down to 9 μm. The most pronounced reduction occurred in ADAM15 E expressing cells, where the total coverage of FA dropped to 0.8% compared with the parental control cell line. The FA disassembly continued for the following 15 min with the FA area reduced down to 0.7%. ADAM15 D expressing cells stood out during this first phase of the experiment. They failed to disassemble their FA to the level comparable with the other cell lines, with the FA coverage being reduced down to only 5% of the total cell area, and the average feret diameter reducing down to 14 μm. These values did not change during the following 15 min of the nocodazole washout. By 45-60

min post nocodazole washout FAs begin to regrow slowly in all cell lines with the exception of ADAM15 B, C and E expressing cells. FA coverage area in these cells remains at approximately 1% of the total cell area, as opposed to 2% in parental and ADAM15 A expressing cells and nearly 6% in ADAM15 D expressing cells. At this time point, while the average FA feret diameter in most cell lines reached 9-12 μm, it remained at 10 μm in ADAM15 C expressing cells, and strikingly, nearly 15 μm in ADAM15 D expressing cells. These observed differences were more striking at the end of the assay period of 120 min post nocodazole washout. FA coverage area was comparable in parental, as well as ADAM15 A, B and E isoform expressing cells, reaching up to 3%, with an average feret diameter of 13 μm. However, in ADAM15 C expressing cells FA coverage remained below 1%, and, on the contrary, in ADAM15 D expressing cells at 6% of the total cell area, with an average feret diamter of 17 μm.

In summary, all cell lines have the ability to form FA irrespective of the expressed ADAM15 isoform. However, the disassembly and re-assembly showed differences. Parental and ADAM15 A, B and E expressing cells showed similar FA turnover while ADAM15 C expressing cells displayed reduced re-assembly. ADAM15 D expressing cells failed to disassemble the FA to a comparable level with the other cell lines, but re-assembled them in a higher rate. Of all the cell lines, only ADAM15 D expressing cells assembled their FA to a degree comparable with the pre-nocodazole stage.

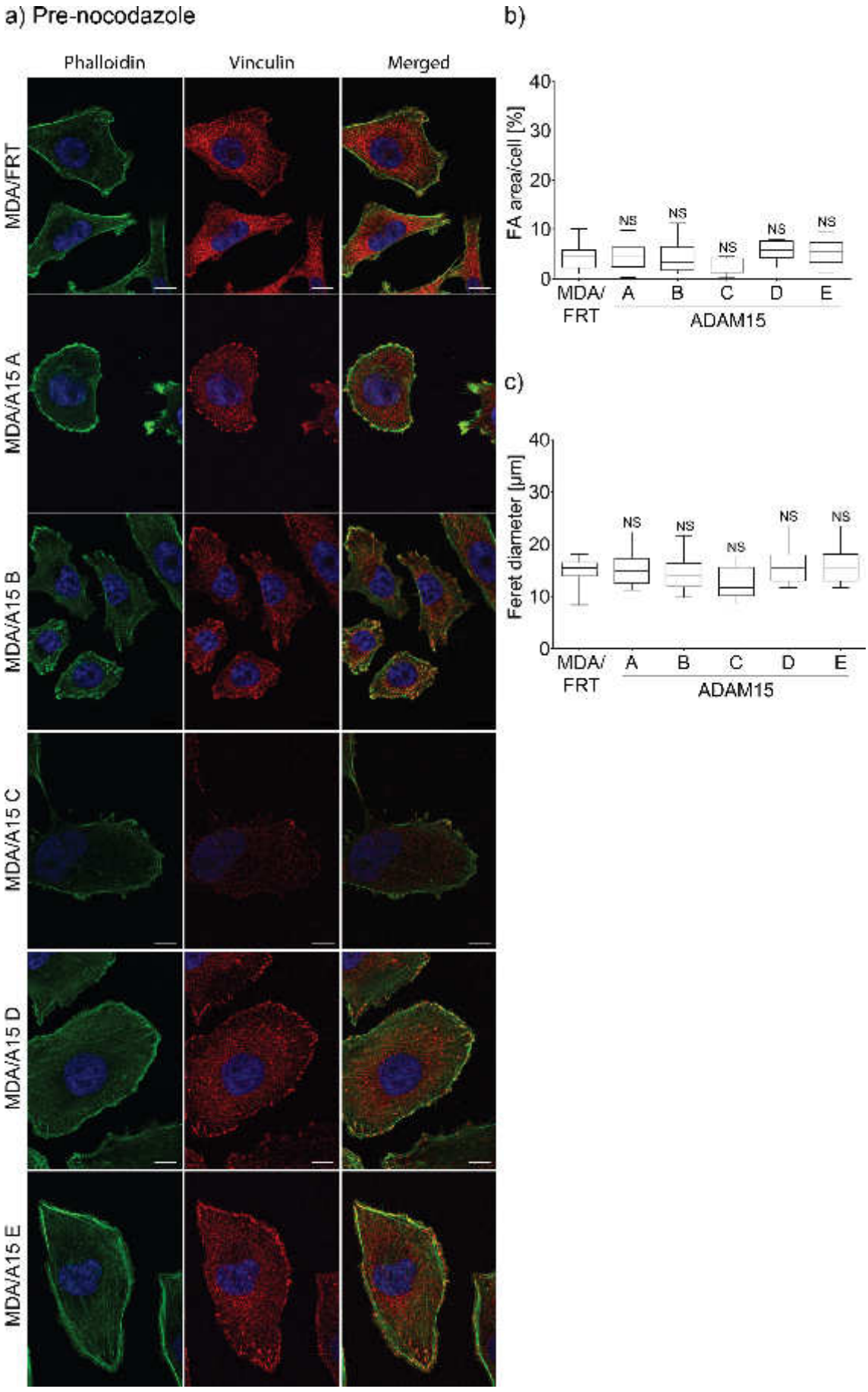

Figure 5.2: Continued on the next page

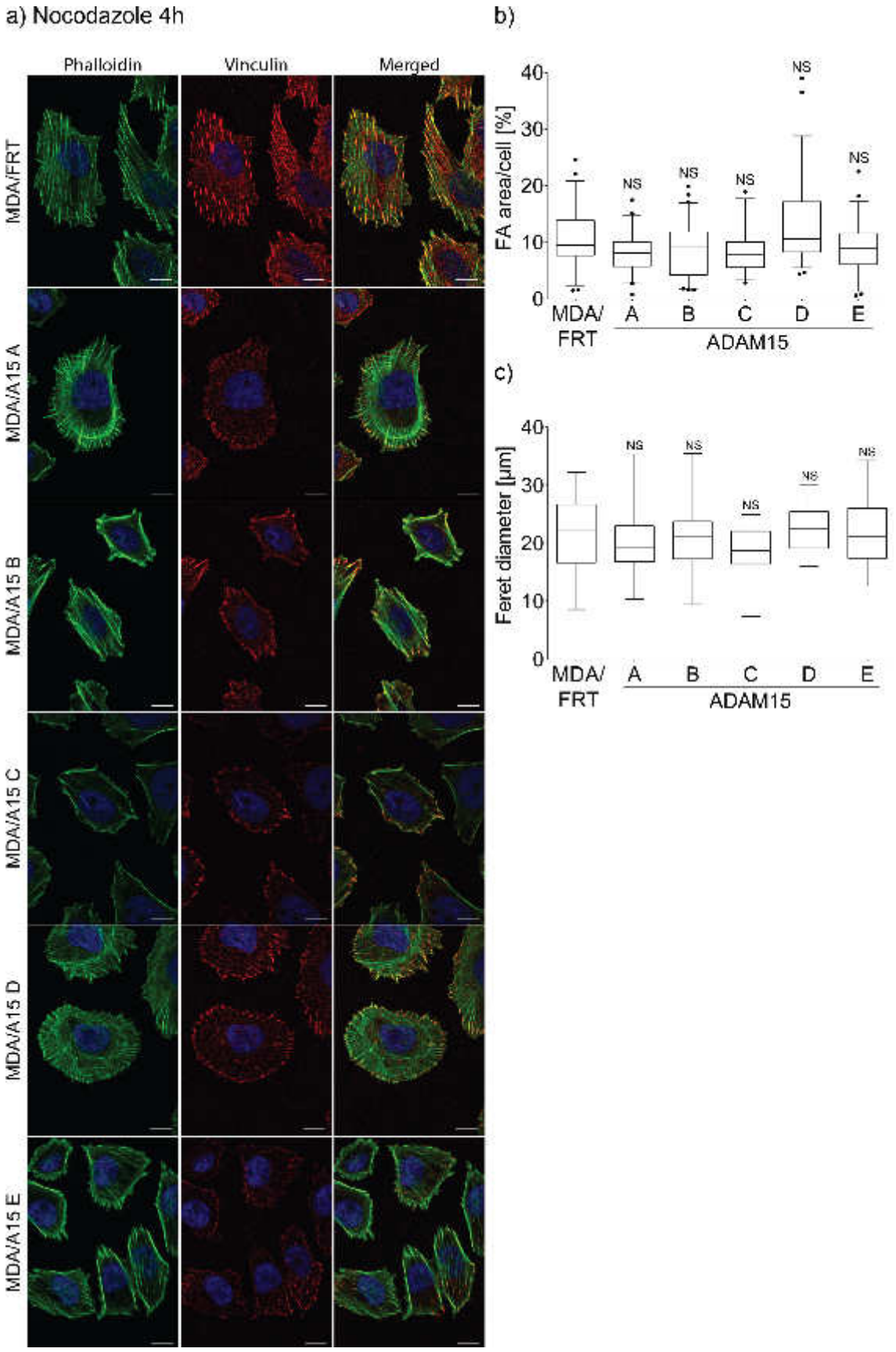

Figure 5.2: Continued on the next page

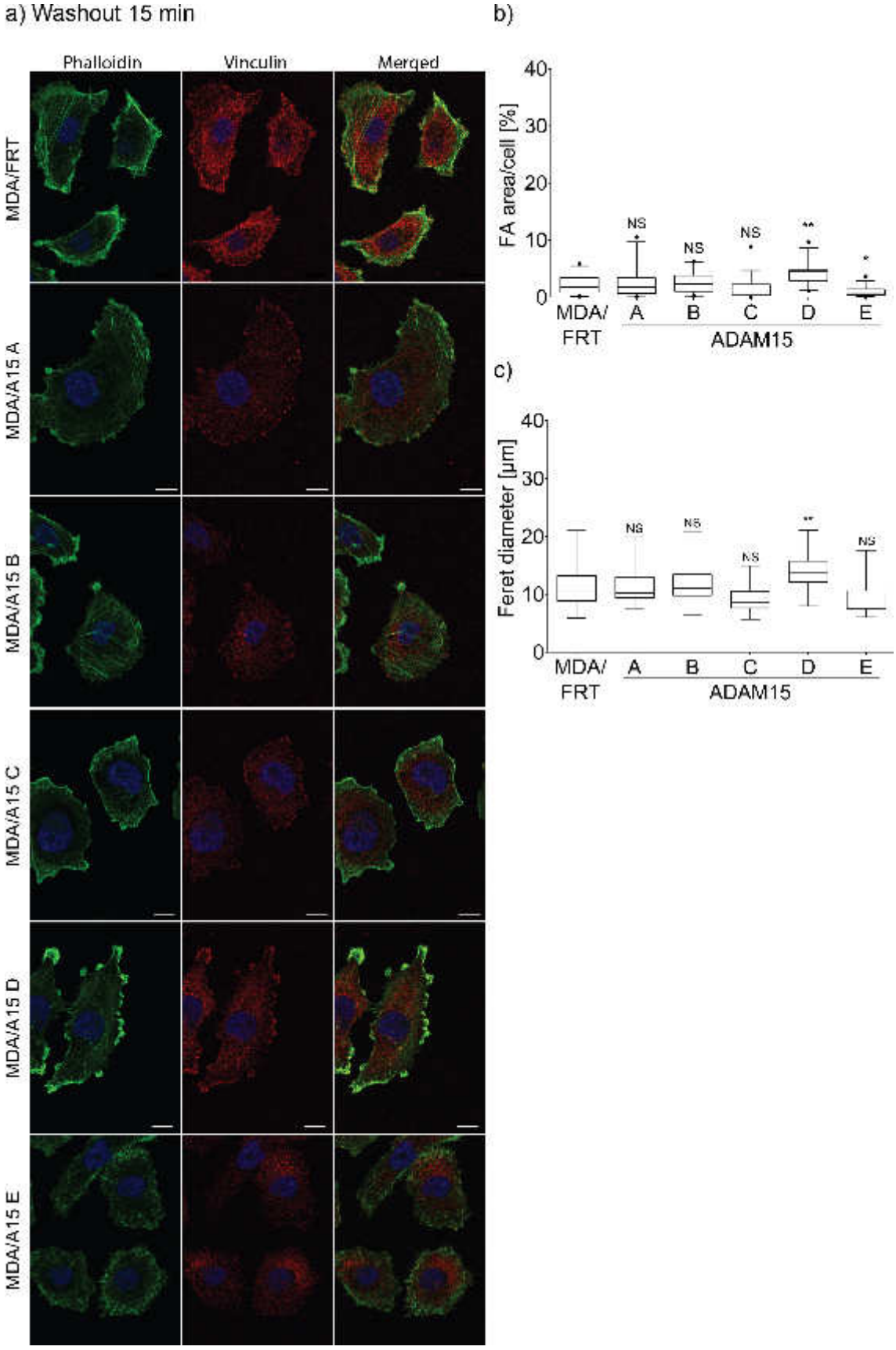

Figure 5.2: Continued on the next page

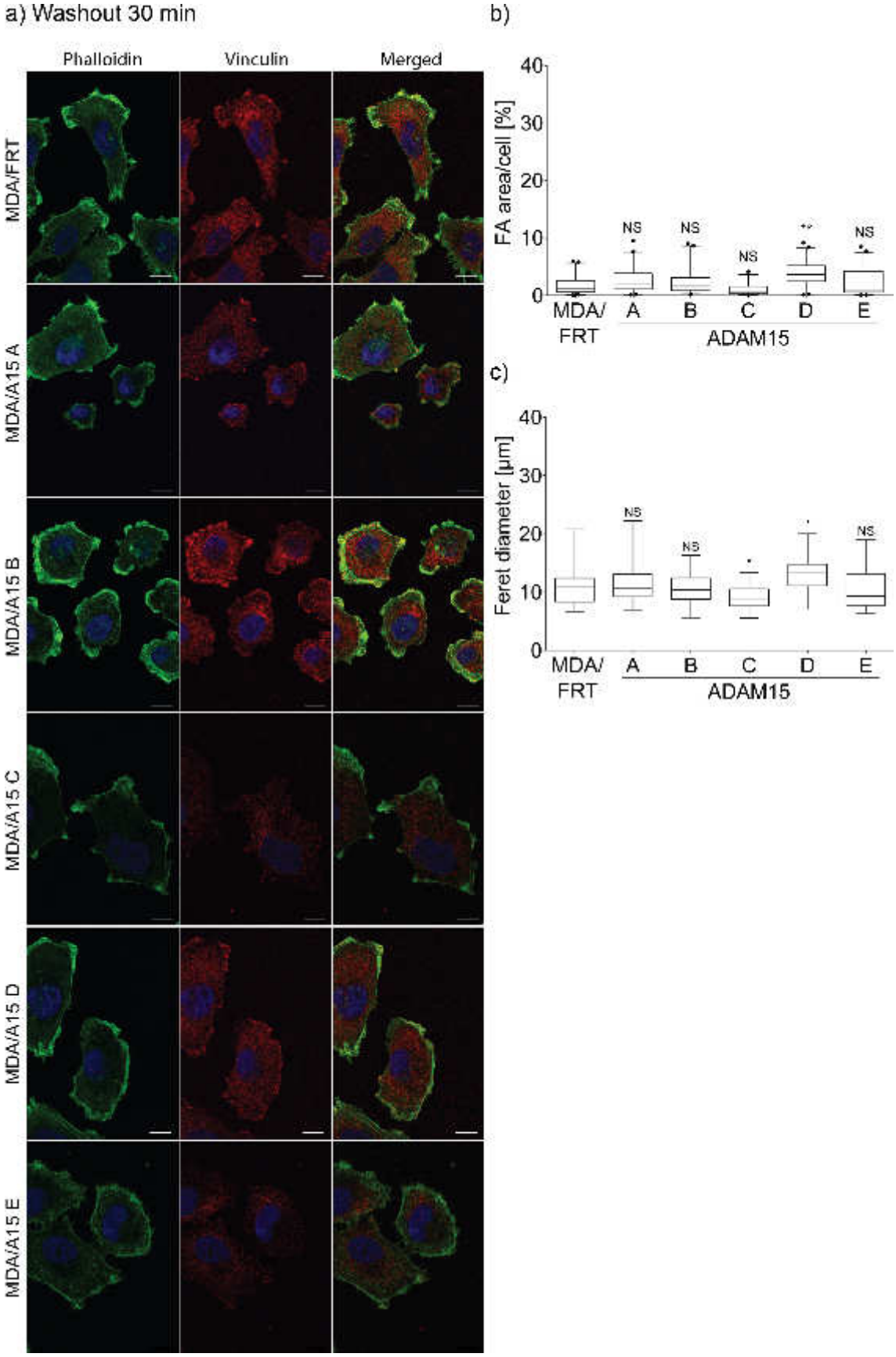

Figure 5.2: Continued on the next page

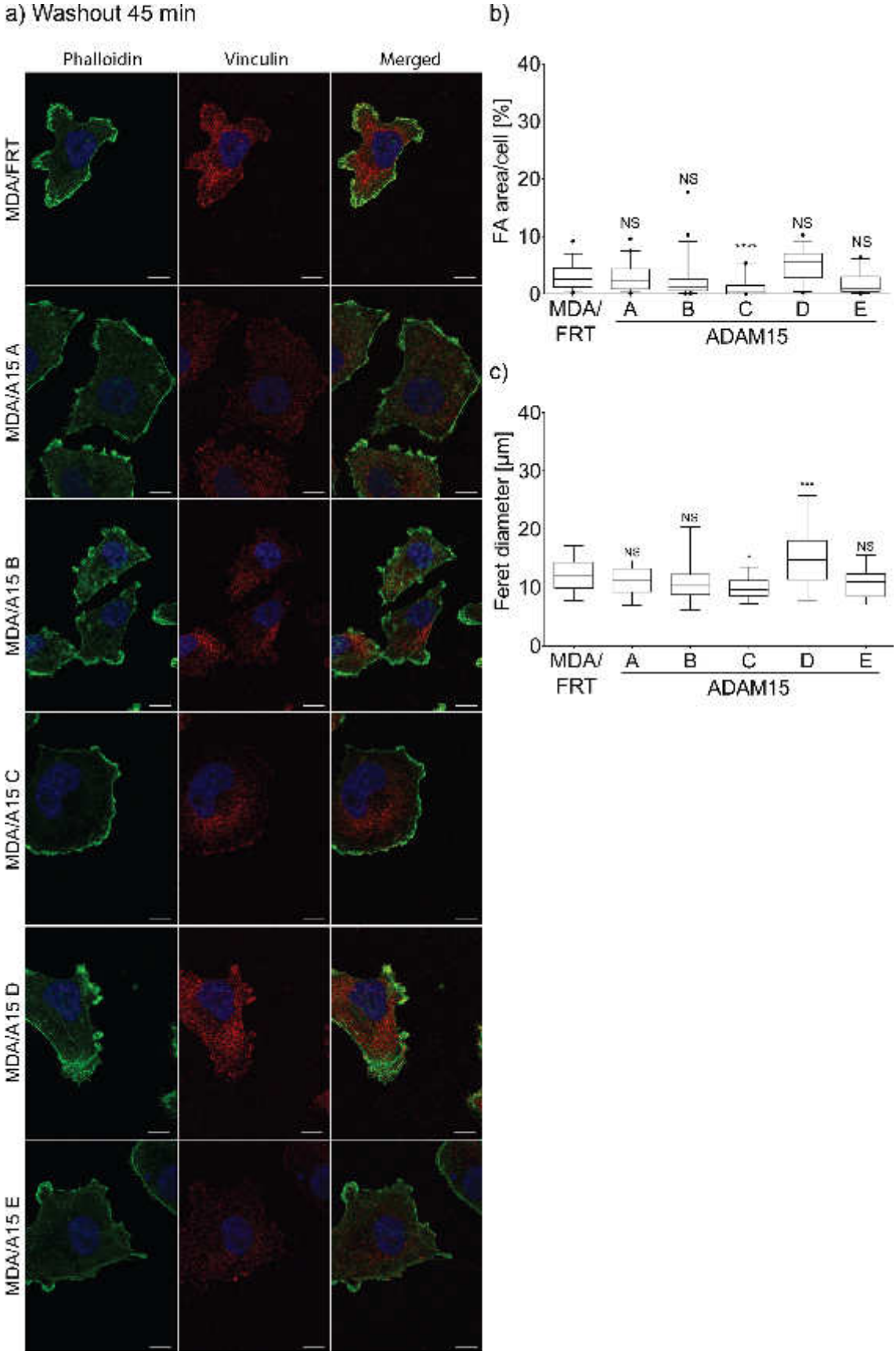

Figure 5.2: Continued on the next page

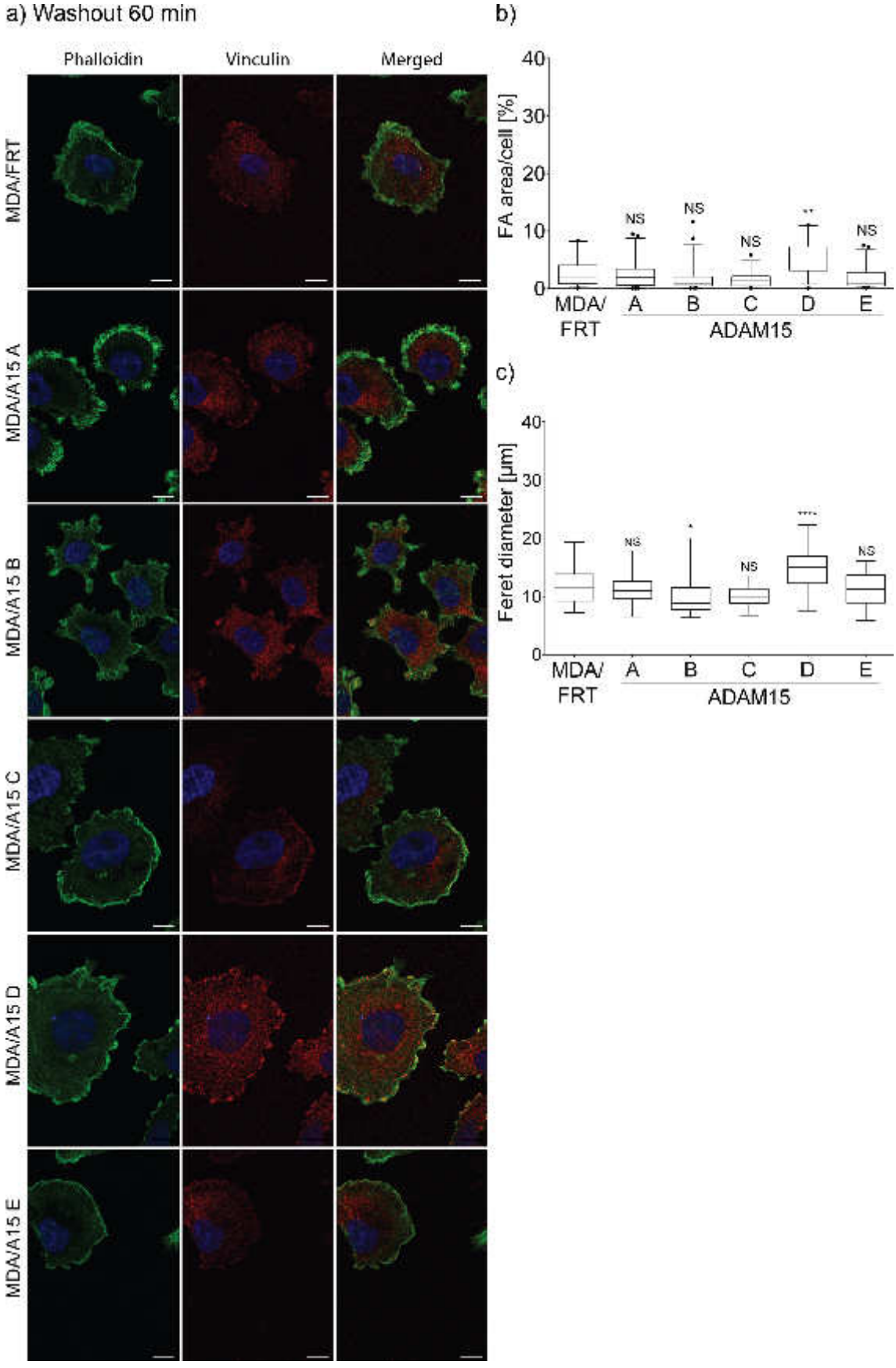

Figure 5.2: Continued on the next page

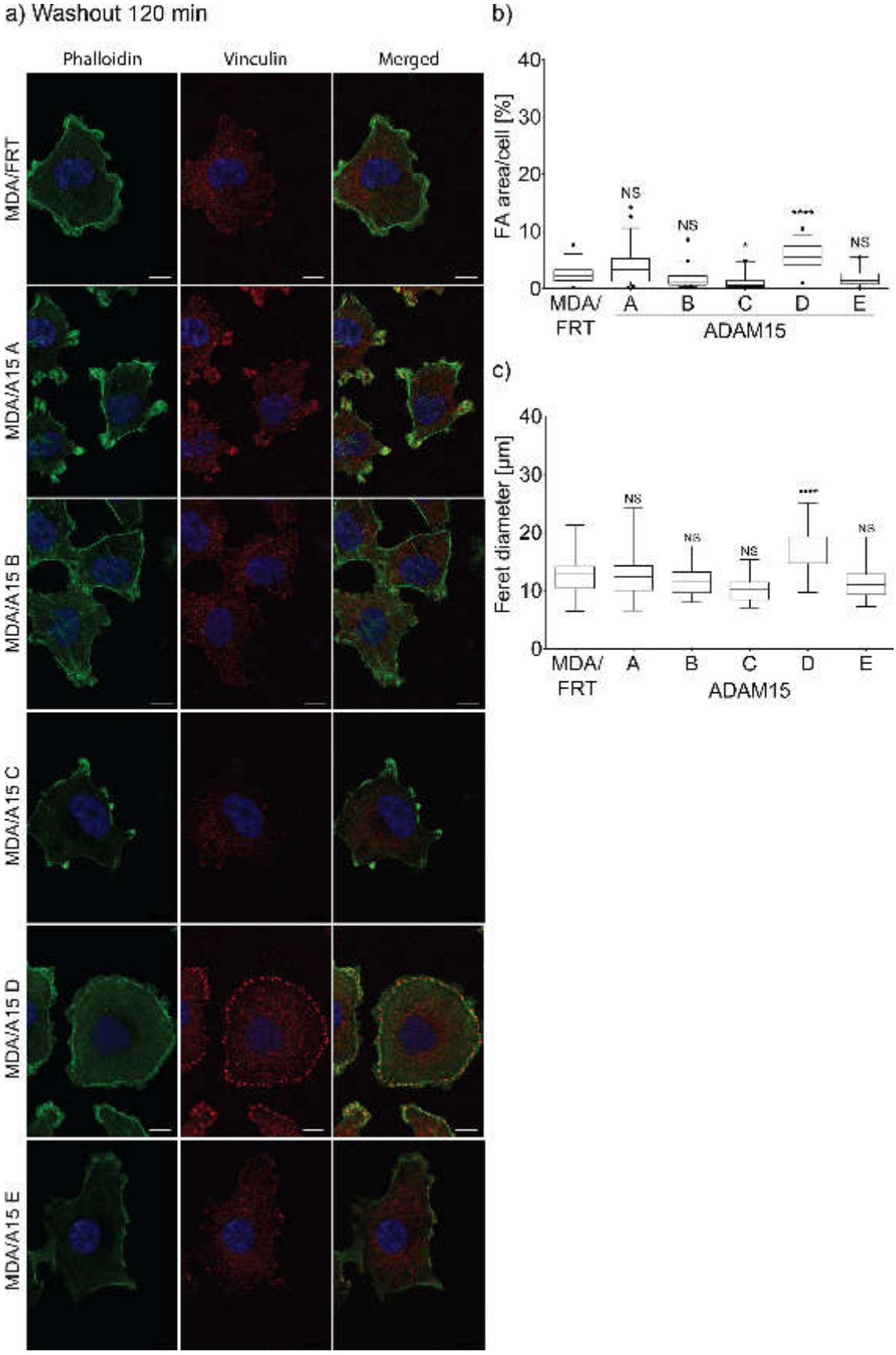

Figure 5.2: Continued on the next page

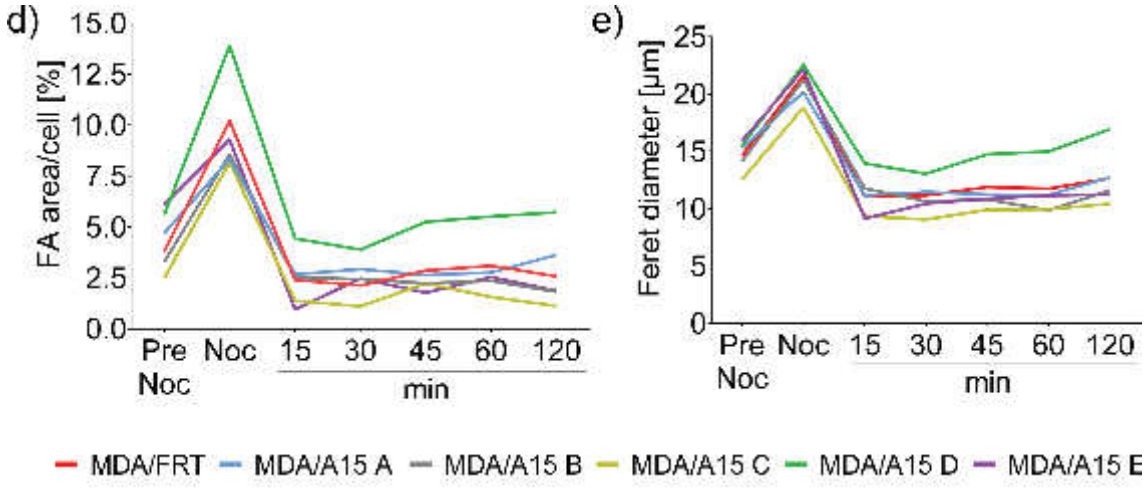

Figure 5.2: Focal adhesion disassembly assay of MDA/FRT and MDA/ADAM15 WT isoform expressing cells. Cells were grown for 72h and serum starved overnight, followed by 4h Noc (10 µM) treatment. Noc was removed and cells were washed twice with serum free medium. Cells were fixed directly before (pre-noc), after 4h of Noc treatment and after 15, 30, 45, 60 and 120 min of washout. The cells were stained for phalloidin (green) and vinculin (red). the nuclei were visualised with DAPI (blue). Images were acquired at a confocal microscope with 630 x magnification and 3 x digital zoom. The cell lines were compared to each other for every time point and shown as box-and-whisker plot. Analysis was performed using the semi-automated script for ImageJ described in section 2.12. The results appear in following order: Pre-noc (n=1); Noc 4h (n=3); 15 min washout (n=2), 30 min washout (n=3), 45 min washout (n=2), 60 min washout (n=3), 120 min washout (n=2). **a)** Representative images of the experiment Left column: Phalloidin staining; Central column: Vinculin staining; Right column: Merged images. Scale bar = 10 µm. **b)** The total area of FA per cell. **c)** Average feret diameter of all FAs combined. Statistical significance was assessed with the post-hoc Dunnet's multiple comparison test after performing one-way ANOVA analysis. MDA/ADAM15 A-E expressing cells were compared to the MDA/FRT control cell lines. Confidence intervals are as follows: $* = p \leq 0.05, ** = p \leq 0.01, *** = p \leq 0.001, **** = p \leq 0.0001$. Scale bar = 10 µm. The experiment was repeated in three independent experiments for 4h nocodazole, 30 and 60 min washout. The time point for 15, 45 and 120 min washout was repeated twice. Analysed images were checked manually to exclude false positive cells which result from the used algorithm. **d)** Summarised total area of FA per cell shown as line graph **e)** Summarised average feret diameter of all FA combined. Red: MDA/FRT; Blue: MDA/ADAM15 A; Grey: MDA/ADAM15 B; Yellow: MDA/ADAM15 C; Green: MDA/ADAM15 D; Purple: MDA/ADAM15 E, Noc: nocodazole.

5.2.2 ADAM15 isoforms affect cell spreading on different ECM substrates

In the previous section we identified that the dynamic turnover of FA is affected by the expression of individual ADAM15 isoforms, whereas the expression of ADAM15 C delays or reduces the FA maturation rate, while the expression of ADAM15 D compromises the disassembly of FA. The dynamic turnover of FA depends on the internalisation and recycling of integrins. Integrins are key proteins in mediating the assembly of FAs linking the ECM to the actin cytoskeleton. On the other hand, integrin endocytosis is one of the events necessary for FA disassembly. Cells use specific integrins receptors to recognise ECM components and bind to them,

facilitating cell adhesion. It is known that ADAM15 disintegrin domain interacts with α5β1 and αvβ3 integrins. We hypothesised that ADAM15 isoform-dependent effects on FA turnover might be due their differential effects on integrin cell surface presentation, or integrin endocytosis and recycling. Thus we decided to investigate which of these integrins might be differentially expressed on the cell surface. The level of cell adhesion and spreading on a specific ECM component can inform us which integrin is mediating the cell attachment. We decided to carry out a pilot experiment to test if ADAM15 isoform expressing cells show differences in their attachment and spreading on FN (α5β1 and αvβ3 ligand), and on VN (αvβ3 ligand). Glass cover slips were coated with either complete medium, FN or VN for 1h at 37°C. Afterwards cells were seeded onto the cover slips and incubated for 60 min. Images were taken at 0, 15, 30, 45 and 60 min. The earliest differences in cell spreading on these substrates were observed at 45 min as demonstrated in figure 5.3.

In this assay the parental, as well as ADAM15 A and B expressing cells behaved similar to each other, and showed better attachment and spreading on FN, although parental cells spread more on FN than ADAM15 A and B expressing cells. ADAM15 E expressing cells adhered and spread equally well on FN and VN compared to medium coated surface. The degree of spreading on FN was more in ADAM15 E expressing cells than ADAM15 A or B expressing cells. ADAM15 C and D isoform expressing cells behaved similar to each other, and, unlike all the other cells, adhered and spread on all surfaces equally efficient, and the degree of spreading on all surfaces was higher compared to the other cell lines.

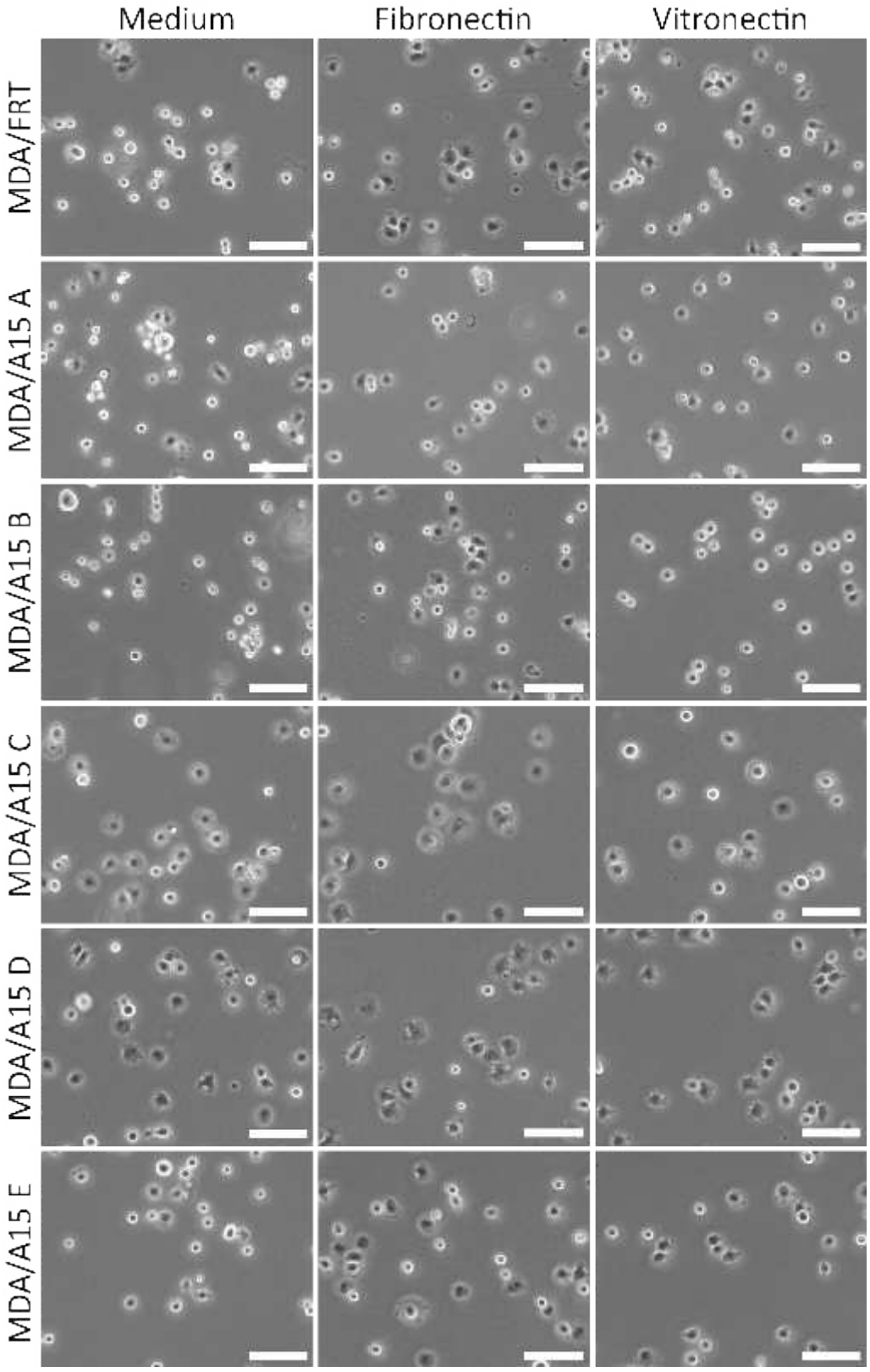

Figure 5.3: Phase-contrast images of MDA/FRT and MDA/ADAM15 WT expressing cells plated on medium, FN (10 µg/mL) or VN (10 µg/mL) coated coverslips. Coverslips were coated with the corresponding substrate for 1h at 37°C. Afterwards MDA/FRT or MDA/ADAM15 WT expressing cells were plated for 45 min and subsequently phase-contrast images were acquired at 100 x magnification. Scale bar = 100 µm

In summary (table 5.2), all cell lines showed best attachment and adherens on FN followed by VN and medium. However, expression of ADAM15 A and B seemed to decrease attachment and spreading while ADAM15 C and D promoted it. ADAM15 E behaved similar to the parental cell line. Thus we conclude expression of ADAM15 isoforms affect substrate dependent cell adhesion and spreading.

Table 5.2: Summary of the adhesion and spreading experiment. Coverslips were coated with medium, FN (10 µg/mL) or VN (10 µg/mL) for 1h at 37°C. Parental and ADAM15 isoform expressing cells were seeded and phase-contrast images were acquired after 0, 15, 30, 45 and 60 min. This table shows the analysed degree of spreading after 45 min as the first differences were observed at this time point.

Cell line	**Result**
MDA/FRT	FN >VN >Medium
MDA/A15 A	FN = VN >Medium
MDA/A15 B	FN >VN >Medium
MDA/A15 C	FN >Medium = VN
MDA/A15 D	Medium = FN = VN
MDA/A15 E	FN = VN >Medium

Our pilot experiment indicated that there are differences in cell attachment and spreading on FN and VN between the cell lines depending on the expression of ADAM15 isoforms. To be able to quantify these differences, we conducted another experiment. Glass coverslips were coated with either complete medium, FN (10 µg/mL) or VN (10 µg/mL) for 1h at 37°C. Cells were trypsinised and plated onto the coverslips for 45 and 105 min. Subsequently, the cells were fixed and stained with phalloidin followed by confocal microscopic examination. Acquired pictures were analysed with ImageJ. The number of cells analysed for each cell line, time point and ECM substrate is shown in table 5.3 below.

Table 5.3: Number of cells analysed on ECM coated substrates after 45 and 105 min.

	Medium		**Fibronectin**		**Vitronectin**	
	45'	**105'**	**45'**	**105'**	**45'**	**105'**
MDA/FRT	61	77	70	53	86	79
ADAM15 A	36	67	73	68	75	69
ADAM15 B	40	89	83	72	86	81
ADAM15 C	43	55	48	49	66	62
ADAM15 D	35	56	64	59	79	79
ADAM15 E	41	50	77	64	77	73

Plating of cells on complete growth medium, FN and VN are shown in figure 5.4, 5.5 and 5.6, respectively. MDA/ADAM15 isoform expressing cells were compared

to MDA/FRT. On medium coating, after 45 min of plating MDA/ADAM15 A, B and E expressing cells showed similar cell surface area and spread, when compared to MDA/FRT (Figure 5.4 a). In contrast, MDA/ADAM15 C and D expressing cells showed increased spreading. One hour later we observed that the MDA/FRT cells reached the same degree of spreading as MDA/ADAM15 C, D, E expressing cells, while the MDA/ADAM15 A and B isoform expressing cells did not increase the spread area to the same extent. Additionally, quantification of cell numbers revealed that the expression of ADAM15 isoforms impaired cell attachment, as significantly more MDA/FRT cells had adhered after 45 min than ADAM15 expressing cells. After the prolonged incubation, at 105 min, comparable numbers of parental and ADAM15 B expressing cells had adhered, while significantly less numbers of ADAM15 A, C, D and E expressing cells adhered on this surface.

To quantify α5β1-dependent cell adhesion and spreading, cells were plated on FN coated coverslips. Analysis of cell surface area revealed significant differences in ADAM15 A and B expressing cells, whose spread area was nearly 50% less at both analysed time points than of all the other cell lines (figure 5.5 b and c). MDA/ADAM15 C and D expressing cells spread somewhat more than the other cell lines. Overall far less ADAM15 isoform expressing cells adhered to FN when compared with the parental cells within the first 45 min. After another hour, however, some of these differences were reduced, with only ADAM15 A and C isoform expressing cells having adhered less then all the other cell lines.

To quantify αvβ3-dependent cell adhesion and spreading cells were plated on VN coated coverslips. Analysis of the cell surface area showed significant differences between ADAM15 B expressing cells compared with all the other cell lines. Throughout the duration of the assay they remained at least 25% smaller then the rest. Additionally, while parental, as well as ADAM15 C, D and E expressing cells continued to spread by 105 min, ADAM15 A and B expressing cells failed to spread to similar levels. Quantification of cell numbers revealed that by 45 min comparable numbers of parental, as well as ADAM15 A, B and D cells adhered to VN, while there were significantly less ADAM15 C and D expressing cells adhered to this surface. By 105 min however, only MDA/FRT and ADAM15 D expressing cells had comparable numbers adhered to VN, and much reduced numbers of the other cell lines adhered, with ADAM15 C expressing cells showing the least number of cells adhered on VN. Comparison of cell spreading on these substrates (figure 5.7) revealed that most preferred FN over VN, but ADAM15 E reduced this preference, and the expression of ADAM15 A altered it in favour of VN over FN. FN is the major ligand for α5β1 and αvβ3 and VN for αvβ3. This results suggest that ADAM15 affects integrin interaction. This may occur due to differential cell surface localisation, general changes in integrin expression or altered ADAM15-integrin interaction.

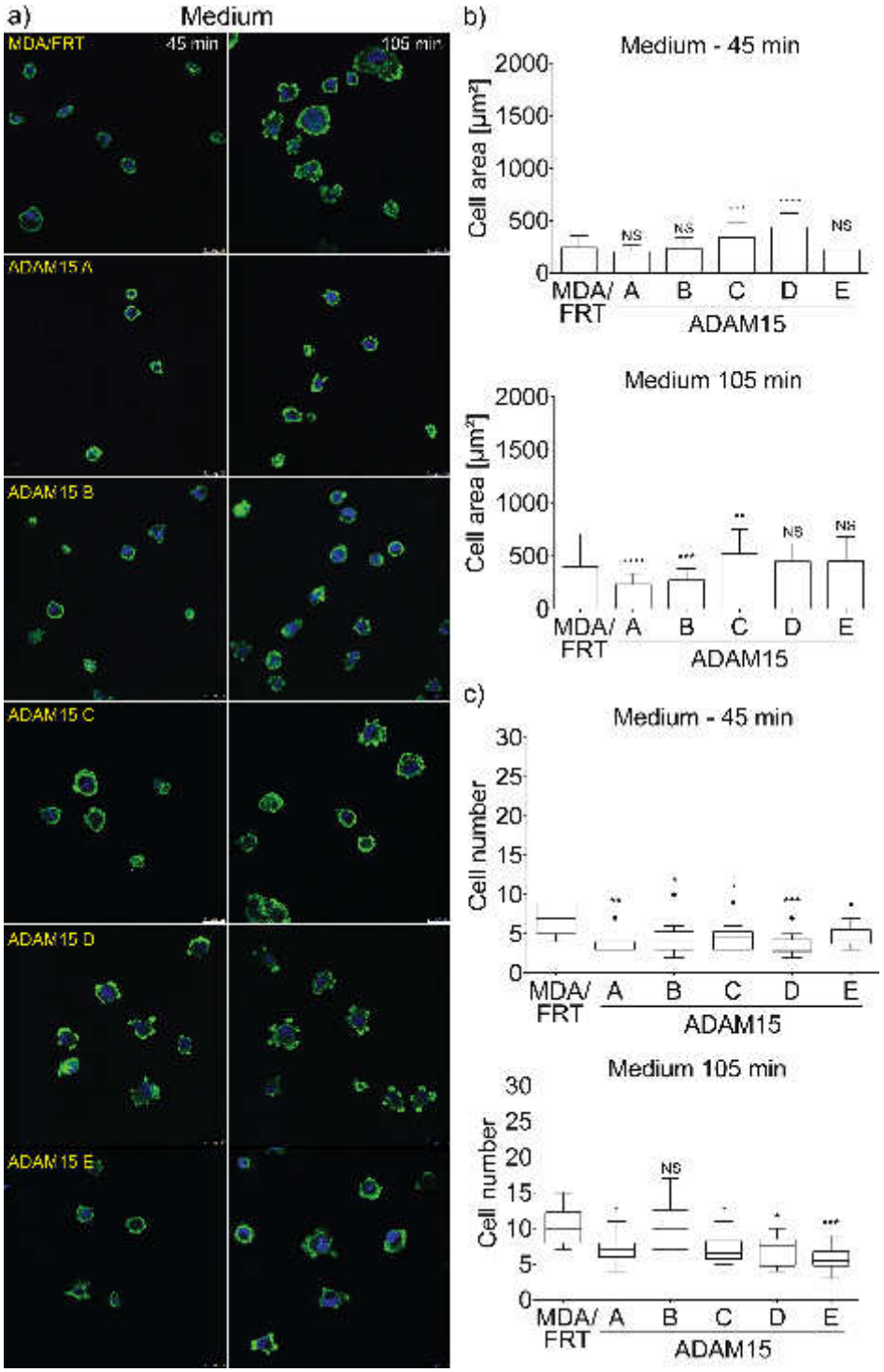

Figure 5.4: Immunofluorescence analysis of MDA/FRT and MDA/ADAM15 isoform expressing cells plated on medium coated surface. Glass cover slips were coated with complete medium for 1h at 37°C. Afterwards MDA/FRT or ADAM15 isoform expressing cells were plated for 45 or 105 min and subsequently fixed and stained with phalloidin-488 (green). Nucleus is stained with DAPI (blue). Images were acquired by a confocal microscopy. Cell area and number were analysed by ImageJ. **a)** Representative images of the acquired images. **b)** Degree of cell spreading shown as bar chart. **c)** The average of counted cells per image shown as box plot. Statistical significance was assessed with the post-hoc Dunnet's multiple comparison test after performing one-way ANOVA analysis. MDA/ADAM15 A-E expressing cells were compared to the MDA/FRT control cell lines. Confidence intervals are as follows: $* = p \leq 0.05, ** = p \leq 0.01, *** = p \leq 0.001, **** = p \leq 0.0001$. The number of analysed cells is shown in table 5.3.

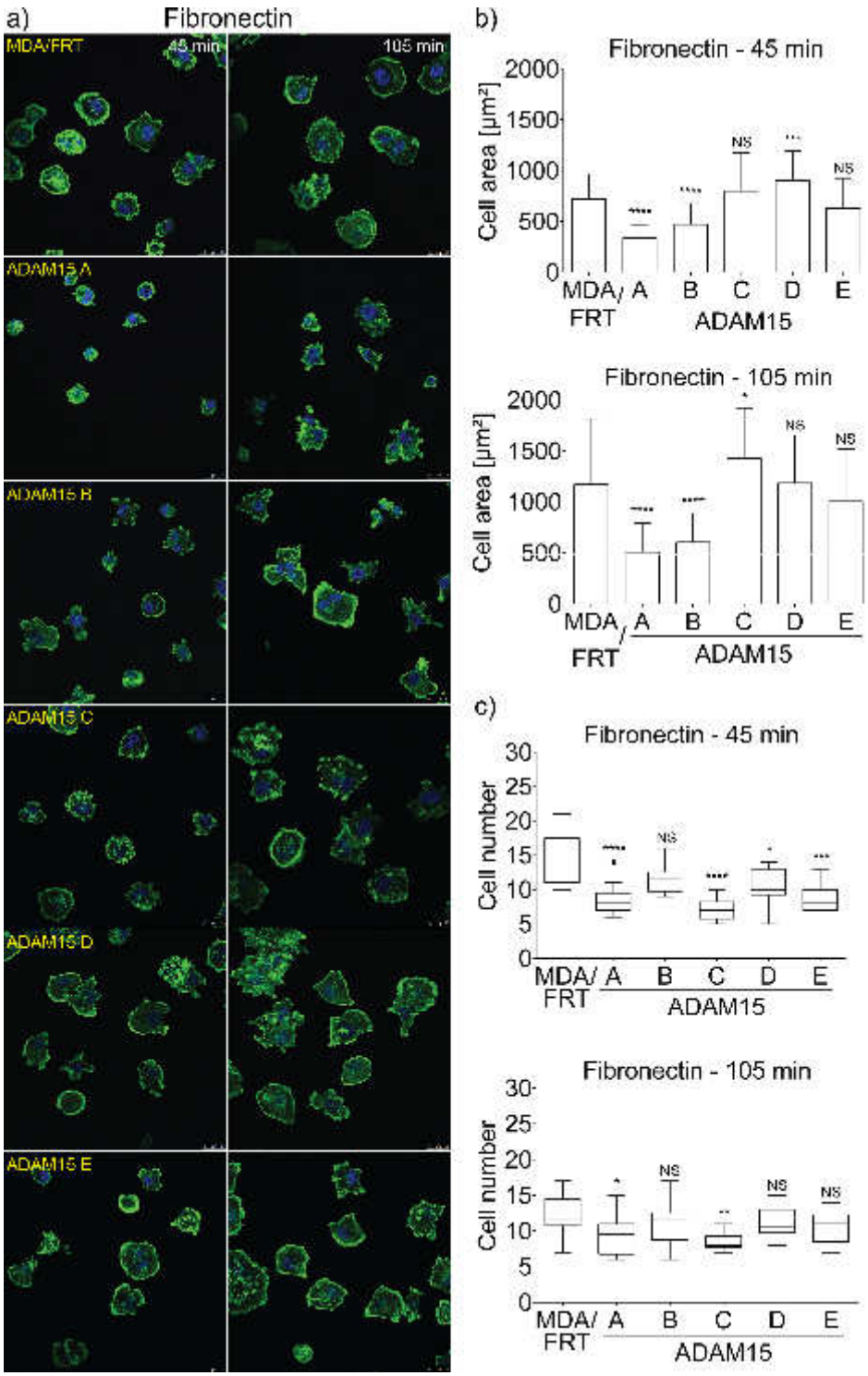

Figure 5.5: Immunofluorescence analysis of MDA/FRT and MDA/ADAM15 isoform expressing cells plated on FN coated surface. Glass cover slips were coated with FN (10 µg/mL) for 1h at 37°C. Afterwards MDA/FRT or ADAM15 isoform expressing cells were plated for 45 or 105 min and subsequently fixed and stained with phalloidin-488 (green). Nucleus is stained with DAPI (blue). Images were acquired by a confocal microscopy. Cell area and number were analysed by ImageJ. **a)** Representative images of the acquired images. **b)** Degree of cell spreading shown as bar chart. **c)** The average of counted cells per image shown as box plot. Statistical significance was assessed with the post-hoc Dunnet's multiple comparison test after performing one-way ANOVA analysis. MDA/ADAM15 A-E expressing cells were compared to the MDA/FRT control cell lines. Confidence intervals are as follows: $* = p \leq 0.05, ** = p \leq 0.01, *** = p \leq 0.001, **** = p \leq 0.0001$. The number of analysed cells is shown in table 5.3.

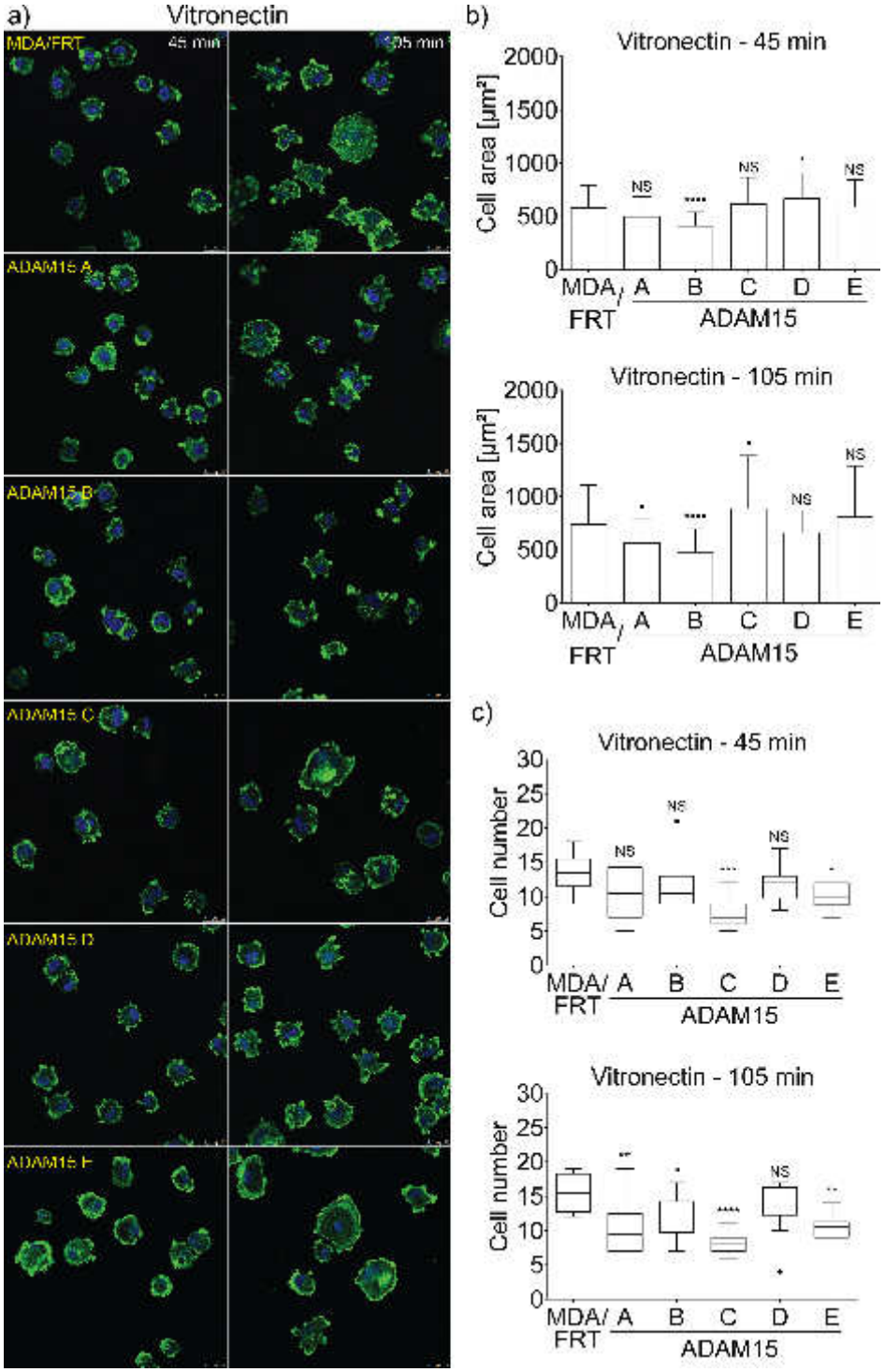

Figure 5.6: [Immunofluorescence analysis of MDA/FRT and MDA/ADAM15 isoform expressing cells plated on medium, FN and VN coated surfaces. Glass cover slips were coated with complete growth medium, FN (10 µg/mL) or VN (10 µg/mL) for 1h at 37°C. Afterwards MDA/FRT and ADAM15 isoform expressing cells were plated for 45 or 105 min and subsequently fixed and stained with phalloidin-488 (green). The nucleus was visualised with DAPI (blue). Images were acquired by a confocal microscopy. Cell area and number were analysed by ImageJ using a semi-automated script descried in section 2.13.2. **a)** Representative images of the acquired images of either medium, FN or VN coated glass cover slips **b)** The corresponding degree of cell spreading shown as bar charts. **c)** The average of counted cells per image shown as box plots. Statistical significance was assessed with the post-hoc Dunnet's multiple comparison test after performing one-way ANOVA analysis. MDA/ADAM15 A-E expressing cells were compared to the MDA/FRT control cell lines. Confidence intervals are as follows: $* = p \leq 0.05, ** = p \leq 0.01, *** = p \leq 0.001, **** = p \leq 0.0001$. The number of analysed cells is shown in table 5.3.

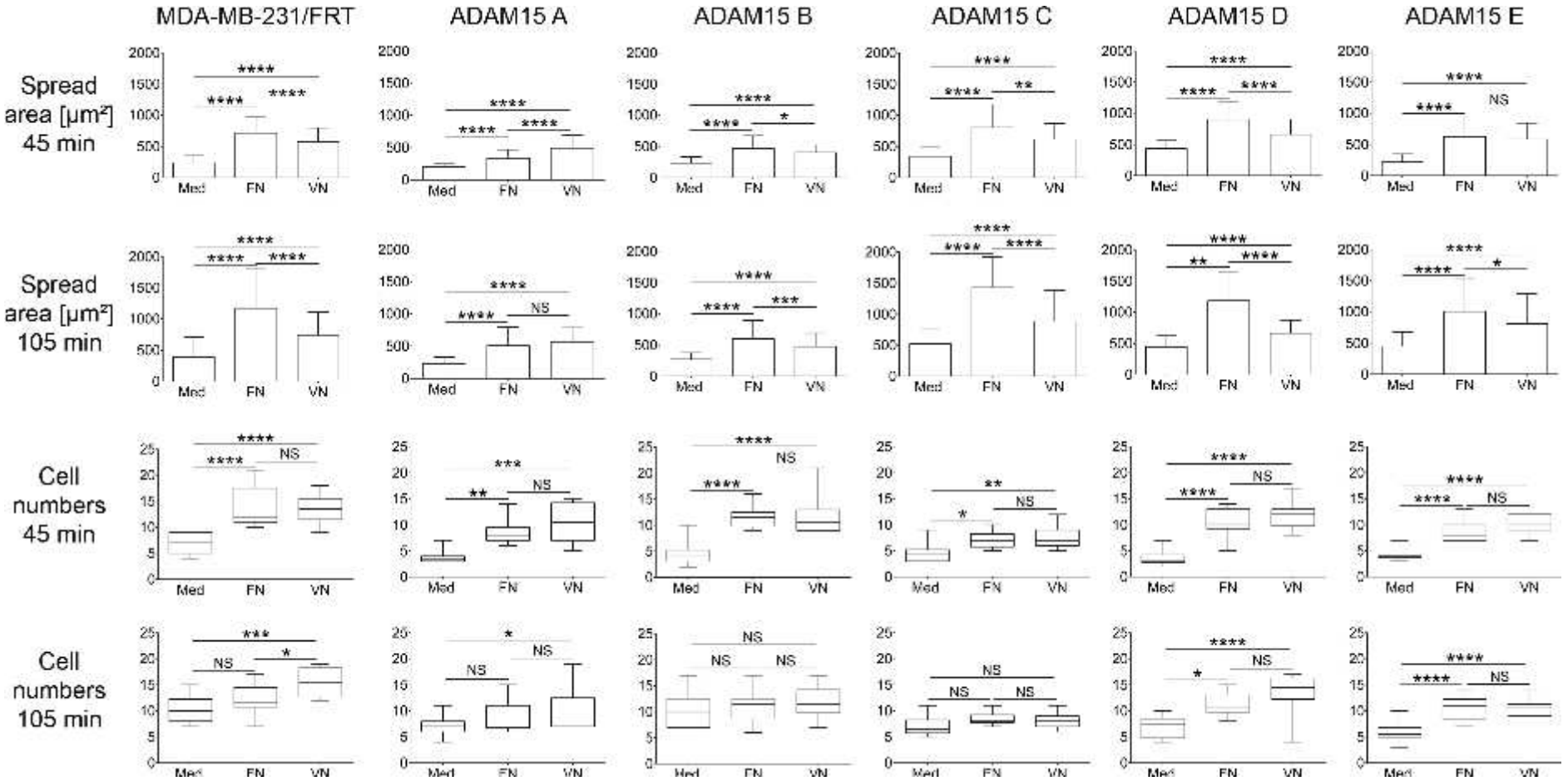

Figure 5.7: Summary of IF analysis of MDA/FRT and MDA/ADAM15 isoform expressing cells plated on medium, FN and VN coated surfaces. Cell area is shown as bar chart while the cell number is displayed as box-and-whiskers plot. Statistical significance was assessed with the post-hoc Dunnet's multiple comparison test after performing one-way ANOVA analysis. All three samples were compared to each other. Confidence intervals are as follows: $* = p \leq 0.05, ** = p \leq 0.01, *** = p \leq 0.001, **** = p \leq 0.0001$. The number of analysed cells is shown in table 5.3.

5.2.3 ADAM15 isoforms may affect integrin cell-surface localisation

Our analysis of FA turnover, as well as of cell spreading on FN and VN suggests that either the cell surface presence, ability to associate with their preferred ECM component, or overall expression of integrins α5β1 and αvβ3 is altered depending on ADAM15 isoform expression. If the expression of specific ADAM15 isoforms affected the internalisation and recycling of these integrins, that would result in differential accumulation of the integrins in the cytoplasm and membrane.

To get better understanding if integrin trafficking is altered, subcellular fractionation experiments were performed from exponential growing cells and subjected to protein analysis by western blot. The membranes were probed with specific antibodies to the β1 and β3 subunits (figure 5.8).

This analysis revealed that the β1 subunit is exclusively localised to the cell membrane. Interestingly, the size of β1 in MDA/ADAM15 D expressing cells is smaller while β1 is larger in MDA/ADAM15 E expressing cells compared to MDA/FRT, MDA/ADAM15 A, B and C expressing cells. On the other hand, differences in subcellular localisation of the β3 subunit were observed, that depended on the expression of specific ADAM15 isoforms. The relative distribution of β3 was comparable in the parental, as well as ADAM15 B, C, and D expressing cells, where it was present in both compartments. However, in ADAM15 D expressing cells there was more β3 in the cytoplasmic than in the membrane fraction. In ADAM15 A and E expressing cells β3 was exclusively in the membrane fraction. As cytoplasmic control HSP90 was used which was primarily located in the cytoplasm. As membrane control, the western blot was probed for R-cadherin which was primarily detected in the membrane.

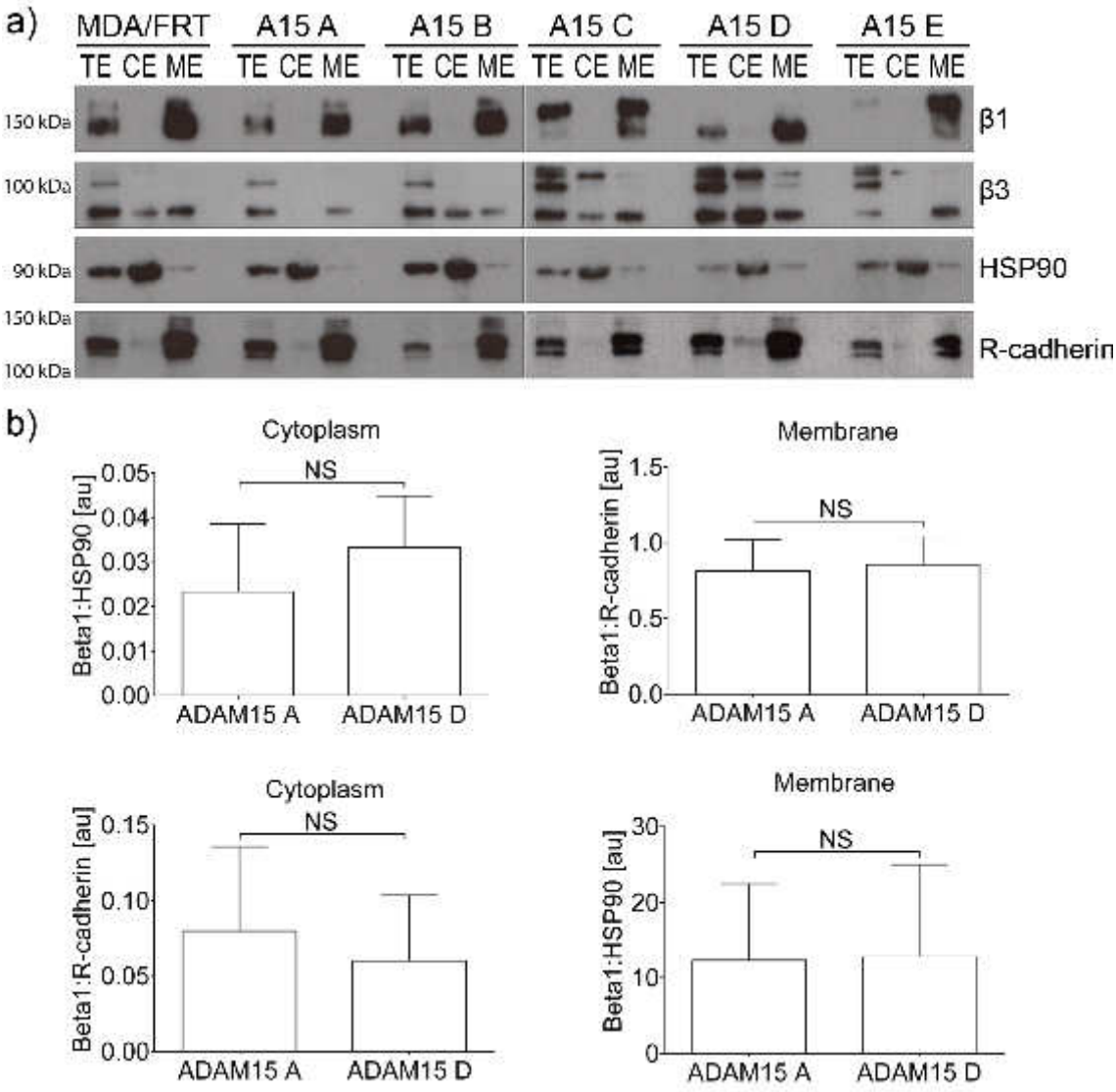

Figure 5.8: Distribution of β1- and β3-integrin in MDA/FRT and ADAM15 isoform expressing cells. The experiment was performed by fractionation and analysis by western blot. **a)** Representative images of the fractionation experiment of the cell panel. Lane 1 shows total cell lysate (TE). Lane 2 shows cytoplasmic extract (CE) with HSP90 as control. Lane 3 shows membrane extract (ME) with R-cadherin as control. **b)** Densitometry of the fractionation experiment where applicable. Statistical analysis was performed by Mann-Whitney t-test by comparing ADAM15 A and D expressing cells. Confidence intervals are as follows: $* = p \leq 0.05, ** = p \leq 0.01, *** = p \leq 0.001, **** = p \leq 0.0001$. Cell panel for β3: n=2; MDA/FRT, MDA/ADAM15 B, C and E for β1: n=2; MDA/ADAM15 A and D: n=3

During the fractionation experiments we observed that the molecular weights of both β1 and β3 varied within the panel. Also, β3 immunobloting revealed multiple bands of different molecular weights which are approximately at 110, 100 and 80 kDa. To confirm whether the observed changes in the size of these integrin subunits were not an artefact of trypsinisation, and, additionally, to investigate if there are changes in the overall expression levels of β1 and β3, I performed WB analysis of the total protein lysates (figure 5.9). We did not observe the same pattern of different

molecular weights for β3, as seen during the fractionation experiment, confirming our suspicion. However, the changes in the molecular weight of β1 were observed using this approach as well. The β1-subunit in MDA/ADAM15 D expressing cells appeared smaller, while the one in MDA/ADAM15 E expressing cells was larger, compared to the other cell lines. There was no difference in the molecular weight of β1 in MDA/FRT, MDA/ADAM15 A-C as well as MDA/ADAM15 A-E E349A expressing cells. Analysis of β3-chain showed that the molecular weights are slightly larger in MDA/15 E WT and cells expressing the catalytic inactive variants of ADAM15.

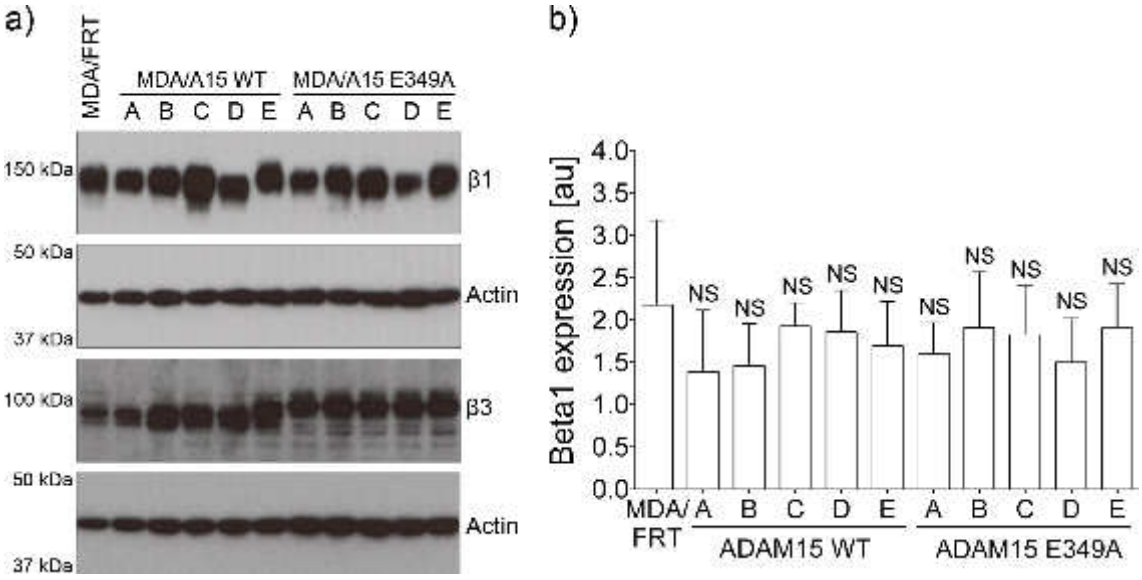

Figure 5.9: Expression of β1- and β3-integrins in MDA/FRT, MDA/ADAM15 WT and MDA/ADAM15 E349A expressing cells. **a)** Representative western blot images of β1 and β3 expression. Actin serves as loading control. **b)** Densitometry analysis of β1 expression presented as bar graphs. Statistical significance was assessed with the post-hoc Dunnet's multiple comparison test after performing one-way ANOVA analysis. MDA/ADAM15 WT and E349A expressing cells were compared to the MDA/FRT control cell line. Confidence intervals are as follows: $* = p \leq 0.05, ** = p \leq 0.01, *** = p \leq 0.001, **** = p \leq 0.0001$. β1: n=5; β3: n=1

5.3 Discussion

In chapter 3 section 3.2.6 we observed that expression of ADAM15 isoforms led to impaired cell migration, especially in ADAM15 C and D expressing cells. In this chapter we sought to get closer understanding of how ADAM15 isoforms might affect cell motility. ADAM15 has the potential to regulate cell motility via several of its functions, such as MP-mediated ECM degradation, disintegrin-mediated integrin and FA regulation, or affecting the activity and localisation of intracellular signalling molecules via ICD-mediated direct protein-protein interactions. Here we focused on elucidating the likely regulation of integrins and integrin-mediated dynamic FA turnover by ADAM15 isoforms. The pilot experiment, looking at general

distribution of FA in cells grown on coverslips for 72h, revealed striking differences in the abundance and intensity of FA between ADAM15 isoform expressing cell lines. ADAM15 B and C expressing cells had fewer, weaker and smaller FA compared to MDA-MB-231 cells while on the other hand, ADAM15 D expressing cells had many large FA. This gave the impression that ADAM15 isoforms have distinct effects on FA maturation and disassembly. More quantitative experiments, using nocodazole as a mean to stabilise FA, confirmed these findings. Nocodazole treatment demonstrated that all the cell lines have the capacity to form mature, large FA. However, we found that MDA/ADAM15 C expressing cells have a much slower rate of reassembly of FA compared to the parental cell lines whereas ADAM15 D expression significantly reduces disassembly and enhances assembly of FA. One reason for this finding could be due to effects on microtuble re-growth. FA disassembly relies on microtuble re-growth post nocodazole washout. If re-growth is impaired cells fail to disassemble FAs[443]. Alterations in microtuble dynamics in our cell panel were not investigated, but may explain our findings. Repeating the FA disassembly assay with vinculin/tubulin co-staining could answer whether microtuble formation is affected in these cells.

In ADAM15 D expressing cells the FA stay larger throughout the time course as judged by the average feret diameter. These impairments in FA turnover might explain why the expression of ADAM15 C and D reduce cell migration. The reduced ability of ADAM15 C expressing cells to form mature FA would compromise the ability of cells to pull the cell body forward. On the other hand, the reduced disassembly of FA in ADAM15 D expressing cells would not allow the cell to retract the trailing edge.

There are many factors that influence the dynamic turnover of FA. One such factor is FAK. While phosphorylation of FAK is necessary for FA assembly, the dephosphorylation of FAK is essential for FA disassembly. Reduced migration due to high numbers of FAs was demonstrated by You et al[525]. Knockdown of the Src homology phosphotyrosyl phosphatase 2 (SHP2) led to increased numbers of FA while reducing the migration rate. Biochemical analysis demonstrated that FAK dephosphorylation was significantly decreased. Hartman et al. confirmed that upon knockdown of SHP2 migration is reduced in MDA-MB-231 and MDA-MB-468 cells[526]. SHP2 is recruited to FAs where it dephosphorylates FAK at Y397[526]. SHP2 possesses two SH2 domains[525,526] which could potentially interact with phosphorylated tyrosines in the cytoplasmic domain of ADAM15. Thus ADAM15 may recruit a phosphatase to FA to modulate FAK activity. Other phosphatases involved in FAK-Y397 dephosphorylation are the protein-tyrosine phosphatase 1B (PTP-1B)[527] and the PEST-sequence containing protein-tyrosine phosphatase-PEST[528]. Both phosphatases contain multiple proline-rich regions which could form a ternary complex with ADAM15 via

Grb2. Indeed we have observed that ADAM15 D expressing cells contain hyperactivated FAK by persistent phosphorylation of Y397, Y576/577 and Y925 (Appendix: figure 9.4). Due to the truncated ICD of ADAM15 D no potential interaction with phosphatases or adaptor proteins is possible. Therefore, ADAM15 D may fail to recruit these to the FA complex to dephoshphorylate FAK, which would lead to stabilisation and reduced disassembly of FA in this cell line.

ADAM15 is known to interact with integrins and their endocytosis is crucial for focal adhesion disassembly. Therefore, it may be possible that ADAM15 isoforms have differential affinity towards integrins which maybe regulated by the ICD. The lack of the ICD of ADAM15 D could enhance extracellular binding to the integrins and thus impair the endocytosis.

Integrins are endocytosed via a clathrin-dependent route which leads to the disassembly of FA. It was shown that this mechanism relies on the clathrin adaptors AP2 and DAB2 as well as dynamin-2[370]. An interesting link between clathrin-mediated endocytosis and ADAM15 is provided by SNX9. SNX9 and dynamin-2 assemble in the cytoplasm as a resting complex. In the presence of ATP this complex is activated. RNAi experiments showed that SNX9 is an essential mediator of dynamin-2 trafficking to the membrane[529]. As shown in table 1.6 SNX9 is a known interaction partner of ADAM15 with very high affinity towards ADAM15 A, B, C and E, but does not interact with ADAM15 D. One hypothesis could be that this resting complex consists of several molecules with distict function including ADAM15. That the resting complex is composed of more than dynamin-2 and SNX9 is known[529]. An additional molecule within this complex was identified as aldolase. Aldolase binds to an acidic sequence of SNX9 blocking the binding activity of SNX9. SNX9 phosphorylation releases aldolase and turns SNX9 competent for membrane binding. ADAM15 as potential member of the resting complex could bring an SH3 domain containing kinase close which does the phosphorylation of SNX9. Since dynamin-2 is crucial for integrin endocytosis and SNX9 essential for dynamin-2 recruitment endocytosis would be impaired with ADAM15 D since it lacks the interaction motifs to participate in the resting complex. Since we still saw disassembly of FA it may have been rescued by endogenous full length ADAM15 or other adaptor proteins.

Another hypothesis involves Intersectin 1/2. Intersectins are molecular scaffolds that play essential roles at the early stage of clathrin-mediated endocytosis (CME) by clustering the membrane sculpting FCHo1/2 proteins which mark the assembly sites of clathrin-coated pits. Intersectin 1/2 are known binding partner for ADAM15[180,181]. Continuous interaction with ADAM15 could reduce the rate of endocytosis. As integrins are mainly dependent on CME, reduced endocytosis may have a negative influence on cell motility and migration, but may enhance cell adhesion. On the other site, ADAM15 could recruit intersectins to the membrane

marking integrins for endocytosis. Since ADAM15 D is unable to bind Intersectins, the endocytosis of those integrins might be impaired. In order to recycle α5β1 and αvβ3 it follows a Rab11 dependent-route which requires inactivation of GSK3β by Akt[530]. Akt activity is also required to phosphorylate a protein which recruits β1 into a recycling coat complex containing clathrin[531,532]. In chapter 4 we identified that the PI3K signalling pathway is modulated by ADAM15. Since Akt is downstream of PI3K it may be influenced by ADAM15 isoforms indirectly. ADAM15 C may influence the localisation of Akt in way to prevent β1 to be recruited to the recycling coat complex.

Another potential mechanism could involve PKCε mediated integrin recycling. PKCε phosphorylates the intermediate filament protein vimentin (expressed in mesenchymal cells) which releases the β1-subunit to allow recycling[533,534]. A way this mechanism could be influenced is via substrate competition. PKCε phosphorylates ADAM17 which induces release of amphiregulin from the cell membrane[535]. Amphiregulin is also a known substrate of ADAM15[197], but the underlying mechanism of how ADAM15 is activated to release amphiregulin is not well understood yet. Therefore, ADAM15 isoforms may be a potential substrate for PKCε phosphorylation too, which could be even isoform dependent. As described in the introduction, ILK is a kinase which is recruited to the plasma membrane during FA formation. ILK was identified as a binding partner for ADAM12[536], thus ADAM15 could potentially interact with ILK as well. In ruffles, ILK was found in a complex with Nck and co-localised with α5β1-integrin[415]. Nck is also an adptor protein known to interact with ADAM15[179].

Adhesion of cells to a substrate is mediated by integrins. The more efficient a cell is able to bind the substrate the quicker cells spread. Our pilot cell spreading experiment suggested that MDA/ADAM15 A and B expressing cells spread less compared to the control (MDA/FRT) on all surfaces. In contrast, MDA/ADAM15 C and D expressing cells spread much more compared to the control.

The more detailed and quantified analysis confirmed the findings of the pilot experiment. In parental cells we observed that cells adhere and spread quicker on FN over VN. This is likely to happen because FN interacts with both α5β1 and αvβ3 integrins[537] while VN binds only to αvβ3[538,539]. In these cells there are theoretical twice as many receptors for FN compared to VN (assuming the quantities are even). Expression of ADAM15 A and B leads to reduced adhesion and spreading on FN as well as VN when compared with the parental cells. This could potentially be as a result of these isoforms interacting with α5β1 and αvβ3 with much higher affinity, thus reducing the availability of these integrins to interact with their substrates. Interestingly, while all the cell lines prefer spreading onto FN rather than VN, the expression of ADAM15 A changes this preference in favour of VN. This suggests

that perhaps ADAM15 A interacts more with α5β1 than with αvβ3, leaving more of this integrin to bind to VN. To address this question ligand binding assays could be used to determine the affinity of integrins to the individual ADAM15 isoforms.

On the other hand, the expression of ADAM15 C and D isoforms led to more spreading on FN as well as VN, when compared with the parental cell line. This increased spread area could be either because these cells are generally larger (as discussed in chapter 3) or because there are more of these integrins free and available to bind to the ECM components facilitating adhesion.

We did not observe any changes in the total expression levels of β1- and β3-integrin subunits. However, the molecular weight of β1 differed in our cell lines, smaller in ADAM15 D expressing cells and larger in ADAM15 E expressing cells compared with the rest of the cell panel. No differences were observed in subcellular localisation of β1. In contrast, subcellular fractionation demonstrated that there is more β3 in the cytoplasmic fraction of ADAM15 D expressing cells than in the membrane fraction when compared with the rest of the cell panel. In cardiac rat myocytes and fibroblasts a 55 kDa fragment of β1-integrin was found[540]. This fragment stimulated the size and shape of these cells and altered ECM interaction. In myocytes the adhesion to collagen was enhanced. Interestingly, the MMP inhibitor GM6001 decreased the β1 shedding in myocytes, but not in fibroblasts. This suggests that other proteinases, such as ADAMs, might be involved. Also integrin shedding seems highly dependent on the cell type. Up to date no ADAM is known to shed integrins. Beside β1, it was also demonstrated that β2 is cleaved as well[541,542]. In a model for synovial inflammation it has been demonstrated that β2 is shed from the surface of leukocytes in a TNFα-dependent manner[541]. Another study demonstrated that β2 integrin is cleaved in mouse macrophages in a MMP-dependent manner. However, we do not think that part of β1 is shed in our ADAM15 D expressing cells, as the same short molecular weight β1 is recognised by an antibody specific to the amino-terminus of the protein (data not shown). A potential reason for altered molecular weight of β1-integrin in ADAM15 expressing cells could be post-translational modification such as differential glycosylation. In keratinocytes it was demonstrated that N-glycosylation of β4-integrin was essential to control adhesion and locomotion[543]. Posttranslational modifications involve many enzymes including kinases, phosphatases, transferases and ligases. Src was found to regulate O-glycosylation by redistributing N-acetylgalactosaminyl transferases from the golgi complex to the endoplasmic reticulum[544]. Their redistribution occurs either in cells with constitutively increased Src-activity or upon EGF or platelet derived growth factor stimulation in a Src-dependent manner[544]. Since ADAM15 is a well known binding partner of Src kinase, potential changes in affinity of ADAM15 isoforms towards Src could contribute to differences in β1 glycosylation.

ADAM15 may modulate integrin function by its disintegrin-like domain which is able to bind integrins. It may be possible that the ICD play an important role in molecule shape by changing the ADAM structure. Some could make the disintegrin domain accessible for integrin binding which induces downstream signalling via Rac or Serine/threonine-protein kinase (PAK) through FAK. Integrins can modulate cell adhesion, migration, actin polymerisation and mitogen-activated protein (MAP) kinase signalling[545]. Src might be an important player in ADAM15 mediated signalling, because its SH3 domain is required for binding β1 subunits[546] and to the proline rich regions in ADAM15.

Overall, here we identified that ADAM15 isoforms have distinct effects on the dynamic turnover of FA, as well as cell adhesion on FN and VN. However, neither cell spreading on the ECM substrates, nor subcellular localisation of these integrins could explain altered FA turnover, and, consequently, the altered cell motility, in our cell panel. Additionally, the subcellular fractionation approach provides a more qualitative, rather than quantitative evaluation regarding the localisation of a particular protein. This makes comparative analysis between the cell lines very difficult, if not impossible. An alternative approach would be FACS analysis that could provide quantitative information and would allow a comprehensive comparison of the cell surface localised integrins between our cell panel. FACS analysis with integrin conformation-specific antibodies would allow us to evaluate if the presence of individual ADAM15 isoforms affects the ECM ligand binding abilities of these integrins. This in turn would enable us to evaluate if α5β1 and αvβ3 are involved in altered FA dynamics in our cell panel. As integrin internalisation and recycling are crucial factors in regulating FA turnover, it will be necessary to carry out detailed comparative analysis of integrin trafficking in our cell panel.

One common link of how ADAM15 mediates changes in cell-cell junctions and cell-adhesion could be provided by ILK. In chapter 4 we showed that overexpression of ADAM15 isoforms lead to upregulation of claudin1 in ADAM15 A, C and E expressing cells, depending on their catalytic function. In this chapter we revealed changes in FA turnover in ADAM15 C and D expressing cells. ILK functions as scaffold protein promoting cell-cell contacts we as well as localisation to AJ and TJ proteins[547,548]. ILK localised to ZO1[548] which we identified as novel interaction partner for ADAM15. ILK is recruited to β1- and β3-ICDs[549] and part of FAs and involved in several cellular mechanisms such as cell polarisation, spreading, proliferation, migration and survival[550]. ILK-phosphorylation is regulated by PI3K, since inhibition of PI3K reduced ILK acitvity[420]. We found that claudin1 upregulation is also mediated via PI3K pathway. In ruffles, ILK was found in a complex with Nck and co-localised with α5β1-integrin[415]. Nck is an adaptor protein known to interact with ADAM15[179]. It may be that ADAM15 could influences ILK activity

via complex formation via its ICD domain, or indirect via direct binding to integrins via its ECD. Or ECD cleaves an unknown substrate which activates RTKs.
We demonstrated that expression of β1 and β3 does not change. Differential ability of ADAM15 isoform expressing cells to adhere to substrates was observed. This may be due to higher affinity of ADAM15 isoform binding to the integrins (extracellular or intracellular via adaptor proteins) or due to changes in cell surface localisation of integrins. The latter was observed for β3 integrin. IF analysis of integrins co-stained with V5-ADAM15 would provide necessary information. To address whether the interaction differs between integrins and ADAM15 I would perform IP analysis with corresponding antibodies. Additionally, using the flow cytometre I could characterise the integrin localisation on the cell surface of ADAM15 isoform expressing cells. Using antibodies to active/inactive integrins could also provide information about their activity in these cells. To address whether ADAM15-integrin interaction occurs extra- or intracellularly, cells can be treated with various integrin-interacting molecules such as osteopontin, RGD peptides or recombinant disintegrin domain of ADAM15. The results of the FA disassembly assay indicate that endocytosis and recycling are affected by ADAM15 isoform expression. I would analyse the trafficking of α5β1 and αvβ3-integrins by antibody- and biotin-IP/ELISA-based integrin internalisation and recycling assays as described by Arjonen et al[551]. In antibody-based internalisation and recycling assays cells are grown in dishes and labelled with AlexaFluor-conjugated anti-integrin (e.g. β1) antibodies on ice. Incubation at 37°C stimulates integrin internalisation. Remaining fluorescent signal on the surface is quenched with antibodies against the primary antibody. The internalised integrins are then measured with a plate reader. In order to determine the rate of recycling the procedure is repeated, but with and additional incubation/quenching step prior to measurement. During the additional step integrins are recycled and translocate to the surface. However the second quenching step eliminates the signal again. The higher the signal the slower the recycling would be, or the lower the signal the faster the recycling.
An alternative approach is via biotin labelling. Cell surface proteins are labelled with biotin at 4°C and unbound biotin is washed off. Incubation at 37°C allows internalisation of the biotinylated integrins. For recycling measurements this a prolonged time point is necessary to ensure complete internalisation. On the cell surface remaining biotin is removed by sodium 2-mercaptoethanesulfonate (MesNA) treatment with consecutive quenching using iodoacetamide to block reactive sulfhydryl groups. In case of recycling experiments the cells are incubated again at 37°C to allow translocation to the cell membrane followed by MesNa treatment and quenching. Cells are lysed and subjected to IP with antibodies against the integrin of interest (e.g. β1). Western blot analysis using biotin targeting antibodies are used for detec-

tion. Alternatively to the IP approach, lysed cells can also be transferred to micro titre plates with immobilised anti-β1 antibodies. Streptavidin-conjugated HRP is used to detect the internalised integrins[552]. I hypothesised that ADAM15 is in a complex with SNX9/Aldolase in which ADAM15 recruits a kinase that phosphorylates SNX9 releasing aldolase. In order to confirm this I would perform IF analysis to our cell panel and co-staining of ADAM15-SNX9, ADAM15-Aldolase and SNX9-Aldolase. This should provide information whether they remain in a complex and where it is localised. Co-localisation is expected to be absent in ADAM15 D expressing cells. With IP analysis I would attempt to confirm direct interaction of ADAM15, SNX9 and aldolase within this complex.

A common problem with work on 2D substrates is that cells grow on a surface which does not resemble the natural environment. Jayo and Parsons discussed different methods of imaging cell adhesion events in 3D matrix environments[553]. Most of the knowledge about adhesive structures is derived from experiments on rigid 2D structures. The disadvantage is that ECM proteins face the cell only on one site, but *in vivo* ECM proteins surround the cell that leads to differences in cellular behaviour and migration. However, other technical issues occur within 3D matrices. For example, cell protrusions can be thicker in 3D matrices which then needs to be examined by microscopes with a larger field of vision such as confocal or widefield microscopes. Therefore, adhesion-specific fluorescently labelled proteins may result in diffuse fluorescent signal in the cytoplasm, masking neighbouring proteins[554]. Also matrix stiffness could cause issues. The closer the cells grow to the border where the 3D matrix is attached the greater the stiffness is. Also the size of structures such as those for adhesion appear in generally smaller compared to 2D environments.

However, 3D models are likely to provide new insights in cellular behaviour which is overseen when investigated in 2D environment. Thus it would be interesting to see how ADAM15 isoform expressing cells behave in 3D. One of the most widely used models depend on basement membrane-based gels or Matrigel^{TM}. It is made of collagen type IV, laminin and proteoglycans. It is commonly used for migration assays and invadopodia research. Matrigel also demonstrates how a 3D matrix affects the morphology of a cell. While fibroblasts are growing elongated on a 2D surface, do they appear rounded in matrigel.

Another type of 3D matrix are type I collagen-based gels. They are commonly used to study motility as an connective tissue model. However, depending on how it is produced variations in collagen fibre thickness and length as well as pore size and rigidity.

Fibrin gels are another type of gels which are mainly composed of fibrin. These fibres are thinner, shorter and straighter than collagen and engage with several integrins such as α5β1 and αvβ3. Based on the FA adhesion disassembly assay and

ECM spreading experiments we have first indications that ADAM15 isoforms have an affect on integrin dynamics it would be interesting to see how ADAM15 isoform expressing cells behave in fibrin gels.

Another type of matrices are the cell-based complex matrices which are rich in FN and collagen. They provide high stiffness, are generally ordered and highly fibrous. It is widely used to study cell motility.

There are also artificial matrices which can be made of polyacrylamide. The advantage is that the stiffness can be precisely adjusted (similar to SDS-PAGE gels). Together with collagen it was used to analyse effects of matrix flexibility and FA formation.

Due to time constraints we only looked at these two integrins, as they are known to interact with ADAM15. It is however possible that ADAM15 isoforms have other, yet unknown, distinct integrins interaction partners. And it is possible that the altered behaviour of these unknown integrins dictates the dynamics of FA turnover in our cell panel. Future directions on continuing this work will be discussed in chapter 7.

Chapter 6

Summary

In this project we observed many changes how ADAM15 isoforms affected cell behaviour. A summary of all findings throughout the project are summarised in table 6.1.

In chapter 3 I described how we generated isogenic cells expressing each ADAM15 isoform in MDA-MB-231 cells. ADAM15 C and D are subjected to hypermethylation in these cells to a varying degree. ADAM15 isoforms introduced morphological changes depending on catalytic function. Especially ADAM15 A expressing cells showed tight cobblestone-like appearance. ADAM15 C and E expressing cells were larger compared to the other isoforms or the parental cells. All cells expressing ADAM15 isoforms were rounder compared to parental cells. Introduction of ADAM15 A, D and E reduced the growth rate independently of the catalytic function. ADAM15 B expression did not alter the proliferation while ADAM15 C reduced growth in WT, but not in cells expressing the catalytically inactive ADAM15. We also found changes in the cytoskeletal rearrangement analysed by IF. ECM degrading, invadopodia-like structures, were found in all ADAM15 isoform expressing cells, but to a greater degree in cell expressing ADAM15 D. ADAM15 A expressing cells had more ruffles, while ADAM15 expressing cells showed more curved actin bundles. ADAM15 E expressing cells showed more stress fibres than the other cell lines. We did not observe changes in total RhoA or Rac1 activity. Scratch wound experiments revealed that introduction of ADAM15 reduced the migration rate of ADAM15 A and B and to a greater degree also in ADAM15 C and D expressing cells. Overexpression of ADAM15 E did not influence the migration rate.

In chapter 4 we showed that the morphological changes of ADAM15 isoform expressing cells are not due to mesenchymal-epithelial transition. Also changes of expression in the tight junctions proteins ZO1, ZO2 and occludin were not observed. However, upregulation of claudin1 in ADAM15 A, C and E expressing cells were observed depending on their catalytic activity. With increasing cell density these cells expressed more claudin1. ZO1 and ZO2 were identified as potential novel interaction partners of ADAM15. Claudin1 was found to co-localise with ADAM15 at cell-cell junctions and along the cell periphery. Some claudin1 also localised in the nucleus of ADAM15 A expressing cells. The upregulation of claudin1 in ADAM15 A, C and E expressing cells is mediated by the PI3K/mTOR pathway. The reduction of migration in ADAM15 A expressing cells was not due to claudin1 which was investigated by scratch wound asays with shClaudin1 knockdown cells.

In chapter 5 we attempted to investigate the reason for reduced migration. FA disassembly assays demonstrated that ADAM15 D expressing cells have impaired FA disassembly and enhanced reassembly. In contrast, ADAM15 C expressing cells disassemble FA at the same rate as parental or the other ADAM15 isoform expressing cells, but fail to reassemble FA at the same rate. To get an indication whether

ADAM15 affects interaction of integrins with ECM substrates we performed experiments on FN and VN, the major ligands for α5β1 as well as αvβ3 and α5β1, respectively. We observed that by comparing the spreading of these substrates that most cell lines preferred FN over VN. However, the expression of ADAM15 E reduced this preference. ADAM15 A expressing cells even preferred VN over FN. Subcellular localisation showed that in all ADAM15 isoform expressing cells including the parental cell line β1 integrin is exclusively localised in the membrane. However, in ADAM15 D expressing cells the molecular weight of the β1-subunit is smaller while it is larger in ADAM15 E expressing cells. The localisation of β3-integrin was comparable in MDA/FRT and ADAM15 B, C and D expressing cells. In these cells localisation was observed in both, the cytoplasm and the membrane. Contrary, in ADAM15 A and E expressing cells β3 exclusively localised in the membrane. Total expression of both subunits did not change. Interestingly, we observed that the molecular weight of β3 is slightly larger in the catalytically inactive ADAM15 isoform expressing cells, compared to WT and parental cells.

We found that ADAM15 expression reduces cell migration in ADAM15 A-D, but not in ADAM15 E expressing cells. Migration is decreased most in cells expressing ADAM15 C and D. To address weather claudin1 upregulation in ADAM15 A expressing cells negatively influences the migration rate I performed wound healing experiments on MDA/ADAM15 A shClaudin1 knockdown cells. In many cell lines claudin1 upregulation is known to cause reduced migration[55,516]. However, we did not observe any differences in migration depending on claudin1 expression in ADAM15 A expressing cells. Keeping in mind that ADAM15 D expression does not upregulate claudin1, but decreases the migration most further suggests migration rate is independent of claudin1 in MDA-MB-231 cells.

FA require to be assembled at the leading edge which indicates the direction a cell moves to. The turnover of FA involves the disassembling at the rear tail. We found that ADAM15 C and D expressing cells have impaired FA turnover. While all ADAM15 isoform expressing cells disassemble FA quickly, it is significantly reduced in ADAM15 D expressing cells. This also leads to a quicker reassembly rate which enhances the adherens to the substrate before the cell actually moved forward. In contrast, ADAM15 C expressing cells cannot reassemble FA which may slow down the formation of the leading edge indicated by slow migration.

Table 6.1: Summary of findings of this project. The cell for MDA/FRT is kept empty if cells are compared to these cells. If information is available it will be displayed. – = Strong reduction; - = Moderate reduction; 0 = no change; + = Moderate increase; ++ = Strong increase. N/A = no data available.

	MDA/FRT	**ADAM15 A**	**ADAM15 B**	**ADAM15 C**	**ADAM15 D**	**ADAM15 E**
Methylation of ADAM15 gene	N/A	N/A	N/A	yes	yes (less than C)	N/A
Morphology (WT/E349A)	Spindle-like	Cobblestone-like/Mixed	Spindle-like/ Spindle-like	Clustered/ Mixed	Clustered/ Clustered	Mixed/ Mixed
Cell size		0	0	++	0	+
Cell circularity		+	+	+	+	+
Growth rate WT/E349A		-/-	0/0	–/0	-/-	–/–
Stress fibre formation	present	0	0	0	0	++
Curved actin bundles	present	0	0	++	0	0
Invadopodia-like structures	not present	+	+	+	++	+
Ruffles	not present	0	++	0	0	0
Total RhoA activity		0	0	0	0	0
Total Rac1 activity		0	0	0	0	0
Migration		-	-	–	–	0

Table 6.1 Continued: Summary of findings of this project. The cell for MDA/FRT is kept empty if cells are compared to these cells. If information is available it will be displayed. – = Strong reduction; - = Moderate reduction; 0 = no change; + = Moderate increase; ++ = Strong increase. N/A = no data available.

	MDA/FRT	**ADAM15 A**	**ADAM15 B**	**ADAM15 C**	**ADAM15 D**	**ADAM15 E**
Claudin1 expression WT/E349	no claudin1	yes/no	no/no	yes/no	no/no	yes/no
Claudin1 expression increases with cell density	no	yes	no	yes	no	yes
Co-localisation of ADAM15 with claudin1	N/A	yes (also in T47D)	N/A	N/A	N/A	N/A
Complex formation of ADAM15 with ZO1	N/A	yes	yes	yes	no	yes
Complex formation of ADAM15 with ZO2	N/A	yes	yes	yes	yes (indirectly)	yes
Nuclear claudin1	N/A	yes	N/A	N/A	N/A	N/A

Table 6.1 Continued: Summary of findings of this project. The cell for MDA/FRT is kept empty if cells are compared to these cells. If information is available it will be displayed. – = Strong reduction; - = Moderate reduction; 0 = no change; + = Moderate increase; ++ = Strong increase. N/A = no data available.

	MDA/FRT	**ADAM15 A**	**ADAM15 B**	**ADAM15 C**	**ADAM15 D**	**ADAM15 E**
Claudin1 via PI3K/mTOR	no claudin1	yes	no claudin1	yes	no claudin1	yes
FA disassembly assay		no changes	no changes	reduced reassembly	impaired disassembly, enhanced reassembly	no changes
ECM spreading	FN>VN>Med	VN>FN>Med	FN>VN>Med	FN>VN>Med	FN>VN>Med	FN=VN>Med
β1 **localisation Membrane**	Membrane	Membrane	Membrane	Membrane	Membrane	Membrane
β3 **localisation**	Cytoplasm & Membrane	Membrane	Cytoplasm & Membrane	Cytoplasm & Membrane	Cytoplasm & Membrane (more in cytoplasm)	Membrane
Molecular weight of β1 **(WT/E349A)**		0/0	0/0	0/0	-/0	+/0
Molecular weight of β3 **(WT/E349A)**		0/+	0/+	0/+	0/+	0/+

Table 6.1 Continued: Summary of findings of this project. The cell for MDA/FRT is kept empty if cells are compared to these cells. If information is available it will be displayed. – = Strong reduction; - = Moderate reduction; 0 = no change; + = Moderate increase; ++ = Strong increase. N/A = no data available.

	MDA/FRT	ADAM15 A	ADAM15 B	ADAM15 C	ADAM15 D	ADAM15 E
Total β1 **expression**		0	0	0	0	0
Total β3 **expression**		0	0	0	0	0

Chapter 7

Future directions

Characterisation of MDA/ADAM15 isoform expressing cells opened up many avenues which can be followed leading to various exciting topics.

My work will have important implications for future ADAM15 research, as it highlighted major ADAM15 isoform-, as well as catalytic function dependent effects on various aspects of cell biology.

I showed that ADAM15 regulates cell proliferation (chapter 3), as well as gene expression (chapter 4) in an isoform dependent and catalytic function dependent manner, providing a strong evidence that ADAM15 isoforms are individually distinct proteases, that shed different transmembrane proteins. Thus a major follow on project will be identification of ADAM15 isoform-specific substrates. This can be achieved by a sophisticated Tandem-Mass-Tag® (TMT) mass spectroscopic (MS) terminal amino isotopic labelling of substrates (TAILS) approach. This approach, developed by Christopher Overall (Canada Research Chair in Proteinase Proteomics and Systems Biology, University of British Columbia, Canada) is a powerful proteomics method used to identify proteolytic events in mammalian cells. TAILS identifies both the identity of the substrate and the exact cleavage site and can distinguish specific proteolytic events from background cleavages[555]. TMT-MS-TAILS approach, combined with phosphoproteomic analysis using KINEXUS phospho-antibody arrays, will allow identification of the ADAM15 isoform-specific substrates, as well as the major signalling pathways that are regulated by ADAM15 isoforms. Further RNA sequencing will allow identification of ADAM15 isoform-specific gene expression signatures.

I showed that ADAM15 isoforms regulate cell-cell junction formation in isoform-dependent and catalytic function dependent manner. Key questions remain: Which other TJ and AJ proteins are changed? Which cadherins localise to these junctions? Detailed MS analysis of β-catenin immunoprecipitates will help to elucidate which other junctional proteins are regulated by ADAM15.

I showed ADAM15 isoform-dependent effects on cell migration and actin cytoskeleton structure (chapter 3), FA dynamic turnover and cell adhesion on different ECM components (chapter 5), providing strong evidence that ADAM15 isoforms regulate integrin behaviour differently. Thus another major follow on project will be detailed characterisation of how ADAM15 isoform regulate integrins, their activity, availability for ECM adhesion, endocytosis and recycling. So far only three integrins have been shown to interact with the disintegrin domain of ADAM15 (α5β1, αvβ3 and α9β1). My data suggest that ADAM15 isoforms might have other integrin interaction partners, which will be important to identify. Followed with 3D organotipic invasion modelling, will allow us to understand how ADAM15 isoforms contribute to tumour cell adhesion, migration, invasion, as well as interaction with the tumour microenvironment.

A common emerging theme eluded to throughout my work is the role of differential protein-protein interactions with individual ADAM15 ICDs that regulate ADAM15 isoforms and dictate ADAM15 isoform specific effects on cell behavior. ADAM15 isoforms have a vast number of common, as well as distinct interaction partners (described in chapter 3). We could speculate that ADAM15 mediated shedding events are likely to be controlled by specific ADAM15 ICD kinase interactions as shown previously for ADAM15 B and Src[207]. To identify which interaction regulates a specific shedding event, it would be necessary to identify the shed substrate(s) first as described earlier. We can then use an shRNA approach to deplete the candidate intracellular interacting protein(s) and monitor if the shedding of that particular substrate by ADAM15 is compromised. Similarly, we could speculate that ADAM15 mediated effects on integrin trafficking are likely to be controlled by sorting nexins or intersectins that interact with ADAM15 ICDs. These proteins have prominent roles in regulating endocytic transport of various cargos. It is possible that integrin endocytosis depends on ADAM15 integrin interaction via the disintegrin domain, and the role of ADAM15 in that interaction is to provide an endocytosis route to the integrins by bringing sorting nexins or itersectins into the complex. Again, to verify that we would need detailed characterisation of integrin trafficking as a function of ADAM15 splicing first, followed by an shRNA approach to validate the role of specified ADAM15 ICD interacting partners in that trafficking.

My work suggests that ADAM15 represents an important master switch in regulating the behaviour of tumour cells and potentially their ability to invade the body to establish metastatic disease. Further work is necessary to investigate how ADAM15 is contributing to tumour invasion to understand in detail how this enzyme works. This is a prerequisite of developing new therapies that will lead to new strategies to suppress tumour cell invasion and block metastasis.

Chapter 8

References

1. Schulz, W. A. in *Molecular Biology of Human Cancer* 1–23 (Springer, Dordrecht, 2005).

2. Cancer Research UK. *Cancer mortality statistics UK* 2016. (Visited on 12/15/2016).

3. Hanahan, D. & Weinberg, R. a. Hallmarks of cancer: the next generation. *Cell* **144,** 646–74 (2011).

4. Hanahan, D., Weinberg, R. A. & Francisco, S. The Hallmarks of Cancer Review University of California at San Francisco. *Cell* **100,** 57–70 (2000).

5. Macleod, K. Tumor suppressor genes. *Current Opinion in Genetics & Development* **10,** 81–93 (2000).

6. Yang, L., Pang, Y. & Moses, H. L. TGF-β and immune cells: an important regulatory axis in the tumor microenvironment and progression. *Trends in Immunology* **31,** 220–227 (2010).

7. Goedegebuure, P, Mitchem, J. B., Porembka, M. R., Tan, M. C. B., Belt, B. a., Wang-Gillam, a, Gillanders, W. E., Hawkins, W. G. & Linehan, D. C. Myeloid-derived suppressor cells: general characteristics and relevance to clinical management of pancreatic cancer. *Current cancer drug targets* **11,** 734–51 (2011).

8. Wright, W. E., Pereira-Smith, O. M. & Shay, J. W. Reversible cellular senescence: implications for immortalization of normal human diploid fibroblasts. *Molecular and cellular biology* **9,** 3088–92 (1989).

9. Feng, J., Funk, W., Wang, S., Weinrich, S., Avilion, A., Chiu, C., Adams, R., Chang, E., Allsopp, R., Yu, J. & Al., e. The RNA component of human telomerase. en. *Science* **269,** 1236–1241 (1995).

10. Sakurai, T., He, G., Matsuzawa, A., Yu, G.-y., Maeda, S. & Karin, M. Hepatocyte necrosis induced by oxidative stress and IL-1α release mediate carcinogen-induced compensatory proliferation and liver tumorigenesis. *Cancer Cell* **14,** 156–165 (2009).

11. Barnes, D. E. & Lindahl, T. Repair and genetic consequences of endogenous DNA base damage in mammalian cells. *Annual review of genetics* **38,** 445–76 (2004).

12. Vander Heiden, M., Cantley, L. & Thompson, C. Understanding the Warburg effect: The metabolic Requiremetns of cell proliferation. *Science* **324,** 1029–1033 (2009).

13. Krzeslak, A., Wojcik-Krowiranda, K., Forma, E., Jozwiak, P., Romanowicz, H., Bienkiewicz, A. & Brys, M. Expression of GLUT1 and GLUT3 glucose transporters in endometrial and breast cancers. *Pathology and Oncology Research* **18,** 721–728 (2012).

14. Interantional Union Against Cancer. *TNM Classification of Malignant Tumours* 7th (eds Sobin, L., Gospodarowicz, M. & Wittekind, C.) (Wiley-Blackwell, Singapore, 2009).

15. American Joint Committee on Cancer. *AJCC Cancer Staging Manual* 7th (eds Edge, S. B., Byrd, D. R., Compton, C. C., Fritz, A. G., Greene, F. L. & Trotti, A. I.) (Springer, New York, NY, 2010).

16. Goldhirsch, A., Winer, E. P., Coates, A. S., Gelber, R. D., Piccart-Gebhart, M., Thürlimann, B., Senn, H. J., Albain, K. S., André, F., Bergh, J., Bonnefoi, H., Bretel-Morales, D., Burstein, H., Cardoso, F., Castiglione-Gertsch, M., Colleoni, M., Costa, A., Curigliano, G., Davidson, N. E., Leo, A. D., Ejlertsen, B., Forbes, J. F., Gnant, M., Goodwin, P., Goss, P. E., Harris, J. R., Hayes, D. F., Hudis, C. A., Ingle, J. N., Jassem, J., Jiang, Z., Karlsson, P., Loibl, S., Morrow, M., Namer, M., Osborne, C. K., Partridge, A. H., Penault-Llorca, F., Perou, C. M., Pritchard, K. I., Rutgers, E. J. T., Sedlmayer, F., Semiglazov, V., Shao, Z. M., Smith, I., Toi, M., Tutt, A., Untch, M., Viale, G., Watanabe, T., Wilcken, N. & Wood, W. C. Personalizing the treatment of women with early breast cancer: Highlights of the st gallen international expert consensus on the primary therapy of early breast Cancer 2013. *Annals of Oncology* **24,** 2206–2223 (2013).

17. Inic, Z., Zegarac, M., Inic, M., Markovic, I., Kozomara, Z., Djurisic, I., Inic, I., Pupic, G. & Jancic, S. Difference between Luminal A and Luminal B subtypes according to Ki-67, tumor size, and progesterone receptor negativity providing prognostic information. *Clinical Medicine Insights: Oncology* **8,** 107–111 (2014).

18. Senkus, E., Kyriakides, S., Ohno, S., Penault-Llorca, F., Poortmans, P., Rutgers, E., Zackrisson, S. & Cardoso, F. Primary breast cancer: ESMO Clinical Practice Guidelines for diagnosis, treatment and follow-up. *Annals of Oncology* **26,** v8–v30 (2015).

19. Zagouri, F., Liakou, P., Bartsch, R., Peccatori, F. A., Tsigginou, A., Dimitrakakis, C., Zografos, G. C., Dimopoulos, M. A. & Azim, H. A. Discrepancies between ESMO and NCCN breast cancer guidelines: An appraisal. *Breast* **24,** 513–523 (2015).

20. Lohrisch, C., Paltiel, C., Gelmon, K., Speers, C., Taylor, S., Barnett, J. & Olivotto, I. A. Impact on survival of time from definitive surgery to initiation of adjuvant chemotherapy for early-stage breast cancer. *Journal of Clinical Oncology* **24,** 4888–4894 (2006).

21. Coates, A. S., Winer, E. P., Goldhirsch, A., Gelber, R. D., Gnant, M., Piccart-Gebhart, M., Thürlimann, B. & Senn, H. J. Tailoring therapies - improving the management of early breast cancer: St Gallen International Expert Consensus on the Primary Therapy of Early Breast Cancer 2015. *Annals of Oncology* **26,** 1533–1546 (2015).

22. Buerger, H, Otterbach, F, Simon, R., Schafer, K.-L., Poremba, C., Diallo, R., Brinkschmidt, C., Dockhorn-Dworniczak, B. & Boecker, W. Different genetic pathways in the evolution of invasive breast cancer are associated with distinct morphological subtypes. *The Journal of Pathology* **189,** 521–526 (1999).

23. Lee, S., Stewart, S., Nagtegaal, I., Luo, J., Wu, Y., Colditz, G., Medina, D. & Allred, C. D. Differentially Expressed Genes Regulating the Progression of Ductal Carcinoma In Situ to Invasive Breast Cancer Sangjun. *Cancer Research* **72,** 4574–4586 (2012).

24. Torrisi, R., Rota, S., Losurdo, A., Zuradelli, M., Masci, G. & Santoro, A. Aromatase inhibitors in premenopause: Great expectations fulfilled? *Critical Reviews in Oncology/Hematology* **107,** 82–89 (2016).

25. Anderson, W. F., Chatterjee, N., Ershler, W. B. & Brawley, O. W. Estrogen receptor breast cancer phenotypes in the Surveillance, Epidemiology, and End Results database. *Breast Cancer Research and Treatment* **76,** 27–36 (2002).

26. Early Breast Cancer Trialists Collaborative Group. Effects of chemotherapy and hormonal therapy for early breast cancer on recurrence and 15-year survival: an overview of the randomised trials. *Lancet* **365,** 1687–717 (2005).

27. Johnston, S. R. D. New strategies in estrogen receptor-positive breast cancer. *Clinical Cancer Research* **16,** 1979–1987 (2010).

28. Santen, R. J. & Harvey, H. A. Use of aromatase inhibitors in breast carcinoma. *Endocrine-Related Cancer* **6,** 75–92 (1999).

29. Hiscox, S., Davies, E. L. & Barrett-Lee, P. Aromatase inhibitors in breast cancer. *Maturitas* **63,** 275–279 (2009).

30. Gligorov, J., Pritchard, K. & Goss, P. Adjuvant and extended adjuvant use of aromatase inhibitors: Reducing the risk of recurrence and distant metastasis. *Breast* **16,** 1–9 (2007).

31. Minotti, G., Menna, P., Salvatorelli, E., Cairo, G. & Gianni, L. Anthracyclines: Molecular Advances and Pharmacologic Developments in Antitumor Activity and Cardiotoxicity. *Pharmacological Reviews* **56,** 185–229 (2004).

32. Szuławska, A. & Czyz, M. Molecular mechanisms of anthracyclines action. *Postepy higieny i medycyny doswiadczalnej (Online)* **60,** 78–100 (2006).

33. Pang, B., Qiao, X., Janssen, L., Velds, A., Groothuis, T., Kerkhoven, R., Nieuwland, M., Ovaa, H., Rottenberg, S., van Tellingen, O., Janssen, J., Huijgens, P., Zwart, W. & Neefjes, J. Drug-induced histone eviction from open chromatin contributes to the chemotherapeutic effects of doxorubicin. *Nature Communications* **4,** 1908 (2013).

34. Perez, E. A., Romond, E. H., Suman, V. J., Jeong, J. H., Sledge, G., Geyer, C. E., Martino, S., Rastogi, P., Gralow, J., Swain, S. M., Winer, E. P., Colon-Otero, G., Davidson, N. E., Mamounas, E., nne Zujewski, J. A. & Wolmark, N. Trastuzumab plus adjuvant chemotherapy for human epidermal growth factor receptor 2-positive breast cancer: planned joint analysis of overall survival from NSABP B-31 and NCCTG N9831. *Journal of Clinical Oncology* **32,** 3744–3752 (2014).

35. Tan, A. R. & Swain, S. M. Therapeutic Strategies for Triple-Negative Breast Cancer OF DNA-DAMAGING AGENTS. *Practice of Oncology: Recent Advances* **14,** 343–351 (2008).

36. Wang, D. & Lippard, S. J. Cellular processing of platinum anticancer drugs. *Nature Reviews Drug Delivery* **4,** 307–320 (2005).

37. Sirohi, B., Arnedos, M., Popat, S., Ashley, S., Nerurkar, A., Walsh, G., Johnston, S. & Smith, I. E. Platinum-based chemotherapy in triple-negative breast cancer. *Annals of Oncology* **19,** 1847–1852 (2008).

38. Meche, A, Cimpean, A. M. & Raica, M. Immunohistochemical expression and significance of epidermal growth factor receptor (EGFR) in breast cancer. *Romanian journal of morphology and embryology = Revue roumaine de morphologie et embryologie* **50,** 217–221 (2009).

39. De Ruijter, T. C., Veeck, J., De Hoon, J. P. J., Van Engeland, M. & Tjan-Heijnen, V. C. Characteristics of triple-negative breast cancer. *Journal of Cancer Research and Clinical Oncology* **137,** 183–192 (2011).

40. Harari, P. M. Epidermal growth factor receptor inhibition strategies in oncology. *Endocrine-Related Cancer* **11,** 689–708 (2004).

41. Green, M. D., Francis, P. A., Gebski, V., Harvey, V., Karapetis, C., Chan, A., Snyder, R., Fong, A., Basser, R., Forbes, J. F., Underhill, C., Moylan, E., Paterson, K., McCarthy, N. & Synder, R. Gefitinib treatment in hormone-resistant and hormone receptor-negative advanced breast cancer. *Annals of Oncology* **20,** 1813–1817 (2009).

42. Corkery, B, Crown, J, Clynes, M & O 'donovan, N. Epidermal growth factor receptor as a potential therapeutic target in triple-negative breast cancer. *Annals of Oncology* **20,** 862–867 (2009).

43. Yvon, A.-M. M, Wadsworth, P. & Jordan, M. A. Taxol suppresses dynamics of individual microtubules in living human tumor cells. *Molecular biology of the cell* **10,** 947–59 (1999).

44. Somlo, G., Martel, C. L., Lau, S. K., Frankel, P., Ruel, C., Gu, L., Hurria, A., Chung, C., Luu, T., Morgan, R., Leong, L., Koczywas, M., McNamara, M., Russell, C. A. & Kane, S. E. A phase I/II prospective, single arm trial of gefitinib, trastuzumab, and docetaxel in patients with stage IV HER-2 positive metastatic breast cancer. *Breast Cancer Research and Treatment* **131,** 899–906 (2012).

45. Burris, H. A., Taylor, C. W., Jones, S. F., Koch, K. M., Versola, M. J., Arya, N., Fleming, R. A., Smith, D. A., Pandite, L., Spector, N. & Wilding, G. A phase I and pharmacokinetic study of oral lapatinib administered once or twice daily in patients with solid malignancies. *Clinical cancer research : an official journal of the American Association for Cancer Research* **15,** 6702–8 (2009).

46. Sorlie, T, Perou, C. M., Tibshirani, R, Aas, T, Geisler, S, Johnsen, H, Hastie, T, Eisen, M. B., van de Rijn, M, Jeffrey, S. S., Thorsen, T, Quist, H, Matese, J. C., Brown, P. O., Botstein, D, Eystein Lonning, P & Borresen-Dale, A. L. Gene expression patterns of breast carcinomas distinguish tumor subclasses with clinical implications. *Proceedings of the National Academy of Sciences of the United States of America* **98,** 10869–10874 (2001).

47. Bertucci, F., Finetti, P., Cervera, N., Esterni, B., Hermitte, F., Viens, P. & Birnbaum, D. How basal are triple-negative breast cancers? *International Journal of Cancer* **123,** 236–240 (2008).

48. Morris, G. J., Naidu, S., Topham, A. K., Guiles, F., Xu, Y., McCue, P., Schwartz, G. F., Park, P. K., Rosenberg, A. L., Brill, K. & Mitchell, E. P. Differences in breast carcinoma characteristics in newly diagnosed African-American and Caucasian patients: A single-institution compilation

compared with the national cancer institute's surveillance, epidemiology, and end results database. *Cancer* **110,** 876–884 (2007).

49. Rakha, E. A., Elsheikh, S. E., Aleskandarany, M. A., Habashi, H. O., Green, A. R., Powe, D. G., El-Sayed, M. E., Benhasouna, A., Brunet, J. S., Akslen, L. A., Evans, A. J., Blamey, R., Reis-Filho, J. S., Foulkes, W. D. & Ellis, I. O. Triple-negative breast cancer: Distinguishing between basal and nonbasal subtypes. *Clinical Cancer Research* **15,** 2302–2310 (2009).

50. Van Laere, S. J., Van Den Eynden, G. G., Van Der Auwera, I., Vandenberghe, M., Van Dam, P., Van Marck, E. A., Van Golen, K. L., Vermeulen, P. B. & Dirix, L. Y. Identification of cell-of-origin breast tumor subtypes in inflammatory breast cancer by gene expression profiling. *Breast Cancer Research and Treatment* **95,** 243–255 (2006).

51. Guérin, M, Gabillot, M, Mathieu, M. C., Travagli, J. P., Spielmann, M, Andrieu, N & Riou, G. Structure and expression of c-erbB-2 and EGF receptor genes in inflammatory and non-inflammatory breast cancer: prognostic significance. *International journal of cancer. Journal international du cancer* **43,** 201–8 (1989).

52. Gonzalez-Angulo, A. M., Sneige, N., Buzdar, A. U., Valero, V., Kau, S.-W., Broglio, K., Yamamura, Y., Hortobagyi, G. N. & Cristofanilli, M. P53 Expression As a Prognostic Marker in Inflammatory Breast Cancer. *Clinical cancer research : an official journal of the American Association for Cancer Research* **10,** 6215–6221 (2004).

53. Van Golen, K. L., Davies, S., Wu, Z. F., Wang, Y., Bucana, C. D., Root, H., Chandrasekharappa, S., Strawderman, M., Ethier, S. P. & Merajver, S. D. A novel putative low-affinity insulin-like growth factor-binding protein, LIBC (lost in inflammatory breast cancer), and RhoC GTPase correlate with the inflammatory breast cancer phenotype. *Clinical Cancer Research* **5,** 2511–2519 (1999).

54. Van Golen, K. L., Wu, Z. F., Xiao Tan Qiao, Li Wei Bao & Merajver, S. D. RhoC GTPase, a novel transforming oncogene for human mammary epithelial cells that partially recapitulates the inflammatory breast cancer phenotype. *Cancer Research* **60,** 5832–5838 (2000).

55. Chao, Y.-C., Pan, S.-H., Yang, S.-C., Yu, S.-L., Che, T.-F., Lin, C.-W., Tsai, M.-S., Chang, G.-C., Wu, C.-H., Wu, Y.-Y., Lee, Y.-C., Hong, T.-M. & Yang, P.-C. Claudin-1 is a metastasis suppressor and correlates with clinical outcome in lung adenocarcinoma. *American journal of respiratory and critical care medicine* **179,** 123–133 (2009).

56. Blanchard, A. A., Skliris, G. P., Watson, P. H., Murphy, L. C., Penner, C., Tomes, L., Young, T. L., Leygue, E. & Myal, Y. Claudins 1, 3, and 4 protein expression in ER negative breast cancer correlates with markers of the basal phenotype. *Virchows Archiv* **454,** 647–656 (2009).

57. Lu, S., Singh, K., Mangray, S., Tavares, R., Noble, L., Resnick, M. B. & Yakirevich, E. Claudin expression in high-grade invasive ductal carcinoma of the breast: correlation with the molecular subtype. *Modern pathology : an official journal of the United States and Canadian Academy of Pathology, Inc* **26,** 485–95 (2013).

58. Toft, D. J. & Cryns, V. L. Minireview: Basal-like breast cancer: from molecular profiles to targeted therapies. *Molecular endocrinology (Baltimore, Md.)* **25,** 199–211 (2011).

59. Blanchard, A. a., Ma, X., Dueck, K. J., Penner, C., Cooper, S. C., Mulhall, D., Murphy, L. C., Leygue, E. & Myal, Y. Claudin 1 expression in basal-like breast cancer is related to patient age. *BMC cancer* **13,** 268 (2013).

60. Heerma van Voss, M. R., van Diest, P. J., Smolders, Y. H. C. M., Bart, J., van der Wall, E. & van der Groep, P. Distinct claudin expression characterizes BRCA1-related breast cancer. *Histopathology* **65,** 814–827 (2014).

61. Chen, S. & Parmigiani, G. Meta-Analysis of BRCA1 and BRCA2 Penetrance Sining. *Journal of Clinical Oncology* **11,** 1329–1333 (2007).

62. Antoniou, A, Pharoah, P., Narod, S, Risch, H., Eyfjord, J., Hopper, J., Loman, N, Olsson, H, Johannsson, O, Borg, Å., Pasini, B, Radice, P, Manoukian, S, Eccles, D., Tang, N, Olah, E, Anton-Culver, H, Warner, E, Lubinski, J, Gronwald, J, Gorski, B, Tulinius, H, Thorlacius, S, Eerola, H, Nevanlinna, H, Syrjäkoski, K, Kallioniemi, O.-P., Thompson, D, Evans, C., Peto, J, Lalloo, F, Evans, D. & Easton, D. Average Risks of Breast and Ovarian Cancer Associated with BRCA1 or BRCA2 Mutations Detected in Case Series Unselected for Family History: A Combined Analysis of 22 Studies. *The American Journal of Human Genetics* **72,** 1117–1130 (2003).

63. Breastcancer.org. *Risk of Developing Breast Cancer* 2016. <http://www.breastcancer.org/symptoms/understand{_}bc/risk/understanding> (visited on 01/12/2017).

64. Konishi, H., Mohseni, M., Tamaki, A., Garay, J. P., Croessmann, S., Karnan, S., Ota, A., Wong, H. Y., Konishi, Y., Karakas, B., Tahir, K., Abukhdeir, A. M., Gustin, J. P., Cidado, J., Wang, G. M., Cosgrove, D., Cochran, R., Jelovac, D., Higgins, M. J., Arena, S., Hawkins, L., Lauring, J., Gross, A. L., Heaphy, C. M., Hosokawa, Y., Gabrielson, E., Meeker, A. K., Visvanathan, K., Argani, P., Bachman, K. E. & Park, B. H. Mutation of a single allele of the cancer susceptibility gene BRCA1 leads to genomic instability in human breast epithelial cells. *Proceedings of the National Academy of Sciences of the United States of America* **108,** 17773–8 (2011).

65. Dantzer, F, de La Rubia, G, Menissier-De Murcia, J, Hostomsky, Z, de Murcia, G & Schreiber, V. Base excision repair is impaired in mammalian cells lacking Poly(ADP-ribose) polymerase-1. *Biochemistry* **39,** 7559–7569 (2000).

66. Ashworth, A. & Tutt, A. The relationship between the roles of BRCA genes in DNA repair and cancer predisposition. *TRENDS in Molecular Medicine* **8,** 571–576 (2002).

67. Fong, P., Boss, D. S., Yap, T. A., Tutt, A., Wu, P., Margui-Roelvink, M., Mortimer, P., Swaiswald, H., Lau, A., O'Connor, M., Ashworth, A., Carmichael, J., Kaye, S. B., Schellens, J. H. & de Bono, J. S. Inhibition of Poly(ADP-Ribose) Polymerase in Tumors from BRCA Mutation Carriers. *The New England Journal of Medicine* **361,** 123–134 (2009).

68. Tutt, A., Robson, M., Garber, J. E., Domchek, S. M., Audeh, M. W., Weitzel, J. N., Friedlander, M., Arun, B., Loman, N., Schmutzler, R. K., Wardley, A., Mitchell, G., Earl, H., Wickens, M. & Carmichael, J. Oral poly(ADP-ribose) polymerase inhibitor olaparib in patients with BRCA1 or BRCA2 mutations and recurrent ovarian cancer: A proof-of-concept trial. *The Lancet* **376,** 235–244 (2010).

69. Comen, E. & Robson, M. Poly(ADP-Ribose) Polymerase Inhibitors in Triple-Negative Breast Cancer. *Cancer journal (Sudbury, Mass.)* **16,** 48–52 (2010).

70. Zhou, B., Moodie, A., Blanchard, A. A. A., Leygue, E. & Myal, Y. Claudin 1 in Breast Cancer: New Insights. *Journal of clinical medicine* **4,** 1960–76 (2015).

71. Prat, A., Parker, J. S., Karginova, O., Fan, C., Livasy, C., Herschkowitz, J. I., He, X. & Perou, C. M. Phenotypic and molecular characterization of the claudin-low intrinsic subtype of breast cancer. *Breast cancer research : BCR* **12,** R68 (2010).

72. Sabatier, R., Finetti, P., Guille, A., Adelaide, J., Chaffanet, M., Viens, P., Birnbaum, D. & Bertucci, F. Claudin-low breast cancers: clinical, pathological, molecular and prognostic characterization. *Molecular cancer* **13,** 228 (2014).

73. White, J. M. & Wolfsberg, T. G. *Table of the ADAMs* 2005. (Visited on 02/16/2016).

74. Vandenbroucke, R. & Libert, C. Is there new hope for therapeutic matrix metalloproteinase inhibition? *Nature Reviews. Drug Discovery* **13,** 904–927 (2014).

75. Edwards, D. R., Handsley, M. M. & Pennington, C. J. The ADAM metalloproteinases. *Molecular aspects of medicine* **29,** 258–89 (2008).

76. Kuno, K, Kanada, N, Nakashima, E, Fujiki, F, Ichimura, F & Matsushima, K. Molecular cloning of a gene encoding a new type of metalloproteinase-disintegrin family protein with thrombospondin motifs as an inflammation associated gene. *J Biol Chem* **272,** 556–562 (1997).

77. Kumar, S., Rao, N. & Ge, R. Emerging roles of ADAMTSS in angiogenesis and cancer. *Cancers* **4,** 1252–1299 (2012).

78. Takeda, S., Takeya, H. & Iwanaga, S. Snake venom metalloproteinases: Structure, function and relevance to the mammalian ADAM/ADAMTS family proteins. *Biochimica et Biophysica Acta - Proteins and Proteomics* **1824,** 164–176 (2012).

79. Bernardes, C. P., Santos-Filho, N. A., Costa, T. R., Gomes, M. S. R., Torres, F. S., Costa, J., Borges, M. H., Richardson, M., dos Santos, D. M., de Castro Pimenta, A. M., Homsi-Brandeburgo, M. I., Soares, A. M. & de Oliveira, F. Isolation and structural characterization of a new fibrin(ogen)olytic metalloproteinase from Bothrops moojeni snake venom. *Toxicon* **51,** 574–584 (2008).

80. Wu, W. B., Chang, S. C., Liau, M. Y. & Huang, T. F. Purification, molecular cloning and mechanism of action of graminelysin I, a snake-venom-derived metalloproteinase that induces apoptosis of human endothelial cells. *The Biochemical journal* **357,** 719–28 (2001).

81. Takeya, H., Nishida, S., Miyata, T., Kawada, S. I., Saisaka, Y., Morita, T. & Iwanaga, S. Coagulation factor X activating enzyme from Russell's viper venom (RVV-X): A novel metalloproteinase with disintegrin (platelet aggregation inhibitor)-like and C-type lectin-like domains. *Journal of Biological Chemistry* **267,** 14109–14117 (1992).

82. Siigur, E., Tõnismägi, K., Trummal, K., Samel, M., Vija, H., Subbi, J. & Siigur, J. Factor X activator from Vipera lebetina snake venom, molecular characterization and substrate specificity. *Biochimica et Biophysica Acta - General Subjects* **1568,** 90–98 (2001).

83. Yamada, D., Sekiya, F. & Morita, T. Isolation and characterization of carinactivase, a novel prothrombin activator in Echis carinatus venom with a unique catalytic mechanism. *Journal of Biological Chemistry* **271,** 5200–5207 (1996).

84. Yamada, D. & Morita, T. Purification and characterization of a Ca2+-dependent prothrombin activator, multactivase, from the venom of Echis multisquamatus. *Journal of Biochemistry* **122,** 991–997 (1997).

85. Calvete, J. J., Marcinkiewicz, C., Monleón, D., Esteve, V., Celda, B., Juárez, P. & Sanz, L. Snake venom disintegrins: Evolution of structure and function. *Toxicon* **45,** 1063–1074 (2005).

86. Lochter, A., Galosy, S., Muschler, J., Freedman, N., Werb, Z. & Bissell, M. J. Matrix metalloproteinase stromelysin-1 triggers a cascade of molecular alterations that leads to stable epithelial-to-mesenchymal conversion and a premalignant phenotype in mammary epithelial cells. *Journal of Cell Biology* **139,** 1861–1872 (1997).

87. Lelongt, B, Bengatta, S, Delauche, M, Lund, L. R., Werb, Z & Ronco, P. M. Matrix metalloproteinase 9 protects mice from anti-glomerular basement membrane nephritis through its fibrinolytic activity. *J Exp Med* **193,** 793–802 (2001).

88. Filippov, S., Caras, I., Murray, R., Matrisian, L. M., Chapman, H. A., Shapiro, S. & Weiss, S. J. Matrilysin-dependent elastolysis by human macrophages. *The Journal of experimental medicine* **198,** 925–35 (2003).

89. Maeda, S., Dean, D. D., Gomez, R., Schwartz, Z. & Boyan, B. D. The first stage of transforming growth factor β1 activation is release of the large latent complex from the extracellular matrix of growth plate chondrocytes by matrix vesicle stromelysin-1 (MMP-3). *Calcified Tissue International* **70,** 54–65 (2002).

90. Bergers, G., Brekken, R., Mcmahon, G., Vu, T. H., Itoh, T., Tamaki, K., Tanzawa, K., Thorpe, P., Itohara, S. & Hanahan, D. Matrix metalloproteinase-9 triggers the angiogenic switch during. *Nature cell biology* **2,** 737–744 (2010).

91. Nomura, H, Fujimoto, N, Seiki, M, Mai, M & Okada, Y. Enhanced production of matrix metalloproteinases and activation of matrix metalloproteinase 2 (gelatinase A) in human gastric carcinomas. *International journal of cancer. Journal international du cancer* **69,** 9–16 (1996).

92. Dufour, A., Zucker, S., Sampson, N. S., Kuscu, C. & Cao, J. Role of matrix metalloproteinase-9 dimers in cell migration: Design of inhibitory peptides. *Journal of Biological Chemistry* **285,** 35944–35956 (2010).

93. Airola, K, Karonen, T, Vaalamo, M, Lehti, K, Lohi, J, Kariniemi, A. L., Keski-Oja, J & Saarialho-Kere, U. K. Expression of collagenases-1 and -3 and their inhibitors TIMP-1 and -3 correlates with the level of invasion in malignant melanomas. *British journal of cancer* **80,** 733–43 (1999).

94. Zhang, S., Mercado-Uribe, I., Xing, Z., Sun, B., Kuang, J. & Liu, J. Generation of Cancer Stem-like Cells through Formation of Polyploid Giant Cancer Cells. **33,** 1–23 (2015).

95. Yang, W., Arii, S., Gorrin-Rivas, M. J., Mori, A., Onodera, H. & Imamura, M. Human macrophage metalloelastase gene expression in colorectal carcinoma and its clinicopathologic significance. *Cancer* **91,** 1277–1283 (2001).

96. Takeha, S, Fujiyama, Y, Bamba, T, Sorsa, T, Nagura, H & Ohtani, H. Stromal expression of MMP-9 and urokinase receptor is inversely associated with liver metastasis and with infiltrating growth in human colorectal cancer: a novel approach from immune/inflammatory aspect. *Japanese journal of cancer research : Gann* **88,** 72–81 (1997).

97. Wolfsberg, T. G. & White, J. M. ADAMs in fertilization and development. *Developmental biology* **180,** 389–401 (1996).

98. Tang, B. L. ADAMTS: A novel family of extracellular matrix proteases. *International Journal of Biochemistry and Cell Biology* **33,** 33–44 (2001).

99. Parks, W. C., Wilson, C. L. & López-Boado, Y. S. Matrix metalloproteinases as modulators of inflammation. *Nature Reviews Immunology* **4,** 617–629 (2004).

100. Krätzschmar, J., Lum, L. & Blobel, C. P. anchored Metalloprotease-Disintegrin Protein with an RGD Integrin Binding Sequence *. *The Journal of biological chemistry* **271,** 4593–4597 (1996).

101. Charrier, L., Yan, Y., Driss, A., Laboisse, C. L., Sitaraman, S. V. & Merlin, D. ADAM-15 inhibits wound healing in human intestinal epithelial cell monolayers. *American journal of physiology. Gastrointestinal and liver physiology* **288,** G346–53 (2005).

102. Roghani, M., Becherer, J. D., Moss, M. L., Atherton, R. E., Erdjument-Bromage, H., Arribas, J., Blackburn, R. K., Weskamp, G., Tempst, P. & Blobel, C. P. Metalloprotease-disintegrin MDC9: Intracellular maturation and catalytic activity. *Journal of Biological Chemistry* **274,** 3531–3540 (1999).

103. Van Wart, H. E. & Birkedal-Hansen, H. The cysteine switch: a principle of regulation of metalloproteinase activity with potential applicability to the entire matrix metalloproteinase gene family. *Proceedings of the National Academy of Sciences of the United States of America* **87,** 5578–82 (1990).

104. McKie, N, Edwards, T, Dallas, D. J., Houghton, a, Stringer, B, Graham, R, Russell, G & Croucher, P. I. Expression of members of a novel membrane linked metalloproteinase family (ADAM) in human articular chondrocytes. *Biochemical and biophysical research communications* **230,** 335–339 (1997).

105. Roberts, C. M., Tani, P. H., Bridges, L. C., Laszik, Z. & Bowditch, R. D. MDC-L, a novel metalloprotease disintegrin cysteine-rich protein family member expressed by human lymphocytes. *Journal of Biological Chemistry* **274,** 29251–29259 (1999).

106. Weskamp, G., Krätzschmar, J., Reid, M. S. & Blobel, C. P. MDC9, a widely expressed cellular disintegrin containing cytoplasmic SH3 ligand domains. *Journal of Cell Biology* **132,** 717–726 (1996).

107. Hosaka, M., Nagahama, M., Kim, W. S., Watanabe, T., Hatsuzawa, K., Ikemizu, J., Murakami, K. & Nakayama, K. Arg-X-Lys/Arg-Arg motif as a signal for precursor cleavage catalyzed by furin within the constitutive secretory pathway. *Journal of Biological Chemistry* **266,** 12127–12130 (1991).

108. Cao, J. A., Rehemtulla, A, Bahou, W & Zucker, S. Membrane Type Matrix Metalloproteinase-1 Activates Pro- Gelatinase-A Without Furin Cleavage of the N-Terminal Domain. *Journal of Biological Chemistry* **Vol 271,** 30174–30180 (1996).

109. Tallant, C., García-Castellanos, R., Baumann, U. & Gomis-Rüth, F. X. On the relevance of the met-turn methionine in metzincins. *Journal of Biological Chemistry* **285,** 13951–13957 (2010).

110. Garcia-Castellanos, R., CynthiaTallant, Marrero, A., Sola, M., Baumann, U. & Gomis-Rüth, F. X. Substrate specificity of a metalloprotease of the pappalysin family revealed by an inhibitor and a product complex. *Archives of Biochemistry and Biophysics* **457,** 57–72 (2007).

111. Niewiarowski, S, McLane, M. A., Kloczewiak, M & Stewart, G. J. Disintegrins and other naturally occurring antagonists of platelet fibrinogen receptors. *Seminars in hematology* **31,** 289–300 (1994).

112. White, J. M. ADAMs: Modulators of cell-cell and cell-matrix interactions. *Current Opinion in Cell Biology* **15,** 598–606 (2003).

113. Eto, K., Huet, C., Tarui, T., Kupriyanov, S., Liu, H. Z., Puzon-McLaughlin, W., Zhang, X. P., Sheppard, D., Engvall, E. & Takada, Y. Functional classification of ADAMs based on a conserved motif for binding to integrin α9β1. Implications for sperm-egg binding and other cell interactions. *Journal of Biological Chemistry* **277,** 17804–17810 (2002).

114. Nath, D, Slocombe, P. M., Stephens, P. E., Warn, A, Hutchinson, G. R., Yamada, K. M., Docherty, a. J. & Murphy, G. Interaction of metargidin (ADAM-15) with αvβ3 and α5β1 integrins on different haemopoietic cells. *Journal of cell science* **112,** 579–587 (1999).

115. Zhang, X. P., Kamata, T., Yokoyama, K., Puzon-McLaughlin, W. & Takada, Y. Specific interaction of the recombinant disintegrin-like domain of MDC- 15 (Metargidin, ADAM-15) with integrin αvβ3. *Journal of Biological Chemistry* **273,** 7345–7350 (1998).

116. Lu, X., Williams, J. A., Deadman, J. J., Salmon, G. P., Kakkar, V. V. & Wilkinson, J. M. Preferential antagonism of the interactions of the integrin allbf3 with immobilized glycoprotein ligands by snake-venom RGD (Arg-Gly-Asp) proteins. *Biochemical Journal* **936,** 929–936 (1994).

117. Lu, X., Rahman, S., Kakkar, V. V. & Authi, K. S. Substitutions of proline 42 to alanine and methionine 46 to asparagine around the RGD domain of the neurotoxin dendroaspin alter its preferential antagonism to that resembling the disintegrin elegantin. *Journal of Biological Chemistry* **271,** 289–294 (1996).

118. Huovila, A.-p. J., Almeida, E. A. & White, J. M. ADAMs and cell fusion Ari-Pekka J Huovila, Eduardo AC Almeida and Judith M White. *Current Opinion in Cell Biology* **8,** 692–699 (1996).

119. Abe, E, Mocharla, H, Yamate, T, Taguchi, Y & Manolagas, S. C. Meltrin-α, a fusion protein involved in multinucleated giant cell and osteoclast formation. *Calcified tissue international* **64,** 508–15 (1999).

120. Yagami-Hiromasa, T., Sato, T., Kurisaki, T., Kamijo, K., Nabeshima, Y.-i. & Fujisawa-Sehara, A. *A metalloprotease-disintegrin participating in myoblast fusion* 1995.

121. Iba, K., Albrechtsen, R., Gilpin, B. J., Loechel, F. & Wewer, U. M. Cysteine-Rich Domain of Human ADAM 12 (Meltrin α) Supports Tumor Cell Adhesion. *The American Journal of Pathology* **154,** 1489–1501 (1999).

122. Iba, K., Albrechtsen, R., Gilpin, B., Fröhlich, C., Loechel, F., Zolkiewska, A., Ishiguro, K., Kojima, T., Liu, W., Langford, J. K., Sanderson, R. D., Brakebusch, C., Fässler, R. & Wewer, U. M. The cysteine-rich domain of human ADAM 12 supports cell adhesion through syndecans and triggers signaling events that lead to β1 integrin-dependent cell spreading. *Journal of Cell Biology* **149,** 1143–1155 (2000).

123. Schrijver, I, Liu, W, Brenn, T, Furthmayr, H & Francke, U. Cysteine substitutions in epidermal growth factor-like domains of fibrillin-1: distinct effects on biochemical and clinical phenotypes. *American journal of human genetics* **65,** 1007–20 (1999).

124. Wouters, M. A., Rigoutsos, I., Chu, C. K., Feng, L. L., Sparrow, D. B. & Dunwoodie, S. L. Evolution of distinct EGF domains with specific functions. *Protein science : a publication of the Protein Society* **14,** 1091–103 (2005).

125. Kansas, G. S., Saunders, K. B., Ley, K, Zakrzewicz, A, Gibson, R. M., Furie, B. C., Furie, B & Tedder, T. F. A role for the epidermal growth factor-like domain of P-selectin in ligand recognition and cell adhesion. *The Journal of cell biology* **124,** 609–18 (1994).

126. Zhou, T., Zhang, Y., Sun, G., Zhang, Y., Zhang, D., Zhao, Y. & Chen, N. Anti-P-selectin lectin-EGF domain monoclonal antibody inhibits the maturation of human immature dendritic cells. *Experimental and Molecular Pathology* **80,** 171–176 (2006).

127. Janes, P. W., Saha, N., Barton, W. A., Kolev, M. V., Wimmer-Kleikamp, S. H., Nievergall, E., Blobel, C. P., Himanen, J.-P., Lackmann, M. & Nikolov, D. B. Adam meets Eph: an ADAM substrate recognition module acts as a molecular switch for ephrin cleavage in trans. *Cell* **123,** 291–304 (2005).

128. Lorenzen, I., Trad, A. & Grötzinger, J. Multimerisation of A disintegrin and metalloprotease protein-17 (ADAM17) is mediated by its EGF-like domain. *Biochemical and Biophysical Research Communications* **415,** 330–336 (2011).

129. The UniProt Consortium. UniProt: a hub for protein information. *Nucleic Acids Research* **43,** D204–212 (2014).

130. Blobel, C. P., Wolfsberg, T. G., Turck, C. W., Myles, D. G., Primakoff, P. & White, J. M. A potential fusion peptide and an integrin ligand domain in a protein active in sperm-egg fusion. *Nature* **356,** 248–252 (1992).

131. Primakoff, P, Hyatt, H & Tredick-Kline, J. Identification and purification of a sperm surface protein with a potential role in sperm-egg membrane fusion. *J Cell Biol* **104,** 141–149 (1987).

132. Lum, L & Blobel, C. P. Evidence for distinct serine protease activities with a potential role in processing the sperm protein fertilin. *Developmental biology* **191,** 131–145 (1997).

133. Jia, L.-g., Wang, X.-m., Shannon, J. D., Bjarnason, J. B. & Fox, J. W. Function of Disintegrin-like / Cysteine-rich Domains of Atrolysin A. **272,** 13094–13102 (1997).

134. Yuan, R., Primakoff, P. & Myles, D. G. A role for the disintegrin domain of cyritestin, a sperm surface protein belonging to the ADAM family, in mouse sperm-egg plasma membrane adhesion and fusion. *Journal of Cell Biology* **137,** 105–112 (1997).

135. Takahashi, E., Sagane, K., Nagasu, T. & Kuromitsu, J. Altered nociceptive response in ADAM11-deficient mice. *Brain Research* **1097,** 39–42 (2006).

136. Galliano, M. F., Huet, C., Frygelius, J., Polgren, A., Wewer, U. M. & Engvall, E. Binding of ADAM12, a marker of skeletal muscle regeneration, to the muscle-specific actin-binding protein, α-actinin-2, is required for myoblast fusion. *Journal of Biological Chemistry* **275,** 13933–13939 (2000).

137. Sagane, K, Ohya, Y, Hasegawa, Y & Tanaka, I. Metalloproteinase-like, disintegrin-like, cysteine-rich proteins MDC2 and MDC3: novel human cellular disintegrins highly expressed in the brain. *The Biochemical journal* **334,** 93–98 (1998).

138. D'Abaco, G. M., Ng, K., Paradiso, L., Godde, N. J., Kaye, A. & Novak, U. ADAM22, expressed in normal brain but not in high-grade gliomas, inhibits cellular proliferation via the disintegrin domain. *Neurosurgery* **58,** 179–186 (2006).

139. Almeida, E. a., Huovila, a. P., Sutherland, a. E., Stephens, L. E., Calarco, P. G., Shaw, L. M., Mercurio, a. M., Sonnenberg, A, Primakoff, P, Myles, D. G. & White, J. M. Mouse egg integrin α6β1 functions as a sperm receptor. *Cell* **81,** 1095–1104 (1995).

140. Scheller, J., Chalaris, A., Garbers, C. & Rose-John, S. ADAM17: A molecular switch to control inflammation and tissue regeneration. *Trends in Immunology* **32,** 380–387 (2011).

141. Moss, M. L., Jin, S. L., Milla, M. E., Bickett, D. M., Burkhart, W, Carter, H. L., Chen, W. J., Clay, W. C., Didsbury, J. R., Hassler, D, Hoffman, C. R., Kost, T. a., Lambert, M. H., Leesnitzer, M. a., McCauley, P, McGeehan, G, Mitchell, J, Moyer, M, Pahel, G, Rocque, W, Overton, L. K., Schoenen, F, Seaton, T, Su, J. L. & Becherer, J. D. Cloning of a disintegrin metalloproteinase that processes precursor tumour-necrosis factor-α. *Nature* **385,** 733–736 (1997).

142. Black, R. A. Tumor necrosis factor-α converting enzyme. *The International Journal of Biochemistry & Cell Biology* **34,** 1–5 (2002).

143. Cissé, M. A., Sunyach, C., Lefranc-Jullien, S., Postina, R., Vincent, B. & Checler, F. The disintegrin ADAM9 indirectly contributes to the physiological processing of cellular prion by modulating ADAM10 activity. *Journal of Biological Chemistry* **280,** 40624–40631 (2005).

144. Vincent, B., Paitel, E., Saftig, P., Frobert, Y., Hartmann, D., De Strooper, B., Grass, J., Lopez-Perez, E. & Checler, F. The disintegrins ADAM10 and TACE contribute to the constitutive and phorbol ester-regulated normal cleavage of the cellular prion protein. *The Journal of biological chemistry* **276,** 37743–37756 (2001).

145. Fourie, A. M., Coles, F., Moreno, V. & Karlsson, L. Catalytic activity of ADAM8, ADAM15, and MDC-L (ADAM28) on synthetic peptide substrates and in ectodomain cleavage of CD23. *The Journal of biological chemistry* **278,** 30469–77 (2003).

146. Weskamp, G., Ford, J. W., Sturgill, J., Martin, S., Docherty, A. J. P., Swendeman, S., Broadway, N., Hartmann, D., Saftig, P., Umland, S., Sehara-Fujisawa, A., Black, R. a., Ludwig, A., Becherer, J. D., Conrad, D. H. & Blobel, C. P. ADAM10 is a principal 'sheddase' of the low-affinity immunoglobulin E receptor CD23. *Nature immunology* **7,** 1293–1298 (2006).

147. Meng, J.-F., McFall, C & Rosenwasser, L. J. Polymorphism R62W results in resistance of CD23 to enzymatic cleavage in cultured cells. *Genes and immunity* **8,** 215–23 (2007).

148. Yuan, X., Wu, H., Xu, H., Xiong, H., Chu, Q., Yu, S., Wu, G. S. & Wu, K. Notch signaling: An emerging therapeutic target for cancer treatment. *Cancer Letters* **369,** 20–27 (2015).

149. Weber, S. & Saftig, P. Ectodomain shedding and ADAMs in development. *Development* **139,** 3693–3709 (2012).

150. Plumb, J, McQuaid, S, Cross, a. K., Surr, J, Haddock, G, Bunning, R. a. D. & Woodroofe, M. N. Upregulation of ADAM-17 expression in active lesions in multiple sclerosis. *Multiple sclerosis (Houndmills, Basingstoke, England)* **12,** 375–385 (2006).

151. Worley, J. R., Hughes, D. A., Dozio, N., Gavrilovic, J. & Sampson, M. J. Low density lipoprotein from patients with Type 2 diabetes increases expression of monocyte matrix metalloproteinase and ADAM metalloproteinase genes. *Cardiovascular diabetology* **6,** 21 (2007).

152. Gomez-Gaviro, M, Dominguez-Luis, M, Canchado, J, Calafat, J, Janssen, H, Lara-Pezzi, E, Fourie, A, Tugores, A, Valenzuela-Fernandez, A, Mollinedo, F, Sanchez-Madrid, F & Diaz-Gonzalez, F. Expression and regulation of the metalloproteinase ADAM-8 during human neutrophil pathophysiological activation and its catalytic activity on L-selectin shedding. *J Immunol* **178,** 8053–8063 (2007).

153. Charbonneau, M., Harper, K., Grondin, F., Pelmus, M., McDonald, P. P. & Dubois, C. M. Hypoxia-inducible factor mediates hypoxic and tumor necrosis factor α-induced increases in tumor necrosis factor-α converting enzyme/ADAM17 expression by synovial cells. *Journal of Biological Chemistry* **282,** 33714–33724 (2007).

154. Schulz, B., Pruessmeyer, J., Maretzky, T., Ludwig, A., Blobel Carl, P., Saftig, P. & Reiss, K. Disintegrin Metalloprotease (ADAM) 10 Regulates Endothelial Permeability and T Cell Transmigration by Proteolysis of Vascular Endothelial Cadherin. *Circulation Research* **102,** 1192–1201 (2008).

155. Van Eerdewegh, P., Little, R. D., Dupuis, J., Del Mastro, R. G., Falls, K., Simon, J., Torrey, D., Pandit, S., McKenny, J., Braunschweiger, K., Walsh, A., Liu, Z., Hayward, B., Folz, C., Manning, S. P., Bawa, A., Saracino, L., Thackston, M., Benchekroun, Y., Capparell, N., Wang, M., Adair, R., Feng, Y., Dubois, J., FitzGerald, M. G., Huang, H., Gibson, R., Allen, K. M., Pedan, A., Danzig, M. R., Umland, S. P., Egan, R. W., Cuss, F. M., Rorke, S., Clough, J. B., Holloway, J. W., Holgate, S. T. & Keith, T. P. Association of the ADAM33 gene with asthma and bronchial hyperresponsiveness. *Nature* **418,** 426–30 (2002).

156. Arima, T., Enokida, H., Kubo, H., Kagara, I., Matsuda, R., Toki, K., Nishimura, H., Chiyomaru, T., Tatarano, S., Idesako, T., Nishiyama, K. & Nakagawa, M. Nuclear translocation of ADAM-10 contributes to the

pathogenesis and progression of human prostate cancer. *Cancer Science* **98,** 1720–1726 (2007).

157. Kveiborg, M, Frohlich, C, Albrechtsen, R, Tischler, V, Dietrich, N, Holck, P, Kronqvist, P, Rank, F, Mercurio, a. M. & Wewer, U. M. A role for ADAM12 in breast tumor progression and stromal cell apoptosis. *Cancer Res* **65,** 4754–4761 (2005).

158. Wildeboer, D., Naus, S., Amy Sang, Q.-X., Bartsch, J. W. & Pagenstecher, A. Metalloproteinase disintegrins ADAM8 and ADAM19 are highly regulated in human primary brain tumors and their expression levels and activities are associated with invasiveness. *Journal of neuropathology and experimental neurology* **65,** 516–527 (2006).

159. Eichenauer, D. A., Simhadri, V. L., Von Strandmann, E. P., Ludwig, A., Matthews, V., Reiners, K. S., Von Tresckow, B., Saftig, P., Rose-John, S., Engert, A. & Hansen, H. P. ADAM10 inhibition of human CD30 shedding increases specificity of targeted immunotherapy in vitro. *Cancer Research* **67,** 332–338 (2007).

160. Komiya, K., Enomoto, H., Inoki, I., Okazaki, S., Fujita, Y., Ikeda, E., Ohuchi, E., Matsumoto, H., Toyama, Y. & Okada, Y. Expression of ADAM15 in rheumatoid synovium: up-regulation by vascular endothelial growth factor and possible implications for angiogenesis. *Arthritis research & therapy* **7,** R1158–R1173 (2005).

161. Fedak, P. W. M., Moravec, C. S., McCarthy, P. M., Altamentova, S. M., Wong, A. P., Skrtic, M., Verma, S., Weisel, R. D. & Li, R. K. Altered expression of disintegrin metalloproteinases and their inhibitor in human dilated cardiomyopathy. *Circulation* **113,** 238–245 (2006).

162. Sun, C., Wu, M. H., Lee, E. S. & Yuan, S. Y. A disintegrin and metalloproteinase 15 contributes to atherosclerosis by mediating endothelial barrier dysfunction via Src family kinase activity. *Arteriosclerosis, thrombosis, and vascular biology* **32,** 2444–51 (2012).

163. Carl-McGarth, S., Lendeckel, U., Ebert, M., Roessner, A. & Röcken, C. The disintegrin-metalloproteinases ADAM9, ADAM12, and ADAM15 are upregulated in gastric cancer. *International Journal of Oncology* **26,** 17–24 (2005).

164. Kuefer, R., Day, K. C., Kleer, C. G., Sabel, M. S., Hofer, M. D., Varambally, S., Zorn, C. S., Chinnaiyan, A. M., Rubin, M. a. & Day, M. L. ADAM15 disintegrin is associated with aggressive prostate and breast cancer disease. *Neoplasia (New York, N.Y.)* **8,** 319–29 (2006).

165. Ortiz, R. M., Kärkkäinen, I. & Huovila, A. P. J. Aberrant alternative exon use and increased copy number of human metalloprotease-disintegrin ADAM15 gene in breast cancer cells. *Genes Chromosomes and Cancer* **41,** 366–378 (2004).

166. Kleino, I., Ortiz, R. M. & Huovila, A.-P. J. ADAM15 gene structure and differential alternative exon use in human tissues. *BMC molecular biology* **8,** 90 (2007).

167. Fairbrother, W. G. Predictive Identification of Exonic Splicing Enhancers in Human Genes. *Science* **297,** 1007–1013 (2002).

168. Blencowe, B. J. Exonic splicing enhancers: Mechanism of action, diversity and role in human genetic diseases. *Trends in Biochemical Sciences* **25,** 106–110 (2000).

169. Long, J. C. & Caceres, J. F. The SR protein family of splicing factors: master regulators of gene expression. *The Biochemical journal* **417,** 15–27 (2009).

170. Goren, A., Ram, O., Amit, M., Keren, H., Lev-Maor, G., Vig, I., Pupko, T. & Ast, G. Comparative Analysis Identifies Exonic Splicing Regulatory Sequences-The Complex Definition of Enhancers and Silencers. *Molecular Cell* **22,** 769–781 (2006).

171. Jin, Y., Suzuki, H., Maegawa, S., Endo, H., Sugano, S., Hashimoto, K., Yasuda, K. & Inoue, K. A vertebrate RNA-binding protein Fox-1 regulates tissue-specific splicing via the pentanucleotide GCAUG. *EMBO Journal* **22,** 905–912 (2003).

172. Villate, O., Turatsinze, J.-V., Mascali, L. G., Grieco, F. a., Nogueira, T. C., Cunha, D. a., Nardelli, T. R., Sammeth, M., Salunkhe, V. a., Esguerra, J. L. S., Eliasson, L., Marselli, L., Marchetti, P. & Eizirik, D. L. Nova1 is a master regulator of alternative splicing in pancreatic beta cells. *Nucleic acids research* **42,** 11818–30 (2015).

173. Barreau, C., Paillard, L., Méreau, A. & Osborne, H. B. Mammalian CELF/Bruno-like RNA-binding proteins: molecular characteristics andÂ biological functions. *Biochimie* **88,** 515–525 (2006).

174. Holt, I., Jacquemin, V., Fardaei, M., Sewry, C. A., Butler-Browne, G. S., Furling, D., Brook, J. D. & Morris, G. E. Muscleblind-Like Proteins. *The American Journal of Pathology* **174,** 216–227 (2009).

175. Konieczny, P., Stepniak-Konieczna, E. & Sobczak, K. MBNL proteins and their target RNAs, interaction and splicing regulation. *Nucleic acids research* **42,** 10873–10887 (2014).

176. Miriami, E., Margalit, H. & Sperling, R. Conserved sequence elements associated with exon skipping. *Nucleic acids research* **31,** 1974–1983 (2003).

177. Warzecha, C. C., Shen, S., Xing, Y. & Carstens, R. P. The epithelial splicing factors ESRP1 and ESRP2 positively and negatively regulate diverse types of alternative splicing events. *RNA Biology* **6,** 546–562 (2009).

178. Warzecha, C. C., Sato, T. K., Nabet, B., Hogenesch, J. B. & Carstens, R. P. ESRP1 and ESRP2 Are Epithelial Cell-Type-Specific Regulators of FGFR2 Splicing. *Molecular Cell* **33,** 591–601 (2009).

179. Zhong, J. L., Poghosyan, Z., Pennington, C. J., Scott, X., Handsley, M. M., Warn, A., Gavrilovic, J., Honert, K., Krüger, A., Span, P. N., Sweep, F. C. G. J. & Edwards, D. R. Distinct functions of natural ADAM-15 cytoplasmic domain variants in human mammary carcinoma. *Molecular cancer research* **6,** 383–94 (2008).

180. Kleino, I., Ortiz, R. M., Yritys, M., Huovila, A.-P. J. & Saksela, K. Alternative splicing of ADAM15 regulates its interactions with cellular SH3 proteins. *Journal of cellular biochemistry* **108,** 877–85 (2009).

181. Kleino, I., Järviluoma, A., Hepojoki, J., Huovila, A. P. & Saksela, K. Preferred SH3 domain partners of ADAM metalloproteases include shared and ADAM-specific SH3 interactions. *PLoS ONE* **10,** 1–19 (2015).

182. Poghosyan, Z., Robbins, S. M., Houslay, M. D., Webster, A., Murphy, G. & Edwards, D. R. Phosphorylation-dependent interactions between ADAM15 cytoplasmic domain and Src family protein-tyrosine kinases. *The Journal of biological chemistry* **277,** 4999–5007 (2002).

183. Horiuchi, K. & Weskamp, G. Potential role for ADAM15 in pathological neovascularization in mice. *Molecular and cellular biology* **23,** 5614–5624 (2003).

184. Böhm, B. B., Aigner, T, Gehrsitz, A, Blobel, C. P., Kalden, J. R. & Burkhardt, H. Up-regulation of MDC15 (metargidin) messenger RNA in human osteoarthritic cartilage. *Arthritis and rheumatism* **42,** 1946–50 (1999).

185. Bohm, B. B., Aigner, T., Roy, B., Brodie, T. A., Blobel, C. P. & Burkhardt, H. Homeostatic effects of the metalloproteinase disintegrin ADAM15 in degenerative cartilage remodeling. *Arthritis and Rheumatism* **52,** 1100–1109 (2005).

186. Yuan, S. Y., Ustinova, E. E., Wu, M. H., Tinsley, J. H., Xu, W, Korompai, F. L. & Taulman, A. C. Protein kinase C activation contributes to microvascular barrier dysfunction in the heart at early stages of diabetes. *Circ Res* **87,** 412–417 (2000).

187. Cinel, I & Dellinger, R. P. Advances in pathogenesis and management of sepsis. *Current Opinion in Infectious Diseases* **20,** 345–352 (2007).

188. Franses, J. W., Drosu, N. C., Gibson, W. J., Chitalia, V. C. & Edelman, E. R. Dysfunctional endothelial cells directly stimulate cancer inflammation and metastasis. *International Journal of Cancer* **133,** 1334–1344 (2013).

189. Sun, C., Wu, M. H., Guo, M., Day, M. L., Lee, E. S., Yuan, Y & Yuan, S. Y. ADAM15 regulates endothelial permeability and neutrophil migration via Src/ERK1/2 signaling. *Cardiovscular Research* **87,** 348–355 (2010).

190. Rabiet, M.-J., Plantier, J.-L., Rival, Y., Genoux, Y., Lampugnani, M.-G. & Dejana, E. Thrombin-Induced Increase in Endothelial Permeability Is Associated With Changes in Cell-to-Cell Junction Organization. *Arteriosclerosis, Thrombosis, and Vascular Biology* **16,** 488–496 (1996).

191. Sun, C., Beard, R. S., McLean, D. L., Rigor, R. R., Konia, T., Wu, M. H. & Yuan, S. Y. ADAM15 deficiency attenuates pulmonary hyperpermeability and acute lung injury in lipopolysaccharide-treated mice. *American journal of physiology. Lung cellular and molecular physiology* **304,** L135–42 (2013).

192. Chatterjee, V., Beard, R. S., Reynolds, J. J., Haines, R., Guo, M., Rubin, M., Guido, J., Wu, M. H. & Yuan, S. Y. MicroRNA-147b Regulates Vascular Endothelial Barrier Function by Targeting ADAM15 Expression. *PLoS ONE* **9** (ed Fu, J.) e110286 (2014).

193. Schütz, a, Härtig, W, Wobus, M, Grosche, J, Wittekind, C. & Aust, G. Expression of ADAM15 in lung carcinomas. *Virchows Archiv : an international journal of pathology* **446,** 421–9 (2005).

194. Dong, D.-D., Zhou, H. & Li, G. ADAM15 targets MMP9 activity to promote lung cancer cell invasion. *Oncology reports* **34,** 2451–60 (2015).

195. Duan, X., Mao, X. & Sun, W. ADAM15 is involved in MICB shedding and mediates the effects of gemcitabine on MICB shedding in PANC-1 pancreatic cancer cells. *Molecular Medicine Reports* **7,** 991–997 (2013).

196. Martin, J., Eynstone, L. V., Davies, M., Williams, J. D. & Steadman, R. The role of ADAM 15 in glomerular mesangial cell migration. *The Journal of biological chemistry* **277,** 33683–9 (2002).

197. Schäfer, B., Gschwind, A. & Ullrich, A. Multiple G-protein-coupled receptor signals converge on the epidermal growth factor receptor to promote migration and invasion. *Oncogene* **23,** 991–9 (2004).

198. Hart, S., Fischer, O. M., Prenzel, N., Zwick-Wallasch, E., Schneider, M., Hennighausen, L. & Ullrich, A. GPCR-induced migration of breast carcinoma cells depends on both EGFR signal transactivation and EGFR-independent pathways. *Biological chemistry* **386,** 845–55 (2005).

199. Najy, A. J., Day, K. C. & Day, M. L. The ectodomain shedding of E-cadherin by ADAM15 supports ErbB receptor activation. *Journal of Biological Chemistry* **283,** 18393–18401 (2008).

200. Maretzky, T., Yang, G., Ouerfelli, O., Overall, C. M., Worpenberg, S., Hassiepen, U., Eder, J. & Blobel, C. P. Characterization of the catalytic activity of the membrane-anchored metalloproteinase ADAM15 in cell-based assays. *The Biochemical journal* **420,** 105–113 (2009).

201. Tousseyn, T., Thathiah, A., Jorissen, E., Raemaekers, T., Konietzko, U., Reiss, K., Maes, E., Snellinx, A., Serneels, L., Nyabi, O., Annaert, W., Saftig, P., Hartmann, D. & de Strooper, B. ADAM10, the rate-limiting protease of regulated intramembrane proteolysis of notch and other proteins, is processed by ADAMS-9, ADAMS-15, and the gamma-secretase. *Journal of Biological Chemistry* **284,** 11738–11747 (2009).

202. Bonnefoy, J. Y., Plater-Zyberk, C., Lecoanet-Henchoz, S., Gauchat, J. F., Aubry, J. P. & Graber, P. A new role for CD23 in inflammation. *Immunology Today* **17,** 418–420 (1996).

203. Märten, A., von Lilienfeld-Toal, M., Büchler, M. W. & Schmidt, J. Soluble MIC is elevated in the serum of patients with pancreatic carcinoma diminishing gammadelta T cell cytotoxicity. *International journal of cancer. Journal international du cancer* **119,** 2359–2365 (2006).

204. Diefenbach, A., Jensen, E. R., Jamieson, A. M. & Raulet, D. H. Rae1 and H60 ligands of the NKG2D receptor stimulate tumor immunity. *Nature* **413,** 165–171 (2001).

205. Groh, V., Wu, J., Yee, C. & Spies, T. Tumour-derived soluble MIC ligands impair expression of NKG2D and T-cell activation. *Nature* **419,** 734–738 (2002).

206. Schäfer, B., Marg, B., Gschwind, A. & Ullrich, A. Distinct ADAM metalloproteinases regulate G protein-coupled receptor-induced cell proliferation and survival. *The Journal of biological chemistry* **279,** 47929–38 (2004).

207. Maretzky, T., Le Gall, S. M., Worpenberg-Pietruk, S., Eder, J., Overall, C. M., Huang, X.-Y., Poghosyan, Z., Edwards, D. R. & Blobel, C. P. Src stimulates fibroblast growth factor receptor-2 shedding by an ADAM15 splice variant linked to breast cancer. *Cancer research* **69,** 4573–6 (2009).

208. Hochegger, H., Takeda, S. & Hunt, T. Cyclin-dependent kinases and cell-cycle transitions: does one fit all? *Nature reviews. Molecular cell biology* **9,** 910–916 (2008).

209. Graham, A. The neural crest. *Curr Biol* **13,** R381–4 (2003).

210. Spano, D., Heck, C., De Antonellis, P., Christofori, G. & Zollo, M. Molecular networks that regulate cancer metastasis. *Seminars in Cancer Biology* **22,** 234–249 (2012).

211. Friedl, P., Locker, J., Sahai, E. & Segall, J. E. Classifying collective cancer cell invasion. *Nature Cell Biology* **14,** 777–783 (2012).

212. Charras, G. & Sahai, E. Physical influences of the extracellular environment on cell migration. *Nature Reviews Molecular Cell Biology* **15,** 813–824 (2014).

213. Batson, J., Astin, J. W. & Nobes, C. D. Regulation of contact inhibition of locomotion by Eph-ephrin signalling. *Journal of Microscopy* **251,** 232–241 (2013).

214. Huttenlocher, A. & Horwitz, A. R. Integrins in cell migration. *Cold Spring Harbor perspectives in biology* **3,** a005074 (2011).

215. Chorev, D. S., Moscovitz, O., Geiger, B. & Sharon, M. Regulation of focal adhesion formation by a vinculin-Arp2/3 hybrid complex. *Nature communications* **5,** 3758 (2014).

216. Swaminathan, V., Fischer, R. S. & Waterman, C. M. The FAK-Arp2/3 interaction promotes leading edge advance and haptosensing by coupling nascent adhesions to lamellipodia actin. *Molecular Biology of the Cell* **27,** mbc.E15–08–0590– (2016).

217. Skau, C. T. & Waterman, C. M. Specification of Architecture and Function of Actin Structures by Actin Nucleation Factors. *Annual review of biophysics* **44,** 285–310 (2015).

218. Mullins, R. D., Heuser, J. a. & Pollard, T. D. The interaction of Arp2/3 complex with actin: nucleation, high affinity pointed end capping, and formation of branching networks of filaments. *Proceedings of the National Academy of Sciences of the United States of America* **95,** 6181–6186 (1998).

219. Rebowski, G, Boczkowska, M, Hayes, D. B., Guo, L, Irving, T. C. & Dominguez, R. X-ray scattering study of actin polymerization nuclei assembled by tandem W domains. *Proceedings of the National Academy of Sciences of the United States of America* **105,** 10785–10790 (2008).

220. Kovar, D. R. & Pollard, T. D. Insertional assembly of actin filament barbed ends in association with formins produces piconewton forces. *Proceedings of the National Academy of Sciences of the United States of America* **101,** 14725–14730 (2004).

221. Tschumperlin, D. J. Fibroblasts and the ground they walk on. *PHYSIOLOGY* **28,** 380–90 (2013).

222. Webb, D. J., Donais, K., Whitmore, L. A., Thomas, S. M., Turner, C. E., Parsons, J. T. & Horwitz, A. F. FAK-Src signalling through paxillin, ERK and MLCK regulates adhesion disassembly. *Nature cell biology* **6,** 154–161 (2004).

223. Lawson, M. A. & Maxfield, F. R. Ca2+ and calcineurin-dependent recycling of an integrin to the front of migrating neutrophils. *Nature* **377,** 75–79 (1995).

224. Herren, B, Garton, K. J., Coats, S, Bowen-Pope, D. F., Ross, R & Raines, E. W. ADAM15 overexpression in NIH3T3 cells enhances cell-cell interactions. *Experimental cell research* **271,** 152–60 (2001).

225. Chen, Q., Meng, L.-H., Zhu, C.-H., Lin, L.-P., Lu, H. & Ding, J. ADAM15 suppresses cell motility by driving integrin α5β1 cell surface expression via Erk inactivation. *The international journal of biochemistry & cell biology* **40,** 2164–2173 (2008).

226. Hou, Y, Chu, M, Du, F. F., Lei, J. Y., Chen, Y, Zhu, R. Y., Gong, X. H., Ma, X & Jin, J. Recombinant disintegrin domain of ADAM15 inhibits the proliferation and migration of Bel-7402 cells. *Biochemical and biophysical research communications* **435,** 640–5 (2013).

227. Najy, A. J., Day, K. C. & Day, M. L. ADAM15 supports prostate cancer metastasis by modulating tumor cell-endothelial cell interaction. *Cancer Research* **68,** 1092–1099 (2008).

228. Gao, J., Zheng, W., Wang, L. & Song, B. A disintegrin and metallproteinase 15 knockout decreases migration of fibroblast-like synoviocytes and inflammation in rheumatoid arthritis. *Molecular Medicine Reports* **11,** 4389–4396 (2015).

229. Kalluri, R. & Neilson, E. G. Epithelial-mesenchymal transition and its implications for fibrosis. *Journal of Clinical Investigation* **112,** 1776–1784 (2003).

230. Kalluri, R. & Weinberg, R. a. Review series The basics of epithelial-mesenchymal transition. *Journal of Clinical Investigation* **119,** 1420–1428 (2009).

231. Huang, L., Wu, R.-L. & Xu, A.-M. Epithelial-mesenchymal transition in gastric cancer. *American journal of translational research* **7,** 2141–2158 (2015).

232. Puisieux, A., Brabletz, T. & Caramel, J. Oncogenic roles of EMT-inducing transcription factors. *Nature cell biology* **16,** 488–94 (2014).

233. Huber, O. & Petersen, I. 150th Anniversary Series: Desmosomes and the Hallmarks of Cancer. *Cell Communication and Adhesion* **22,** 15–28 (2015).

234. Freund-Michel, V., Muller, B., Marthan, R., Savineau, J.-P. & Guibert, C. Expression and role of connexin-based gap junctions in pulmonary inflammatory diseases. *Pharmacology & Therapeutics,* 1–15 (2016).

235. Meng, W. & Takeichi, M. Adherens junction: molecular architecture and regulation. *Cold Spring Harbor perspectives in biology* **1,** 1–13 (2009).

236. Niessen, C. M. Tight junctions/adherens junctions: basic structure and function. *The Journal of investigative dermatology* **127,** 2525–32 (2007).

237. Pokutta, S., Herrenknecht, K., Kemler, R. & Engel, J. Conformational changes of the recombinant extracellular domain of E-cadherin upon calcium binding. *European Journal of Biochemistry* **223,** 1019–1026 (1994).

238. Xiao, K., Oas, R. G., Chiasson, C. M. & Kowalczyk, A. P. Role of p120-catenin in cadherin trafficking. *Biochimica et Biophysica Acta - Molecular Cell Research* **1773,** 8–16 (2007).

239. Anastasiadis, P. Z. p120-ctn: A nexus for contextual signaling via Rho GTPases. *Biochimica et Biophysica Acta - Molecular Cell Research* **1773,** 34–46 (2007).

240. Drees, F., Pokutta, S., Yamada, S., Nelson, W. J. & Weis, W. I. α-Catenin is a molecular switch that binds E-cadherin-β-catenin and regulates actin-filament assembly. *Cell* **123,** 903–915 (2005).

241. Irie, K., Shimizu, K., Sakisaka, T., Ikeda, W. & Takai, Y. Roles and modes of action of nectins in cell-cell adhesion. *Seminars in Cell and Developmental Biology* **15,** 643–656 (2004).

242. Saito, K., Shiino, T., Kurihara, H., Harita, Y., Hattori, S. & Ohta, Y. Afadin regulates RhoA/Rho-associated protein kinase signaling to control formation of actin stress fibers in kidney podocytes. *Cytoskeleton* **72,** 146–156 (2015).

243. Linnemann, T, Geyer, M, Jaitner, B. K., Block, C, Kalbitzer, H. R., Wittinghofer, A & Herrmann, C. Thermodynamic and kinetic characterization of the interaction between the Ras binding domain of AF6 and memberas of the Ras subfamily. *The Journal of Biological Chemistry* **274,** 13556–13562 (1999).

244. Ham, C., Levkau, B., Raines, E. W. & Herren, B. ADAM15 Is an Adherens Junction Molecule Whose Surface Expression Can Be Driven by VE-Cadherin. *Experimental Cell Research* **279,** 239–247 (2002).

245. Ikenouchi, J., Furuse, M., Furuse, K., Sasaki, H., Tsukita, S. & Tsukita, S. Tricellulin constitutes a novel barrier at tricellular contacts of epithelial cells. *Journal of Cell Biology* **171,** 939–945 (2005).

246. Guillemot, L., Spadaro, D. & Citi, S. The Junctional Proteins Cingulin and Paracingulin Modulate the Expression of Tight Junction Protein Genes through GATA-4. *PLoS ONE* **8** (2013).

247. Ebnet, K. Junctional Adhesion Molecule (JAM) interacts with the PDZ domain containing proteins AF-6 and ZO-1. *Journal of Biological Chemistry* (2000).

248. Hirabayashi, S., Tajima, M., Yao, I., Nishimura, W., Mori, H. & Hata, Y. JAM4, a Junctional Cell Adhesion Molecule Interacting with a Tight Junction Protein, MAGI-1. *Molecular and cellular biology* **23,** 4267–4282 (2003).

249. Mandell, K. J., McCall, I. C. & Parkos, C. A. Involvement of the Junctional Adhesion Molecule-1 (JAM1) Homodimer Interface in Regulation of Epithelial Barrier Function. *Journal of Biological Chemistry* **279,** 16254–16262 (2004).

250. Bauer, H., Zweimueller-Mayer, J., Steinbacher, P., Lametschwandtner, A. & Bauer, H. C. The dual role of zonula occludens (ZO) proteins. *Journal of Biomedicine and Biotechnology* **2010** (2010).

251. Gottardi, C. J., Arpin, M, Fanning, a. S. & Louvard, D. The junction-associated protein, zonula occludens-1, localizes to the nucleus before the maturation and during the remodeling of cell-cell contacts. *Proceedings of the National Academy of Sciences of the United States of America* **93,** 10779–10784 (1996).

252. Islas, S., Vega, J., Ponce, L. & González-Mariscal, L. Nuclear localization of the tight junction protein ZO-2 in epithelial cells. *Experimental cell research* **274,** 138–148 (2002).

253. Katahira, J., Sugiyama, H., Inoue, N., Horiguchi, Y., Matsuda, M. & Sugimoto, N. Clostridium perfringens enterotoxin utilizes two structurally related membrane proteins as functional receptors in vivo. *Journal of Biological Chemistry* **272,** 26652–26658 (1997).

254. Fujita, K., Katahira, J., Horiguchi, Y., Sonoda, N., Furuse, M. & Tsukita, S. Clostridium perfringens enterotoxin binds to the second extracellular loop of claudin-3, a tight junction integral membrane protein. *FEBS Letters* **476,** 258–261 (2000).

255. Sonoda, N., Furuse, M., Sasaki, H., Yonemura, S., Katahira, J., Horiguchi, Y. & Tsukita, S. Clostridium perfringens Enterotoxin Fragment Removes Specific Claudins from Tight Junction Strands. *The Journal of Cell Biology* **147,** 195–204 (1999).

256. Wu, Z., Nybom, P. & Magnusson, K. E. Distinct effects of Vibrio cholerae haemagglutinin/protease on the structure and localization of the tight junction-associated proteins occludin and ZO-1. *Cellular Microbiology* **2,** 11–17 (2000).

257. Fujita, H., Sugimoto, K., Inatomi, S., Maeda, T., Osanai, M., Uchiyama, Y., Yamamoto, Y., Wada, T., Kojima, T., Yokozaki, H., Yamashita, T., Kato, S., Sawada, N. & Chiba, H. Tight Junction Proteins Claudin-2 and -12 Are Critical for Vitamin D-dependent Ca2+ Absorption between Enterocytes. *Molecular biology of the Cell* **19,** 1912–1921 (2008).

258. Tobioka, H., Isomura, H., Kokai, Y. & Sawada, N. Polarized distribution of carcinoembryonic antigen is associated with a tight junction molecule in human colorectal adenocarcinoma. *Journal of Pathology* **198,** 207–212 (2002).

259. Tobioka, H., Isomura, H., Kokai, Y., Tokunaga, Y., Yamaguchi, J. & Sawada, N. Occludin Expression Decreases with the Progression of Human Endometrial Carcinoma. *Human Pathology* **35,** 159–164 (2004).

260. Cummins, P. M. Occludin: one protein, many forms. *Molecular and cellular biology* **32,** 242–250 (2012).

261. Krause, G., Winkler, L., Mueller, S. L., Haseloff, R. F., Piontek, J. & Blasig, I. E. Structure and function of claudins. *Biochimica et Biophysica Acta - Biomembranes* **1778,** 631–645 (2008).

262. Ebnet, K., Suzuki, A., Ohno, S. & Vestweber, D. Junctional adhesion molecules (JAMs): more molecules with dual functions? *Journal of cell science* **117,** 19–29 (2004).

263. Bazzoni, G & Dejana, E. Endothelial cell-to-cell junctions: molecular organization and role in vascular homeostasis. *Physiol Rev.* **84,** 869–901 (2004).

264. Myal, Y., Leygue, E. & Blanchard, A. A. Claudin 1 in breast tumorigenesis: Revelation of a possible novel "claudin high" subset of breast cancers. *Journal of Biomedicine and Biotechnology* **2010** (2010).

265. Singh, A. B., Sharma, A. & Dhawan, P. Claudin family of proteins and cancer: an overview. *Journal of oncology* **2010,** 541957 (2010).

266. Colegio, O. R., Van Itallie, C. M., McCrea, H. J., Rahner, C. & Anderson, J. M. Claudins create charge-selective channels in the paracellular pathway between epithelial cells. *American journal of physiology. Cell physiology* **283,** C142–C147 (2002).

267. Laurila, J. J., Karttunen, T., Koivukangas, V., Laurila, P. A., Syrjala, H., Saarnio, J., Soini, Y. & Ala-Kokko, T. I. Tight Junction Proteins in Gallbladder Epithelium: Different Expression in Acute Acalculous and Calculous Cholecystitis. *Journal of Histochemistry and Cytochemistry* **55,** 567–573 (2007).

268. Sakai, N., Chiba, H., Fujita, H., Akashi, Y., Osanai, M., Kojima, T. & Sawada, N. Expression patterns of claudin family of tight-junction proteins in the mouse prostate. *Histochemistry and Cell Biology* **127,** 457–462 (2007).

269. Rahner, C, Mitic, L. L. & Anderson, J. M. Heterogeneity in expression and subcellular localization of claudins 2, 3, 4, and 5 in the rat liver, pancreas, and gut. *Gastroenterology* **120,** 411–422 (2001).

270. Günzel, D., Haisch, L., Pfaffenbach, S., Krug, S. M., Milatz, S., Amasheh, S., Hunziker, W. & Müller, D. Claudin function in the thick ascending limb of henle's loop. *Annals of the New York Academy of Sciences* **1165,** 152–162 (2009).

271. Mrsny, R. J., Brown, G. T., Gerner-Smidt, K., Buret, A. G., Meddings, J. B., Quan, C., Koval, M. & Nusrat, A. A key claudin extracellular loop domain is critical for epithelial barrier integrity. *The American journal of pathology* **172,** 905–15 (2008).

272. Huber, J. D., Egleton, R. D. & Davis, T. P. Molecular physiology and pathophysiology of tight junctions in the blood-brain barrier. *Trends in neurosciences* **24,** 719–725 (2001).

273. Tökés, A.-M., Kulka, J., Paku, S., Szik, A., Páska, C., Novák, P. K., Szilák, L., Kiss, A., Bögi, K. & Schaff, Z. Claudin-1, -3 and -4 proteins and mRNA expression in benign and malignant breast lesions: a research study. *Breast cancer research* **7,** R296–R305 (2005).

274. Soini, Y. Expression of claudins 1, 2, 3, 4, 5 and 7 in various types of tumours. *Histopathology* **46,** 551–560 (2005).

275. Furuse, M., Hata, M., Furuse, K., Yoshida, Y., Haratake, A., Sugitani, Y., Noda, T., Kubo, A. & Tsukita, S. Claudin-based tight junctions are crucial for the mammalian epidermal barrier: A lesson from claudin-1-deficient mice. *Journal of Cell Biology* **156,** 1099–1111 (2002).

276. Hadj-Rabia, S., Baala, L., Vabres, P., Hamel-Teillac, D., Jacquemin, E., Fabre, M., Lyonnet, S., De Prost, Y., Munnich, A., Hadchouel, M. & Smahi, A. Claudin-1 gene mutations in neonatal sclerosing cholangitis associated with ichthyosis: A tight junction disease. *Gastroenterology* **127,** 1386–1390 (2004).

277. Baala, L., Hadj-Rabia, S., Hamel-Teillac, D., Hadchouel, M., Prost, C., Leal, S. M., Jacquemin, E., Sefiani, A., De Prost, Y., Courtois, G., Munnich, A., Lyonnet, S. & Vabres, P. Homozygosity mapping of a locus for a novel syndromic ichthyosis to chromosome 3q27-q28. *Journal of Investigative Dermatology* **119,** 70–76 (2002).

278. Feldmeyer, L., Huber, M., Fellmann, F., Beckmann, J., Frenk, E. & Hohl, D. Mutational Spectrum and Genotype - Phenotype Correlations in Mevalonate Kinase Deficiency. *Human Mutation* **27,** 408–410 (2006).

279. Furuse, M, Fujita, K, Hiiragi, T, Fujimoto, K & Tsukita, S. Claudin-1 and -2: novel integral membrane proteins localizing at tight junctions with no sequence similarity to occludin. *The Journal of cell biology* **141,** 1539–50 (1998).

280. Furuse, M., Sasaki, H., Fujimoto, K. & Tsukita, S. A single gene product, claudin-1 or -2, reconstitutes tight junction strands and recruits occludin in fibroblasts. *Journal of Cell Biology* **143,** 391–401 (1998).

281. Leotlela, P. D., Wade, M. S., Duray, P. H., Rhode, M. J., Brown, H. F., Rosenthal, D. T., Dissanayake, S. K., Earley, R, Indig, F. E., Nickoloff, B. J., Taub, D. D., Kallioniemi, O. P., Meltzer, P, Morin, P. J. & Weeraratna, a. T. Claudin-1 overexpression in melanoma is regulated by PKC and contributes to melanoma cell motility. *Oncogene* **26,** 3846–3856 (2007).

282. Poritz, L. S., Harris, L. R., Kelly, A. A. & Koltun, W. A. Increase in the tight junction protein claudin-1 in intestinal inflammation. *Digestive Diseases and Sciences* **56,** 2802–2809 (2011).

283. Saeedi, B. J., Kao, D. J., Kitzenberg, D. A., Dobrinskikh, E., Schwisow, K. D., Masterson, J. C., Kendrick, A. A., Kelly, C. J., Bayless, A. J., Kominsky, D. J., Campbell, E. L., Kuhn, K. A., Furuta, G. T., Colgan, S. P. & Glover, L. E. HIF-dependent regulation of claudin-1 is central to intestinal epithelial tight junction integrity. *Molecular biology of the cell* **26,** 2252–2262 (2015).

284. Rüffer, C. & Gerke, V. The C-terminal cytoplasmic tail of claudins 1 and 5 but not its PDZ-binding motif is required for apical localization at epithelial and endothelial tight junctions. *European journal of cell biology* **83,** 135–44 (2004).

285. Cell Signalling Technolgies. *Phosphorylation sites of claudin1* 2013. <`http://www.phosphosite.org/proteinAction.action?id=5091`> (visited on 09/01/2016).

286. Fujibe, M., Chiba, H., Kojima, T., Soma, T., Wada, T., Yamashita, T. & Sawada, N. Thr203 of claudin-1, a putative phosphorylation site for MAP kinase, is required to promote the barrier function of tight junctions. *Experimental cell research* **295,** 36–47 (2004).

287. Nunbhakdi-Craig, V., Machleidt, T., Ogris, E., Bellotto, D., White, C. L. & Sontag, E. Protein phosphatase 2A associates with and regulates atypical PKC and the epithelial tight junction complex. *Journal of Cell Biology* **158,** 967–978 (2002).

288. Donaldson, R., Sun, Y., Liang, D.-y., Zheng, M., Sahbaie, P., Dill, D. L., Peltz, G., Buck, K. J. & Clark, J. D. The multiple PDZ domain protein Mpdz / MUPP1 regulates opioid tolerance and opioid-induced hyperalgesia. *BMC Genomics* **313,** 1–12 (2016).

289. Baumgart, S., Jansen, F., Bintig, W., Kalbe, B., Herrmann, C., Klumpers, F., Ko, S. D., Scholz, P., Rasche, S., Dooley, R., Metzler-nolte, N., Spehr, M., Hatt, H. & Neuhaus, E. M. The scaffold protein MUPP1 regulates odorant-mediated signaling in olfactory sensory neurons. *The Company of Biologists* **127,** 2518–2527 (2014).

290. Harris, H. J., Farquhar, M. J., Mee, C. J., Davis, C., Reynolds, G. M., Jennings, A., Hu, K., Yuan, F., Deng, H., Hubscher, S. G., Han, J. H., Balfe, P. & Mckeating, J. A. CD81 and Claudin 1 Coreceptor Association: Role in Hepatitis C Virus Entry. *Journal of Virology* **82,** 5007–5020 (2008).

291. Itoh, M, Furuse, M, Morita, K, Kubota, K, Saitou, M & Tsukita, S. Direct binding of three tight junction-associated MAGUKs, ZO-1, ZO-2, and ZO-3, with the COOH termini of claudins. *The Journal of cell biology* **147,** 1351–63 (1999).

292. Che, P., Tang, H. & Li, Q. The interaction between claudin-1 and dengue viral prM/M protein for its entry. *Virology* **446,** 303–313 (2013).

293. Evans, M. J., von Hahn, T., Tscherne, D. M., Syder, A. J., Panis, M., Wölk, B., Hatziioannou, T., McKeating, J. a., Bieniasz, P. D. & Rice, C. M. Claudin-1 is a hepatitis C virus co-receptor required for a late step in entry. *Nature* **446,** 801–805 (2007).

294. Barmeyer, C., Schulzke, J. D. & Fromm, M. Claudin-related intestinal diseases. *Seminars in Cell and Developmental Biology* **42,** 30–38 (2015).

295. Weber, C. R., Nalle, S. C., Tretiakova, M., Rubin, D. T. & Turner, J. R. Claudin-1 and claudin-2 expression is elevated in inflammatory bowel disease and may contribute to early neoplastic transformation. *Laboratory investigation; a journal of technical methods and pathology* **88,** 1110–20 (2008).

296. Bertiaux-Vandaële, N., Youmba, S. B., Belmonte, L., Lecleire, S., Antonietti, M., Gourcerol, G., Leroi, A.-M., Déchelotte, P., Ménard, J.-F., Ducrotté, P. & Coëffier, M. The expression and the cellular distribution of the tight junction proteins are altered in irritable bowel syndrome patients with differences according to the disease subtype. *The American journal of gastroenterology* **106,** 2165–73 (2011).

297. Fluge, O, Bruland, O, Akslen, L. A., Lillehaug, J. R. & Varhaug, J. E. Gene expression in poorly differentiated papillary thyroid carcinomas. *Thyroid* **16,** 161–175 (2006).

298. Iacobuzio-Donahue, C. a., Maitra, A., Shen-Ong, G. L., van Heek, T., Ashfaq, R., Meyer, R., Walter, K., Berg, K., Hollingsworth, M. a., Cameron, J. L., Yeo, C. J., Kern, S. E., Goggins, M. & Hruban, R. H. Discovery of novel tumor markers of pancreatic cancer using global gene expression technology. *The American journal of pathology* **160,** 1239–1249 (2002).

299. Miwa, N., Furuse, M., Tsukita, S., Niikawa, N., Nakamura, Y. & Furukawa, Y. Involvement of Claudin-1 in the β-Catenin/Tcf Signaling Pathway and its Frequent Upregulation in Human Colorectal Cancers. *Oncology Research* **12,** 469–476 (2001).

300. Huang, J., Zhang, L., He, C., Qu, Y., Li, J., Zhang, J., Chen, X., Yu, Y., Liu, B. & Zhu, Z. Claudin-1 enhances tumor proliferation and metastasis by regulating cell anoikis in gastric cancer. *Oncotarget* **6,** 1652–1665 (2015).

301. Dhawan, P., Singh, A. B., Deane, N. G., No, Y., Shiou, S.-r., Schmidt, C., Neff, J., Washington, M. K. & Beauchamp, R. D. Claudin-1 regulates cellular transformation and metastatic behavior in colon cancer. *The Journal of Clinical Investigation* **115,** 1765–1776 (2005).

302. Higashi, Y., Suzuki, S., Sakaguchi, T., Nakamura, T., Baba, S., Reinecker, H.-C., Nakamura, S. & Konno, H. Loss of claudin-1 expression correlates with malignancy of hepatocellular carcinoma. *The Journal of surgical research* **139,** 68–76 (2007).

303. Paschoud, S., Bongiovanni, M., Pache, J.-C. & Citi, S. Claudin-1 and claudin-5 expression patterns differentiate lung squamous cell carcinomas from adenocarcinomas. *Modern Pathology* **20,** 947–954 (2007).

304. Krämer, F, White, K, Kubbies, M, Swisshelm, K & Weber, B. H. Genomic organization of claudin-1 and its assessment in hereditary and sporadic breast cancer. *Human genetics* **107,** 249–56 (2000).

305. Hoevel, T., Macek, R., Swisshelm, K. & Kubbies, M. Reexpression of the TJ protein CLDN1 induces apoptosis in breast tumor spheroids. *International Journal of Cancer* **108,** 374–383 (2004).

306. Hoevel, T., Macek, R., Mundigl, O., Swisshelm, K. & Kubbies, M. Expression and targeting of the tight junction protein CLDN1 in CLDN1-negative human breast tumor cells. *Journal of Cellular Physiology* **191,** 60–68 (2002).

307. Kulawiec, M., Safina, A., Desouki, M. M., Still, I., Matsui, S.-I., Bakin, A. & Singh, K. K. Tumorigenic transformation of human breast epithelial cells induced by mitochondrial DNA depletion. *Cancer biology & therapy* **7,** 1732–43 (2008).

308. Morohashi, S., Kusumi, T., Sato, F., Odagiri, H., Chiba, H., Yoshihara, S., Hakamada, K., Sasaki, M. & Kijima, H. Decreased expression of claudin-1 correlates with recurrence status in breast cancer. *International Journal of Molecular Medicine* **20,** 139–143 (2007).

309. Di Cello, F., Cope, L., Li, H., Jeschke, J., Wang, W., Baylin, S. B. & Zahnow, C. A. Methylation of the Claudin 1 Promoter Is Associated with Loss of Expression in Estrogen Receptor Positive Breast Cancer. *PLoS ONE* **8,** 1–8 (2013).

310. Qin, W., Ren, Q., Liu, T., Huang, Y. & Wang, J. MicroRNA-155 is a novel suppressor of ovarian cancer-initiating cells that targets CLDN1. *FEBS Letters* **587,** 1434–1439 (2013).

311. Roth, C., Rack, B., Müller, V., Janni, W., Pantel, K. & Schwarzenbach, H. Circulating microRNAs as blood-based markers for patients with primary and metastatic breast cancer. *Breast cancer research* **12,** R90 (2010).

312. Liu, J., Mao, Q., Liu, Y., Hao, X., Zhang, S. & Zhang, J. Analysis of miR-205 and miR-155 expression in the blood of breast cancer patients. *Chinese journal of cancer research = Chung-kuo yen cheng yen chiu* **25,** 46–54 (2013).

313. Polyak, K. Science in medicine Breast cancer: origins and evolution. *Cell* **117,** 3155–63 (2007).

314. Itoh, M. & Bissel, M. J. The Organization of Tight Junctions in Epithelia: Implications for Mammary Gland Biology and Breast Tumorigenesis. *Journal of Mammary Gland Biology and Neoplasia* **8,** 449–462 (2003).

315. Suh, Y, Yoon, C.-H., Kim, R.-K., Lim, E.-J., Oh, Y. S., Hwang, S.-G., An, S, Yoon, G, Gye, M. C., Yi, J.-M., Kim, M.-J. & Lee, S.-J. Claudin-1 induces epithelial-mesenchymal transition through activation of the c-Abl-ERK signaling pathway in human liver cells. *Oncogene* **32,** 4873–82 (2013).

316. Singh, A. B., Sharma, A., Smith, J. J., Krishnan, M., Chen, X., Eschrich, S., Washington, M. K., Yeatman, T. J., Beauchamp, R. D. & Dhawan, P. Claudin-1 up-regulates the repressor ZEB-1 to inhibit E-cadherin expression in colon cancer cells. *Gastroenterology* **141,** 2140–2153 (2011).

317. Zhou, B., Blanchard, A., Wang, N., Ma, X., Han, J., Schroedter, I., Leygue, E. & Myal, Y. Claudin 1 Promotes Migration and Increases Sensitivity to Tamoxifen and Anticancer Drugs in Luminal-like Human Breast Cancer Cells MCF7. *Cancer Investigation* **33,** 429–439 (2015).

318. Martinez-Estrada, O. M., Culleres, A, Soriano, F. X., Peinado, H, Bolos, V, Martinez, F. O., Reina, M, Cano, A, Fabre, M & Vilaro, S. The transcription factors Slug and Snail act as repressors of Claudin-1 expression in epithelial cells. *Biochem J* **394,** 449–457 (2006).

319. Miyamori, H., Takino, T., Kobayashi, Y., Tokai, H., Itoh, Y., Seiki, M. & Sato, H. Claudin Promotes Activation of Pro-matrix Metalloproteinase-2 Mediated by Membrane-type Matrix Metalloproteinases. *Journal of Biological Chemistry* **276,** 28204–28211 (2001).

320. Oku, N., Sasabe, E., Ueta, E., Yamamoto, T. & Osaki, T. Tight junction protein claudin-1 enhances the invasive activity of oral squamous cell carcinoma cells by promoting cleavage of laminin-5 γ2 chain via matrix metalloproteinase (MMP)-2 and membrane-type MMP-1. *Cancer Research* **66,** 5251–5257 (2006).

321. Yilmaz, M. & Christofori, G. Mechanisms of motility in metastasizing cells. *Molecular cancer research* **8,** 629–642 (2010).

322. Fortier, A.-M., Asselin, E. & Cadrin, M. Keratin 8 and 18 loss in epithelial cancer cells increases collective cell migration and cisplatin sensitivity through claudin1 up-regulation. *The Journal of biological chemistry* **288,** 11555–71 (2013).

323. Kinzler, K. W. & Vogelstein, B. Lessons from hereditary colorectal cancer. *Cell* **87,** 159–70 (1996).

324. Ayrolles-Torro, A., Vezzio-Vie, N., Denis, V., Boissiere-Michot, F., Garambois, V., Busson, M., Ait Arsa, I., Mollevi, C., Pugniere, M., Bibeau, F., Martineau, P., Gongora, C. & Del Rio, M. Abstract B245: Claudin-1 (CLDN1) as a new therapeutic target in colorectal cancer: Inhibition of cell growth and survival by an anti-CLDN1 monoclonal antibody. *Mol. Cancer Ther.* **12** (2013).

325. Fofana, I., Krieger, S. E., Grunert, F., Glauben, S., Xiao, F., Fafikremer, S., Soulier, E., Royer, C., Thumann, C., Mee, C. J., McKeating, J. A., Dragic, T., Pessaux, P., Stollkeller, F., Schuster, C., Thompson, J. & Baumert, T. F. Monoclonal anti-claudin 1 antibodies prevent hepatitis C virus infection of primary human hepatocytes. *Gastroenterology* **139,** 953–964.e4 (2010).

326. Polivka Jr., J. & Janku, F. Molecular targets for cancer therapy in the PI3K/AKT/mTOR pathway. *Pharmacology & Therapeutics* **142,** 164–175 (2014).

327. Walker, E. H., Perisic, O., Ried, C., Stephens, L. & Williams, R. L. Structural insights into phosphoinositide 3-kinase catalysis and signalling. *Nature* **402,** 313–320 (1999).

328. Yasui, M., Matsuoka, S. & Ueda, M. PTEN Hopping on the Cell Membrane Is Regulated via a Positively-Charged C2 Domain. *PLoS Computational Biology* **10** (2014).

329. Zhao, L & Vogt, P. K. Class I PI3K in oncogenic cellular transformation. *Oncogene* **27,** 5486–96 (2008).

330. Aitio, O., Hellman, M., Kazlauskas, A., Vingadassalom, D. F., Leong, J. M., Saksela, K. & Permi, P. Recognition of tandem PxxP motifs as a unique Src homology 3-binding mode triggers pathogen-driven actin assembly. *Proceedings of the National Academy of Sciences* **107,** 21743–21748 (2010).

331. Zhou, S., Shoelson, S. E., Chaudhuri, M., Gish, G., Pawson, T., Haser, W. G., King, F., Roberts, T., Ratnofsky, S., Lechleider, R. J., Neel, B. G., Birge, R. B., Fajardo, J. E., Chou, M. M., Hanafusa, H., Schaffhausen, B. & Cantley, L. C. SH2 domains recognize specific phosphopeptide sequences. *Cell* **72,** 767–778 (1993).

332. Zheng, Y., Bagrodia, S. & Cerione, R. A. Activation of phosphoinositide 3-kinase activity by Cdc42Hs binding to p85. *Journal of Biological Chemistry* **269,** 18727–18730 (1994).

333. Tolias, K. F., Cantley, L. C. & Carpenter, C. L. *Rho family GTPases bind to phosphoinositide kinases* 1995.

334. Alessi, D. R., James, S. R., Downes, C. P., Holmes, A. B., Gaffney, P. R., Reese, C. B. & Cohen, P. Characterization of a 3-phosphoinositide-dependent protein kinase which phosphorylates and activates protein kinase Bα. *Curr Biol* **7,** 261–269 (1997).

335. Vanhaesebroeck, B., Guillermet-Guibert, J., Graupera, M. & Bilanges, B. The emerging mechanisms of isoform-specific PI3K signalling. *Nature reviews. Molecular cell biology* **11,** 329–341 (2010).

336. Lempiäinen, H. & Halazonetis, T. D. Emerging common themes in regulation of PIKKs and PI3Ks. *The EMBO Journal* **28,** 3067–73 (2009).

337. Sabatini, D. M., Erdjument-Bromage, H., Lui, M., Tempst, P. & Snyder, S. H. RAFT1: A mammalian protein that binds to FKBP12 in a rapamycin-dependent fashion and is homologous to yeast TORs. *Cell* **78,** 35–43 (1994).

338. Cargnello, M., Tcherkezian, J. & Roux, P. P. The expanding role of mTOR in cancer cell growth and proliferation. *Mutagenesis* **30,** 169–176 (2015).

339. Wang, L., Lawrence, J. C., Sturgill, T. W. & Harris, T. E. Mammalian target of rapamycin complex 1 (mTORC1) activity is associated with phosphorylation of raptor by mTOR. *The Journal of biological chemistry* **284,** 14693–14697 (2009).

340. Peterson, T. R., Laplante, M., Thoreen, C. C., Sancak, Y., Kang, S. A., Kuehl, W. M., Gray, N. S. & Sabatini, D. M. DEPTOR is an mTOR Inhibitor Whose Frequent Overexpression in Multiple Myeloma Cells Promotes their Survival Timothy. *Cell* **137,** 873–886 (2009).

341. Guertin, D. A., Stevens, D. M., Thoreen, C. C., Burds, A. A., Kalaany, N. Y., Moffat, J., Brown, M., Fitzgerald, K. J. & Sabatini, D. M. Ablation in Mice of the mTORC Components raptor, rictor, or mLST8 Reveals that mTORC2 Is Required for Signaling to Akt-FOXO and PKCα, but Not S6K1. *Developmental Cell* **11,** 859–871 (2006).

342. Jacinto, E., Facchinetti, V., Liu, D., Soto, N., Wei, S., Jung, S. Y., Huang, Q., Qin, J. & Su, B. SIN1/MIP1 Maintains rictor-mTOR Complex Integrity and Regulates Akt Phosphorylation and Substrate Specificity. *Cell* **127,** 125–137 (2006).

343. Frias, M. A., Thoreen, C. C., Jaffe, J. D., Schroder, W., Sculley, T., Carr, S. A. & Sabatini, D. M. mSin1 Is Necessary for Akt/PKB Phosphorylation, and Its Isoforms Define Three Distinct mTORC2s. *Current Biology* **16,** 1865–1870 (2006).

344. Siekierka, J. J., Hung, S. H., Poe, M, Lin, C. S. & Sigal, N. H. A cytosolic binding protein for the immunosuppressant FK506 has peptidyl-prolyl isomerase activity but is distinct from cyclophilin. *Nature* **341,** 755–757 (1989).

345. Lyutova, E. M., Kasakov, A. S. & Gurvits, B. Y. Chaperone-like activity of immunophilin FKBP12 from bovine brain, a cytoplasmic receptor of immunosuppressor FK506. *Neurochemical Journal* **1,** 196–203 (2007).

346. Knuefermann, C., Lu, Y., Liu, B., Jin, W., Liang, K., Wu, L., Schmidt, M., Mills, G. B., Mendelsohn, J. & Fan, Z. HER2/PI-3K/Akt activation leads to a multidrug resistance in human breast adenocarcinoma cells. *Oncogene* **22,** 3205–3212 (2003).

347. Stern, D. F. ERBB3/HER3 and ERBB2/HER2 duet in mammary development and breast cancer. *Journal of Mammary Gland Biology and Neoplasia* **13,** 215–223 (2008).

348. Rodriguez-Viciana, P, Warne, P. H., Dhand, R, Vanhaesebroeck, B, Gout, I, Fry, M. J., Waterfield, M. D. & Downward, J. Phosphatidylinositol-3-OH kinase as a direct target of Ras. *Nature* **370,** 527–532 (1994).

349. Cantley, L. C. The Phosphoinositide 3-Kinase Pathway. *Science* **296,** 1655–1658 (2002).

350. Sarbassov, D. D., Guertin, D. a., Ali, S. M. & Sabatini, D. M. Phosphorylation and regulation of Akt/PKB by the rictor-mTOR complex. *Science (New York, N.Y.)* **307,** 1098–1101 (2005).

351. Manning, B. D. & Cantley, L. C. Rheb fills a GAP between TSC and TOR. *Trends in Biochemical Sciences* **28,** 573–576 (2003).

352. Stambolic, V., Suzuki, A., De la Pompa, J. L., Brothers, G. M., Mirtsos, C., Sasaki, T., Ruland, J., Penninger, J. M., Siderovski, D. P. & Mak, T. W. Negative regulation of PKB/Akt-dependent cell survival by the tumor suppressor PTEN. *Cell* **95,** 29–39 (1998).

353. Andjelković, M, Jakubowicz, T, Cron, P, Ming, X. F., Han, J. W. & Hemmings, B. A. Activation and phosphorylation of a pleckstrin homology domain containing protein kinase (RAC-PK/PKB) promoted by serum and protein phosphatase inhibitors. *Proceedings of the National Academy of Sciences of the United States of America* **93,** 5699–704 (1996).

354. Wang, H., Ji, Y., Wu, G., Sun, K., Sun, Y., Li, W., Wang, B., He, B., Zhang, Q., Dai, Z., Wu, Z., Affiliations, A. & Affiliations, A. L -Tryptophan Activates Mammalian Target of Rapamycin and Enhances Expression of Tight Junction Proteins in Intestinal, 1–2 (2015).

355. Yu, C., Jia, G., Deng, Q., Zhao, H., Chen, X., Liu, G. & Wang, K. The effects of Glucagon-like peptide-2 on the tight junction and barrier function in IPEC-J2 cells through phosphatidylinositol 3-kinase-protein kinase B-mammalian target of rapamycin signaling pathway. *Asian-Australasian Journal of Animal Sciences* **29,** 731–738 (2016).

356. Humphries, J. D., Byron, A. & Humphries, M. J. Integrin ligands at a glance. *Journal of Cell Science* **119,** 3901–3903 (2006).

357. Cattaneo, F., Guerra, G., Parisi, M., De Marinis, M., Tafuri, D., Cinelli, M. & Ammendola, R. Cell-surface receptors transactivation mediated by G protein-coupled receptors. *International Journal of Molecular Sciences* **15,** 19700–19728 (2014).

358. Burridge, K, Chrzanowska-Wodnicka, M & Zhong, C. Focal adhesion assembly. *Trends in cell biology* **7,** 342–7 (1997).

359. Eto, K., Puzon-McLaughlin, W., Sheppard, D., Sehara-Fujisawa, A., Zhang, X. P. & Takada, Y. RGD-independent binding of integrin α9β1 to the ADAM-12 and -15 disintegrin domains mediates cell-cell interaction. *Journal of Biological Chemistry* **275,** 34922–34930 (2000).

360. Yang, J. T., Rayburn, H & Hynes, R. O. Embryonic mesodermal defects in α5 integrin-deficient mice. *Development (Cambridge, England)* **119,** 1093–1105 (1993).

361. Huang, X. Z., Wu, J. F., Ferrando, R, Lee, J. H., Wang, Y. L., Farese Jr., R. V. & Sheppard, D. Fatal bilateral chylothorax in mice lacking the integrin α9β1. *Mol Cell Biol* **20,** 5208–5215 (2000).

362. Bader, B. L., Rayburn, H, Crowley, D & Hynes, R. O. Extensive vasculogenesis, angiogenesis, and organogenesis precede lethality in mice lacking all αv integrins. *Cell* **95,** 507–519 (1998).

363. Fassler, R. & Meyer, M. Consequences of lack of β1 integrin gene expression in mice. *Genes & Development* **9,** 1896–1908 (1995).

364. Stephens, L. E., Sutherland, A. E., Klimanskaya, I. V., Andrieux, A., Meneses, J., Pedersen, R. A. & Damsky, C. H. Deletion of β1 integrins in mice results in inner cell mass failure and peri-implantation lethality. *Genes and Development* **9,** 1883–1895 (1995).

365. Hodivala-Dilke, K. M., McHugh, K. P., Tsakiris, D. A., Rayburn, H., Crowley, D., Ullman-Culleré, M., Ross, F. P., Coller, B. S., Teitelbaum, S. & Hynes, R. O. β3-integrin-deficient mice are a model for Glanzmann thrombasthenia showing placental defects and reduced survival. *Journal of Clinical Investigation* **103,** 229–238 (1999).

366. Friedlander, M, Theesfeld, C. L., Sugita, M, Fruttiger, M, Thomas, M. A., Chang, S & Cheresh, D. A. Involvement of integrins αvβ3 and αβ5 in ocular neovascular diseases. *Proceedings of the National Academy of Sciences of the United States of America* **93,** 9764–9 (1996).

367. Fotin, A., Cheng, Y., Sliz, P., Grigorieff, N., Harrison, S. C., Kirchhausen, T. & Walz, T. Molecular model for a complete clathrin lattice from electron cryomicroscopy. *Nature* **432,** 573–9 (2004).

368. Pearse, B. M., Smith, C. J. & Owen, D. J. Clathrin coat construction in endocytosis. *Current Opinion in Structural Biology* **10,** 220–228 (2000).

369. Calderwood, D. a., Fujioka, Y., de Pereda, J. M., García-Alvarez, B., Nakamoto, T., Margolis, B., McGlade, C. J., Liddington, R. C., Ginsberg, M. H., Garcia-Alvarez, B., Nakamoto, T., Margolis, B., McGlade, C. J., Liddington, R. C. & Ginsberg, M. H. Integrin β cytoplasmic domain interactions with phosphotyrosine-binding domains: A structural prototype for diversity in integrin signaling. *Proceedings of the National Academy of Sciences of the United States of America* **100,** 2272–2277 (2003).

370. Chao, W.-T. & Kunz, J. Focal adhesion disassembly requires clathrin-dependent endocytosis of integrins. *FEBS Letters* **583,** 1337–1343 (2009).

371. Teckchandani, A., Toida, N., Goodchild, J., Henderson, C., Watts, J., Wollscheid, B. & Cooper, J. A. Quantitative proteomics identifies a Dab2/integrin module regulating cell migration. *Journal of Cell Biology* **186,** 99–111 (2009).

372. Valdembri, D., Caswell, P. T., Anderson, K. I., Schwarz, J. P., König, I., Astanina, E., Caccavari, F., Norman, J. C., Humphries, M. J., Bussolino, F. & Serini, G. Neuropilin-1/GIPC1 signaling regulates α5β1 integrin traffic and function in endothelial cells. *PLoS Biology* **7** (2009).

373. Chao, Y. Y., Jan, C. R., Ko, Y. C., Chen, J. J. & Chen, I. S. Interaction of nocodazole with tubulin isotypes. *Drug Development Research* **55,** 91–96 (2002).

374. Nishimura, T. & Kaibuchi, K. Numb Controls Integrin Endocytosis for Directional Cell Migration with aPKC and PAR-3. *Developmental Cell* **13,** 15–28 (2007).

375. Pellinen, T., Tuomi, S., Arjonen, A., Wolf, M., Edgren, H., Meyer, H., Grosse, R., Kitzing, T., Rantala, J. K., Kallioniemi, O., Fässler, R., Kallio, M. & Ivaska, J. Integrin Trafficking Regulated by Rab21 Is Necessary for Cytokinesis. *Developmental Cell* **15,** 371–385 (2008).

376. Pellinen, T., Arjonen, A., Vuoriluoto, K., Kallio, K., Fransen, J. A. M. & Ivaska, J. Small GTPase Rab21 regulates cell adhesion and controls endosomal traffic of β1-integrins. *Journal of Cell Biology* **173,** 767–780 (2006).

377. Shi, F. & Sottile, J. Caveolin-1-dependent β1 integrin endocytosis is a critical regulator of fibronectin turnover. *Journal of Cell Science* **212,** 2360–2371 (2008).

378. Ng, T., Shima, D., Squire, A., Bastiaens, P. I. H., Gschmeissner, S., Humphries, M. J. & Parker, P. J. PKCα regulates β1 integrin-dependent cell motility through association and control of integrin traffic. *The EMBO Journal* **18,** 3909–3923 (1999).

379. Upla, P., Marjomäki, V., Kankaanpää, P., Ivaska, J., Hyypiä, T. & van der Goot, F. G. Clustering Induces a Lateral Redistribution of α2β1 Integrin from Membrane Rafts to Caveolae and Subsequent Protein Kinase C-dependent Internalization. *Molecular biology of the cell* **15,** 625–636 (2004).

380. Fabbri, M., Di Meglio, S., Gagliani, M. C., Consonni, E., Molteni, R., Bender, J. R., Tacchetti, C. & Pardi, R. Dynamic Partitioning into Lipid Rafts Controls the Endo- Exocytic Cycle of the αL/β2 Integrin, LFA-1, during Leukocyte Chemotaxis. *Molecular Biology of the Cell* **16,** 5793–5803 (2005).

381. Wu, J, Wu, M. C., Zhang, L. F., Lei, J. Y., Feng, L & Jin, J. Identification of binding peptides of the ADAM15 disintegrin domain using phage display. *J Biosci* **34,** 213–220 (2009).

382. Jeon, O. H., Kim, D., Choi, Y. J., Kim, S. H., Choi, W. S. & Kim, D. S. Novel function of human ADAM15 disintegrin-like domain and its derivatives in platelet aggregation. *Thrombosis Research* **119,** 609–619 (2007).

383. Lee, H. D., Koo, B.-H., Kim, Y. H., Jeon, O.-H. & Kim, D.-S. Exosome release of ADAM15 and the functional implications of human macrophage-derived ADAM15 exosomes. *The FASEB Journal* **26,** 3084–3095 (2012).

384. Böhm, B. B., Freund, I., Krause, K., Kinne, R. W. & Burkhardt, H. ADAM15 Adds to Apoptosis Resistance of Synovial Fibroblasts by Modulating Focal Adhesion Kinase Signaling. *Arthritis & Rheumatism* **65,** 2826–2834 (2013).

385. Fried, D., Böhm, B. B., Krause, K. & Burkhardt, H. ADAM15 protein amplifies focal adhesion kinase phosphorylation under genotoxic stress conditions. *The Journal of biological chemistry* **287,** 21214–23 (2012).

386. Mosnier, J.-F., Jarry, A., Bou-Hanna, C., Denis, M. G., Merlin, D. & Laboisse, C. L. ADAM15 upregulation and interaction with multiple binding partners in inflammatory bowel disease. *Laboratory investigation; a journal of technical methods and pathology* **86,** 1064–73 (2006).

387. Toquet, C., Colson, A., Jarry, A., Bezieau, S., Volteau, C., Boisseau, P., Merlin, D., Laboisse, C. L. & Mosnier, J.-F. ADAM15 to α5β1 integrin switch in colon carcinoma cells: a late event in cancer progression associated with tumor dedifferentiation and poor prognosis. *International journal of cancer. Journal international du cancer* **130,** 278–87 (2012).

388. Beck, V., Herold, H., Benge, A., Luber, B., Hutzler, P., Tschesche, H., Kessler, H., Schmitt, M., Geppert, H.-G. & Reuning, U. ADAM15 decreases integrin αvβ3/vitronectin-mediated ovarian cancer cell adhesion and motility in an RGD-dependent fashion. *The international journal of biochemistry & cell biology* **37,** 590–603 (2005).

389. Hall, A. Rho GTPases and the Actin Cytoskeleton. *Science* **279,** 509–514 (1998).

390. Huveneers, S. & Danen, E. H. J. Adhesion signaling - crosstalk between integrins, Src and Rho. *Journal of cell science* **122,** 1059–1069 (2009).

391. Nimnual, A. S., Taylor, L. J. & Bar-Sagi, D. Redox-dependent downregulation of Rho by Rac. *Nature cell biology* **5,** 236–241 (2003).

392. Ohta, Y., Hartwig, J. H. & Stossel, T. P. FilGAP, a Rho- and ROCK-regulated GAP for Rac binds filamin A to control actin remodelling. *Nature cell biology* **8,** 803–814 (2006).

393. Mitra, S. K. & Schlaepfer, D. D. Integrin-regulated FAK-Src signaling in normal and cancer cells. *Current Opinion in Cell Biology* **18,** 516–523 (2006).

394. Chodniewicz, D. & Klemke, R. L. Regulation of integrin-mediated cellular responses through assembly of a CAS/Crk scaffold. *Biochimica et Biophysica Acta - Molecular Cell Research* **1692,** 63–76 (2004).

395. Brugnera, E., Haney, L., Grimsley, C., Lu, M., Walk, S. F., Tosello-Trampont, A.-C., Macara, I. G., Madhani, H., Fink, G. R. & Ravichandran, K. S. Unconventional Rac-GEF activity is mediated through the Dock180-ELMO complex. *Nature cell biology* **4,** 574–582 (2002).

396. Ten Klooster, J. P., Jaffer, Z. M., Chernoff, J. & Hordijk, P. L. Targeting and activation of Rac1 are mediated by the exchange factor β-Pix. *Journal of Cell Biology* **172,** 759–769 (2006).

397. Dráber, P., Sulimenko, V. & Dráberová, E. Cytoskeleton in mast cell signaling. *Frontiers in Immunology* **3,** 1–19 (2012).

398. Mains, P. E., Sulston, I. A. & Wood, W. B. Dominant maternal-effect mutations causing embryonic lethality in Caenorhabditis elegans. *Genetics* **125,** 351–369 (1990).

399. Feng, Q., Baird, D., Peng, X., Wang, J., Ly, T., Guan, J.-L. & Cerione, R. a. Cool-1 functions as an essential regulatory node for EGFreceptor- and Src-mediated cell growth. *Nature Cell Biology* **8,** 945–956 (2006).

400. Arthur, W. T., Petch, L. A. & Burridge, K. Integrin engagement suppresses RhoA activity via a c-Src-dependent mechanism. *Current Biology* **10,** 719–722 (2000).

401. Heasman, S. J. & Ridley, A. J. Mammalian Rho GTPases: new insights into their functions from in vivo studies. *Nature reviews. Molecular cell biology* **9,** 690–701 (2008).

402. Carlier, M. F., Nioche, P., Broutin-L'hermite, I., Boujemaa, R., Le Clainche, C., Egile, C., Garbay, C., Ducruix, A., Sansonetti, P. & Pantaloni, D. GRB2 links signaling to actin assembly by enhancing interaction of neural wiskott-aldrich syndrome protein (N-WASp) with actin-related protein (ARP2/3) complex. *Journal of Biological Chemistry* **275,** 21946–21952 (2000).

403. Spiering, D. & Hodgson, L. Dynamics of the rho-family small GTPases in actin regulation and motility. *Cell Adhesion and Migration* **5,** 170–180 (2011).

404. Bartolini, F., Moseley, J. B., Schmoranzer, J., Cassimeris, L., Goode, B. L. & Gundersen, G. G. The formin mDia2 stabilizes microtubules independently of its actin nucleation activity. *Journal of Cell Biology* **181,** 523–536 (2008).

405. Bhattacharya, M, Babwah, a. V. & Ferguson, S. S. G. Small GTP-binding protein-coupled receptors. *Biochemical Society transactions* **32,** 1040–4 (2004).

406. DeMali, K. a., Wennerberg, K. & Burridge, K. Integrin signaling to the actin cytoskeleton. *Current Opinion in Cell Biology* **15,** 572–582 (2003).

407. Siehler, S. Regulation of RhoGEF proteins by G12/13-coupled receptors. *British journal of pharmacology* **158,** 41–9 (2009).

408. Wang, D., Tan, Y.-c., Kreitzer, G. E., Nakai, Y., Shan, D., Zheng, Y. & Huang, X.-Y. G proteins G12 and G13 control the dynamic turnover of growth factor-induced dorsal ruffles. *The Journal of biological chemistry* **281,** 32660–7 (2006).

409. Miao, H., Li, S., Hu, Y.-L., Yuan, S., Zhao, Y., Chen, B. P. C., Puzon-McLaughlin, W., Tarui, T., Shyy, J. Y.-J., Takada, Y., Usami, S. & Chien, S. Differential regulation of Rho GTPases by β1 and β3 integrins: the role of an extracellular domain of integrin in intracellular signaling. *Journal of cell science* **115,** 2199–206 (2002).

410. Wolfenson, H., Bershadsky, A., Henis, Y. I. & Geiger, B. Actomyosin-generated tension controls the molecular kinetics of focal adhesions. *Journal of Cell Science* **124,** 1425–1432 (2011).

411. Critchley, D. R. Genetic, biochemical and structural approaches to talin function. *Biochemical Society transactions* **33,** 1308–12 (2005).

412. Tadokoro, S., Shattil, S. J., Eto, K., Tai, V., Liddington, R. C., de Pereda, J. M., Ginsberg, M. H. & Calderwood, D. a. Talin binding to integrin β tails: a final common step in integrin activation. *Science* **302,** 103–106 (2003).

413. Kiema, T., Lad, Y., Jiang, P., Oxley, C. L., Baldassarre, M., Wegener, K. L., Campbell, I. D., Ylänne, J. & Calderwood, D. A. The molecular basis of filamin binding to integrins and competition with talin. *Molecular Cell* **21,** 337–347 (2006).

414. Hannigan, G. E., Leung-Hagesteijn, C, Fitz-Gibbon, L, Coppolino, M. G., Radeva, G, Filmus, J, Bell, J. C. & Dedhar, S. Regulation of cell adhesion and anchorage-dependent growth by a new β1-integrin-linked protein kinase. *Nature* **379,** 91–96 (1996).

415. Tu, Y, Li, F, Goicoechea, S & Wu, C. The LIM-only protein PINCH directly interacts with integrin-linked kinase and is recruited to integrin-rich sites in spreading cells. *Molecular and cellular biology* **19,** 2425–2434 (1999).

416. Yamaji, S., Suzuki, A., Sugiyama, Y., Koide, Y. I., Yoshida, M., Kanamori, H., Mohri, H., Ohno, S. & Ishigatsubo, Y. A novel integrin-linked kinase-binding protein, affixin, is involved in the early stage of cell-substrate interaction. *Journal of Cell Biology* **153,** 1251–1264 (2001).

417. Tu, Y, Huang, Y, Zhang, Y, Hua, Y & Wu, C. A new focal adhesion protein that interacts with integrin-linked kinase and regulates cell adhesion and spreading. *The Journal of cell biology* **153,** 585–598 (2001).

418. Nikolopoulos, S. N. & Turner, C. E. Integrin-linked Kinase (ILK) Binding to Paxillin LD1 Motif Regulates ILK Localization to Focal Adhesions. *Journal of Biological Chemistry* **276,** 23499–23505 (2001).

419. Leung-Hagesteijn, C., Mahendra, A., Naruszewicz, I. & Hannigan, G. E. Modulation of integrin signal transduction by ILKAP, a protein phosphatase 2C associating with the integrin-linked kinase, ILK1. *EMBO Journal* **20,** 2160–2170 (2001).

420. Delcommenne, M, Tan, C, Gray, V, Rue, L, Woodgett, J & Dedhar, S. Phosphoinositide-3-OH kinase-dependent regulation of glycogen synthase kinase 3 and protein kinase B/AKT by the integrin-linked kinase. *Proceedings of the National Academy of Sciences of the United States of America* **95,** 11211–11216 (1998).

421. Persad, S, Attwell, S, Gray, V, Delcommenne, M, Troussard, a, Sanghera, J & Dedhar, S. Inhibition of integrin-linked kinase (ILK) suppresses activation of protein kinase B/Akt and induces cell cycle arrest and apoptosis of PTEN-mutant prostate cancer cells. *Proceedings of the National Academy of Sciences of the United States of America* **97,** 3207–3212 (2000).

422. Legate, K. R. & Fässler, R. Mechanisms that regulate adaptor binding to β-integrin cytoplasmic tails. *Journal of cell science* **122,** 187–98 (2009).

423. Westhoff, M. A., Serrels, B, Fincham, V. J., Frame, M. C. & Carragher, N. O. Src-Mediated Phosphorylation of Focal Adhesion Kinase Couples Actin and Adhesion Dynamics to Survival Signaling Src-Mediated Phosphorylation of Focal Adhesion Kinase Couples Actin and Adhesion Dynamics to Survival Signaling. *Mol Cell Biol* **24,** 8113–8133 (2004).

424. Lawson, C., Lim, S. T., Uryu, S., Chen, X. L., Calderwood, D. A. & Schlaepfer, D. D. FAK promotes recruitment of talin to nascent adhesions to control cell motility. *Journal of Cell Biology* **196,** 223–232 (2012).

425. Ling, K., Doughman, R. L., Firestone, A. J., Bunce, M. W. & Anderson, R. a. Type Iγ phosphatidylinositol phosphate kinase targets and regulates focal adhesions. *Nature* **420,** 89–93 (2002).

426. Mitra, S. K., Hanson, D. a. & Schlaepfer, D. D. Focal adhesion kinase: in command and control of cell motility. *Nature reviews. Molecular cell biology* **6,** 56–68 (2005).

427. Felsenfeld, D. P., Schwartzberg, P. L., Venegas, a, Tse, R & Sheetz, M. P. Selective regulation of integrin–cytoskeleton interactions by the tyrosine kinase Src. *Nature cell biology* **1,** 200–206 (1999).

428. Nada, S, Okada, M, MacAuley, A, Cooper, J. A. & Nakagawa, H. Cloning of a complementary DNA for a protein-tyrosine kinase that specifically phosphorylates a negative regulatory site of p60c-src. *Nature* **351,** 69–72 (1991).

429. Imamoto, A. & Soriano, P. Disruption of the csk gene, encoding a negative regulator of Src family tyrosine kinases, leads to neural tube defects and embryonic lethality in mice. *Cell* **73,** 1117–1124 (1993).

430. Li, L., Okura, M. & Imamoto, A. Focal Adhesions Require Catalytic Activity of Src Family Kinases To Mediate Integrin-Matrix Adhesion Focal Adhesions Require Catalytic Activity of Src Family Kinases To Mediate Integrin-Matrix Adhesion. *Mol Cell Biol* **22,** 1203–1217 (2002).

431. Howell, B. W. & Cooper, J. a. Csk suppression of Src involves movement of Csk to sites of Src activity. *Molecular and cellular biology* **14,** 5402–11 (1994).

432. Yam, J. W. P., Ko, F. C. F., Chan, C. Y., Jin, D. Y. & Ng, I. O. L. Interaction of deleted in liver cancer 1 with Tensin2 in caveolae and implications in tumor suppression. *Cancer Research* **66,** 8367–8372 (2006).

433. Braun, A. C. & Olayioye, M. A. Rho regulation: DLC proteins in space and time. *Cellular Signalling* **27,** 1643–1651 (2015).

434. Lo, S. H. Tensin. *International Journal of Biochemistry and Cell Biology* **36,** 31–34 (2004).

435. Lo, S. H., Weisberg, E & Chen, L. B. Tensin: a potential link between the cytoskeleton and signal transduction. *BioEssays : news and reviews in molecular, cellular and developmental biology* **16,** 817–823 (1994).

436. Lo, S. H., Janmey, P. A., Hartwig, J. H. & Chen, L. B. Interactions of tensin with actin and identification of its three distinct actin-binding domains. *Journal of Cell Biology* **125,** 1067–1075 (1994).

437. Katz, B. Z., Zohar, M, Teramoto, H, Matsumoto, K, Gutkind, J. S., Lin, D. C., Lin, S & Yamada, K. M. Tensin can induce JNK and p38 activation. *Biochemical and biophysical research communications* **272,** 717–20 (2000).

438. Deakin, N. O. & Turner, C. E. Paxilin comes of age. *Journal of Cell Science* **121,** 2435–2444 (2008).

439. Parton, R. G. & del Pozo, M. a. Caveolae as plasma membrane sensors, protectors and organizers. *Nature reviews. Molecular cell biology* **14,** 98–112 (2013).

440. Nethe, M. & Hordijk, P. L. A model for phospho-caveolin-1 driven turnover of focal adhesions. *Cell Adhesion and Migration* **5,** 59–64 (2011).

441. Zimnicka, A. M., Husain, Y. S., Shajahan, A. N., Sverdlov, M., Chaga, O., Chen, Z., Toth, P. T., Klomp, J., Karginov, A. V., Tiruppathi, C., Malik, A. B. & Minshall, R. D. Src-dependent phosphorylation of caveolin-1 Tyr-14 promotes swelling and release of caveolae. *Mol Biol Cell* **27,** 2090–2106 (2016).

442. Liu, B. P., Chrzanowska-Wodnicka, M & Burridge, K. Microtubule depolymerization induces stress fibers, focal adhesions, and DNA synthesis via the GTP-binding protein Rho. *Cell adhesion and communication* **5,** 249–255 (1998).

443. Ezratty, E. J., Partridge, M. A. & Gundersen, G. G. Microtubule-induced focal adhesion disassembly is mediated by dynamin and focal adhesion kinase. *Nature cell biology* **7,** 581–590 (2005).

444. American Type Culture Collection. *MDA-MB-231* <http://www.lgcstandards-atcc.org/products/all/HTB-26.aspx?> (visited on 11/22/2015).

445. Satya-Prakash, K. L., Pathak, S, Hsu, T. C., Olivé, M & Cailleau, R. Cytogenetic analysis on eight human breast tumor cell lines: high frequencies of 1q, 11q and HeLa-like marker chromosomes. *Cancer genetics and cytogenetics* **3,** 61–73 (1981).

446. Neve, R. M., Chin, K., Fridlyand, J., Baehner, F. L., Yeh, J., Fevr, T., Clark, L., Bayani, N., Coppe, J.-P. P., Speed, T., Tong, F., Spellman, P. T., DeVries, S., Lapuk, A., Wang, N. J., Kuo, W.-L. L., Stilwell, J. L., Pinkel, D., Albertson, D. G., Waldman, F. M., McCormick, F., Dickson, R. B., Johnson, M. D., Lippman, M., Ethier, S., Gazdar, A. & Gray, J. W. A collection of breast cancer cell lines for the study of functionally distinct cancer subtypes. *Cancer cell* **10,** 515–527 (2006).

447. Price, J. E., Polyzos, a, Dan Zhang, R & Daniels, L. M. Tumorigenicity and metastasis of human breast carcinoma cell lines in nude mice. *Cancer research* **50,** 717 (1990).

448. Walker, E. H., Pacold, M. E., Perisic, O., Stephens, L., Hawkins, P. T., Wymann, M. P. & Williams, R. L. Structural Determinants of Phosphoinositide 3-Kinase Inhibition by Wortmannin, LY294002, Quercetin, Myricetin, and Staurosporine. *Molecular Cell* **6,** 909–919 (2000).

449. Knight, Z. A., Chiang, G. G., Alaimo, P. J., Kenski, D. M., Ho, C. B., Coan, K., Abraham, R. T. & Shokat, K. M. Isoform-specific phosphoinositide 3-kinase inhibitors from an arylmorpholine scaffold. *Bioorganic and Medicinal Chemistry* **12,** 4749–4759 (2004).

450. Raynaud, F. I., Eccles, S. A., Patel, S., Alix, S., Box, G., Chuckowree, I., Folkes, A., Gowan, S., De Haven Brandon, A., Di Stefano, F., Hayes, A., Henley, A. T., Lensun, L., Pergl-Wilson, G., Robson, A., Saghir, N., Zhyvoloup, A., McDonald, E., Sheldrake, P., Shuttleworth, S., Valenti, M., Wan, N. C., Clarke, P. A. & Workman, P. Biological properties of potent inhibitors of class I phosphatidylinositide 3-kinases: from PI-103 through PI-540, PI-620 to the oral agent GDC-0941. *Molecular cancer therapeutics* **8,** 1725–38 (2009).

451. Knight, Z. A., Gonzalez, B., Feldman, M. E., Zunder, E. R., Goldenberg, D. D., Williams, O., Loewith, R., Stokoe, D., Balla, A., Toth, B., Balla, T., Weiss, W. A., Williams, R. L. & Shokat, K. M. A Pharmacological Map of the PI3-K Family Defines a Role for p110α in Insulin Signaling. *Cell* **125,** 733–747 (2006).

452. Vézina, C., Kudelski, A. & Sehegal, S. N. Rapamycin (AY-22,989), a new antifungal antibiotic. I. Taxonomy of the producing streptomycete and isolation of the active principle. *The Journal of Antibiotics* **28,** 721–726 (1975).

453. Heitman, J, Movva, N. R. & Hall, M. N. Targets for cell cycle arrest by the immunosuppressant rapamycin in yeast. *Science (New York, N.Y.)* **253,** 905–909 (1991).

454. Brown, E. J., Albers, M. W., Shin, T. B., Ichikawa, K, Keith, C. T., Lane, W. S. & Schreiber, S. L. A mammalian protein targeted by G1-arresting rapamycin-receptor complex. *Nature* **369,** 756–758 (1994).

455. García-Martínez, J. M., Moran, J., Clarke, R. G., Gray, A., Cosulich, S. C., Chresta, C. M. & Alessi, D. R. Ku-0063794 is a specific inhibitor of the mammalian target of rapamycin (mTOR). *The Biochemical journal* **421,** 29–42 (2009).

456. Saalfeld, S. *Enhance Local Contrast (CLAHE)* 2010. <`http://fiji.sc/Enhance{\_}Local{\_}Contrast{\_}(CLAHE)`> (visited on 01/01/2015).

457. Zuiderveld, K. in *Graphics gems IV* 474–485 (Academic Press Professional, Inc., San Diego, CA, USA, 1994).

458. Sage, D., Neumann, F. R., Hediger, F., Gasser, S. M. & Unser, M. Automatic tracking of individual fluorescence particles: application to the study of chromosome dynamics. *IEEE Transactions on Image Processing* **14,** 1372–1383 (2005).

459. Yen, J. C., Chang, F. J. & Chang, S. A new criterion for automatic multilevel thresholding. *IEEE Transactions on Image Processing* **4,** 370–378 (1995).

460. Sezgin, M. & Sankur, B. Survey over image thresholding techniques and quantitative performance evaluation Mehmet. *Journal of Electronic Imaging* **13,** 146–165 (2004).

461. Longobardi Givan, A. in *Flow Cytometry - First principles* 2nd, 15–31 (Wiley-Liss, New York, NY, 2001).

462. Givan, A. L. in *Flow Cytometry Protocols* (eds Hawley, T. S. & Hawley, R. G.) 3rd, 1–30 (Humana Press, London, 2011).

463. Meade, S. O., Godin, J., Chen, C.-H., Cho, S. H., Tsai, F. S., Qiao, W. & Lo, Y.-H. in *Advanced Optical Flow Cytometry - Methods and Disease Diagnoses* (ed Tuchin, V. V.) 273–310 (Wiley-VCH Verlag & Co. KGaA, Weinheim, 2011).

464. The 1000 Genomes Project Consortium. A map of human genome variation from population scale sequencing. *Nature* **476,** 1061–1073 (2010).

465. Scrimieri, F., Calhoun, E. S., Patel, K., Gupta, R., Huso, D. L., Hruban, R. H. & Kern, S. E. FAM190A rearrangements provide a multitude of individualized tumor signatures and neo-antigens in cancer. *Oncotarget* **2,** 69–75 (2011).

466. Patel, K., Scrimieri, F., Ghosh, S., Zhong, J., Kim, M.-S., Ren, Y. R., Morgan, R. a., Iacobuzio-Donahue, C. a., Pandey, A. & Kern, S. E. FAM190A Deficiency Creates a Cell Division Defect. *The American journal of pathology* **183,** 1–9 (2013).

467. Heijink, A. M., Blomen, V. A., Bisteau, X., Degener, F., Matsushita, F. Y., Kaldis, P., Foijer, F. & van Vugt, M. A. T. M. A haploid genetic screen identifies the G1/S regulatory machinery as a determinant of Wee1 inhibitor sensitivity. *Proceedings of the National Academy of Sciences* **112,** 15160–15165 (2015).

468. Vanhaecke, T., Papeleu, P., Elaut, G. & Rogiers, V. Trichostatin A-like hydroxamate histone deacetylase inhibitors as therapeutic agents: toxicological point of view. *Current medicinal chemistry* **11,** 1629–43 (2004).

469. Lodish, H., Berk, A., Matsudaira, P., Kaiser, C. A., Krieger, M., Scott, M. P., Zipursky, L. & Darnell, J. in *Molecular Cell Biology* 5th, 1–28 (Palgrave Macmillan, Basingstoke, 2004).

470. Weinberg, R. A. The retinoblastoma protein and cell cycle control. *Cell* **81,** 323–330 (1995).

471. Yamazaki, D., Kurisu, S. & Takenawa, T. Regulation of cancer cell motility through actin reorganization. *Cancer science* **96,** 379–86 (2005).

472. Yin, J., Lu, J. & Yu, F.-S. X. Role of Small GTPase Rho in Regulating Corneal Epithelial Wound Healing. *Investigative Ophthalmology and Visual Science* **49,** 900–909 (2008).

473. Pellegrin, S. & Mellor, H. Rho GTPase activation assays. *Current Protocols in Cell Biology,* 1–19 (2008).

474. Pertz, O., Hodgson, L., Klemke, R. L. & Hahn, K. M. Spatiotemporal dynamics of RhoA activity in migrating cells. *Nature* **440,** 1069–72 (2006).

475. Lakhani, V. V., Hinde, E., Gratton, E. & Elston, T. C. Spatio-temporal regulation of Rac1 mobility by actin islands. *PLoS ONE* **10,** 1–14 (2015).

476. Aspenstrom, P, Fransson, A & Saras, J. Rho GTPases have diverse effects on the organization of the actin filament system. *The Biochemical journal* **377,** 327–337 (2004).

477. Guasch, R. M., Scambler, P, Jones, G. E. & Ridley, A. J. RhoE regulates actin cytoskeleton organization and cell migration. *Molecular and cellular biology* **18,** 4761–71 (1998).

478. De Araujo, R. M. S., Oba, Y., Kuroda, S., Tanaka, E. & Moriyama, K. RhoE regulates actin cytoskeleton organization in human periodontal ligament cells under mechanical stress. *Archives of Oral Biology* **59,** 187–192 (2014).

479. Foster, R., Hu, K.-Q. Q., Lu, Y., Nolan, K. M., Thissen, J. & Settleman, J. Identification of a novel human Rho protein with unusual properties: GTPase deficiency and in vivo farnesylation. *Molecular and cellular biology* **16,** 2689–2699 (1996).

480. Weed, S. A. & Parsons, J. T. Cortactin: coupling membrane dynamics to cortical actin assembly. *Oncogene* **20,** 6418–6434 (2001).

481. Maekawa, M. Signaling from Rho to the Actin Cytoskeleton Through Protein Kinases ROCK and LIM-kinase. *Science* **285,** 895–898 (1999).

482. DerMardirossian, C., Rocklin, G., Seo, J.-Y. & Bokoch, G. M. Phosphorylation of RhoGDI by Src Regulates Rho GTPase Binding and Cytosol-Membrane Cycling. *Molecular biology of the Cell* **17,** 4760–4768 (2006).

483. Murphy, D. A. & Courtneidge, S. A. The 'ins' and 'outs' of podosomes and invadopodia: characteristics, formation and function. *Nature reviews. Molecular cell biology* **12,** 413–26 (2011).

484. Anderl, J., Ma, J. & Armstrong, L. *Fluorescent Gelatin Degradation-Assays for Investigating-Invadopodia Formation* 2012. <http://www.nature.com/app{_}notes/nmeth/2012/121007/pdf/an8622.pdf>.

485. Shikatani, E. A., Trifonova, A., Mandel, E. R., Liu, S. T. K., Roudier, E., Krylova, A., Szigiato, A., Beaudry, J., Riddell, M. C. & Haas, T. L. Inhibition of proliferation, migration and proteolysis contribute to corticosterone-mediated inhibition of angiogenesis. *PloS one* **7,** e46625 (2012).

486. Tomasz, M. Mitomycin C: Small, fast and deadly (but very selective). *Chemistry and Biology* **2,** 575–579 (1995).

487. Alberts, B., Johnson, A., Lewis, J., Raff, M., Roberts, K. & Walter, P. *Molecular Biology of the Cell* 5th editio, 1115 (Garland Science, 2008).

488. Eriksson, J. E., Dechat, T., Grin, B., Helfand, B., Mendez, M., Pallari, H.-m. & Goldman, R. D. Review series Introducing intermediate filaments : from discovery to disease. **119** (2009).

489. Kojima, T., Takano, K.-i., Yamamoto, T., Murata, M., Son, S., Imamura, M., Yamaguchi, H., Osanai, M., Chiba, H., Himi, T. & Sawada, N. Transforming growth factor-β induces epithelial to mesenchymal transition by down-regulation of claudin-1 expression and the fence function in adult rat hepatocytes. *Liver international : official journal of the International Association for the Study of the Liver* **28,** 534–45 (2008).

490. Singh, A. B. & Harris, R. C. Epidermal Growth Factor Receptor Activation Differentially Regulates Claudin Expression and Enhances Transepithelial Resistance in Madin-Darby Canine Kidney Cells. *Journal of Biological Chemistry* **279,** 3543–3552 (2004).

491. Hu, L.-L. *STAT3 in intestinal epithelial cells regulates barrier function and anti-bacterial response* PhD thesis (University of California, 2009), 1–74.

492. Pope, J. L., Bhat, A. A., Sharma, A., Ahmad, R., Krishnan, M., Washington, M. K., Beauchamp, R. D., Singh, A. B. & Dhawan, P. Claudin-1 Regulates Intestinal Epithelial Homeostasis through the Modulation of Notch Signaling. *Gut* **4,** 622–634 (2011).

493. Wanger, T. M., Dewitt, S., Collins, A., Maitland, N. J., Poghosyan, Z. & Knäuper, V. Differential regulation of TROP2 release by PKC isoforms through vesicles and ADAM17. *Cellular Signalling* **27,** 1325–1335 (2015).

494. Dodd, K. M., Yang, J, Shen, M. H., Sampson, J. R. & Tee, a. R. mTORC1 drives HIF-1α and VEGF-A signalling via multiple mechanisms involving 4E-BP1, S6K1 and STAT3. *Oncogene* **34,** 1–12 (2014).

495. Davis, T., Brook, A. J. C., Rokicki, M. J., Bagley, M. C. & Kipling, D. Evaluating the Role of p38 MAPK in the Accelerated Cell Senescence of Werner Syndrome Fibroblasts. *Pharmaceuticals* **9,** 23 (2016).

496. Stephens, P., Grenard, P., Aeschlimann, P., Langley, M., Blain, E., Errington, R., Kipling, D., Thomas, D. & Aeschlimann, D. Crosslinking and G-protein functions of transglutaminase 2 contribute differentially to fibroblast wound healing responses. *Journal of cell science* **117,** 3389–403 (2004).

497. Boller, K., Vestweber, D. & Kemler, R. Cell-adhesion molecule uvomorulin is localized in the intermediate junctions of adult intestinal epithelial cells. *Journal of Cell Biology* **100,** 327–332 (1985).

498. Otto, T, Rembrink, K, Goepel, M, Meyer-Schwickerath, M & Rübben, H. E-cadherin: a marker for differentiation and invasiveness in prostatic carcinoma. *Urological research* **21,** 359–62 (1993).

499. Hajra, K. M., Chen, D. Y.-s. & Fearon, E. R. The SLUG Zinc-Finger Protein Represses E-Cadherin in Breast Cancer Advances in Brief The SLUG Zinc-Finger Protein Represses E-Cadherin in Breast Cancer 1. *Cancer Research* **62,** 1613–1618 (2002).

500. Franke, W. W., Schmid, E., Osborn, M. & Weber, K. Intermediate-sized filaments of human endothelial cells. *Journal of Cell Biology* **81,** 570–580 (1979).

501. Balda, M. S. & Matter, K. The tight junction protein ZO-1 and an interacting transcription factor regulate ErbB-2 expression. *The EMBO journal* **19,** 2024–2033 (2000).

502. Balda, M. S., Garrett, M. D. & Matter, K. The ZO-1-associated Y-box factor ZONAB regulates epithelial cell proliferation and cell density. *Journal of Cell Biology* **160,** 423–432 (2003).

503. Matter, K. & Balda, M. S. Signalling to and from tight junctions. *Nature reviews. Molecular cell biology* **4,** 225–236 (2003).

504. Matter, K. & Balda, M. S. Functional analysis of tight junctions. *Methods* **30,** 228–234 (2003).

505. Srinivasan, B., Kolli, A. R., Esch, M. B., Abaci, H. E., Shuler, M. L. & Hickman, J. J. *Systems* **2,** 107–126 (2016).

506. Balda, M. S. & Matter, K. *Size-selective assessment of tight junction paracellular permeability using fluorescently labelled dextrans* tech. rep. 3401 (2007).

507. Fanning, A. S., Jameson, B. J., Lynne, a, Anderson, J. M., Jesaitis, L. a. & Melvin, J. CELL BIOLOGY AND METABOLISM : The Tight Junction Protein ZO-1 Establishes a Link between the Transmembrane Protein Occludin and the Actin Cytoskeleton The Tight Junction Protein ZO-1 Establishes a Link between the Transmembrane Protein Occludin and the Ac. **273,** 29745–29753 (1998).

508. Wachtel, M, Frei, K, Ehler, E, Fontana, a, Winterhalter, K & Gloor, S. M. Occludin proteolysis and increased permeability in endothelial cells through tyrosine phosphatase inhibition. *Journal of cell science* **112 (Pt 2,** 4347–56 (1999).

509. Liu, J., Jin, X., Liu, K. J. & Liu, W. Matrix Metalloproteinase-2-Mediated Occludin Degradation and Caveolin-1-Mediated Claudin-5 Redistribution Contribute to Blood-Brain Barrier Damage in Early Ischemic Stroke Stage. *Journal of Neuroscience* **32,** 3044–3057 (2012).

510. French, A. D., Fiori, J. L., Camilli, T. C., Leotlela, P. D., O'Connell, M. P., Frank, B. P., Subaran, S., Indig, F. E., Taub, D. D. & Weeraratna, A. T. PKC and PKA Phosphorylation Affect the Subcellular Localization of Claudin-1 in Melanoma Cells. *International Journal of Medical Sciences* **6,** 93–101 (2009).

511. Jian, Y., Chen, C., Li, B. & Tian, X. Delocalized Claudin-1 promotes metastasis of human osteosarcoma cells. *Biochemical and Biophysical Research Communications* **466,** 356–361 (2015).

512. Li, L., Sampat, K., Hu, N., Zakari, J. & Yuspa, S. H. Protein kinase C negatively regulates Akt activity and modifies UVC-induced apoptosis in mouse keratinocytes. *Journal of Biological Chemistry* **281,** 3237–3243 (2006).

513. Gentili, C., Morelli, S. & De Boland, A. R. Involvement of PI3-kinase and its association with c-Src in PTH-stimulated rat enterocytes. *Journal of Cellular Biochemistry* **86,** 773–783 (2002).

514. Lei, J. & Ingbar, D. H. Src kinase integrates PI3K/Akt and MAPK/ERK1/2 pathways in T3-induced Na-K-ATPase activity in adult rat alveolar cells. *American journal of physiology. Lung cellular and molecular physiology* **301,** L765–71 (2011).

515. Holleran, J. L., Egorin, M. J., Zuhowski, E. G., Parise, R. A., Musser, S. M. & Pan, S. S. Use of high-performance liquid chromatography to characterize the rapid decomposition of wortmannin in tissue culture media. *Analytical Biochemistry* **323,** 19–25 (2003).

516. Zhang, G. J., Xiao, H. X., Tian, H. P., Liu, Z. L., Xia, S. S. & Zhou, T. Upregulation of microRNA-155 promotes the migration and invasion of colorectal cancer cells through the regulation of claudin-1 expression. *International Journal of Molecular Medicine* **31,** 1375–1380 (2013).

517. Izraely, S., Sagi-Assif, O., Klein, A., Meshel, T., Ben-Menachem, S., Zaritsky, A., Ehrlich, M., Prieto, V. G., Bar-Eli, M., Pirker, C., Berger, W., Nahmias, C., Couraud, P.-O., Hoon, D. S. B. & Witz, I. P. The Metastatic Microenvironment: Claudin-1 Suppresses the Malignant Phenotype of Melanoma Brain Metastasis. *International journal of cancer. Journal international du cancer* **00,** 1–12 (2014).

518. Shiozaki, A., Shimizu, H., Ichikawa, D., Konishi, H., Komatsu, S., Kubota, T., Fujiwara, H., Okamoto, K., Iitaka, D., Nakashima, S., Nako, Y., Liu, M. & Otsuji, E. Claudin 1 mediates tumor necrosis factor alpha-induced cell migration in human gastric cancer cells. *World Journal of Gastroenterology* **20,** 17863–17876 (2014).

519. Shiozaki, A., Bai, X.-h., Shen-Tu, G., Moodley, S., Takeshita, H., Fung, S.-Y., Wang, Y., Keshavjee, S. & Liu, M. Claudin 1 mediates TNFα-induced gene expression and cell migration in human lung carcinoma cells. *PloS one* **7,** e38049 (2012).

520. Zhang, K., Yao, H. P. & Wang, M. H. Activation of RON differentially regulates claudin expression and localization: Role of claudin-1 in RON-mediated epithelial cell motility. *Carcinogenesis* **29,** 552–559 (2008).

521. Friedl, P. & Gilmour, D. Collective cell migration in morphogenesis, regeneration and cancer. *Nature reviews. Molecular cell biology* **10,** 445–457 (2009).

522. Rørth, P. Collective cell migration. *Annual review of cell and developmental biology* **25,** 407–29 (2009).

523. Du Roure, O., Saez, A., Buguin, A., Austin, R. H., Chavrier, P., Silberzan, P. & Ladoux, B. Force mapping in epithelial cell migration. *Proceedings of the National Academy of Sciences of the United States of America* **102,** 2390–2395 (2005).

524. Villari, G., Jayo, A., Zanet, J., Fitch, B., Serrels, B., Frame, M., Stramer, B. M., Goult, B. T. & Parsons, M. A direct interaction between fascin and microtubules contributes to adhesion dynamics and cell migration. *Journal of cell science* **128,** 4601–4614 (2015).

525. Yu, D. H., Qu, C. K., Henegariu, O., Lu, X. & Feng, G. S. Protein-tyrosine phosphatase Shp-2 regulates cell spreading, migration, and focal adhesion. *Journal of Biological Chemistry* **273,** 21125–21131 (1998).

526. Hartman, Z. R., Schaller, M. D. & Agazie, Y. M. The tyrosine phosphatase SHP2 regulates focal adhesion kinase to promote EGF-induced lamellipodia persistence and cell migration. *Molecular cancer research* **11,** 651–64 (2013).

527. Zhang, Z., Lin, S. Y., Neel, B. G. & Haimovich, B. Phosphorylated α-actinin and protein-tyrosine phosphatase 1B coregulate the disassembly of the focal adhesion kinase·Src complex and promote cell migration. *Journal of Biological Chemistry* **281,** 1746–1754 (2006).

528. Zheng, Y, Yang, W, Xia, Y, Hawke, D, Liu, D. X. & Lu, Z. Ras-induced and extracellular signal-regulated kinase 1 and 2 phosphorylation-dependent isomerization of protein tyrosine phosphatase (PTP)-PEST by PIN1 promotes FAK dephosphorylation by PTP-PEST. *Mol Cell Biol* **31,** 4258–4269 (2011).

529. Lundmark, R. & Carlsson, S. R. Regulated membrane recruitment of dynamin-2 mediated by sorting nexin 9. *Journal of Biological Chemistry* **279,** 42694–42702 (2004).

530. Roberts, M. S., Woods, A. J., Dale, T. C., Van Der Sluijs, P. & Norman, J. C. Protein kinase B/Akt acts via glycogen synthase kinase 3 to regulate recycling of αvβ3 and α5β1 integrins. *Molecular and cellular biology* **24,** 1505–1515 (2004).

531. Li, J., Ballif, B. A., Powelka, A. M., Dai, J., Gygi, S. P. & Hsu, V. W. Phosphorylation of ACAP1 by Akt regulates the stimulation-dependent recycling of integrin β1 to control cell migration. *Developmental Cell* **9,** 663–673 (2005).

532. Li, J., Peters, P. J., Bai, M., Dai, J., Bos, E., Kirchhausen, T., Kandror, K. V. & Hsu, V. W. An ACAP1-containing clathrin coat complex for endocytic recycling. *Journal of Cell Biology* **178,** 453–464 (2007).

533. Ivaska, J., Whelan, R. D. H., Watson, R. & Parker, P. J. PKCε controls the traffic of β1 integrins in motile cells. *EMBO Journal* **21,** 3608–3619 (2002).

534. Ivaska, J., Vuoriluoto, K., Huovinen, T., Izawa, I., Inagaki, M. & Parker, P. J. PKCepsilon-mediated phosphorylation of vimentin controls integrin recycling and motility. *The EMBO journal* **24,** 3834–3845 (2005).

535. Lemjabbar-Alaoui, H., Sidhu, S. S., Mengistab, A., Gallup, M. & Basbaum, C. TACE/ADAM-17 phosphorylation by PKC-epsilon mediates premalignant changes in Tobacco smoke-exposed lung cells. *PLoS ONE* **6** (2011).

536. Leyme, a., Bourd-Boittin, K., Bonnier, D., Falconer, a., Arlot-Bonnemains, Y. & Theret, N. Identification of ILK as a new partner of the ADAM12 disintegrin and metalloprotease in cell adhesion and survival. *Molecular Biology of the Cell* **23,** 3461–3472 (2012).

537. Danen, E. H. J., Sonneveld, P., Brakebusch, C., Fässler, R. & Sonnenberg, A. The fibronectin-binding integrins α5β1 and αvβ3 differentially modulate RhoA-GTP loading, organization of cell matrix adhesions, and fibronectin fibrillogenesis. *Journal of Cell Biology* **159,** 1071–1086 (2002).

538. Pytela, R., Pierschbacher, M. D. & Ruoslahti, E. Identification and isolation of a 140 kd cell surface glycoprotein with properties expected of a fibronectin receptor. *Cell* **40,** 191–198 (1985).

539. Horton, M. a. The αvβ3 integrin "vitronectin receptor". *The international journal of biochemistry & cell biology* **29,** 721–725 (1997).

540. Goldsmith, E. C., Carver, W., McFadden, A., Goldsmith, J. G., Price, R. L., Sussman, M., Lorell, B. H., Cooper, G. & Borg, T. K. Integrin shedding as a mechanism of cellular adaptation during cardiac growth. *American journal of physiology. Heart and circulatory physiology* **284,** H2227–34 (2003).

541. Gjelstrup, L. C., Boesen, T., Kragstrup, T. W., Jørgensen, A., Klein, N. J., Thiel, S., Deleuran, B. W. & Vorup-Jensen, T. Shedding of large functionally active CD11/CD18 Integrin complexes from leukocyte membranes during synovial inflammation distinguishes three types of arthritis through differential epitope exposure. *Journal of immunology (Baltimore, Md. : 1950)* **185,** 4154–68 (2010).

542. Gomez, I. G., Tang, J., Wilson, C. L., Yan, W., Heinecke, J. W., Harlan, J. M. & Raines, E. W. Metalloproteinase-mediated shedding of integrin β2 promotes macrophage efflux from inflammatory sites. *Journal of Biological Chemistry* **287,** 4581–4589 (2012).

543. Kariya, Y. & Gu, J. N-glycosylation of β4 integrin controls the adhesion and motility of keratinocytes. *PLoS ONE* **6** (2011).

544. Gill, D. J., Chia, J., Senewiratne, J. & Bard, F. Regulation of O-glycosylation through Golgi-to-ER relocation of initiation enzymes. *Journal of Cell Biology* **189,** 843–858 (2010).

545. Parsons, J. T., Martin, K. H., Slack, J. K., Taylor, J. M. & Weed, S. a. Focal adhesion kinase: a regulator of focal adhesion dynamics and cell movement. *Oncogene* **19,** 5606–13 (2000).

546. Arias-Salgado, E. G., Lizano, S., Sarkar, S., Brugge, J. S., Ginsberg, M. H. & Shattil, S. J. Src kinase activation by direct interaction with the integrin β cytoplasmic domain. *Proceedings of the National Academy of Sciences of the United States of America* **100,** 13298–302 (2003).

547. Vespa, A., Darmon, A. J., Turner, C. E., D'Souza, S. J. A. & Dagnino, L. Ca2+-dependent localization of integrin-linked kinase to cell junctions in differentiating keratinocytes. *Journal of Biological Chemistry* **278,** 11528–11535 (2003).

548. Vespa, A., D'Souza, S. J. A. & Dagnino, L. A Novel Role for Integrin-linked Kinase in Epithelial Sheet Morphogenesis. *Molecular Biology of the Cell* **16,** 4084–4095 (2005).

549. Widmaier, M., Rognoni, E., Radovanac, K., Azimifar, S. B. & Fassler, R. Integrin-linked kinase at a glance. *Journal of Cell Science* **125,** 1839–1843 (2012).

550. Legate, K. R., Montañez, E., Kudlacek, O. & Fässler, R. ILK, PINCH and parvin: the tIPP of integrin signalling. *Nature reviews. Molecular cell biology* **7,** 20–31 (2006).

551. Arjonen, A., Alanko, J., Veltel, S. & Ivaska, J. Distinct Recycling of Active and Inactive β1 Integrins. *Traffic* **13,** 610–625 (2012).

552. Roberts, M., Barry, S., Woods, A., Van der Sluijs, P. & Norman, J. PDGF-regulated rab4-dependent recycling of αvβ3 integrin from early endosomes is necessary for cell adhesion and spreading. *Current Biology* **11,** 1392–1402 (2001).

553. Jayo, A. & Parsons, M. Imaging of cell adhesion events in 3D matrix environments. *European Journal of Cell Biology* **91,** 824–833 (2012).

554. Kubow E. Kristopher, H. A. R., Kubow, K. E., Horwitz, A. R. & Kubow E. Kristopher, H. A. R. Reducing background fluorescence reveals adhesion in 3D matrices. *Nature Cell Biology* **13,** 3–7 (2011).

555. Kleifeld, O., Doucet, A., Kizhakkedathu, J & Overall, C. M. System-wide proteomic identification of protease cleavage products by terminal amine isotopic labeling of substrates. *Nature Protocols* **28,** 1578–1611 (2010).

Chapter 9

Appendix

9.1 Supplementary Data

9.1.1 Negative controls of claudin1 co-localisation experiment

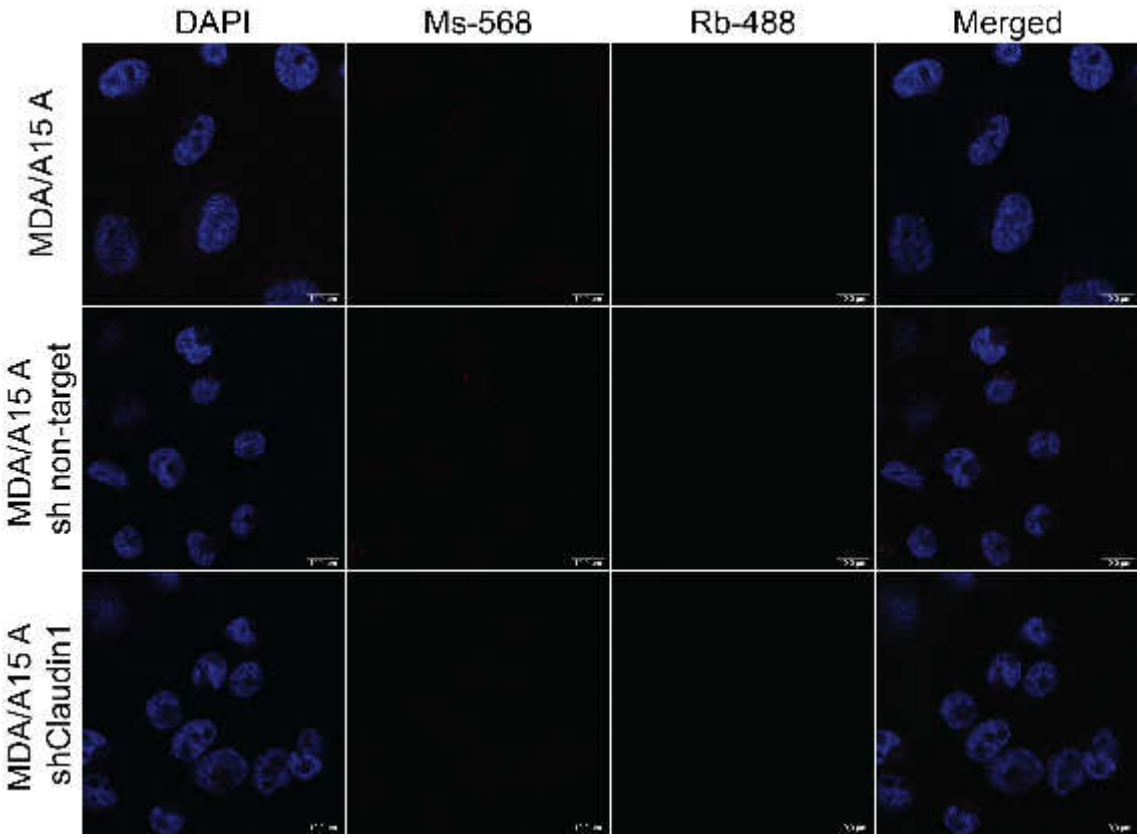

Figure 9.1: Control images of ADAM15 and claudin1 co-localisation in MDA/A15 A, MDA/A15 A non-target shRNA and MDA/A15 A shClaudin1 expressing cells. Columns from left to right: DAPI, Ms-568 (goat), Rb-488 (goat) and merged image. Scale bar = 10 µm

9.1.2 Negative controls of antibody validation experiment

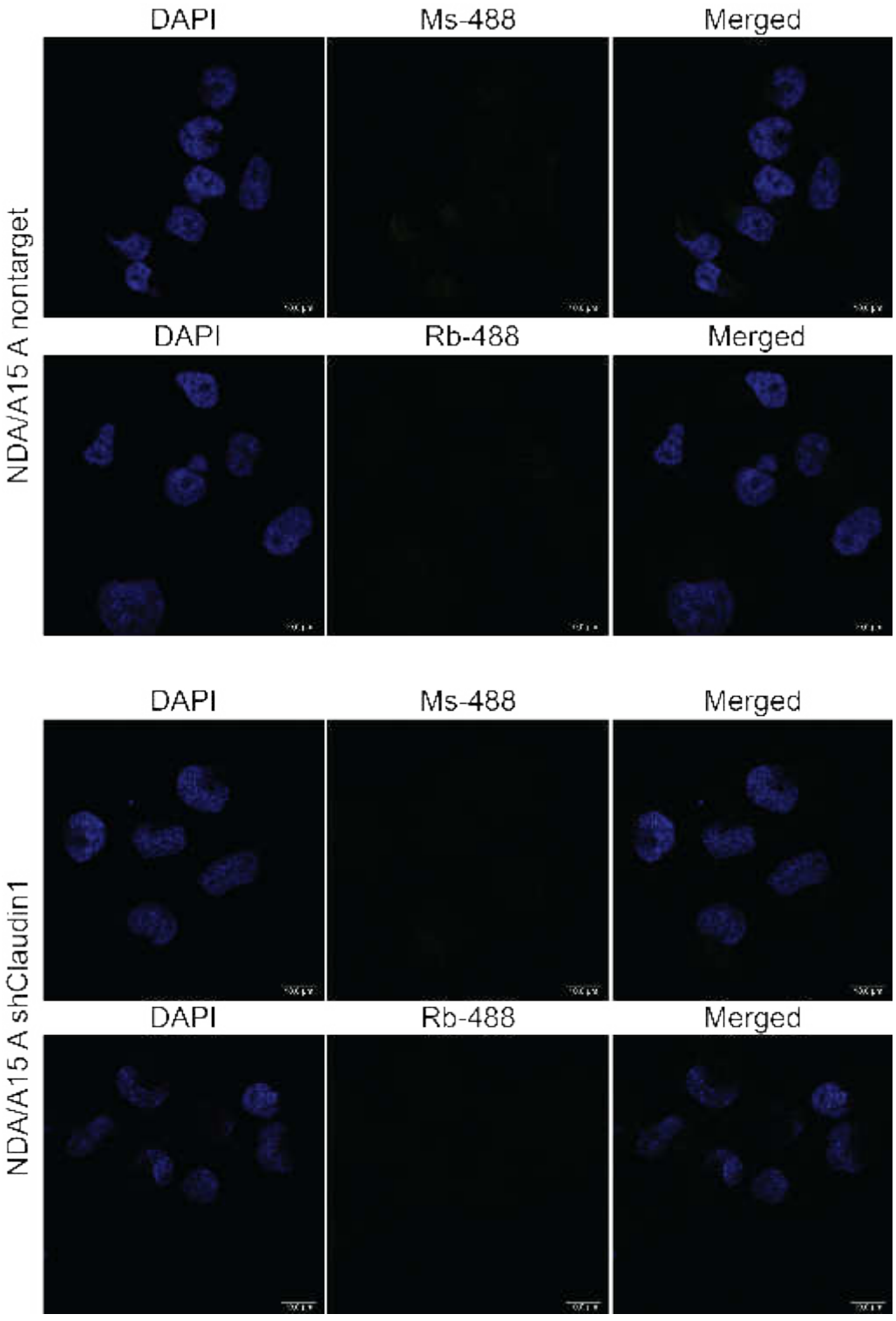

Figure 9.2: Negative controls of claudin1 antibody validation in MDA/A15 A non-target shRNA and shClaudin1 expressing cells. Left column: DAPI staining; Middle column: α-Ms- or Rb-488 (goat); Right column: Merged images. Scale bar = 10 µm

9.1.3 Negative controls of the focal adhesion disassembly assay

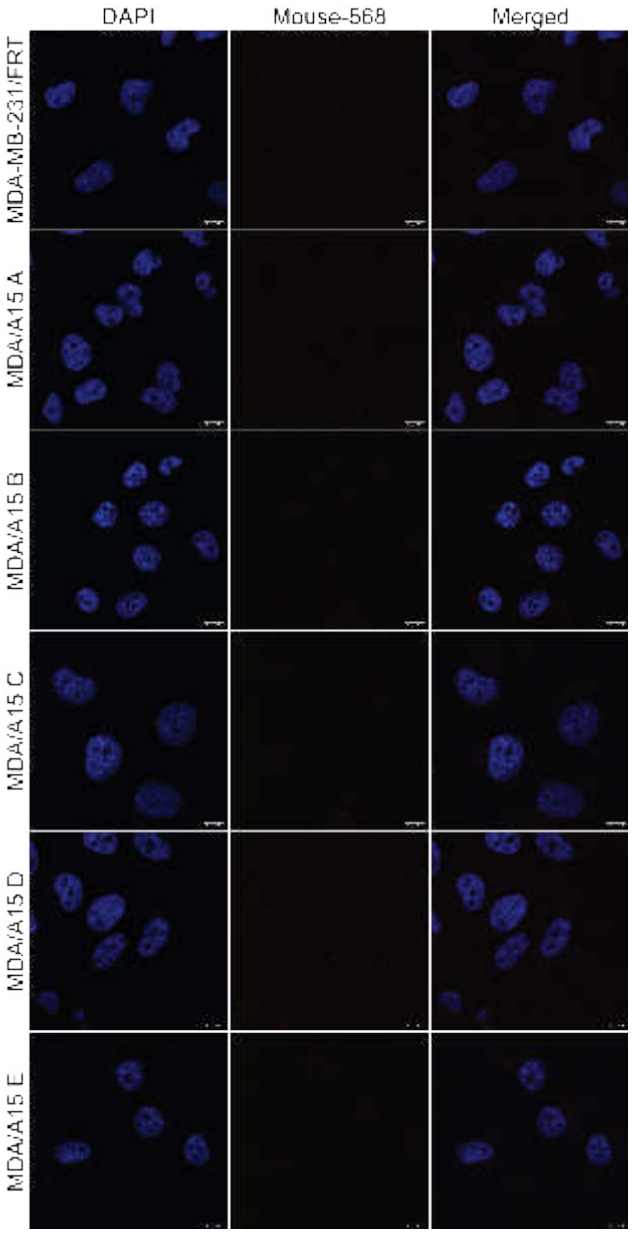

Figure 9.3: Negative controls of MDA/FRT and MDA/A15 A-E WT expressing cells for focal adhesion disassembly assay. Slides were exactly treated as the analysed once but the primary antibody incubation was done with 1% BSA. Left column: DAPI staining; Middle column: α – mouse – 568 (goat); Right column: Merged images. Scale bar = 10 μm

9.1.4 FAK and Src phosphorylation in MDA/FRT and MDA/ADAM15 WT isoform expressing cells

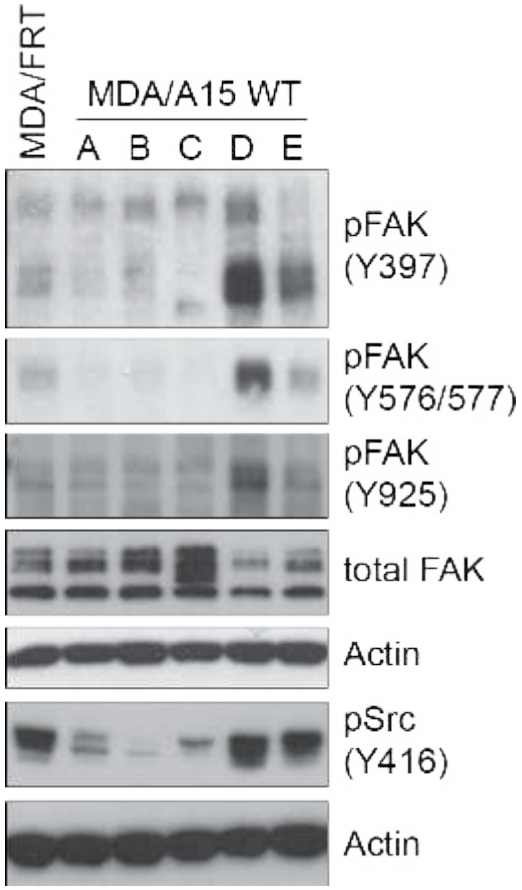

Figure 9.4: Preliminary western blot analysis of FAK and Src phosphorylation in MDA/FRT and MDA/ADAM15 WT isoform expressing cells. Exponential growing cells were lysed and subjected to protein analysis. A summary of the used antibodies is shown in table 9.1. n=1

Table 9.1: Detailed information about antibodies used to detect FAK and Src phosphorylation

Antibody	**Supplier**	**Catalogue number**	**Source**	**Detected band(s)**	**Primary antibody dilution**	**Secondary antibody dilution**
Actin	Sigma	A2066	Rabbit	42 kDa	1:4,000	1:5,000
FAK[1]	SantaCruz	sc-557	Rabbit	125 kDa	1:1,000	1:5,000
pFAK (Y397)[1]	Invitrogen	44-624G	Rabbit	125 kDa	1:1,000	1:5,000
pFAK (Y576/577)	CST	#3281	Rabbit	125 kDa	1:1,000	1:5,000
pFAK (Y925)	CST	#3284	Rabbit	125 kDa	1:1,000	1:5,000
pSrc (Y416)	CST	#2101	Rabbit	60 kDa	1:1,000	1:5,000

[1]Blocking and primary antibody incubation in 3% BSA in TBST

9.2 Software

Table 9.2: Detailed information about used software

Software	Version	Company
CFlow Plus	1.0.264.15 Build 20140714.264.15	BD Oxford, Oxfordshire, UK
FlowJo	10.0.7	FlowJo, LLC Ashland, OR, USA
Illustrator	CC 2014	Adobe Systems, Inc. San José, CA, USA
ImageJ/Fiji	1.49m	National Institutes of Health Bethesda, MD, USA
Leica LAS AF Lite	4.0.0 Build 11706	Leica Microsystems Wetzler, Hessen, Germany
Mendeley Desktop	1.16	Mendeley Ltd. London, UK
Office	365	Microsoft Redmond, WA, USA
Photoshop	CC 2014	Adobe Systems, Inc. San José, CA, USA
Prism	6.01	GraphPad Software, Inc. La Jolla, CA, USA
TeXstudio	2.10.8	Free Software Foundation

9.3 Materials

9.3.1 Consumables

Table 9.3: Detailed information about used consumables

Product	Catalogue number	Supplier
10 cm cell culture dish (TC treated dish, standard)	734-0006	VWR International Lutterworth, Leicestershire, UK
150 mm cell culture dish (TC treated dish, with 20 mm moulded grid)	734-0013	VWR International Lutterworth, Leicestershire, UK

Table 9.3 Continued: Detailed information about used consumables

Product	Catalogue number	Supplier
35 mm cell culture dish (TC treated dish, Easy-Grip)	734-0005	VWR International Lutterworth, Leicestershire, UK
6 cm cell culture dish (TC treated dish, Easy-Grip)	734-0007	VWR International Lutterworth, Leicestershire, UK
96-well plate (BD Falcon, flat bottom with lid)	734-0023	VWR International Lutterworth, Leicestershire, UK
Annexin V-FITC Apoptosis Detection Kit	BMS500FI	eBioscience, Ltd. Hatfield, Hertfordshire , UK
BCA Protein Assay Kit	23225	Fisher Scientific Loughborough, Leicestershire, UK
Dispenser tips 0.5 mL (Classic, individual blister pack)	613-1027	VWR International Lutterworth, Leicestershire, UK
Dispenser tips 2.5 mL (Classic, individual blister pack)	613-1011	VWR International Lutterworth, Leicestershire, UK
Dispenser tips 5 mL (Classic, individual blister pack)	613-1012	VWR International Lutterworth, Leicestershire, UK
Falcon tube 15 mL (flat top)	11849650	Fisher Scientific Loughborough, Leicestershire, UK
Falcon tube 50 mL (flat top)	FB55958	Fisher Scientific Loughborough, Leicestershire, UK
Filter paper (WYPALL X60, white, 420 x 310 mm)	115-2166	VWR International Lutterworth, Leicestershire, UK
G-LISA RhoA Activation Assay	BK124	Cytoskeleton Inc. Denver, CO, USA

Table 9.3 Continued: Detailed information about used consumables

Product	Catalogue number	Supplier
G-LISA Rac1 Activation Assay	BK128	Cytoskeleton Inc. Denver, CO, USA
Gel loading tips (1-200 µ/L)	732-3501	VWR International Lutterworth, Leicestershire, UK
Gloves (Nitrile, Semperguard comfort, PPE category III)	11867192	Fisher Scientific Loughborough, Leicestershire, UK
Immobilon-P membrane, PVDF 0.45 µm	IPVH00010	Millipore Ltd. Watford, Hertfordshire, UK
KAPA 2G Robust Hot Start Ready mix	KK5702	Kapa Biosystems Ltd. London, UK
MTS assay solution (CellTiter 96® AQueous One Solution Cell Proliferation Assay (MTS))	G3580	Promega UK Southampton, Hampshire, UK
QIAshredder	79654	Qiagen Manchester, UK
RNeasy Mini Kit	74104	Qiagen Manchester, UK
Stripettes 5 mL (Corning Costar, sterile)	10127400	Fisher Scientific Loughborough, Leicestershire, UK
Stripettes 10 mL (Corning Costar, sterile)	10677341	Fisher Scientific Loughborough, Leicestershire, UK
Stripettes 25 mL (Corning Costar, sterile)	TKV671070H	Fisher Scientific Loughborough, Leicestershire, UK
T25 cell culture flask (70 mL, vented, 25cm^2, canted)	734-0045	VWR International Lutterworth, Leicestershire, UK
T75 cell culture flask (250 mL, vented, 75cm^2, canted)	734-0050	VWR International Lutterworth, Leicestershire, UK

9.3.2 Chemicals

In this subsection all used chemicals are listed in alphabetic order in table 9.4. Different companies may helf the same distributor which are indicated in the footnote. Antibodies and inhibitors are listed separately in their corresponding sections.

Table 9.4: Detailed information about used chemicals

Product	Supplier	Catalogue number	Solvent	Stock concentration	Final concentration	Function
α-V5 affinity gel	Sigma	A7345	PBS	-	10 µL/IP	Binds to V5 tag; Used in IP
β-Mercaptoethanol	Bio-Rad	161-0710	-	-	See methods	Reducing agent
1,10-Phenanthroline monohydrate	Sigma	P9375	Methanol	200 mM	10 mM	MMP inhibitor
5-Aza-2'-deoxycytidine (Decitabine)	Sigma	A3656	Growth medium	50 mM	33.3 - 50 µM	Hypomethylation agent
6-Aminohexanoic acid	Sigma	07260	MilliQ water	-	25 mM	Component of Cathode buffer
Acrylamide/bis solution, 40%, 29:1	Bio-Rad	161-0146	MilliQ water	40%	7-17%	Monomers for PAA gels
Agarose	Fisher	BP160-500	1 x TAE	-	1-2%	Component of DNA gels
Ammonium persulfate	Bio-Rad	161-0700	MilliQ water	10%	0.1%	Oxidizing agent/ Provides free radicals

Table 9.4 Continued: Detailed information about used chemicals

Product	Supplier	Catalogue number	Solvent	Stock concentration	Final concentration	Function
Beads (Protein G Sepharose)	Sigma	P3296	EtOH	-	-	Binds to Fc-region of antibodies
BSA	Appli-Chem	A1391	PBS or TBST 0.1%	-	1-5 %	Blocking reagent
Bromophenol blue	Sigma	B0126	Methanol	10 mg/mL	100 µg/mL	Dye
cOmplete EDTA-free protease inhibitor cocktail	Roche	11873580001	Lysis buffer	20 x	1 x	Proteinase inhibitor
DMEM	Gibco	11960-085	-	-	-	Cell culture medium
DMSO	Sigma	D2650	-	-	-	Solvent
DNA Ladder (100 bp)	NEB	N3231	MilliQ water	500 µg/mL	35 µg/mL	Marker
dNTP mix	Invitrogen	18427-013	Tris-HCl (pH 7.5)	40 mM	400 µM	Nucleotide monomers in RT-PCR
Dried skimmed milk powder	Marvel	-	0.1% TBST	-	5%	Membrane blocking
DTT	Invitrogen	comes with RT kit	-	0.1 M	400 µM	Reducing agent in RT PCR

Table 9.4 Continued: Detailed information about used chemicals

Product	Supplier	Catalogue number	Solvent	Stock concentration	Final concentration	Function
Ethanol	Fisher	10437341	-	-	-	Solvent; Used in RNAeasy Kit
Fibronectin	Sigma	F1411	PBS	1 mg/mL	10 µL/mL	ECM substrate
FBS	Sigma	F7524	-	100%	10%	Growth media supplement
Formaldehyde (Pierce, Methanol-free)	Fisher	10751395	N/A	16%	4%	Fixative
GelRed	Biotium	41003	1 x TAE	10,000 x	1 x	DNA intercalating agent
Glycine	Fisher	G/0800/60	MilliQ water	-	1.92 M	Component of 10 x SDS running buffer
HCl	VWR	20252.335	-	37%	-	pH adjustment
Hygromycin B	Invitrogen	10687010	Cell culture medium	50 mg/mL	450 µg/mL	Selective antibiotic
Immersol 518 F	Zeiss	630-0340	-	-	-	Oil for confocal microscopy

Table 9.4 Continued: Detailed information about used chemicals

Product	Supplier	Catalogue number	Solvent	Stock concentration	Final concentration	Function
L-Glutamine	Sigma	G7513	Cell culture grade water	200 mM	2 mM	Growth media supplement
Lipofectamine 2000	Invitrogen	11668019	OptiMEM	-	See manual	Transfection reagent
Methanol	Fisher	M/4000/17	-	-	-	Used in SDS-Page and WB
NaCl	Fisher	S/3160/65	MilliQ water	-	-	Buffer ingredient
NaOH	Fisher	10743591	MilliQ water	-	-	WB stripping and pH adjustment
Nocodazole	Sigma	M1404	DMSO	25 mM	10 μM	Disrupt mitotic spindle function
OptiMEM	Gibco	31985062	-	-	-	Treatments and transfections
PBS tablets	Sigma	P4417	MilliQ water	-	1x	Buffer
Penicillin/Streptomycin	Sigma	P0781	0.9% NaCl	100x	1x	Growth media antibiotic

Table 9.4 Continued: Detailed information about used chemicals

Product	Supplier	Catalogue number	Solvent	Stock concentration	Final concentration	Function
PhosSTOP	Roche	4906845001	Lysis buffer	20 x	1 x	Phosphotase inhibitor
Polybrene	Sigma	107689	MilliQ water	800 µg/mL	8 µg/mL	Enhances viral infection
Puromycin	Thermo	A1113803	-	10 mg/mL	1 µg/mL	Selective antibiotic
Precision Plus Protein Dual Colour Standards	Bio-Rad	161-0394	-	-	5-7 µL per well (15 well combs)	Protein marker
ProLong Gold Antifade Mountant with DAPI	Invitrogen	P-36931	-	-	Approx. 30 µL	Mounting and staining of cover slips
Propidium iodide	Sigma	P4170	MilliQ water	400 µg/mL	10 µg/mL	Nucleic acid dye
Random hexamers	Invitrogen	N8080127	-	50 µM	500 nM	RNA primer for RT-PCR
RIPA buffer	Sigma	R0278	-	-	-	Lysis buffer
ScaI	NEB	R3122L	Neb buffer 3 in MilliQ water	1,000 u	10 u	Restriction enzyme
SDS solution	Appli-Chem	MilliQ water	A0675	20%	various	Micelle formation/negatively charges proteins

Table 9.4 Continued: Detailed information about used chemicals

Product	Supplier	Catalogue number	Solvent	Stock concentration	Final concentration	Function
Staurosporine solution	Sigma	S6942	DMSO	1 mM	1-10 µM	Apoptosis inducing agent
Sulfuric acid	Sigma	258105	-	-	-	Component of G-LISA HRP stop solution
Superscript II RT	Thermo	18064-071	Invitrogen storage buffer	10,000 u	200 u	Reverse Transcriptase
TAE buffer	Appli-chem	A4686	-	50 x	1 x	Electrophoresis buffer
TEMED	Bio-Rad	161-0800	N/A	100%	0.1%	Catalyst for PAA gels
Trichostatin A	Sigma	T1952	Cell culture medium	5 mM	500 nM	Inhibits histone deacetylase
Tris-Base	Fisher	BP152-1	MilliQ water	-	See methods	pH buffer reagent
Trypsin-EDTA	Sigma	T4174	0.9% NaCl	10x	1x (in PBS)	Cell detachment solution
Tween-20	Sigma	P1379	-	100%	0.1%	Soap in TBS buffer
Vitronectin	Gibco	PHE0011	PBS	0.5 mg/mL	10 µL/mL	ECM substrate

Table 9.4 Continued: Detailed information about used chemicals

Product	Supplier	Catalogue number	Solvent	Stock concentration	Final concentration	Function
Western Blot substrate (Pierce ECL 2 WB substrate)	Thermo	11517371	N/A	-	40:1	Substrate for chemiluminescence reaction

9.3.3 Laboratory Equipment

Table 9.5: Detailed information about used equipment

Item	Manufacturer
-86°C Freezer (FormaScientific)	Thermo Fisher Scientific Basingstoke, Hampshire, UK
Analytical balance (MH 124)	Fisher Scientific Loughborough, Leicestershire, UK
Aspirator (Medical Suction Unit SAM12)	MG Electric Ltd. Colchester, Essex, UK
Bright-field microscope (Olympus LH50A)	Olympus Scientific Solutions Americas Inc. Waltham, Massachusetts, USA
Casting stand for PAA gels Mini-PROTEAN® Casting Stand	Bio-Rad Laboratories Ltd. Hemel Hempstead, Hertfordshire, UK
Cell Imaging System (EVOS® XL Core)	Life Technologies Ltd. Paisley, Renfrewshire, UK
Comb for PAA gels Mini-PROTEAN® Comb, 10-well	Bio-Rad Laboratories Ltd. Hemel Hempstead, Hertfordshire, UK
Comb for PAA gels Mini-PROTEAN® Comb, 15-well	Bio-Rad Laboratories Ltd. Hemel Hempstead, Hertfordshire, UK
Confocal microscope (Leica SP5)	Leica Microsystems (UK) Ltd. Milton Keynes, UK
Developer for Western Blot Konica Minolta SRX-101A	Konica Minolta Medical & Graphic Imaging Europe B.V. Banbury, Oxfordshire, UK
Digital Graphic Printer for UV Transilluminator (UP-D 897)	Sony Europe Ltd. Weybridge, Surrey, UK
Electronic Pipette Controller (peqMATE)	PEQLAB c/o VWR International Lutterworth, Leicestershire, UK
Flake ice machine	Thermo Fisher Scientific Basingstoke, Hampshire, UK
Flow Cytometer (Accuri C6)	BD Oxford, Oxfordshire, UK
Freezing Container (Nalgene® Cryo 1°C “Mr. Frosty”)	Thermo Fisher Scientific Basingstoke, Hampshire, UK
Freezer (Labcold Borolabs)	Labcold Ltd. Basingstoke, Hampshire, UK

Table 9.5 Continued: Detailed information about used equipment

Item	Manufacturer
Fridge (Labcold Borolabs)	Labcold Ltd. Basingstoke, Hampshire, UK
Gel electrophoresis tank for PCR (Multi Sub Choice)	Geneflow Ltd. Lichfield, Staffordshire, UK
Gel electrophoresis tank for Western Blot (Mini-PROTEAN Tetra Cell)	Bio-Rad Laboratories Ltd. Hemel Hempstead, Hertfordshire, UK
Heating Block (Techne Dri-Block® DB-2A)	Bibby Scientific Ltd. Stone, Staffordshire, UK
Incubator (HeraCell 240)	Thermo Fisher Scientific Basingstoke, Hampshire, UK
Magnetic stirrer (Stuart stir CB162)	Bibby Scientific Limited Stone, Staffordshire, UK
Magnetic heatable stirrer (Stuart stir SB161)	Bibby Scientific Limited Stone, Staffordshire, UK
NanoDrop® ND-1000	Thermo Fisher Scientific Basingstoke, Hampshire, UK
Counting chamber (Neubauer improved)	Hawksley Lancing, Sussex, UK
Orbital platform shaker (Stuart Mini Orbital Shaker SSM1)	Bibby Scientific Limited Stone, Staffordshire, UK
pH-Meter (S20 SevenEasy pH)	Mettler-Toledo Ltd. Leicester, Leicestershire, UK
Pipettes (2 µL, 20 µL, 200 µL, 1000 µL,)	Gilson Scientific Ltd., Luton, Bedfordshire, UK
Pipettes for cell culture (RAININ Pipet-like XLS)	Anachem Ltd. Luton, Bedfordshire, UK
Plate Reader (Fluostar Optima)	BMG Labtech Ortenberg, Baden-Württemberg, Germany
Platform rocker (STR)	Bibby Scientific Limited Stone, Staffordshire, UK
Power supply for PCR (Bio-Rad Model 200/2.0)	Bio-Rad Laboratories Ltd. Hemel Hempstead, Hertfordshire, UK

Table 9.5 Continued: Detailed information about used equipment

Item	Manufacturer
Power supply for Western Blot (GE electophoresis power supply EPS30)	GE Healthcare Little Chalfont, Buckinghamshire, UK
Precision balance (GX-6100)	A&D Medical San Jose, California, USA
Rotary wheel (Stuart Rotary Drive STR4)	Bibby Scientific Limited Stone, Staffordshire, UK
Safety Cabinet for cell culture (HeraSafe KS)	Thermo Fisher Scientific Basingstoke, Hampshire, UK
Scanner (Canon CanoScan LiDE 210)	Canon UK Ltd. Reigate, Surrey, UK
Sonicator	Diagenode Seraing (Ougrée), Belgium
Spectrophotometer Ultrospec™ 2100 Pro	GE Healthcare UK Limited Little Chalfont, Buckinghamshire, UK
Stepper/Repetitive pipette (peqSTEPPER)	PEQLAB c/o VWR International Lutterworth, Leicestershire, UK
Table top autoclave (Classic 2100 Portable)	Prestige Medical Ltd. Blackburn, Lancashire , UK
Table top centrifuge for cell culture (SANYO MSE Centaur2)	MSE (UK) Ltd Lower Sydenham, London, UK
Table top centrifuge for cell culture (SANYO MSE Micro Centaur)	MSE (UK) Ltd Lower Sydenham, London, UK
Table top centrifuge (Perfect 24 Plus)	PEQLAB c/o VWR International Lutterworth, Leicestershire, UK
Table top centrifuge refrigerated (Heraeus Fresco21)	Thermo Fisher Scientific Basingstoke, Hampshire, UK
ThermoCycler (MJ Research Peltier PTC-225)	Bio-Rad Laboratories Ltd. Hemel Hempstead, Hertfordshire, UK
Trans-Blot® Turbo Transfer System	Bio-Rad Laboratories Ltd. Hemel Hempstead, Hertfordshire, UK
Vortexer (Stuart SA7)	Bibby Scientific Limited Stone, Staffordshire, UK
Water bath (Grant SUB36)	Fisher Scientific Loughborough, Leicestershire, UK

Table 9.5 Continued: Detailed information about used equipment

Item	Manufacturer
UV Transilluminator	Ultra-Violet Products Ltd.
(BioDoc-It® Imaging Systems)	Cambridge, Cambridgeshire, UK